

# Phase Behaviour of Colloid-Micelle Mixtures

Linda A Galloway

Thesis submitted for the degree of Doctor of Philosophy



Department of Physics and Astronomy  
University of Edinburgh

2000



*For My Family*

# Abstract

Under suitable conditions surfactant molecules self-assemble into wormlike micelles. These micelles behave as polymers in many ways. There are, however, some important differences. The micelles can break and reform. The average size of the micelles increases as the surfactant concentration increases, and they have an exponential size distribution. Wormlike micelles are used in many industrial products, such as shampoos, where they are mixed with oil droplets. The phase behaviour of this type of mixture is therefore extremely interesting to study.

The phase behaviour of a model colloid-polymer system has already been investigated. It agrees well with theoretical predictions of a depletion model. We have therefore extended beyond the standard colloid-polymer system and investigated the behaviour of a mixture of colloids and wormlike micelles. Do wormlike micelles act as depletants? This more complicated system provides an interesting test of the generality of the depletion model.

We have studied the phase behaviour of both charged and uncharged hard colloidal particles in a solution of wormlike micelles of the nonionic surfactant  $C_{16}E_6$ . The behaviour found is similar to that in the case of colloid-polymer mixtures. The phase boundaries agree well with theoretical predictions of an adapted colloid-polymer depletion model that accounts for the concentration induced growth and the exponential size distribution of the micelles. In the case of uncharged colloids a stable one phase fluid region is found at low surfactant concentrations. As the concentration of  $C_{16}E_6$  increases, phase separation into coexisting colloid-rich and colloid-poor phases is observed, as a result of the increase of the concentration and/or average length of the micelles. At still higher concentrations a metastable gel is found. Similar behaviour is

found in the case of charged colloid, both with and without added electrolyte to screen the coulombic repulsion between the particles.

A more realistic, industrial type system with charged colloids in an aqueous solution of anionic micelles of sodium lauryl ether sulfate (SLES) and cocoamidopropylbetaine (CAPB) was also investigated. A ternary phase diagram of SLES/H<sub>2</sub>O/NaCl, where the salt is used to promote the formation of wormlike micelles, resembles that found in the C<sub>16</sub>E<sub>6</sub> systems and can be rationalised by the depletion attraction. At low surfactant/salt concentrations the mixture is a one phase fluid. As the concentration of surfactant and/or salt is increased first phase separation into coexisting colloid-rich and colloid-poor phases, then colloidal gels are observed. The collapse of these gels was studied by diffusive-wave spectroscopy and shows a qualitatively reproducible behaviour of the particle dynamics during the gel collapse.

# Acknowledgements

I would like to thank my supervisors Wilson Poon, Stefan Egelhaaf, and Mike Cates for all their guidance and enthusiasm throughout my PhD. I would also like to thank my industrial supervisors Stan Lam and Peter Fairley. Thanks also to Patrick Warren for developing the theoretical model for this thesis and for many interesting discussions.

I am also grateful to the postdocs who have worked in this group, particularly to; Jérôme Arrault for introducing me to rheology; George Petekidis for all his help with DWS; Mark Haw for many useful discussions and for reading this manuscript; and Andy Schofield for synthesising particles and for his help with all things chemical. Thanks also to Peter Tuffy for taking the photographs of my samples.

Thanks to all members of the condensed matter group, both past and present, for making JCMB more interesting and for fun nights out.

*“Life’s a rollercoaster ride, the ups and downs will make you scream and shout”*

Jon Bon Jovi

A special thanks to my family and friends who have been there through the “ups and downs”, for putting up with my “screams and shouts”. You have been FAB.

# Contents

<b>Abstract</b>	<b>v</b>
<b>Declaration</b>	<b>vii</b>
<b>Acknowledgements</b>	<b>ix</b>
<b>1 Introduction</b>	<b>1</b>
1.1 An Introduction to Soft Matter . . . . .	1
1.2 Phase Behaviour . . . . .	2
1.3 Thesis Layout . . . . .	3
<b>2 Background</b>	<b>5</b>
2.1 What is a Colloid? . . . . .	5
2.2 Colloidal Interactions . . . . .	6
2.2.1 Van der Waals Attraction . . . . .	6
2.2.1.1 The Hamaker Constant . . . . .	7
2.2.2 Charge Stabilisation . . . . .	8
2.2.2.1 Potential of One Particle . . . . .	8

## CONTENTS

2.2.2.2	Interactions Between Charged Particles . . . . .	10
2.2.2.3	The Derjaguin-Landau and Verwey-Overbeek (DLVO) Theory . . . . .	11
2.2.2.4	Critical Coagulation Concentrations . . . . .	13
2.2.3	Steric Stabilisation . . . . .	14
2.2.4	The Depletion Attraction . . . . .	15
2.3	Colloidal Phase Behaviour . . . . .	16
2.3.1	Hard-Spheres . . . . .	16
2.3.2	Sterically Stabilised Colloid . . . . .	18
2.3.3	Charge Stabilised Colloid . . . . .	19
2.4	Surfactants . . . . .	21
2.4.1	Types of Surfactant . . . . .	21
2.4.2	Properties of Surfactants . . . . .	22
2.4.3	Geometry of Micelles . . . . .	23
2.4.3.1	Mesophase Formation . . . . .	24
2.4.4	Properties of Wormlike Micelles . . . . .	26
2.4.4.1	Structure . . . . .	26
2.4.4.2	Dynamics . . . . .	29
2.4.5	Typical Surfactant Phase Behaviour . . . . .	31
2.4.5.1	Non-ionic Surfactants . . . . .	31
2.4.5.2	Ionic Surfactants . . . . .	34

<b>3</b>	<b>The Depletion Interaction</b>	<b>37</b>
3.1	Colloid-Polymer Mixtures . . . . .	37
3.1.1	A Depletion Potential . . . . .	37
3.1.2	Predicting the Equilibrium Phase Behaviour . . . . .	39
3.1.2.1	Theory of Gast, Hall & Russel . . . . .	40
3.1.2.2	Theory of Lekkerkerker et al. . . . .	44
3.1.2.3	Comparison of the Theories . . . . .	50
3.1.3	Experimental Observations . . . . .	51
3.1.3.1	Hard Sphere Colloids & Polymer . . . . .	51
3.1.3.2	Charged Colloids & Polymer . . . . .	51
3.1.4	Non-equilibrium Behaviour . . . . .	53
3.1.4.1	Gel Formation . . . . .	53
3.1.4.2	Gel Collapse . . . . .	55
3.1.5	Depletion Restabilisation . . . . .	56
3.2	Binary Mixtures . . . . .	58
3.3	Rod-sphere Mixtures . . . . .	60
3.4	Colloid-Micelle Mixtures . . . . .	61
3.4.1	Colloid-Spherical Micelle Mixtures . . . . .	61
3.4.2	Colloid-Wormlike Micelle Mixtures . . . . .	64
<b>4</b>	<b>Experimental Systems &amp; Methods</b>	<b>67</b>
4.1	The Systems . . . . .	67



## CONTENTS

4.1.1	System A . . . . .	67
4.1.2	Preparation of System A . . . . .	68
4.1.3	System B . . . . .	69
4.1.4	Preparation of System B . . . . .	69
4.1.5	System C . . . . .	70
4.1.6	Preparation of System C . . . . .	71
4.1.7	Errors in Sample Preparation . . . . .	71
4.2	Characterisation of the Colloid . . . . .	72
4.2.1	Conductivity Measurements . . . . .	72
4.2.2	Critical Coagulation Concentration . . . . .	73
4.3	Characterisation of Micelles - Rheology . . . . .	74
4.3.1	Background . . . . .	74
4.3.1.1	Flow . . . . .	74
4.3.1.2	Oscillation . . . . .	75
4.3.2	Apparatus and Technique . . . . .	78
4.4	Phase Studies . . . . .	82
4.5	Direct Observations . . . . .	83
4.6	Diffusing Wave Spectroscopy . . . . .	85
4.6.1	Background . . . . .	85
4.6.2	Experimental Procedure . . . . .	88
4.6.3	Ergodicity Measurements . . . . .	88

4.6.3.1	Background . . . . .	88
4.6.3.2	Apparatus & Technique . . . . .	89
4.6.4	DWS During Gel Collapse . . . . .	91
4.6.4.1	Apparatus & Technique . . . . .	91
<b>5</b>	<b>Characterisation of Components</b>	<b>93</b>
5.1	Characterisation of Colloid . . . . .	93
5.1.1	Surfactant-free (IDC) Latices . . . . .	93
5.1.1.1	Data from IDC . . . . .	93
5.1.1.2	Calculation of the Screening Length . . . . .	94
5.1.1.3	Conductivity Measurements . . . . .	95
5.1.1.4	Comparison of the values of $\kappa^{-1}$ . . . . .	98
5.1.1.5	Critical Coagulation Concentrations . . . . .	98
5.1.1.6	DLVO Potentials . . . . .	99
5.1.2	Rhône-Poulenc Latices . . . . .	103
5.1.3	PEO-Stabilised Latices . . . . .	103
5.2	Characterisation of $C_{16}E_6$ . . . . .	103
5.2.1	Light Scattering Study of $C_{16}E_6$ . . . . .	103
5.2.2	Rheology of $C_{16}E_6$ . . . . .	107
5.3	Characterisation of SLES system . . . . .	110
5.3.1	Salt Dependence . . . . .	110
5.3.2	Effect of Zwitterion . . . . .	113

## CONTENTS

5.3.3	Effect of Octanol . . . . .	114
5.3.4	Temperature Effects . . . . .	116
5.4	Comparison of SLES and C <sub>16</sub> E <sub>6</sub> Systems . . . . .	118
<b>6</b>	<b>Phase Behaviour of Nonionic Surfactant and Colloid</b>	<b>121</b>
6.1	Introduction . . . . .	121
6.2	Differences between Wormlike Micelles and Polymer as Depletants . . .	121
6.2.1	Scission & Recombination of Micelles . . . . .	122
6.2.2	Concentration Effects . . . . .	122
6.2.3	Size Distributions . . . . .	122
6.2.4	Entanglement . . . . .	123
6.2.5	Possibility of Branching . . . . .	124
6.3	System A - Uncharged Colloid . . . . .	125
6.3.1	Experimental Phase Diagram . . . . .	125
6.3.2	Details of Phase Behaviour . . . . .	125
6.3.3	Discussion . . . . .	127
6.4	System B - Charged Colloid with Added Salt . . . . .	128
6.4.1	Experimental Phase Diagrams . . . . .	128
6.4.2	Details of Phase Behaviour . . . . .	132
6.4.3	Discussion . . . . .	138
6.5	System B - Charged Colloid, no Added Salt . . . . .	140
6.5.1	Experimental Phase Diagrams . . . . .	141

6.5.2	Details of Phase Behaviour . . . . .	145
6.5.3	Discussion . . . . .	148
6.5.3.1	Depletion Picture of Charged Colloid and Uncharged Wormlike Micelles . . . . .	148
6.5.3.2	Discussion of Results in Terms of Depletion . . . . .	150
6.6	Comparing Phase Boundaries of the Three Systems . . . . .	152
6.6.1	Salt Dependence . . . . .	154
6.7	Comparison of Experimental Results with Colloid-Polymer Mixtures . .	155
6.7.1	Phase Separation . . . . .	155
6.7.2	Gels . . . . .	157
6.7.3	Depletion Restabilisation . . . . .	158
6.7.4	Redispersibility of Samples . . . . .	158
6.8	Comparison with Theory . . . . .	158
6.8.1	Details of the Theory . . . . .	159
6.8.1.1	Assumptions . . . . .	159
6.8.1.2	Inputs . . . . .	159
6.8.2	Theoretical Phase Diagrams . . . . .	160
6.8.2.1	Effect of Growth Exponent . . . . .	160
6.8.2.2	Effect of Polydispersity . . . . .	164
6.8.2.3	Effect of Size Ratio . . . . .	165
6.8.3	Comparison With Experiment . . . . .	167
6.8.3.1	Qualitative Behaviour . . . . .	168

## CONTENTS

6.8.3.2	Binodals . . . . .	168
6.8.3.3	Validity of the Theory . . . . .	171
6.8.3.4	Tielines . . . . .	171
6.8.3.5	Conclusion . . . . .	172
6.9	Conclusions . . . . .	173
<b>7</b>	<b>Phase Behaviour of Ionic Surfactant and Colloid</b>	<b>175</b>
7.1	Introduction . . . . .	175
7.2	SLES/NaCl/H <sub>2</sub> O Phase Diagram . . . . .	175
7.2.1	Details of the Phase Behaviour . . . . .	176
7.2.1.1	Creaming Behaviour . . . . .	179
7.2.2	Discussion in terms of colloidal interactions . . . . .	180
7.2.3	Conclusion . . . . .	181
7.3	Detailed Studies of Gels . . . . .	181
7.3.1	Observations . . . . .	182
7.3.2	DWS . . . . .	185
7.3.2.1	Results . . . . .	185
7.3.2.2	Fitting . . . . .	195
7.3.2.3	Conclusion . . . . .	201
7.4	Distinguishing between Charge Effects and Depletion Effects . . . . .	201
7.4.1	Varying Zwitterion . . . . .	202
7.4.1.1	Results . . . . .	202

7.4.1.2	Discussion . . . . .	203
7.4.2	SLES/CAPB/Octanol System . . . . .	203
7.4.2.1	Results . . . . .	204
7.4.2.2	Discussion . . . . .	204
7.5	Discussion & Comparison with Other Systems . . . . .	205
7.5.1	Comparison with Theory . . . . .	207
7.6	Conclusions . . . . .	208
<b>8</b>	<b>Conclusions</b>	<b>209</b>
8.1	Depletion Interaction due to Wormlike Micelles . . . . .	209
8.2	Comparison with Experimental Studies of Colloid-Polymer Mixtures . .	210
8.2.1	System A and System B with Added Salt: Approximate Hard-Sphere Systems . . . . .	210
8.2.2	System B with no Added Salt: Strong Electrostatic Interactions	211
8.2.3	System C: An Industrial System . . . . .	212
8.3	Theoretical Predictions of Phase Behaviour . . . . .	212
8.4	Non-equilibrium Behaviour . . . . .	213
8.5	Application to Complex Systems . . . . .	214
8.6	Suggestions for Further Work . . . . .	214
	<b>List of Figures</b>	<b>216</b>
	<b>List of Tables</b>	<b>224</b>

CONTENTS

<b>Bibliography</b>	<b>226</b>
<b>A Sample Making - More Details</b>	<b>237</b>
A.1 System A . . . . .	237
A.1.1 Finding the Volume Fraction of the Colloid . . . . .	237
A.2 System B . . . . .	238
A.2.1 Finding the Required Colloid Volume Fraction . . . . .	238
A.2.2 Sample-making . . . . .	239
A.2.2.1 Sample Error Calculation . . . . .	239
A.3 System C . . . . .	240
A.3.1 Sample-making . . . . .	240
A.3.1.1 Uncertainties . . . . .	240

# Chapter 1

## Introduction

### 1.1 An Introduction to Soft Matter

Complex fluids such as colloids, polymers and surfactants have been well-studied in recent times. A colloidal system consists of a dispersed phase on the nanometre to micrometre scale in a continuous medium. Both the dispersed and the dispersion phases can be gas, liquid or solid. There are many everyday examples of colloids, such as mayonnaise which is formed from liquid droplets dispersed in another liquid and smoke which is solid particles dispersed in a gaseous medium. In this thesis the colloids which are discussed are suspensions of solid particles dispersed in a liquid medium. Polymers are long chain-like molecules built up from a large number of subunits called monomers, e.g. polyethylene (more commonly known as polythene) which is a commonly used plastic. Surfactants are “amphiphilic” molecules which have both a water-loving and a water-hating part. They form the basis of all cleaning products. These types of systems are therefore ubiquitous in both industrial products and nature. The area of research involving complex fluids is known as “soft matter”.

The common characteristic in these systems is their mesoscopic length scale, which lies between the atomic length scale ( $\gtrsim 1\text{nm}$ ) and the bulk length scale ( $\lesssim 1\text{mm}$ ). One advantage of these systems is that their lengthscale makes experimental study relatively straight forward. The wavelength of visible light is comparable to the mesoscopic lengthscale and therefore light scattering and optical microscopy can be used as probes.



Typical interparticle energies in these systems are of the order of 1 to  $20kT$  and they have accessible relaxation times in the range 1s to 1 year. Model systems are also readily available for study in this field.

## 1.2 Phase Behaviour

Phase science involves finding the states in which a system exists as a function of thermodynamic variables. Phase diagrams are plots of these phases as functions of the relevant thermodynamic variables e.g. the phase diagram of water would show ice, liquid and gaseous states and their coexistence regions as a function of temperature and pressure. The chemistry remains constant in this case but under different conditions the microscopic structure and therefore the macroscopic appearance changes. An equilibrium state under given conditions corresponds to the state with the lowest free energy. In soft matter, however, the observed “phase” behaviour often corresponds to nonequilibrium or metastable phases, such as gels and glasses.

Phase behaviour is extremely important both fundamentally and commercially. On a fundamental level investigating the phase behaviour provides information on the interactions present in the system. Also, knowledge of the phase behaviour of a system is essential information for making products such as cosmetics and foodstuffs. A large proportion of studies of soft matter have therefore been phase studies. The phase behaviour of both individual components, such as hard-sphere colloids [1] and aqueous solutions of surfactant [2, 3, 4] and of mixtures such as colloid-polymer mixtures [5, 6, 7] have been investigated.

Colloid-polymer mixtures have been extensively studied and their experimental phase behaviour [7] has been well understood in terms of a macromolecular crowding effect known as the “depletion interaction” [8, 9, 10]. As the polymer concentration increases the colloidal suspension separates into two or more phases. Equilibrium behaviour such as gas/liquid and gas/crystal separation have been observed. This behaviour is dependent on the relative size ratio of the polymer to the colloid ( $\xi = R_g/a$ , where  $\xi$  is the size ratio,  $R_g$  is the radius of gyration of the polymer and  $a$  is the colloidal radius). At high polymer concentrations equilibrium is not reached and the colloid-polymer

mixture is found to exist in long-lived metastable or nonequilibrium states.

In this thesis the more complex system of colloid-wormlike micelle mixtures is studied. Wormlike micelles are self-assembled aggregates of surfactant molecules resembling polymer molecules. However, these micelles continually break and reform unlike polymer molecules. The micelles also have an exponential distribution of lengths. Do these differences alter the phase behaviour drastically from the well understood colloid-polymer mixtures? Do wormlike micelles deplete at all, since they could potentially break into smaller micelles if this is energetically more favourable? Furthermore, colloid-wormlike micelle mixtures are interesting to investigate since a greater range of size ratios than in the case of colloid-polymer can be explored. This is because as the concentration of surfactant is increased the micelles can grow extensively, whereas with colloid-polymer mixtures one is limited by how large the polymer can be synthesised easily, and how small monodisperse (single-sized) colloids could be made.

Moreover, this study has been carried out in order to begin investigations of more realistic systems. Surfactants and therefore micelles are used extensively in cleaning products, such as shower gel, shampoo, and washing-up liquid. To improve the performance of many such commercial products particulate matter is often added. The colloid-wormlike micelle mixture is therefore a good model analogue of these commercial products. Since the behaviour of the similar system of colloid-polymer mixtures is well known there is a framework in which the results can be compared and contrasted. It will allow us to determine the generality with which the colloid-polymer framework can be applied.

### **1.3 Thesis Layout**

This thesis presents experimental studies of the phase behaviour of colloid-wormlike micelle mixtures. Initial studies using an industrial system proved too complex to allow a detailed understanding of the behaviour to be found. Consequently a more detailed study was carried out on a simpler system. The results of this together with those of the complex system have led to significant progress in understanding the phase behaviour and interactions in colloid-wormlike micelle mixtures.

## CHAPTER 1: INTRODUCTION

The thesis is split into two main sections, the background chapters (chapters 2-4) and the results and discussion chapters (chapters 5-7). Chapter 8 draws the results together and establishes the main conclusions of the thesis as well as outlining suggestions for further work.

Chapter 2 is an introductory guide to colloids and surfactants. The interactions and phase behaviour of both colloids and surfactants are discussed in detail. The formation and properties of wormlike micelles are also detailed.

Chapter 3 is essentially a literature review detailing the relevant colloid-depletant mixtures previously studied both experimentally and theoretically.

Chapter 4 introduces the particular systems studied here and explains the various experimental techniques used, including sample making, direct observations, rheology and diffusive-wave spectroscopy.

In chapter 5 the characterisation of the individual components of the systems, i.e. the different colloids and wormlike micelles studied, is discussed.

In chapter 6 the experimental phase behaviour of both charged and uncharged colloids in a solution of uncharged wormlike micelles is presented. The results are compared with studies of other colloidal mixtures and a theory developed for colloid-wormlike micelle mixtures.

In chapter 7 the experimental results of the more complex, industrial-type system of charged colloid in a solution of charged wormlike micelles are discussed.

Chapter 8 summarises the work carried out in this thesis and discusses the main conclusions.

## Chapter 2

# Background

### 2.1 What is a Colloid?

A colloid is a system in which one or more of the components has at least one dimension on the mesoscopic scale i.e. in the nanometer to micrometer range and the solvent can be treated as a continuum. On this lengthscale the particles are large enough to be treated classically, but small enough such that Brownian motion dominates over gravitational settling.

There are many examples of colloids, such as fog (liquid drops suspended in a gas), foams (a gas dispersed in a liquid), mayonnaise (liquid droplets dispersed in another liquid) and micellar solutions (see section 2.4). It is therefore the structure that is important and not the specific materials. One of the most studied colloidal systems is the suspension of solid particles dispersed in a liquid. This is known as a colloidal suspension and is the type of colloidal system discussed in this thesis. These are of scientific interest both in terms of their physical chemistry and because they are analogous to atoms. The colloidal interactions are, however, easily tunable as discussed later and therefore one can get an insight into atomic systems by studying colloids, where the time and length scales make experiments much more accessible. Colloids are important in many different industries, including pharmaceuticals, food, cosmetics and paint. The stability of colloids and therefore the shelf-life of products is one of the most important industrial aspects of colloid science.

## 2.2 Colloidal Interactions

Colloidal interactions are very important, both for the fundamental understanding and when considering the properties of commercial products such as their stability. The following sections therefore discuss the main interactions in some detail. These will be discussed in terms of potentials, however it should be noted that these interactions have also been looked at in terms of free energies in recent times [11].

### 2.2.1 Van der Waals Attraction

Between any two bodies there is a force known as the van der Waals or the London force. This is usually an attractive interaction arising between fluctuating dipoles on the bodies. Even though there is no permanent dipole on the body one is induced by fluctuations of the charge distribution on adjacent bodies. This attraction is short range and goes as  $r^{-6}$  for a pair of molecules/atoms, where  $r$  is the interatomic/molecular distance. For an assembly of molecules the London forces are to a first approximation additive. The attractive interaction between two particles of equal radius in such an assembly is calculated by adding all of the pair potentials. It is found that for an assembly of particles (or a colloidal solution) the van der Waals attraction decays less rapidly than it does for a pair of atoms/molecules. The interaction energy as a function of surface separation  $H$  for two spherical particles of radius  $a$  is [12]

$$V_a = -\frac{A}{12} \left\{ \frac{1}{x(x+2)} + \frac{1}{(x+1)^2} + 2 \ln \left( \frac{x(x+2)}{(x+1)^2} \right) \right\} \quad (2.1)$$

where  $x = H/2a$  is the normalised surface separation.  $A$  is known as the Hamaker constant and depends on both the particles and the solvent. This will be discussed in detail in section 2.2.1.1.

At long interparticle separations,  $x \rightarrow \infty$ , the  $r^{-6}$  behaviour is recovered. At small interparticle separation, such that  $H \ll a$ , the interaction simplifies to

$$V_a = -\frac{Aa}{12H} \quad (2.2)$$

It can be seen that the attractive potential now drops off only as the inverse distance

between the particles. This long range van der Waals attraction induces aggregation of the colloidal particles, unless they are stabilised by some method. Both charge stabilisation and steric stabilisation can be employed for this purpose. The details of these stabilisation techniques are discussed in section 2.2.2 and section 2.2.3 respectively.

### 2.2.1.1 *The Hamaker Constant*

The Hamaker constant is determined by the material properties of the particles and their suspension medium. The evaluation of this constant is difficult and is a major problem in correctly determining the van der Waals interaction in a colloidal suspension.

There are two methods of measuring the Hamaker constant. A microscopic evaluation from the individual atomic polarisabilities and the atomic densities of the materials can be made. This method assumes that the interaction is the sum of the individual pair interactions and that it is centred around a single frequency. The influence of neighbouring atoms will, however, be important, thus introducing errors into the value of the constant. Alternatively, a macroscopic approach has been developed by Lifshitz [13]. This method treats both the particles and medium as continuous phases. It involves a complex calculation, where the bulk optical and dielectric properties of the interacting materials are required over a large frequency range. The macroscopic approach provides a more accurate value of  $A$  at large values of  $H$ .

Hamaker constants for the interaction between single materials in vacuo are found tabulated in many textbooks. They typically have a value of about  $kT$ . When the material is dispersed in a liquid medium an effective Hamaker constant needs to be calculated. This effective value can then be used in equation 2.1 or 2.2 in order to find the van der Waals attraction in this dispersion.

Consider the interaction between two particles, 1 and 2, in a continuous medium, 3. When the particles are far apart the interactions are particle-solvent interactions only, with Hamaker constants  $A_{13}$  and  $A_{23}$ . When the two particles approach each other both particle-particle and solvent-solvent interactions, with Hamaker constants  $A_{12}$  and  $A_{33}$  respectively, need to be considered. The effective Hamaker constant is then given by

$$A_{132} = A_{12} + A_{33} - A_{13} - A_{23} \quad (2.3)$$

The problem with this expression is that the Hamaker constants on the right hand side are all unknown. The effective Hamaker constant is therefore written in terms of tabulated constants for the material in vacuum (e.g.  $A_{11}$  is the Hamaker constant for the interaction for material 1 in vacuo) as,

$$A_{132} = (A_{11}^{1/2} - A_{33}^{1/2})(A_{22}^{1/2} - A_{33}^{1/2}) \quad (2.4)$$

If the two particles are made of the same material, which is the case for most colloidal suspensions this equation can be simplified further to

$$A_{131} = (A_{11}^{1/2} - A_{33}^{1/2})^2 \quad (2.5)$$

It can be seen that the interaction between particles in the same medium is always positive, i.e. the van der Waals forces are always attractive. It can also be seen that a weak interaction will be found when the particles and the medium are made of similar materials. This property is used to find model hard sphere colloidal systems, where the only force is an infinite repulsive force on contact. The minimisation of the van der Waals attraction by index-matching of the dispersion medium and the dispersed particles has therefore been used in experimental model hard-sphere studies.

## 2.2.2 Charge Stabilisation

### 2.2.2.1 Potential of One Particle

Charged colloidal particles have a double layer consisting of counterions and the ions of any electrolyte present in solution surrounding it. As the particles approach one another the double layers overlap, resulting in a repulsive force that can stabilise the colloids against aggregation.

This double layer can be modelled in terms of the Gouy-Chapman-Stern Model. The double layer then consists of two parts. At the particle surface there is a plane of atoms that are specifically adsorbed (temporarily) with a force strong enough to overcome thermal agitation. This is known as the Stern Layer and the potential drops off quickly in this region of the double layer. Ions with centres beyond the Stern layer form the diffuse part of the double layer which was modelled by Gouy and Chapman. Here the potential drops off more slowly. (Figure 2.1)

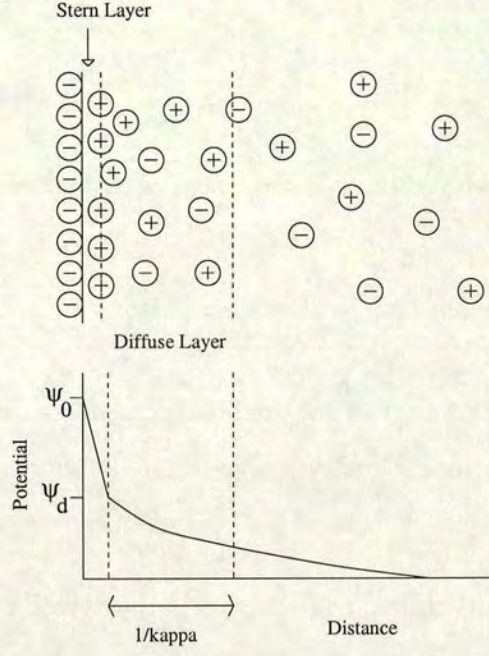


Figure 2.1: Schematic diagram of the structure of the double layer and the corresponding potential versus distance curve.

The Debye Screening length,  $\kappa^{-1}$ , is the distance over which the potential decreases by an exponential factor. It can be thought of as the “thickness” of the double layer. It is found by applying the Poisson equation to a Boltzmann distribution of ions around the colloidal particle, and is given by[12]

$$\kappa = \left( \frac{2e^2 n_0 z^2}{\epsilon \epsilon_0 kT} \right)^{1/2} = \left( \frac{2e^2 N_A c z^2}{\epsilon \epsilon_0 kT M_w} \right)^{1/2} \quad (2.6)$$

where  $n_0$  is the bulk concentration of ionic species,  $z$  is the charge on the ions,  $c$  is the concentration of the electrolyte in  $\text{gl}^{-1}$ , and  $M_w$  is the molecular weight. The addition of electrolyte reduces  $\kappa^{-1}$ , therefore decreasing the thickness of the double layer and allowing the particles to approach more closely. When  $\kappa^{-1}$  is large the van der Waals attraction is screened out by the longer range repulsion, resulting in a stable colloidal suspension. By adding enough electrolyte the screening length can become small enough such that the colloidal particles can aggregate via the van der Waals attraction.

Another useful expression is that relating the potential at the surface,  $\psi_d$  to the charge density at the surface,  $\sigma_d$ ,

$$\sigma_d = (8n_0 \epsilon_0 \epsilon kT)^{1/2} \sinh \frac{ze\psi_d}{2kT} \quad (2.7)$$



which at low potentials reduces to

$$\sigma_d = \epsilon_0 \epsilon \kappa \psi_d \quad (2.8)$$

Further information about the derivation of these equations can be found in Shaw [12].

### 2.2.2.2 Interactions Between Charged Particles

The calculation of the interaction of the double layers proves difficult. No exact analytical expressions can be found, therefore one needs to use numerical solutions or various approximations.

A very simple approximation of the interaction is that given by a screened Coulombic or Yukawa potential, where

$$V_C(r) = \frac{q_e^2}{\epsilon r} \exp(-\kappa r) \quad (2.9)$$

where  $q_e$  is the effective charge on the macroion,  $\kappa$  is the inverse of the Debye length, and  $r$  is the centre-centre distance between the particles. For weak interactions in the presence of added electrolyte the effective charge is given by

$$q_e = \frac{q_0}{1 + \kappa a} \exp(\kappa a) \quad (2.10)$$

A more sophisticated treatment of the problem has been carried out by Healy et al [14, 15], using the Gouy-Chapman-Stern theory as a basis. It is assumed that ion adsorption equilibrium is maintained as the two double layers overlap. There are two distinct cases to consider, depending on the properties of the colloid. Firstly if the surface charge results from the adsorption of ions then the surface potential remains constant and the surface charge density adjusts accordingly. Alternatively the surface charge may be a result of ionisation of the groups on the surface of the colloid. In this case the surface charge density remains constant and the surface potential adjusts accordingly. For spherical particles of equal radius,  $a$ , stern potential,  $\psi_d$  (figure 2.1) and a shortest distance of approach  $H$ , the constant-potential  $V_R^\psi$  and constant-charge,  $V_R^\sigma$  double layer interactions were found to be [12]

$$V_R^\psi = 2\pi\epsilon_0\epsilon a\psi_d^2 \ln(1 + \exp[-\kappa H]) \quad (2.11)$$

and

$$V_R^\sigma = -2\pi\epsilon_0\epsilon a\psi_d^2 \ln(1 - \exp[-\kappa H]) \quad (2.12)$$

For small electric double layer overlap, such that  $\exp[-\kappa H] \ll 1$ , these expressions both reduce to

$$V_R = 2\pi\epsilon a\psi_d^2 \exp[-\kappa H] \quad (2.13)$$

There is of course a problem deciding which equation to use since it is not always clear cut. The assumption of the adsorption equilibrium has been shown by Overbeek [16] to be invalid, since the rate of overlap of the double layers by Brownian motion is too fast for the adsorption equilibrium to be maintained. The true situation therefore lies somewhere in between that of constant charge and constant potential.

There are many other approaches and approximations for the double layer interaction. These won't however be discussed in this thesis and can be found in Shaw [12], Hunter[17] or Russel, Saville & Schowalter[18]

### 2.2.2.3 *The Derjaguin-Landau and Verwey-Overbeek (DLVO) Theory*

Derjaguin and Landau [19] and Verwey and Overbeek [20] independently developed a quantitative theory for the stability of charge stabilised colloids (traditionally known as lyophobic colloids). In this theory colloidal stability is determined from the interaction energy-distance curves, where the total interaction energy is the van der Waals attraction plus the double layer repulsion. DLVO theory can therefore be stated as

$$V_t = V_a + V_R \quad (2.14)$$

The details of the attractive and repulsive energies can be very different depending on which approximations are used, however the trends are the same. The double layer repulsion decreases approximately exponentially, whilst the van der Waals attraction falls off as the inverse power of the distance between particles. The van der Waals attraction therefore dominates at both small and large interparticle distances. In figure 2.2 both a schematic diagram of a typical DLVO potential illustrating the main features, and theoretical potentials for a typical colloidal suspension and varying electrolyte concentration are given. The theoretical DLVO curves have been determined using equations ?? for a  $\phi = 0.01$  solution of 300nm particles with 2000 charge groups per particle in an aqueous solution with various concentrations of salt (NaCl). It can be

seen that at short interparticle distances the finite repulsion and the large attractive energy results in a primary minimum. This is deep (sometimes a few hundred  $kT$ ), but not infinitely so, due to the short range repulsion between the colloid, as illustrated in the schematic DLVO potential (figure 2.2(a)). The DLVO calculations, however, do not provide information about this steep repulsive potential as seen in figure 2.2(b).

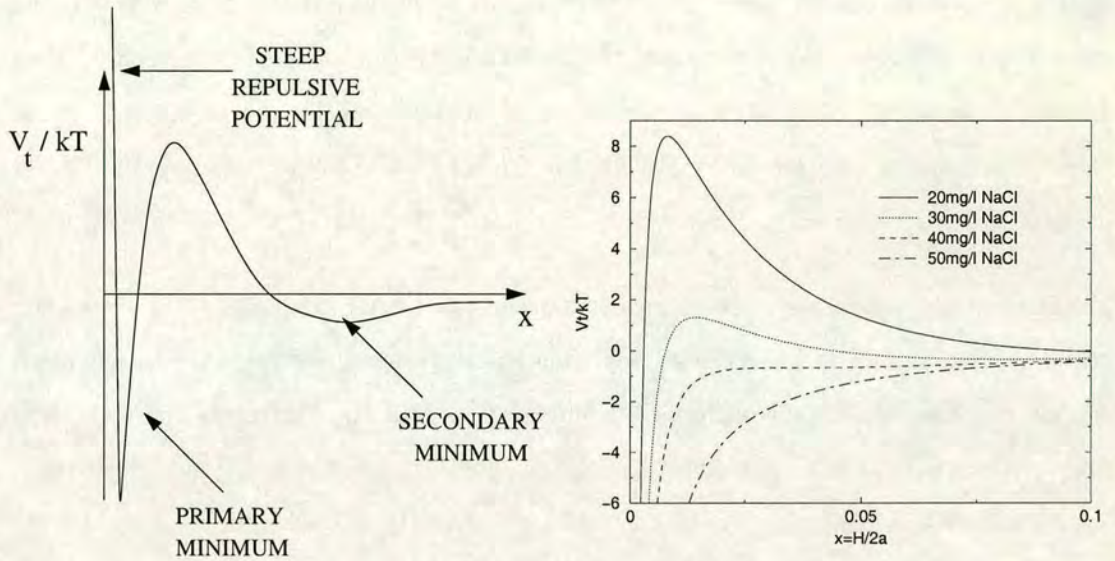
Depending on the electrolyte concentration and colloidal properties there may be a barrier to the primary minimum (see figure 2.2). If this barrier height is greater than a few  $kT$  then the colloidal particles do not aggregate and therefore the solution is said to be stable. As the electrolyte concentration increases the screening length decreases lowering the barrier and therefore reducing the stability. The barrier width is also a factor in the colloidal stability, but it is far less important than the barrier height. By determining the rate of barrier crossing the kinetics of coagulation can be explained. One of the most useful, though approximate approaches to the kinetics problem was devised by Reerink and Overbeek [21], where a stability factor,  $W$  was related to the maximum height of the barrier,  $V_{max}$ . This stability factor is defined as the ratio of the number of collisions between particles to the number of collisions that result in coagulation. It is therefore a measure of the effectiveness of the barrier to the prevention of coagulation and is given by the following equation,

$$W \approx \frac{1}{2\kappa a} \exp\left(\frac{V_{max}}{kT}\right) \quad (2.15)$$

A more accurate stability factor can be found by integrating over the barrier rather than just simplifying it to a barrier height. This theory was developed by Fuchs [22].

At relatively large interparticle separations the van der Waals attraction again dominates over the repulsive forces and a secondary minimum can be found. This can be seen in figure 2.2 (a), the secondary minima found by calculations in figure 2.2 (b) were negligible. When this minimum is a few  $kT$ , the particles become trapped in this minima and form loose, easily reversible aggregates. This is thought to play an important role in the stability of certain emulsions and foams.

DLVO theory cannot explain the coagulation properties in all colloidal systems. Various system specific structural effects must be considered. A structural term,  $V_s$  can be



(a) Schematic diagram of a DLVO potential.

(b) DLVO potentials for a typical charged colloidal suspension with a varying concentration of salt.

Figure 2.2: DLVO potentials for a typical charged colloidal suspension - (a) is a schematic diagram illustrating the type of behaviour found. There is a secondary minima at relatively large interparticle separations, as well as the deep primary minimum. The barrier to the primary minimum in this case is relatively high. Figure 2.2 (b) are calculated DLVO potentials for a colloidal suspension ( $a=300\text{nm}$ ) of  $\phi = 0.01$ , having a charge of  $2000e$  per particle in an aqueous solution with NaCl. As the salt concentration is increased it can be seen that the barrier to the primary minimum gets lower until there is a purely attractive potential.

added to the total potential energy (equation 2.14) taking into account the influence of a surface on the adjacent solvent. This structural term is however difficult to determine, especially in aqueous systems and can either contribute an attractive or repulsive term depending on the hydration forces. Despite these problems DLVO theory was a very important breakthrough in explaining and predicting colloidal stability and is still used extensively today, over 50 years after its development.

#### 2.2.2.4 Critical Coagulation Concentrations

DLVO theory shows the change in intermolecular potential on addition of electrolyte. When enough electrolyte is added there is no barrier to the primary minimum and rapid

aggregation of the colloid takes place. At the point where  $V = 0$  and  $dV/dH = 0$  at the same value of  $H$  the concentration of electrolyte is known as the critical coagulation concentration (ccc). This corresponds to about 40mg/l NaCl in figure 2.2 (b). From these constraints a theoretical expression for the ccc can be found based on the DLVO expression used.

Experimentally a measure of the ccc can be determined even though the crossover from stability to coagulation is a gradual one. The criterion is subjective, therefore it must remain constant for a series of measurements. The minimum electrolyte concentration is that which produces a visible change in the colloidal appearance within a given time, say 30 minutes. These results can then be compared with the predictions of the DLVO theory, though to get good agreement the kinetics of aggregation must also be taken into account.

### 2.2.3 Steric Stabilisation

Steric stabilisation is achieved by coating the colloid with chemically grafted polymer. In general the thickness of the polymer coating is much smaller than the radius of the particle. When the colloidal particles approach one another the polymer layers begin to interpenetrate. This results in a strong repulsive force, since the free energy of the system rises. As the colloids approach, the polymer shells overlap resulting in a higher concentration of polymers in between the particles. This results in an unbalanced osmotic pressure pushing the colloid apart. Alternatively one can consider this in entropic terms. The configuration of polymer will be restricted when the colloids approach too closely, thus reducing the configurational entropy and therefore the particles repel one another.

Due to large differences in the nature of polymers and the way they are grafted there is no general theory for steric stabilisation like charge stabilisation. The temperature of the system plays an important role in the case of sterically stabilised colloid, since the polymer has different behaviour in a solvent at different temperatures. The temperature can change the solvent from a good to a bad solvent for a given polymer. In a poor solvent the monomers of a polymer prefer to be near to other monomers rather than the solvent. The opposite is true in the case of a good solvent, where the monomers

prefer to be near solvent molecules. This results in the polymer coil expanding. The temperature at which these effects are balanced and therefore where the polymer coil can be modelled by a random walk [23] is known as the theta temperature. Steric stabilisation is ineffective in the presence of a poor solvent for the polymer since these polymers will tend to aggregate.

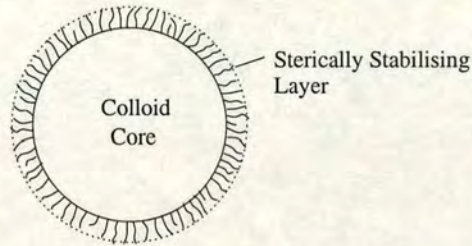


Figure 2.3: Schematic diagram of a sterically stabilised colloid.

Steric stabilisation has some advantages over charge stabilisation. It can be used to stabilise colloid in non-aqueous media, unlike charge stabilisation. Reversible flocculation is also commonly found in the case of sterically stabilised colloid. For charge stabilised colloid the coagulation is often irreversible due to the colloid getting into the deep primary minimum.

#### 2.2.4 The Depletion Attraction

It was found experimentally that the addition of non-adsorbing polymer to a solution of colloidal particles induced phase separation [24, 25, 7]. This was first explained in 1945 by Asakura and Oosawa [8] in terms of a depletion effect. The polymer and particles are mutually impenetrable, thus the centre of a polymer of radius of gyration  $R_g$  is excluded from a region around the colloid. This region is known as the depletion zone and has a thickness of order  $R_g$ . When these depletion zones overlap as shown in figure 2.4 the polymer coils cannot get in between the colloidal particles. This results in an unbalanced osmotic pressure pushing the particles together. An attractive force between the colloidal particles is therefore induced by the added polymer. The resulting phase behaviour and the depletion by other species such as rod-shaped colloids and spherical micelles will be discussed in detail in chapter 3.

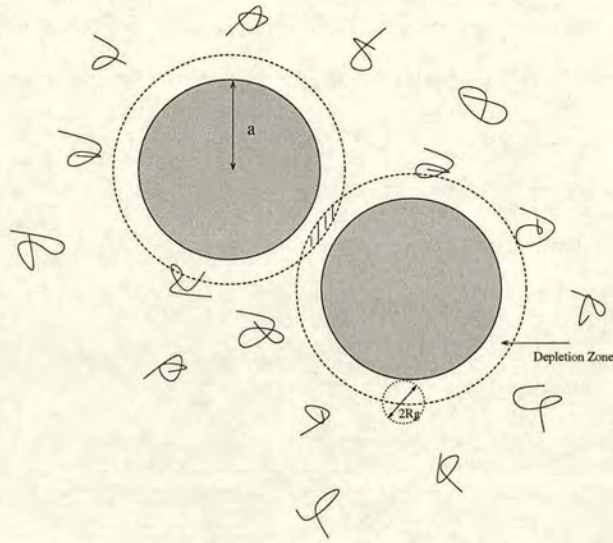


Figure 2.4: Schematic diagram illustrating the depletion attraction induced on addition of non-adsorbing polymer to a colloidal solution. The polymers cannot approach the colloid too closely, i.e. they are excluded from the depletion zones. Therefore when these zones overlap there is an excess osmotic pressure on the outside of the particles, leading to an attractive force.

## 2.3 Colloidal Phase Behaviour

### 2.3.1 Hard-Spheres

The simplest system to consider for colloidal phase behaviour is a model hard sphere system. In a suspension of hard-sphere particles there is no interaction between the particles until they touch when there is an infinite repulsive force. There is therefore no energy scale present and the phase behaviour depends only on the number density of particles,  $\rho$ . More commonly this parameter is discussed in terms of a colloid volume fraction,  $\phi$ , which is given by

$$\phi = \frac{4}{3}\pi a^3 \rho \tag{2.16}$$

where  $a$  is the particle radius.

The phase behaviour for a suspension of monodisperse (single size) particles was determined by computer simulation [26, 27]. A schematic diagram of the phase diagram found is shown in figure 2.5. It can be seen that below a volume fraction of 0.494 (the freezing volume fraction,  $\phi_F$ ), the hard sphere system is a fluid. The particles are therefore able to diffuse freely and there is no long range order present.

Between volume fractions of 0.494 and 0.545 there is a coexistence region. Here the colloid is a coexisting mixture of fluid and crystal. The crystal forms and then sediments to the bottom of the sample cell. Above the melting volume fraction  $\phi = 0.545$  the stable phase is a colloidal crystal. As the volume fraction is increased further above the melting volume fraction the crystal becomes more tightly packed, up to a maximum close packing volume fraction of  $\phi_{CP} = 0.74$ . If however the particles adopt a random close packed arrangement the maximum volume fraction is  $\phi_{RCP} = 0.64$ . The system also exhibits non-equilibrium behaviour. A metastable glass phase is found to form at  $\phi_G = 0.58$ .

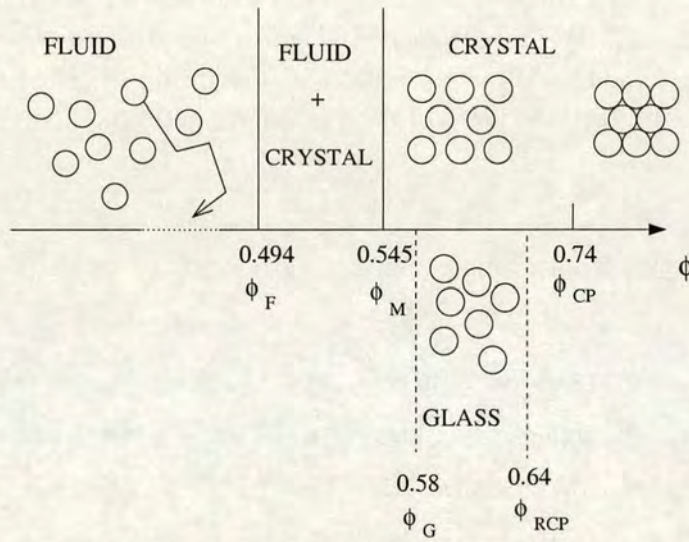


Figure 2.5: Schematic diagram of hard-sphere phase behaviour.

What drives the freezing of hard spheres? Since there is no energy scale the transition must be entropy driven. Intuitively, however, one would expect the crystal phase to have the lower entropy since it is highly ordered. One must also consider the free volume entropy,  $S_{FV}$ , as well as the configurational entropy,  $S_{\text{config}}$ . In figure 2.6 the box on the left hand side contains a random configuration of spheres, whilst that on the right contains a highly ordered crystal of spheres. The configurational entropy of the crystal is lower than that of the random configuration. However in the random configuration the spheres are essentially jammed, thus the free volume entropy is low. In the crystal by contrast the particles can move around a bit and this system therefore has a high free volume entropy. Crystallisation therefore takes place when the decrease in  $S_{\text{config}}$  is more than offset by the increase in  $S_{FV}$ . This takes place at the melting



volume fraction,  $\phi_M = 0.545$ .

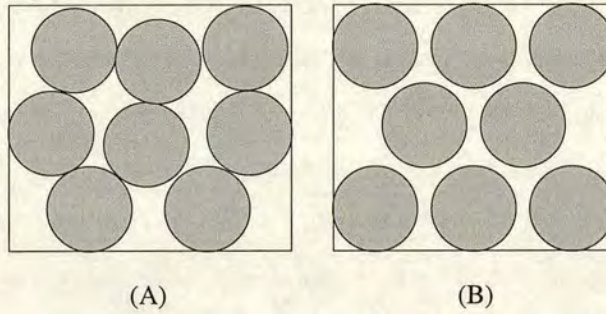


Figure 2.6: Schematic 2-d representation of the entropically-driven freezing transition of hard-spheres. (A) shows a colloidal fluid, which has a low free volume entropy and a high configurational entropy. (B) is a colloidal crystal with a high free volume entropy since the particles can jiggle around easily but a low configurational entropy. The freezing transition therefore arises due to the importance of the free volume entropy.

### 2.3.2 Sterically Stabilised Colloid

Some sterically-stabilised colloids form good model hard spheres. A well studied example is that of colloidal polymethylmethacrylate (PMMA) which is stabilised by chemically grafted poly-12-hydroxystearic acid (PHSA). These colloidal particles can be synthesised with low polydispersities, i.e. with a very small range of sizes about the mean. The refractive index of the PMMA particles is  $n_p = 1.49$ . These colloidal particles can be index-matched by using a mixture of cis-decahydronaphthalene (cis-decalin,  $n = 1.48$ ) and tetrahydronaphthalene (tetralin,  $n = 1.54$ ) or carbon disulphide ( $n = 1.63$ ). This therefore makes the van der Waals attractions negligible as well as making light scattering studies possible. This model system has an interaction close to that of hard spheres.

A detailed study of the experimental phase behaviour of PMMA particles in cis-decalin and carbon disulphide was carried out by Pusey and van Megen [1]. Samples spanning both the freezing and glass transitions were made. These samples were driven into metastable states by slow tumbling, which shear melts any of the fragile crystals in the samples. The samples were then left undisturbed and observed over a number of weeks. It was found that the colloid existed in a fluid state at a volume fraction of below  $\phi = 0.494$ . Coexisting fluid and crystal were observed between  $\phi = 0.494$  and

$\phi = 0.545$ , with the ratio of crystal to fluid increasing linearly as the volume fraction was increased. The presence of the crystal phase is characterised by iridescence. This is a result of Bragg diffraction of white light. Between  $\phi = 0.545$  and  $\phi = 0.58$  small homogeneously nucleated crystals form. Large irregular crystallites are found at still higher volume fractions, from  $\phi \approx 0.59$  to  $\phi \approx 0.61$ . Non-equilibrium glasses were found at volume fractions greater than  $\phi \approx 0.61$ . The overall behaviour observed is in agreement with the predicted hard sphere behaviour in figure 2.5. The minor differences may be explained by the slight softness or attractions in the pair potential and/or polydispersity of the model system.

### 2.3.3 Charge Stabilised Colloid

In the case of charge stabilised colloid there are a number of behaviours which can be observed depending on the colloidal interactions. When the van der Waals attraction is weak the behaviour is dependent on the range of the electrostatic repulsion and therefore the electrolyte concentration. At high electrolyte concentration the double layer thickness is small i.e. there is a small  $\kappa^{-1}$ . There is therefore only significant repulsion when the centre to centre separation is comparable to the diameter of the particle, thus the colloids behave essentially as hard spheres.

At low electrolyte concentration the double layer is large and thus there is a strong repulsive force for a number of particle diameters. Such suspensions show fluid-like ordering and freezing transitions at low volume fractions (as low as  $\phi=10^{-4}$ ). The structure of these crystals are either body centred cubic (BCC) or face centred cubic (FCC). Often charged colloids with low electrolyte concentrations are treated as hard sphere colloids with an effective radius, [28, 29, 30]

$$a_{\text{eff}} = a + \kappa^{-1} \quad (2.17)$$

where  $\kappa^{-1}$  is the Debye screening length. The effect of the electrolyte concentration on the colloidal phase behaviour can be illustrated by an experimental study undertaken in 1973 by Kose et al. [31]. The main results are shown in figure 2.7 along with predicted phase boundaries determined by Russel [32] using a perturbation method. It can be seen at high salt concentrations the volume fraction required for crystal formation is about the same as that for hard spheres,  $\phi \approx 0.48$ . As the salt concentration is lowered

and the double layer becomes more extensive, resulting in a higher effective colloidal radius, the volume fraction required to observe crystals becomes lower. This continues until at very low salt concentrations, very small volume fractions are required in order to see a transition to an ordered phase. The region of coexistence is also observed to get narrower as the salt concentration is decreased.

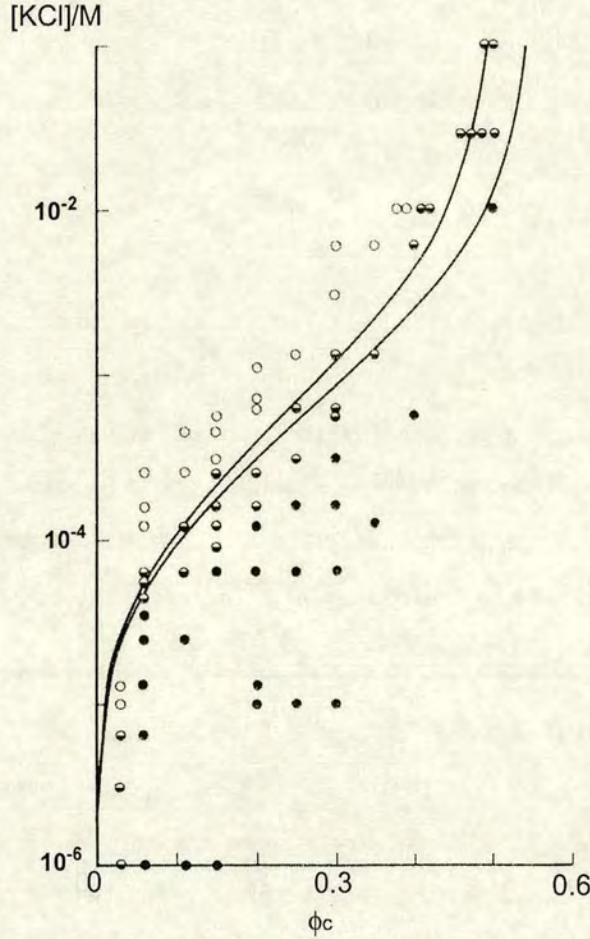


Figure 2.7: Experimental phase diagram of charge stabilised colloids ( $a=0.085\mu m$ ) with varying electrolyte concentration and colloid volume fraction. The data is that of Kose et al. [31]. The open circles represent a fluid phase, the filled circles are ordered phases and the half-filled circles are the two-phase samples. The lines are the phase boundaries predicted by Russel [32]. The diagram is reproduced from reference [18] with the axes changed in order to easily compare these results with those of hard-spheres.

It can be seen that in the case of the charged colloids the behaviour is much more complicated than that of sterically stabilised systems. Here only the main points have

been highlighted. However, further details can be found in reference [33] and references therein.

## 2.4 Surfactants

Surfactants are amphiphilic in nature i.e. they have both hydrophilic (water-loving) and hydrophobic (water-hating) parts. It is because of this property that they are useful and form the basis of detergents, shampoos etc. They are also found in nature e.g. they constitute the main components of cell membranes. In figure 2.8 a schematic diagram of a surfactant molecule is shown.

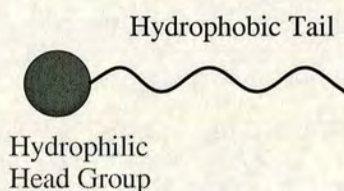


Figure 2.8: A surfactant molecule, with a hydrophilic head group and a hydrophobic tail.

### 2.4.1 Types of Surfactant

The hydrophobic tail of a surfactant is generally a hydrocarbon chain. It typically has between 12 and 20 carbon atoms on the backbone. The nature of the hydrophilic head group can however take a number of different forms. Firstly there are ionic surfactants which have a charged head group. These can be split into two classes, anionics and cationics. Anionics have a negatively charged head group, and a positive counterion that dissociates from the surfactant molecule in solution. A common example is Sodium Dodecyl Sulfate (SDS), which has the ionic group  $-\text{OSO}_3^-$  as the hydrophilic head group and  $\text{Na}^+$  as a counterion. Most traditional soaps and detergents are anionic surfactants, typically with sulfonate or sulfate head groups.

Cationics have a positive charge on the head group and a negative counterion, e.g. cetyltrimethylammonium bromide (CTAB). There are also a range of zwitterionic (or amphoteric) surfactants which have both a positive and negative charge on the head group. Typically the head group is some form of betaine ( $-\text{N}^+(\text{CH}_3)_2\text{CH}_2\text{CO}_2^-$ ). They

are used in many toiletries since they are milder on the skin than anionics. The other major group of surfactants is that of non-ionics. Traditionally the most commonly found non-ionic surfactants are part of the ethoxylate family, with a head group of  $-(\text{OCH}_2\text{CH}_2)_n\text{OH}$ . These are used extensively in low-temperature detergents and as emulsifiers. There has however been a recent move to the more environmentally friendly alkyl polyglucosides (APG) or sugar surfactants, where the saccharide group is the hydrophilic head group [34].

### 2.4.2 Properties of Surfactants

Since surfactants are amphiphilic there is a competition between the head group that wants to be in contact with water and the hydrophobic tail, which has a tendency to be excluded from water. The balance of these competing forces is the basis for all surfactant behaviour; adsorption, aggregation and mesophase (structures and non-isotropic phases formed at high concentrations) formation.

Adsorption at oil-water interfaces allows the hydrophobic chain to be in contact with the oil, while the head group is in contact with the water (figure 2.9) and thus the free energy of the system is reduced. This adsorption can also take place at air/water interfaces and is an equilibrium. Since adsorption is favourable, a high concentration of surfactant molecules are present at the interface. This is energetically favourable and therefore leads to a reduction in surface tension at an oil-water or air-water interface. This is the basis of surface activity, and led to the introduction of the term surfactant (SURFace ACTive ageNT).

Aggregation or self-assembly of the surfactants also allows the hydrophobic tails to get out of contact with water. At a certain concentration of surfactant solution, aggregates of surfactants, more commonly known as micelles, are formed. This concentration is known as the critical micelle concentration (cmc), and can be determined experimentally due to the abrupt change in concentration dependence of many physical properties such as osmotic pressure, surface tension and molar conductivity which accompany it. In micelles the surfactant molecules pack together such that the hydrocarbon chains associate and exclude water from the interior of the micelle. The head groups form the exterior part of the micelle and are in contact with water, maximising the favourable

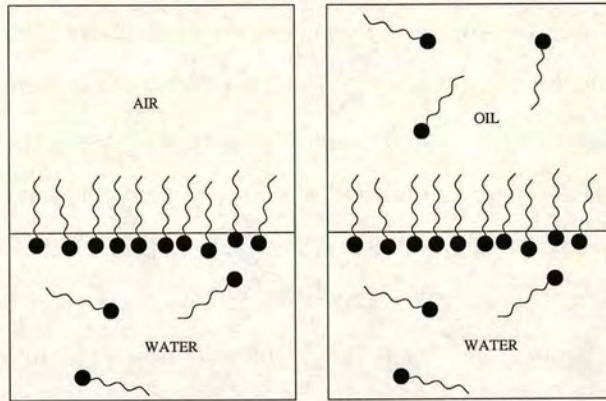


Figure 2.9: Schematic diagram of the adsorption of surfactant molecules at both air/water and oil/water interfaces. A large proportion of surfactant molecules align themselves at the interface with the head group in contact with water and the tail group out of contact with the water. This leads to a lowering of the surface tension. The adsorption is in dynamic equilibrium with surfactant molecules moving between the solution and the interface.

interactions. Micellisation is therefore an alternative method to adsorption by which the interfacial tension of the surfactant solution decreases. This will be discussed in section 2.4.3. The oily interior of a micelle can solubilise oil thus forming a microemulsion. The surfactant forms the interface between the oil droplets and the water. This provides the basis of detergency.

### 2.4.3 Geometry of Micelles

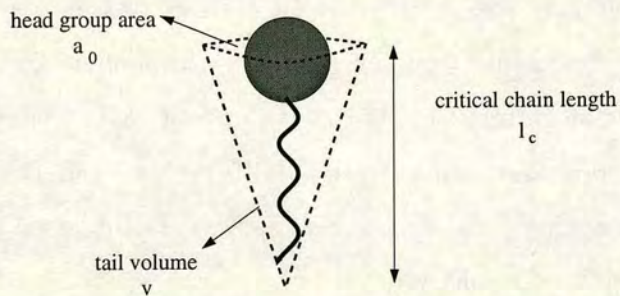


Figure 2.10: Diagram illustrating the packing parameter,  $v/a_0l_c$ , which depends on the head group area  $a_0$ , the volume of the tail  $v$  and the critical chain length  $l_c$ .

As discussed in section 2.4.2 the amphiphilic nature of surfactants leads to the formation of aggregates or micelles in aqueous solution. These micelles can take on a number of shapes depending on the molecular geometric factors of the surfactant molecules and

their concentration. The packing is determined by the relative head group area and tail groups volume and length. (Figure 2.10) This results in a number of geometries. A large headgroup/small tail results in spherical micelles. As the head group becomes smaller and the tail gets bigger cylindrical micelles (figure 2.11) are formed. As these rodlike micelles grow beyond the persistence length,  $l_p$  (figure 2.12) the rods become flexible and behave as polymers. The transition from spheres to worms is continuous. Bilayers (figure 2.11) are formed when the surfactant has small headgroups and large tails. If the tail group becomes larger still and the headgroup continues to get smaller then the inverse of these geometries can also be formed. This theory was developed by Israelachvili [13] and is summarised in figure 2.11.

This table therefore outlines a good model for predicting the geometry of the micelles. In practice, however, it is very difficult to predict the resulting shape for a certain surfactant concentration since it results from a delicate balance of small effects. It is therefore more useful to use the theory when comparing the behaviour of similar surfactants. When the conditions are changed the theory can also be used to predict the likely effect on micelle geometry.

As alluded to, there are many factors which affect the geometric packing factors of surfactants. The chemistry of the surfactant, particularly the head group can play an important role. The apparent head group area can be affected by the salt concentration, pH and temperature. The salt concentration has a very strong influence in the case of ionic surfactants, but may also modify the head group area in non-ionic surfactants. Temperature has a great impact on the geometry of non-ionic surfactants as will be discussed in more detail in section 2.4.5.1. The critical chain length (figure 2.10) can be affected by chain branching, unsaturation of the carbon chain and the temperature. The main effects for nonionic and ionic surfactants will be discussed in detail in section 2.4.5 in terms of their typical phase behaviour.

#### 2.4.3.1 *Mesophase Formation*

Mesophases, where micelles start to pack together, form at high concentrations of surfactant. Spherical micelles pack together to form the cubic phase ( $I_1$ ), while rod-like micelles form bundles to produce a hexagonal phase ( $H_1$ ). The so-called sponge

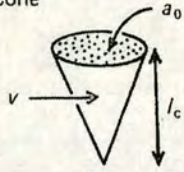


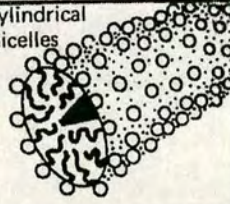
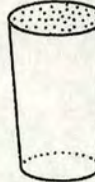
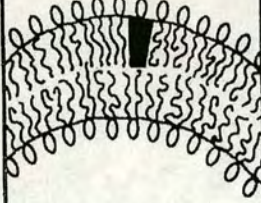
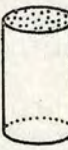
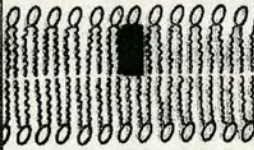

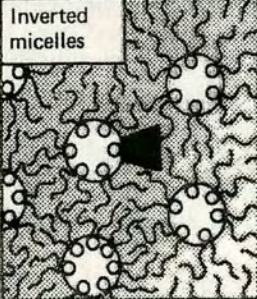
Critical packing parameter $v/a_0l_c$	Critical packing shape	Structures formed
$< 1/3$	Cone 	Spherical micelles 
$1/3-1/2$	Truncated cone 	Cylindrical micelles 
$1/2-1$	Truncated cone 	Flexible bilayers, vesicles 
$\sim 1$	Cylinder 	Planar bilayers 
$> 1$	Inverted truncated cone or wedge 	Inverted micelles 

Figure 2.11: This table, reproduced from [13], shows how the type of micelle formed depends on the packing requirements of the surfactant molecules.



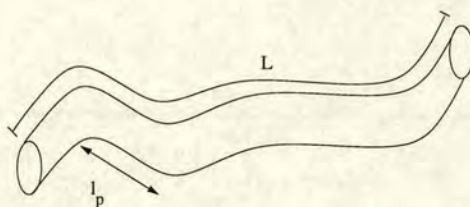


Figure 2.12: Schematic diagram of a wormlike micelle with a persistence length  $l_p$  and contour length  $L$ . The persistence length is defined as the length over which the micelle does not bend.

phase ( $L_3$ ) has two continuous fluid domains separated by a single continuous bilayer. A lamellar phase (known as  $L_\alpha$ ) is one that consists of alternating bilayers and water, and is found at high surfactant concentrations. These type of phases have not been studied in this thesis and are included simply for completeness. The relative positions of the mesophases in surfactant phase diagrams will be seen in section 2.4.5.

## 2.4.4 Properties of Wormlike Micelles

### 2.4.4.1 Structure

As discussed in section 2.4.3, rodlike micelles are formed when the critical packing parameter is between  $1/3$  and  $1/2$ . As these rodlike micelles become longer than the persistence length  $l_p$  the rods become flexible and behave as polymers. These are known as giant wormlike micelles and are the type of system investigated in this thesis. In the case of ionic surfactants, the addition of an electrolyte or cosurfactants such as a zwitterion or an alcohol promote the formation of wormlike micelles. In the case of non-ionics it is the temperature that usually controls the phase behaviour. Theoretically it can be expected that a very large range of surfactants form wormlike micelles under the right conditions. While there are many examples for ionic surfactants, only a few nonionic systems have been found to form wormlike micelles.

Wormlike micelles can grow for two reasons. Firstly there is concentration induced growth on addition of surfactant. Secondly the micelles can grow due to changes in packing parameter, for example when an electrolyte is added to a solution of ionic wormlike micelles. As the average length of the micelles grows it begins to exceed the distance between them and the micelles become entangled. Entanglement can

also take place as the concentration of relatively small micelles increases enough so that they overlap. Above the entanglement threshold the overlapping micelles interact extensively and a transient network of randomly oriented micelles is formed. The viscosity increases dramatically above the overlap concentration, however, under shear this system exhibits shear-thinning. This means that the effective viscosity decreases since the fluid flow orients the micelles and reduces the interaction between them. This property has been utilised in shampoos; where as one lathers the shampoo into the hair a reduction in viscosity is desirable.

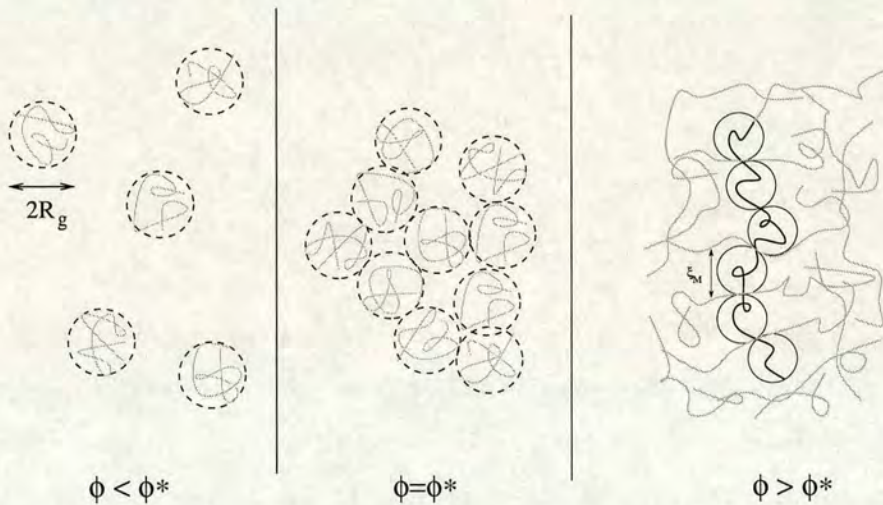


Figure 2.13: Diagram illustrating the state of a solution of wormlike micelles as the volume fraction of surfactant is increased. The dilute regime is shown on the left, where  $\phi < \phi^*$ . In the middle the solution is at the overlap concentration,  $c^*$ , where the micelles just begin to touch one another. In both of these regimes the important length scale is the radius of gyration,  $R_g$ . Finally on the right is the semi-dilute regime where the micelles are entangled. The lengthscale in the semidilute regime is the mesh size  $\xi_M$  as indicated.

Wormlike micelles have many properties in common with polymers. Like polymer systems there is a dilute regime, where  $\phi$  the volume fraction of surfactant is less than the overlap concentration  $\phi^*$ , and a semi-dilute regime, where  $\phi > \phi^*$  (figure 2.13). In the semi-dilute regime the important length-scale is the correlation length,  $\xi_M$  (figure 2.13), and it can be modelled by blobs of this size as shown. In both polymer systems and those of wormlike micelles, the semi-dilute regime exhibits viscoelastic properties. There are however differences between polymers and wormlike micelles. Firstly since the surfactants self-assemble, micelles are in equilibrium with the surfactant molecules.

This results in a molecular weight distribution (MWD) that is in thermal equilibrium, unlike that of a polymer solution where the MWD is fixed. The MWD of wormlike micelles can be calculated using the Flory-Huggins approach. Flory-Huggins uses a mean field picture where the polymer chains (in this case the wormlike micelles) are represented by random walks on a lattice. Each lattice site is occupied either by one chain monomer or by a solvent molecule [23]. This allows the Helmholtz free energy to be determined, which can then be minimised in order to find the MWD. The size distribution is found to be [35]

$$c(L) \simeq a^{-3} \exp(-E/kT) \exp(-L/\bar{L}) \quad (2.18)$$

where

$$\bar{L} = a\phi^{1/2} \exp(E/2kT) \quad (2.19)$$

The number of chains of arc-length  $L$  is  $c(L)$ ,  $E$  is the end-cap energy i.e. the energy required to create two hemispherical chain ends,  $\phi$  is the volume fraction of the surfactant and  $a$  is the lattice constant. It can therefore be seen that there is a broad exponential length distribution. The average size of this distribution increases slowly with  $\phi$  and rapidly with  $E$ . This growth law has been investigated experimentally via light scattering. It is a difficult experiment as it is hard to distinguish between the contributions from intermicellar interactions and concentration-induced growth. There is therefore a lack of hard supporting evidence for this growth exponent of 0.5. Schurtenberger et al. have, found a growth exponent of about 0.6 for a system of lecithin reverse micelles in deuterated isooctane when the added water is tuned such that the micelles do not grow too long. When the added water is such that large wormlike micelles form a growth exponent of about 1.2 is found [36]. A large growth exponent, of about 1.1, is also found for an aqueous solution of  $C_{16}E_6$  [37]. The evidence for these large exponents is very strong, although there is, as yet, no theoretical explanation for them.

One last difference between polymers and wormlike micelles is that the latter can also form living rings. This property will be ignored in the following sections since it complicates the picture somewhat and their absence is an assumption of the Cates model [38]. Rings are thought to play an important role for ionic micelles at low ionic strength [39].

### 2.4.4.2 Dynamics

The dynamics of entangled polymers is understood in terms of the reptation model [23]. In this model, relaxation of chain conformations occurs by the gradual disengagement of a given chain by curvilinear diffusion along its own contour from a tube-like environment. The tube represents the neighbouring chains, which provides obstacles to diffusion normal to the chain contour. This is illustrated in figure 2.14. Old tube is destroyed and new tube is created as the polymer reptates through the entangled solution.



Figure 2.14: Diagram illustrating the tube model for the reptation of polymers. Other polymer in solution act as obstacles, and are represented by the tube as indicated. (Reproduced from [40]).

When a small strain is applied to the system, a stress is induced which is associated with the entropy loss of the polymer chains on deformation. The chain reptates out of its original tube, creating new tube that is in equilibrium with the strained environment and therefore carries no stress. For a monodisperse system, where all the polymer chains have the same length, the stress relaxation function is nearly a pure exponential.

In an entangled solution of wormlike micelles reptation takes place in a similar manner. There is, however, an additional mode of relaxation. Since the micelles self-assemble they can break and reform in order to remove the applied strain. This is known as reversible scission and is illustrated in figure 2.15. The wormlike micelle B breaks into two smaller micelles, one of which subsequently joins onto micelle A creating a new

micelle C. Wormlike micelles are hence often referred to as living polymers. What effect does reversible scission have on the stress relaxation function?

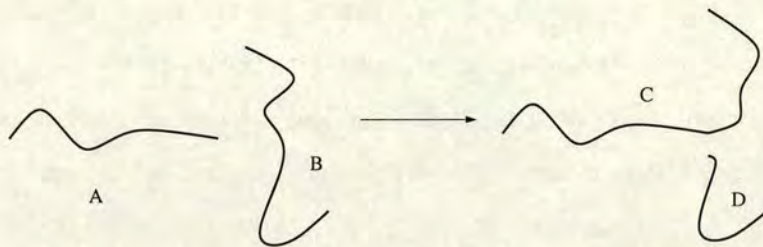


Figure 2.15: Schematic diagram of the scission-recombination reactions of wormlike micelles. Micelle B breaks into two shorter micelles, one of which then joins onto micelle A, forming micelle C. Ends of micelles are created and destroyed.

When the scission kinetics are very slow there is negligible breaking on the timescale of reptation. Reptation of the micelles is therefore the only effective relaxation mode. The micelles have an equilibrium MWD unlike polymers and therefore the stress relaxation function will be extremely non-exponential. Experimentally, however, a pure exponential stress decay curve has been found for entangled wormlike micelles in various surfactant systems (section 4.3.1). The scission and recombination kinetics must therefore be fast enough to directly affect the stress relaxation process.

This regime has been rationalised via the Cates model [38]. The model assumes that the scission of a chain is a unimolecular process, occurring with equal probability per unit time and per unit length on all chains. The recombination is assumed to be a bimolecular process, with a rate independent of the molecular weights of the two reacting subchains. It is also assumed that it is unlikely for a chain to recombine with its previous partner (a mean-field assumption). When the timescale of the micellar scission is shorter than the reptation time ( $\tau_{break} \ll \tau_{rep}$ ) this model finds a clean single exponential stress decay.

The single exponential stress decay can be rationalised by noting that the relaxation mechanism in this regime involves all the tube segments equally. This is because many scission and recombination reactions occur before a given tube segment relaxes, since the reptation time is much slower than the scission kinetics. There is therefore no memory of the initial chain length or the position on the chain initially corresponding to the tube segment. Thus all the tube segments relax at the same rate. This therefore

gives rise to the characteristic monoexponential stress decay.

This rheological behaviour has been found experimentally in many entangled wormlike micelle systems. Khatory et al. found such a behaviour for a solution of the cationic surfactant CTAB and the salt potassium bromide (KBr) [41]. The same surfactant, CTAB has also been found to form wormlike micelles with sodium salicylate (NaSal) [42]. Another system showing this behaviour is that of cetylpyridinium chloride (CPyCl) and NaSal [43]. This will be discussed in more detail in chapter 4.

### 2.4.5 Typical Surfactant Phase Behaviour

The phase behaviour of a typical non-ionic and a typical ionic surfactant will be illustrated in the following sections. These will be treated separately since there are some significant differences. One common feature, however, shared by all surfactants, is the existence of the Krafft temperature ( $T_K$ ). Above this temperature there is a dramatic increase in the solubility of the surfactant. For most practical purposes surfactants should be used above the Krafft temperature.

#### 2.4.5.1 Non-ionic Surfactants

The most well studied non-ionic surfactants are the so called polyoxyethylene surfactants introduced in section 2.4.1. They are usually denoted as  $C_mE_n$  and have the structure  $\text{CH}_3-(\text{CH}_2)_{m-1}-(\text{O}-\text{CH}_2-\text{CH}_2)_n-\text{OH}$ . The head group is the chain of EO groups  $((-\text{OCH}_2\text{CH}_2)_n\text{OH})$ . The greater the number of EO groups the larger volume the head group and therefore the apparent head group area  $a_o$  and the greater is its hydrophilicity. At fixed  $n$ , the head group area is affected primarily by the temperature. This is illustrated in figure 2.16 along with the temperature effect on the tail. As the temperature increases the head group area decreases as shown in figure 2.16. This is a result of the dehydration of the EO groups. The water changes from a good solvent to a bad solvent as the temperature is increased for the polymer PEO (polyethylene oxide), which is just many of the EO groups joined together. The tail group has more gauche conformers at high temperatures and therefore the tail groups cannot pack so close together. This is illustrated in fig 2.16. Both of these effects result in a reduction in the

preferred radius of curvature, thus moving from spherical micelles through to bilayers as the favourable geometry. The head group can also be increased/decreased by the addition of salting-in/salting-out electrolytes. Most commonly electrolytes reduce the head group area by dehydration, since the salt binds strongly to the water. In the case of salting-in the addition of salt induces rehydration and thus increases the head-group area.

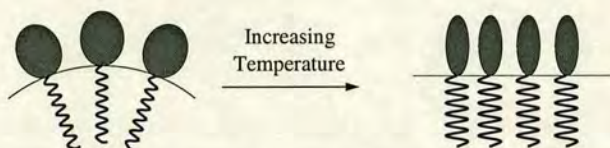


Figure 2.16: Schematic representation of the behaviour of nonionic surfactants when temperature is increased. The increasing temperature causes a dehydration of the EO groups, therefore resulting in a lowering of the head group area as shown. There is also an increase in gauche conformers as the temperature increases, which restricts the packing of the tail groups.

A schematic representation of the phase diagram of non-ionic surfactants from geometrical considerations is shown in figure 2.17. Above the cmc micelles begin to form, the shape of which depends on the preferred curvature as discussed in section 2.4.3. As the concentration of the micelles increases, then treating them as hard-core particles we would expect to see order-disorder transitions. Spherical micelles will close pack into a regular cubic array ( $I_1$ ). This begins to happen at a surfactant volume fraction,  $\phi_{surf} \approx 0.5$  until it reaches the closest packing volume fraction of  $\phi_{surf} = 0.74$  as discussed previously in the case of hard sphere colloids (see section 2.3.1). Similarly rod-like micelles pack to form hexagonal arrays in a volume fraction range of  $\phi_{surf} = 0.7 - 0.91$ . There is, however, no simple rule for the transition from a sponge phase to a lamellar phase. The bilayers nonetheless pack to form the  $L_\alpha$  phase at some point (see reference [44] for more details). At very high surfactant concentrations inverse micelles, in which the head groups point into an aqueous environment and the tails point out into a continuous oil medium, form. The inverse micellar phase, sponge phase, cubic phase and hexagonal phases are denoted by  $L_2$ ,  $L_4$ ,  $I_2$  and  $H_2$  respectively.

Real phase diagrams of one of these surfactants,  $C_{12}E_5$  [3], as a function of temperature and surfactant concentration is shown in figure 2.18. It can be seen that packing factors have predicted most of the observed phase behaviour. There are, however, some

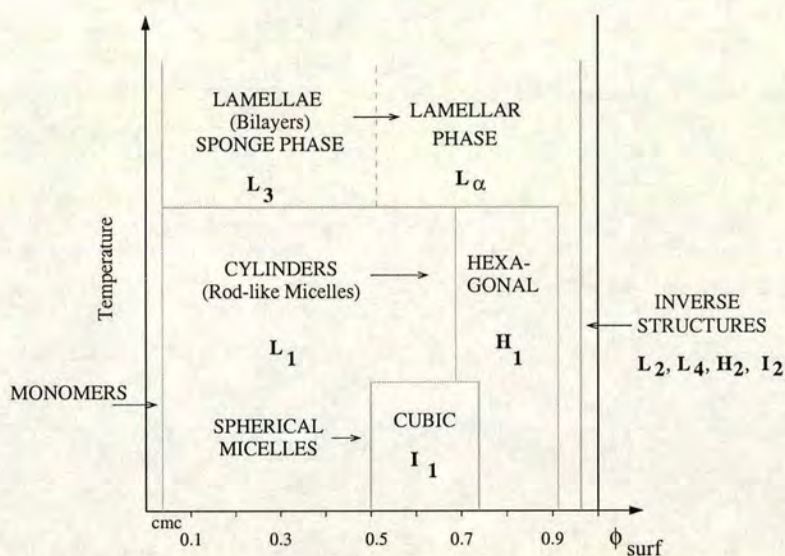


Figure 2.17: Schematic phase diagram for nonionic surfactants based on geometric considerations.

differences in the real phase behaviour. The phase boundaries all curve downwards as the volume fraction increases in the experimental phase diagram (figure 2.18). This is a result of the surfactants competing for water. This therefore has a similar effect to raising the temperature. Another major difference is the appearance of a two-phase region known as the miscibility gap in the micellar region of figure 2.18. The two phases are both micellar in nature. The temperature at which the miscibility gap appears is known as the cloud point, since the solution becomes cloudy. The cloud point depends on the concentration of the surfactant. One last point to make when comparing the schematic phase diagram with the experimental phase diagram for  $C_{12}E_5$  is in the latter there is no cubic ( $I_1$ ) phase observed. The phase behaviour observed must be in the temperature range of water (0-100°C) and therefore in the case of  $C_{12}E_5$  the 0°C is too high a temperature to observe the cubic phase. The limited temperature range therefore limits the phase behaviour available. Other surfactants in the homologous series can form cubic phases and so explore a different area of the theoretical phase diagram (figure 2.17).

By considering the effect on both the geometry and hydrophilicity as the values of  $m$  and  $n$  in  $C_mE_n$  are changed the phase behaviour can be explained. For example as the carbon chain length is increased and the number of EO groups remains the same, the surfactants become more hydrophobic and therefore the cmc decreases.



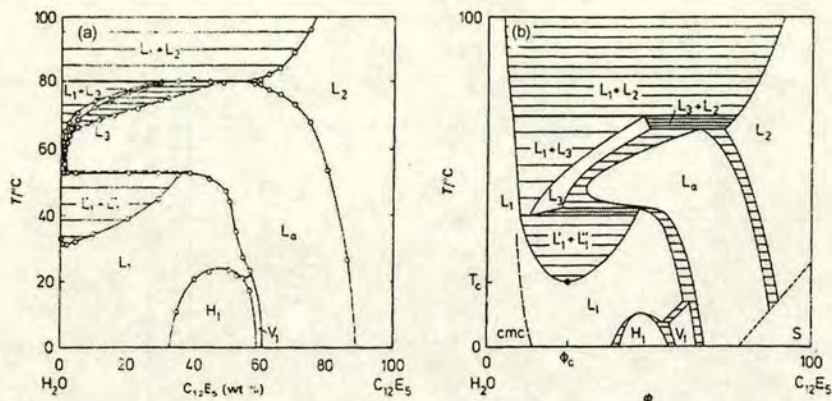


Figure 2.18: Phase diagrams of the water- $C_{12}E_5$  system, reproduced from [3]. Figure (a) is plotted on a linear scale, whilst that in (b) is a log-log scale. In figure (a) the bending of the phase boundaries compared with the schematic diagram 2.17 is clearly visible. Figure (b) shows that the micelles only appear above the cmc and that as the concentration of surfactant increases the phase changes from a micellar phase  $L_1$  to mesophases. As the temperature is increased it can be seen in both diagrams that the micellar solution  $L_1$  phase separates into a mixture of 2 micellar solutions  $L'_1$  and  $L''_1$  above the cloud point ( $T_c$ ).  $V_1$  represents a bicontinuous cubic phase. As the temperature is increased further a mixture of micellar phases and lamellar phases is found.

### 2.4.5.2 Ionic Surfactants

In the case of ionic surfactants the addition of an electrolyte has a major influence on the surfactant geometry and therefore the phase behaviour. By adding salt to the surfactant solution the ions screen the charged head groups from one another therefore reducing their effective size. This can be thought of as a similar effect as raising the temperature in the case of nonionic surfactants. (Figure 2.16) A typical ionic surfactant system therefore has three components, surfactant, salt and water. Keeping the temperature and pressure constant still leaves two degrees of freedom, the mole fractions of two of the components. This can be represented by a triangular phase diagram, also known as a ternary phase diagram. This type of phase diagram will be discussed before looking at an example of a surfactant-salt-water system.

A ternary phase diagram is illustrated in figure 2.19. The vertices of the triangle represent the pure components, in this case A, B and C. Each axis is therefore a binary mixture. Points inside the triangle are mixtures of the three components A, B and C, e.g. point P is made up of mole fractions  $X_A$  (by drawing a line parallel to BC),  $X_B$

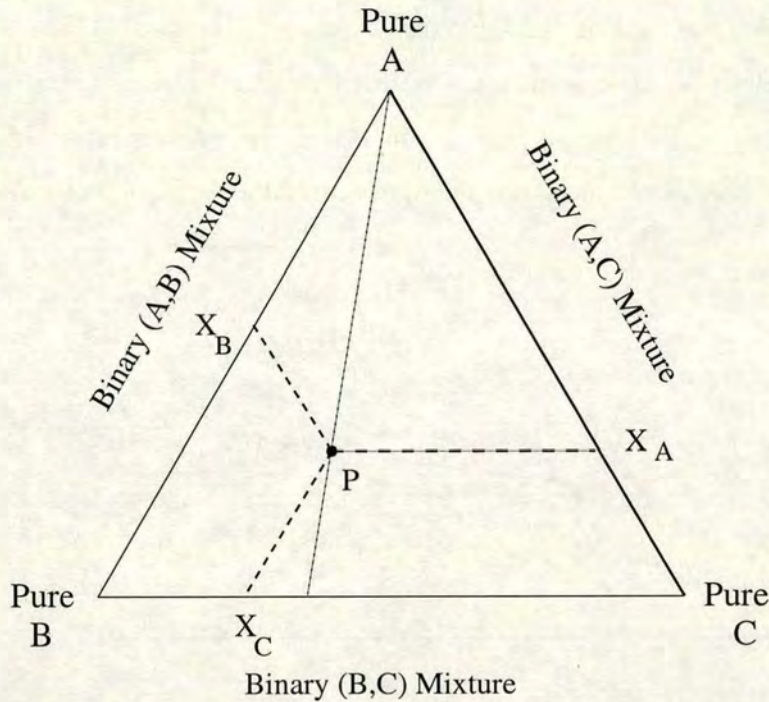


Figure 2.19: A ternary phase diagram for a mixture of three components; A, B and C. The vertices of the triangle represent the pure components while the edges correspond to binary mixtures. A point P has components  $X_A$ ,  $X_B$  and  $X_C$  as illustrated. For each point these mole fractions must add up to 1. The solid line shows a system with a constant proportion of B and C and in increasing amount of component A as the apex is approached.

(by drawing a line parallel to AC) and  $X_C$  (by drawing a line parallel to AB) as shown. The mole fractions of the three components satisfy,

$$X_A + X_B + X_C = 1 \quad (2.20)$$

The components can also be given in percentages as well as mole fractions and thus sum of the components would have to add up to 100. The solid line in figure 2.19 represents a composition that is become increasingly rich in component A as the apex is being reached, but with the same proportions of B and C.

An example of a phase diagram for an ionic surfactant in the presence of salt and water is that of AOT in brine as shown in figure 2.20. AOT (sodium bis(2ethylhexyl)sulfosuccinate) is a two-tailed surfactant and therefore with little added salt the geometric packing factors favour the formation of bilayers and therefore the sponge phase ( $L_3$ ) and lamellar phase ( $L_\alpha$ ). Figure 2.20 shows the dilute corner of the ternary phase diagram for the AOT-brine system [4]. It can be seen that even in

the dilute regime the topology of the phase diagram is complex. The addition of salt has a similar effect on ionic surfactants as temperature has been shown to affect non-ionic surfactants in the previous section. Increasing the concentration of salt reduces the preferred spontaneous curvature thus promoting the formation of worms and then bilayers.

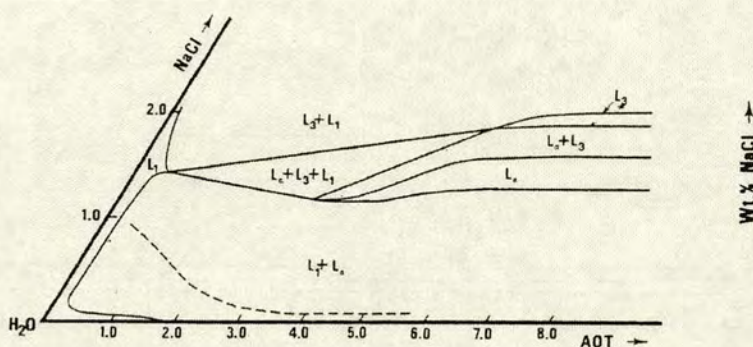


Figure 2.20: Dilute corner of the ternary phase diagram for the AOT-NaCl-H<sub>2</sub>O system (reproduced from [4]).

In the discussion above only the effect of added electrolyte on ionic surfactants has been considered. There are however a few other important methods of influencing the geometry of the surfactant and therefore the phase behaviour. A co-surfactant can be added eg. a zwitterionic surfactant or an n-alkanol. These usually produce mixed micelles with a preference for a lower interface curvature and therefore promote the transition from spherical micelles to wormlike micelles and eventually to bilayers. The counterion can also have an important effect on ionic surfactants and therefore a change of counterion can influence the surfactant phase behaviour dramatically.

## Chapter 3

# The Depletion Interaction

In this chapter a review of the various mixtures of colloids and depletants that have been studied will be undertaken. The main theoretical developments will be discussed and compared with some of the main experimental results. The main emphasis is rather on findings related to my results rather than an exhaustive review.

### 3.1 Colloid-Polymer Mixtures

#### 3.1.1 A Depletion Potential

In section 2.2 the concept of the depletion interaction was introduced. Asakura and Oosawa [8] and Vrij [9] showed that the addition of non-adsorbing polymer to a solution of colloidal particles could induce an attraction. The polymer molecules and colloidal particles are assumed to be mutually impenetrable, thus the centre of a polymer coil of radius of gyration  $R_g$  is excluded from a region of thickness  $R_g$  around the colloidal particles. This is known as the depletion zone. The polymer is therefore restricted to the volume not occupied by the colloids or their depletion zones, the free volume  $V_{free}$ . When the depletion zones overlap polymers are excluded from the zone between the particles, therefore the particles feel an excess osmotic pressure which pushes them together (figure 2.4). Alternatively one can think of the overlap of the depletion zones in entropic terms. Their overlap creates more free volume for the polymer coils (the overlap reduces the total volume inaccessible to the polymers), therefore maximising

entropy, and lowering the free energy of the system.

The induced interparticle attraction can be modelled by a pair potential,  $U_{dep}(r)$ ,

$$U_{dep}(r) = \begin{cases} 0 & r > 2(a + R_g) \\ -\Pi_p V_{over} & 2a < r < 2(a + R_g) \\ \infty & r \leq 2a \end{cases} \quad (3.1)$$

where  $a$  is the colloidal radius,  $r$  is the centre-centre separation of the particles and  $\Pi_p$  is the osmotic pressure exerted on the particles by the polymer coils.  $V_{over}$  is the volume of the overlapping depletion zones between two particles. It is given by

$$V_{over} = \left( 1 - \frac{3r}{4a(1+\xi)} + \frac{1}{2} \left[ \frac{r}{2a(1+\xi)} \right]^3 \right) \frac{4\pi}{3} a^3 (1+\xi)^3 \quad (3.2)$$

where  $\xi = R_g/a$  is the size ratio of polymer radius of gyration to colloid radius. Qualitatively the range of the depletion attraction depends on  $R_g$ , while the depth depends on the polymer concentration.

Assuming that the polymers behave as an ideal gas (experimentally valid when the polymer volume fraction is well below that of overlap, and that the study is carried out at the theta temperature for the polymer) the osmotic pressure is given by the van't Hoff Law,

$$-\Pi_p = \frac{N_p kT}{V_{free}} \quad (3.3)$$

where  $N_p$  is the number of polymer coils.  $V_{free}$  is the free volume available to the polymer coils and is given by,

$$V_{free} = V - V_c - V_{dz} + V_{over} \quad (3.4)$$

where  $V$  is the total volume of the sample,  $V_c$  is the volume taken up by the colloid,  $V_{dz}$  is the volume of the depletion zones, and  $V_{over}$  is the volume of overlapping depletion zones. The free volume,  $V_{free}$  can be written as a fraction of the total volume of the sample  $V$  as follows,

$$V_{free} = \alpha V \quad (3.5)$$

The free-volume fraction  $\alpha$  depends upon the colloid volume fraction  $\phi$ , the number density of polymer coils,  $N_p$ , the size ratio,  $\xi = R_g/a$ , and the positions of all the colloidal particles. An approximate form for  $\alpha$  was obtained using scaled particle theory [10],

$$\alpha = (1 - \phi) \exp[-A\gamma - B\gamma^2 - C\gamma^3] \quad (3.6)$$

where  $\gamma = \phi/(1 - \phi)$ ,  $A = 3\xi + 3\xi^2 + \xi^3$ ,  $B = (9\xi^2)/(2 + 3\xi^3)$  and  $C = 3\xi^3$ .

Scaled particle theory assumes a mean-field average over colloidal particle coordinates, assuming that they are unperturbed by the presence of the polymer. Note that in this approximation there is no dependence on  $N_p/V$  and it can therefore be expected to be valid in the limit  $N_p/V \rightarrow 0$ .

Both the range and the strength of the depletion attraction depend on the size ratio,  $\xi$ . As the size ratio is increased the range of the attraction increases but the well depth becomes shallower for a constant polymer concentration. This is illustrated in figure 3.1. For a high size ratio the polymer is relatively large and therefore the depletion zones will be big and thus can overlap and induce an attraction at a large intercolloidal distance. Therefore the range of the attraction is relatively great. This will be important when considering the phase behaviour in the following sections. For a constant size ratio (therefore for a constant range of attraction) the depletion attraction becomes stronger and therefore the well depth gets larger when the polymer concentration is increased.

### 3.1.2 Predicting the Equilibrium Phase Behaviour

An early method of interpreting and therefore predicting phase behaviour of colloid-polymer mixtures involved finding an effective potential for the system. Sperry [45] determined an effective potential for a system of charged aqueous colloids with non-adsorbing polymer by adding the depletion attraction given by Asakura and Oosawa [8] (section 3.1.1) to the DLVO potential (see section 2.2.2). Effective potentials were determined for an aqueous system of polystyrene latices and hydroxyethyl cellulose (HEC) which Sperry and co-workers had investigated experimentally in a previous study [5]. The barrier to the primary minimum in the potential was found to be very high  $\sim 400kT$  and therefore the secondary minimum is the important feature. The experimental concentration of polymer that was required to induce phase separation

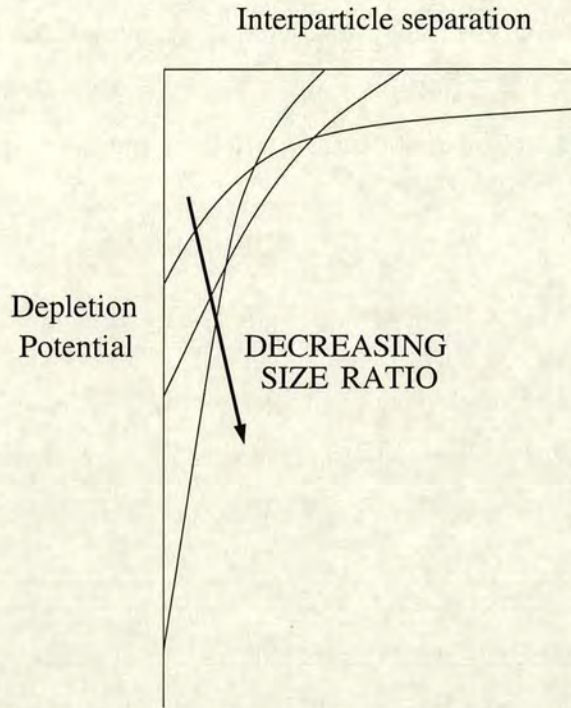


Figure 3.1: Schematic diagram illustrating the effect of size ratio on the depletion potential for a constant polymer concentration. As the size ratio increases the range of the attraction increases, whilst the effectiveness of the attraction falls.

in various colloid-polymer mixtures,  $C_F$  was found to correspond to an approximately constant secondary minimum well depth, with an average value of  $2.7kT$ . This value was therefore subsequently used to calculate concentrations required for flocculation. Joanny et al. invoked a similar criterion for phase separation for semi-dilute polymer solutions in good solvents [46]. There have since been developments in rigorous statistical mechanical methods for determining the phase behaviour of colloid-polymer mixtures. These allow complete phase diagrams to be predicted and therefore provide information on the nature of the resulting phases as well as the polymer concentration that first induces separation. The main two methods developed will be described in the following sections.

### 3.1.2.1 Theory of Gast, Hall & Russel

Gast, Hall and Russel have developed a theory for determining the phase behaviour of colloids in the presence of non-adsorbing polymer in both non-aqueous [47] and aqueous systems [48]. In both cases they have used a perturbation technique, where

the interaction potential is decomposed into a reference potential giving rise to known (i.e. soluble) phase behaviour and a perturbation potential. In the simpler, non-aqueous case the reference potential is the hard sphere potential and the depletion attraction according to Asakura and Oosawa [8] (section 3.1.1) is the perturbation potential. This provides a means for calculating the thermodynamic properties of the system. In addition to the interaction potential the calculations require the radial distribution function and free energy of the hard sphere reference state. The hard sphere system is found to separate into coexisting fluid and solid (see section 2.3.1). These properties must therefore be determined for both a hard sphere fluid, where the particles are disordered and move around in Brownian motion and a hard sphere crystal, where the particles are ordered on a crystal lattice. The free energies used were that of Carnahan and Starling [49] in the case of the fluid and that of Hall [50] for the crystal. The radial distribution functions have also been determined for both a hard sphere fluid and solid. The Percus-Yevick approximation [51] with the improvements made by Verlet and Weis [52] was used for the colloidal fluid. The radial distribution function used for the solid was the equation of Kincaid and Weis [53].

To find the phase behaviour the criterion of equal chemical potentials (or equivalently equal  $G$ ) and pressures in coexisting phases is utilised. Gast et al. used the perturbation theory to determine the Gibbs free energy and the pressure of the system as a function of the temperature and the number density of colloids. The coexisting pressure at the phase transition was then determined by finding the intersection of the fluid and solid  $G/kT$  versus  $p/\rho_0 kT$  and subsequently determining the equivalent densities of the fluid and solid phases.  $G$  is the Gibbs free energy,  $p$  is the pressure, and  $\rho_0$  is the density of colloid at closest packing. Repeating these calculations for different polymer concentrations maps out the phase diagrams.

Modified phase diagrams are reproduced from [47] in figures 3.2 and 3.3. The axes have been interchanged so that the volume fraction of polymer is the y-axis and the volume fraction of colloid is the x-axis. The size ratio used by Gast, Hall and Russel was  $a/R_g$  and therefore in the diagrams these have been changed such that  $\xi = R_g/a$ . These changes are made in order for convenient comparison with the theoretical predictions of Lekkerkerker et al. [10] and the experimental results discussed subsequently. From figure 3.2 it can be seen that the phase boundaries depend only on the size ratio. As



the size ratio increases the polymer volume fraction required to induce phase separation increases. This is a result of the weaker depletion well depth with increased size ratio mentioned earlier. At higher size ratios still there is a qualitative change in behaviour as shown in figure 3.3. For  $\xi \gtrsim 0.33$  critical and triple points appear in the phase diagram. Two fluid phases can coexist above the critical point. The value of the size ratio where the behaviour changes is known as the crossover size ratio,  $\xi_{CO}$ . In the case of no added polymer hard sphere phase behaviour is recovered.

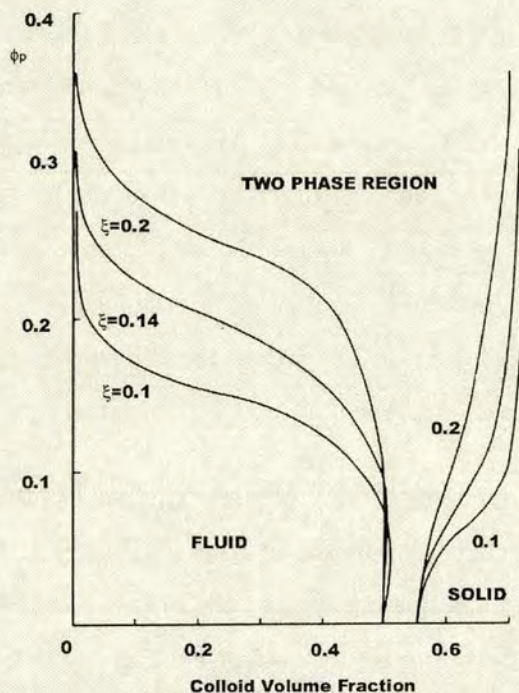


Figure 3.2: Phase diagram reproduced from [47] showing the predicted phase behaviour for colloid-polymer mixtures. It can be seen for the range of size ratios shown that the effect of added polymer is to expand the fluid-solid coexistence region of the hard-sphere system.

For the aqueous system the effective colloid pair potential is a sum of the electrostatic repulsion (see section 2.2.2) and the osmotic attraction of Asakura and Oosawa [8]. The van der Waals attraction is ignored since the colloidal particles are assumed to be kinetically stable (i.e. there is a large barrier to the primary minimum) and the van der Waals contribution to the attractive force is negligible compared to the osmotic attraction at long ranges. The phase behaviour is predicted using a similar perturbative approach as used in the non-aqueous case. More information can be found in reference [48].

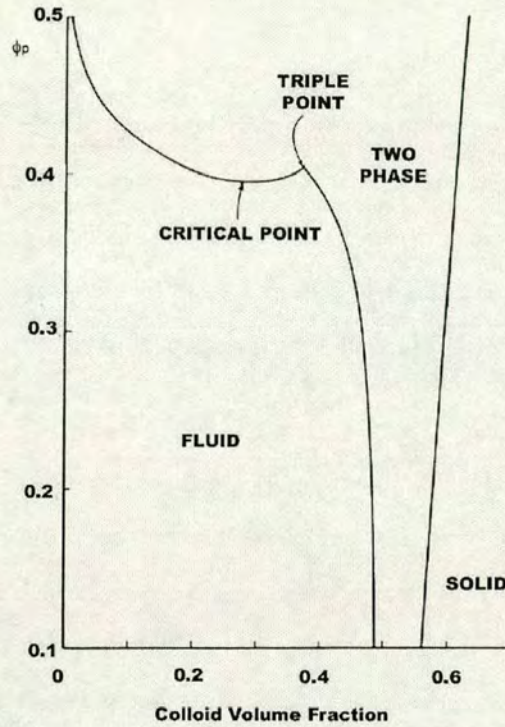


Figure 3.3: Phase diagram reproduced from [47] showing the expected phase behaviour for colloid-polymer mixtures with a size ratio,  $\xi \gtrsim 0.33$ . In this case the fluid-solid coexistence region is expanded as in figure 3.2. Critical and triple points also feature in this phase diagram as the depletion attraction is longer range for larger size ratios.

Modified phase diagrams (as discussed earlier) have been reproduced from reference [48] in figures 3.4 and 3.7. In this case a dimensionless polymer osmotic pressure is plotted against the colloid volume fraction. In figure 3.4 the ionic strength of the system is kept constant, at  $I = 0.010 \text{ mol dm}^{-3}$ , and the size ratio is varied. In the case of no added polymer the fluid solid coexistence moves to a lower volume fraction than the hard sphere case. It corresponds to the phase behaviour of hard spheres with an effective diameter, which is greater than the hard sphere diameter due to the steep repulsive force the colloids feel when the double layers overlap. As the size ratio is decreased the range of the depletion attraction decreases and therefore moves increasingly into the double layer of the particle, where it is shielded. The depletion attraction therefore becomes less effective, resulting in a larger osmotic pressure required to induce phase separation as shown in figure 3.4. The effect of the range of the attraction dominates

over the effect of the depletion well depth in this case. This is illustrated in figure 3.5 and 3.6. The trends shown are therefore opposite to that of the non-aqueous, uncharged system.

Figure 3.7 shows the dependence of the phase behaviour on ionic strength at a fixed size ratio. As the ionic strength is increased the electrostatic repulsion is screened more effectively and therefore doesn't shield the depletion attraction so well. A lower concentration of polymer is therefore required to induce separation (figure 3.7). There is no indication by Gast et al. [48] of the appearance of a critical point in the phase diagram.

In this study into aqueous colloid-polymer mixtures by Gast Hall and Russel [48], the polymer concentration was also increased into the semi-dilute regime (2.4.4). The important lengthscale in this case is the mesh size  $\xi_M$  which decreases as polymer concentration is increased, rather than the individual polymer size. The range of the attractive potential therefore decreases with increasing polymer and reduces the depth of the secondary minimum. Therefore it is predicted that at high enough polymer concentrations the mixture restabilises. Other theories which predict this restabilisation at high polymer concentrations are discussed in section 3.1.5.

### 3.1.2.2 Theory of Lekkerkerker et al.

The phase behaviour of the colloid-polymer mixture was subsequently predicted using a free energy minimisation approach by Lekkerkerker et al [10]. This approach allows for the partitioning of polymer between the phases, unlike the theory of Gast, Hall and Russel [47, 48]. Again, Lekkerkerker et al. treat the polymer as an ideal suspension of freely interpenetrable coils. The centres of these coils are excluded from a region of thickness  $R_g$  from around the colloid as discussed previously. The colloidal particles are assumed to interact as hard spheres. The free energy of such a system can be approximated by,

$$F = F_C(N_C, V) + F_P(N_P, \alpha V). \quad (3.7)$$

$F_C$  is the Helmholtz free energy of the  $N_C$  colloids in a volume  $V$ . This assumes that the polymer does not disturb the colloidal configuration and therefore the free energy of the colloid used is that of the pure colloid (as discussed later). The polymer free energy

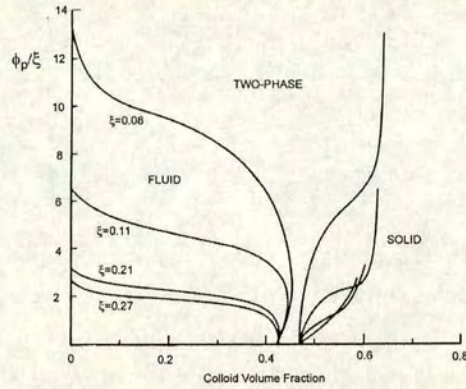


Figure 3.4: Phase diagram reproduced from [48] showing the expected phase behaviour of colloid-polymer mixtures for varying size ratio. The ionic strength is kept constant at  $I = 0.01\text{mol dm}^{-3}$ . It can be seen that the polymer induces a large region of two-phase coexistence due to the depletion attraction.

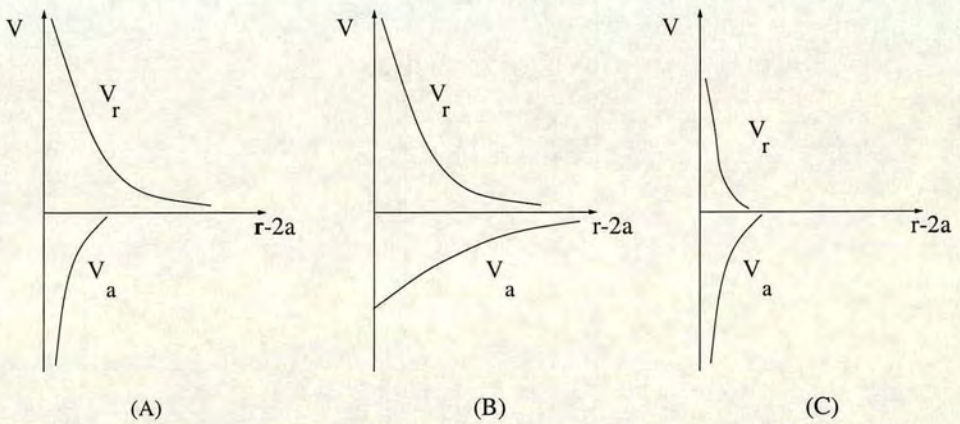


Figure 3.5: Schematic diagram of the effectiveness of the depletion attraction in the presence of an electrostatic repulsion. (A) shows the case where the range of the attractive potential is too short to overcome the repulsive potential. In this case uncharged polymer can move freely in between the colloidal particles. (B) has the same repulsive potential as (A) but with a larger size ratio. In this case the colloids do feel an attraction due to the exclusion of polymer coils. (C) has the same attractive potential as (A) but the repulsive potential is shorter range i.e. the Debye length  $\kappa^{-1}$  is shorter and thus the depletion attraction becomes more important since it is not totally swamped by the electrostatic repulsion.

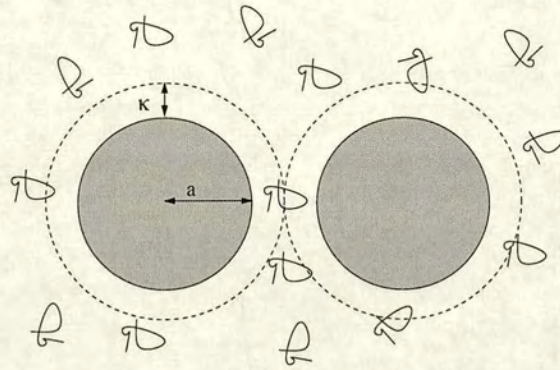


Figure 3.6: Schematic diagram of two charged colloidal particles in a sea of uncharged polymer coils. These colloidal particles repel each other due to the electrostatic interaction. It can be considered that they cannot approach each other closer than  $a + \kappa$ . If the polymer is too small it will not deplete since it will always be able to move all around the colloidal particles as illustrated.

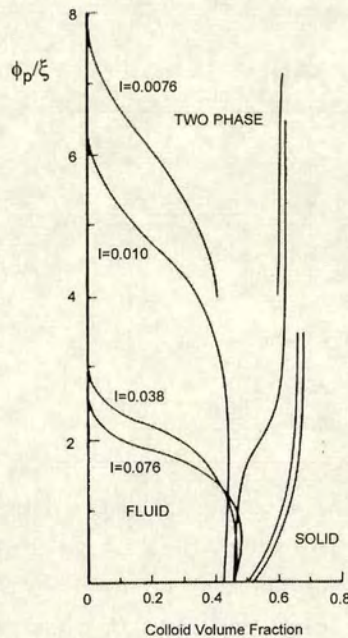


Figure 3.7: Phase diagram reproduced from [48] illustrating the effect of the ionic strength on the phase behaviour of a colloid-polymer mixture according to the theory of Gast, Hall & Russel. The size ratio is constant with a value of  $\xi = 0.11$ .

is that of  $N_P$  ideal polymer coils in a free volume  $\alpha V$ . The parameter,  $\alpha$  contains the excluded volume interaction between the colloid and polymer and is given by equation 3.6. The polymer free energy therefore depends on the colloid volume fraction via  $\alpha(\phi)$ .

Assuming the polymer is a suspension of non-interacting coils the free energy of the polymer is, [10]

$$F_P(N_P, \alpha V) = kTnV \log \frac{n}{\alpha} \quad (3.8)$$

where  $n = N_P/V$ . There are other terms which have been neglected since they are linear in  $N_P$  and  $V$  and therefore do not affect the determination of the phase behaviour. Like Gast, Hall and Russel the colloidal free energy for both a fluid and a crystal were used. The expressions by Carnahan and Starling [49] and Hall [50] were used respectively.

The Helmholtz free energy is an extensive variable and therefore depends on  $N$ . A more useful way to express the free energy is as an intensive free energy density,  $f = F/V$ . Thermal coexistence requires equal pressures, in this case the osmotic pressure ( $\Pi$ ) and equal chemical potentials ( $\mu$ ) in the two phases. In order to determine these conditions in terms of the free energy density let us consider the thermodynamic variable,  $\mu$ ;

$$\begin{aligned} \mu &= \left( \frac{\partial F}{\partial N} \right)_V \\ &= V \left( \frac{\partial f}{\partial N} \right)_V \\ &= V \left( \frac{\partial \rho}{\partial N} \right) \left( \frac{\partial f}{\partial \rho} \right)_V \\ &= \left( \frac{\partial f}{\partial \rho} \right)_V \end{aligned} \quad (3.9)$$

It can be seen from this that the chemical potential,  $\mu$  is given by the slope of the function  $f(\rho)$ . Therefore for phase coexistence equal slopes in  $f(\rho)$  is equivalent to equal chemical potentials.

The pressure must also be constant in coexisting phases. A similar treatment, as above for  $\mu$  can be carried out for pressure showing that the y-axis intercept of  $f(\rho)$  gives the pressure at a given  $\rho$ , as detailed below;

$$\begin{aligned} \Pi &= \left( \frac{\partial F}{\partial V} \right)_N \\ &= f + V \left( \frac{\partial f}{\partial V} \right)_N \end{aligned}$$

$$\begin{aligned}
 &= f + V \left( \frac{\partial \rho}{\partial V} \right) \left( \frac{\partial f}{\partial \rho} \right)_N \\
 &= f - \rho \left( \frac{\partial f}{\partial \rho} \right)_N
 \end{aligned}
 \tag{3.10}$$

Therefore coexisting phases must have the same intercept in the tangents to the  $f(\rho)$  curves. A common tangent approach can therefore be used to determine phase behaviour as illustrated in figure 3.8. This is equivalent to the method used by Gast, Hall and Russel [47], since it is equivalent to equal chemical potential and osmotic pressures in the coexisting phases. In this figure the free energy densities for both fluid and crystal colloidal phases, calculated as described previously, are plotted. It can be seen in figure 3.8 that a homogenised sample with a free energy of  $f_i$  can lower its free energy to  $f_{ps}$  by phase separating into a coexisting fluid and crystal, of densities  $\rho_f$  and  $\rho_c$  respectively. The amounts of each phase can be determined by the Lever rule ( $V_f/V_C = (\rho_c - \rho_i)/(\rho_i - \rho_f)$ ).

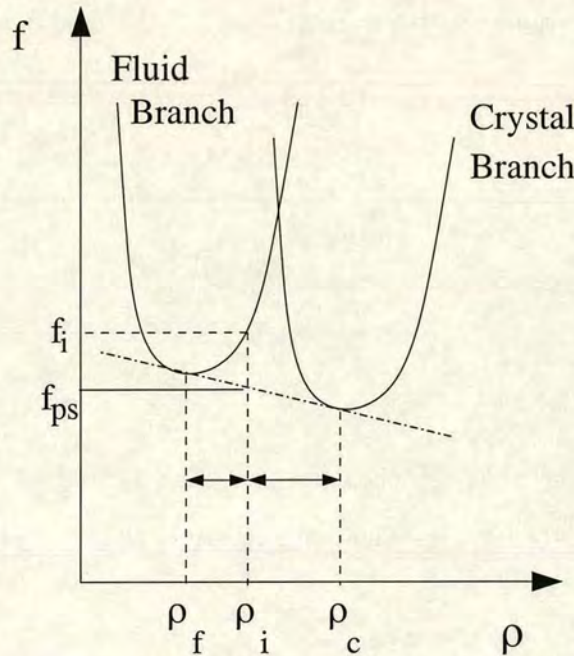


Figure 3.8: Schematic diagram showing the common tangent method for determining phase behaviour. A homogenised sample with a free energy density of  $f_i$  and density  $\rho_i$  will lower its free energy to  $f_{ps}$  by separating into a coexisting fluid and crystal with densities,  $\rho_F$  and  $\rho_C$  respectively. The common tangent is indicated by the dash-dot line.

This procedure can be repeated for an increasing volume fraction of polymer in order

to build up the theoretical phase diagram. This has been determined for various size ratios ( $\xi = R_g/a$ ). In figures 3.9 and 3.10 the phase behaviour of colloid-polymer mixtures determined by the method described is shown for two different size ratios. Lekkerkerker et al. [10], like Gast, Hall and Russel [47] found that the topology of the phase diagram depends on the size ratio. For  $\xi \lesssim 0.32$  the region of fluid-crystal coexistence, (F+C) is simply broadened on addition of polymer. For  $\xi \gtrsim 0.32$  both a critical point (CP) and triple point (TP) appear. Figure 3.9 shows the phase diagrams with the polymer volume fraction in the free volume versus colloid volume fraction, whilst figure 3.10 shows these diagrams in terms of the polymer volume fraction in the total sample volume. This is the experimentally accessible quantity.

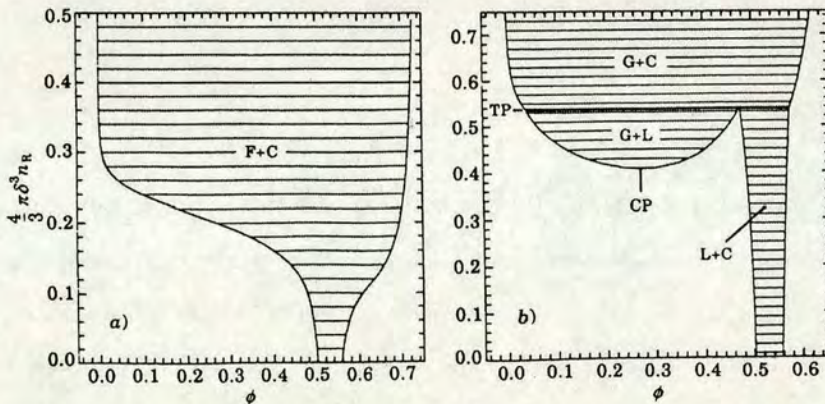


Figure 3.9: Phase diagram of colloids according to the theory of Lekkerkerker et al. for colloid-polymer mixtures. The diagrams are plotted with the polymer concentration in the free volume against the colloid volume fraction and illustrate the two types of behaviour found. Figure a) has size ratio  $\xi = 0.1$ , below the crossover size ratio whilst figure b) has size ratio  $\xi = 0.4$ , above  $\xi_{CO}$  and therefore has a critical point (CP) and a triple point (TP). The symbols denote the following: F, fluid; G, gas; L, liquid; C, crystal; F+C, fluid plus crystal etc. This figure was reproduced from reference [10].

It can also be seen from the phase diagrams that the polymer concentration is significantly different in the two phases, as indicated by the oblique tie-lines in figures 3.10 a) and b).



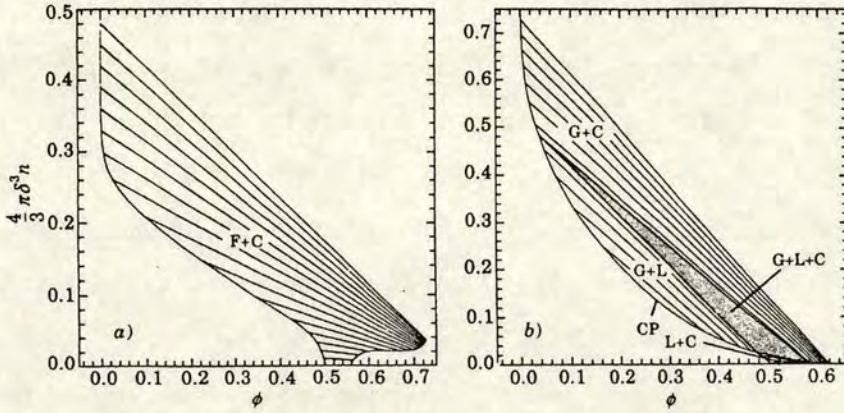


Figure 3.10: Phase diagrams of colloid-polymer mixtures predicted by Lekkerkerker et al. with actual concentration of polymer versus colloid volume fraction. Two size ratios are shown as in figure 3.9; a) has  $\xi = 0.1$  and b) has  $\xi = 0.4$ . This figure was reproduced from reference [10].

### 3.1.2.3 Comparison of the Theories

The theory of Lekkerkerker et al. [10] correctly allows the polymer concentration in the phases to vary, whereas in the case of Gast et al. the polymer concentration must be the same in coexisting phases. Experimental results do indeed indicate uneven polymer partitioning. An investigation by Russel and Patel [25] provided evidence of this partitioning, however the clearest of studies to date indicating this polymer partitioning was carried out by Poon et al. [54]. In this investigation the polymer concentration was measured directly in the two phases using light scattering techniques.

It is in fact unclear in the results of Gast, Hall and Russel [47] whether the volume fraction of polymer is the actual value or the value in the free volume. If it is indeed the latter, then the results agree well with those of Lekkerkerker et al. The crossover size ratio determined by both methods is approximately the same,  $\xi \approx 0.32$ . The phase boundaries for the size ratios  $\xi = 0.10$  and  $\xi = 0.40$  are shown for both theories in figures 3.2, 3.3, 3.9 and 3.10. It can be seen that the values of polymer volume fraction where phase separation begins for a given colloid volume fraction are approximately the same for both theories.

Lekkerkerker et al. have not investigated the effect of charges on the phase behaviour.

### 3.1.3 Experimental Observations

#### 3.1.3.1 *Hard Sphere Colloids & Polymer*

There have been many investigations of systems approximating to hard spheres and polymer, including references [55, 56]. In light of the progress made in the theory by Lekkerkerker et al. [10], the most comprehensive study to date was carried out by Ilett et al. [7] who explored the behaviour of sterically stabilised PMMA particles with polystyrene in *cis*-decalin. The results are shown in figure 3.11 with the corresponding theoretical results from the theory of Lekkerkerker et al. shown in figure 3.12. The results agree reasonably well with the predicted phase behaviour of both Gast et al. and Lekkerkerker et al. At small  $\xi$  the region of fluid-crystal coexistence as observed in hard-sphere systems was expanded on the addition of polymer. At higher size ratios a critical point and three phase coexistence was found. The cross-over size ratio was found to be  $\xi_{CO} \approx 0.25$  in this study. This is lower than the value predicted by both theories. As the size ratio is increased above  $\xi_{CO}$  the region of gas-liquid coexistence increases. Experimentally there is also a type of behaviour observed that is not predicted by theory, that of gelation (section 3.1.4). Particle gels are found at high polymer concentrations for all size ratios investigated. This is non-equilibrium behaviour and therefore cannot be determined by equilibrium statistical mechanics.

#### 3.1.3.2 *Charged Colloids & Polymer*

The experimental study by Sperry [5, 6] mentioned previously was compared by Gast et al. [48] to their theory. The concentration of hydroxyethylcellulose (HEC),  $C_F$  required to induce flocculation of the polystyrene latices was compared with the phase boundaries found by Gast et al. Plots of the experimental results and the theoretical results of Gast, Hall and Russel [48], both for varying size ratio at constant ionic strength and for varying ionic strength at constant size ratio are shown in figures 3.13 and 3.14 respectively. The ionic strength was changed in the experiments by Sperry et al. by the addition of ammonium sulfate.

Gast et al. also carried out investigation into the phase behaviour of polystyrene latices

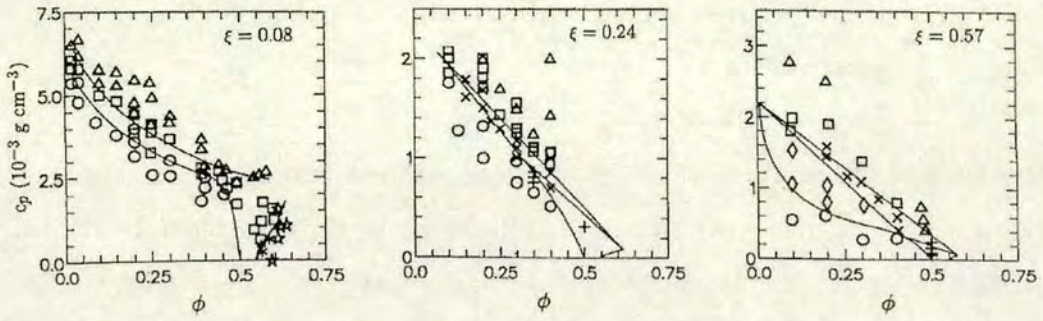


Figure 3.11: Experimental phase diagrams for colloid-polymer mixtures of three size ratios as indicated. The symbols denote the following: circle, fluid; diamond, gas-liquid coexistence; cross, three phase sample, i.e. gas plus liquid plus solid; plus sign, liquid-crystal coexistence; square, gas-crystal coexistence; triangle, gel (for  $\xi = 0.08$ ) or no visible crystallites (for  $\xi = 0.33$  and  $0.57$ ); stars, glass. The lines in these figures are drawn as guides to the eye, except for the triangular regions for  $\xi = 0.24$  and  $0.57$  which have been located with the aid of experimentally determined colloid concentrations in the three coexisting phases. Figure reproduced from [7].

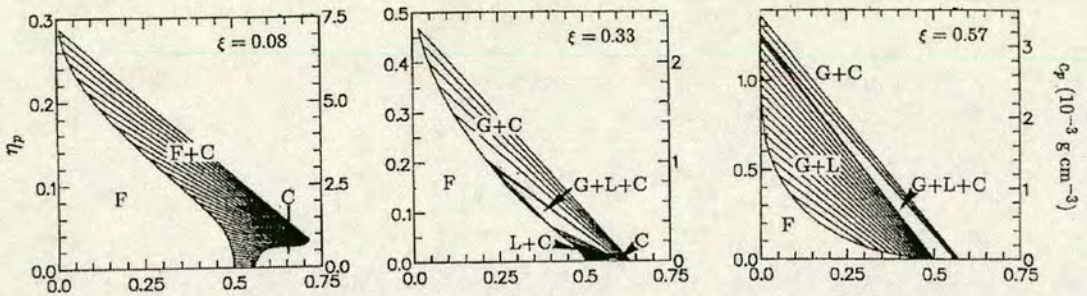


Figure 3.12: Theoretical phase diagrams according to the theory of Lekkerkerker et al. for three different size ratios,  $\xi = 0.08$ ,  $\xi = 0.33$  and  $\xi = 0.57$ . (Reproduced from [7].)

in an aqueous solution of HEC and found that the results compared favourably with the results with their theoretical predictions [57].

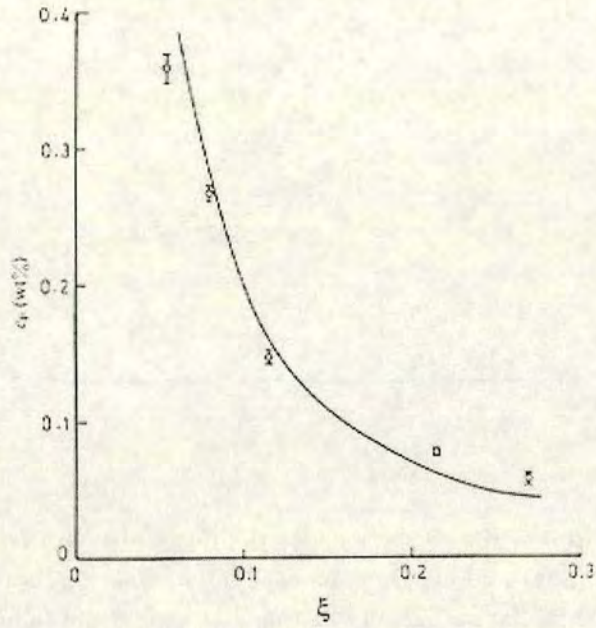


Figure 3.13: Comparison of the predictions for the onset of phase separation between theory and experiments. The line represents the theoretical dependence of the concentration of polymer first inducing separation ( $c_F$ ) on the size ratio ( $\xi$ ), as predicted by Gast, Hall and Russel [48]. The open circles are the experimental results of Sperry et al. [5] for a system of polystyrene particles in an aqueous solution of HEC. The ionic strength is 0.01M. (Reproduced from reference [48])

### 3.1.4 Non-equilibrium Behaviour

As was mentioned in section 3.1.3 non-equilibrium behaviour has been observed as well as the equilibrium behaviour predicted by the theory. These metastable gels, where the particles are aggregated in a space-spanning solid-like network, form at high polymer concentrations. Non-equilibrium behaviour is very important industrially, since many products exist in metastable states, e.g. salad cream.

#### 3.1.4.1 Gel Formation

The aggregation and gelation of colloidal particles has been simulated using a simple model, that of Diffusion Limited Cluster Aggregation (DLCA)[58]. It is assumed in this model that there is a strong short-range attractive force between the particles. Colloidal particles are allowed to diffuse around in space but when two particles touch

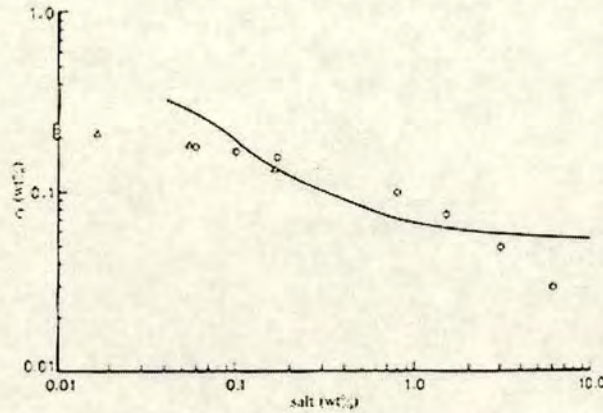


Figure 3.14: Comparison of the predictions for the onset of phase separation between the theory of Gast et al. (line) and experiments by Sperry et al. [5] (both the circles and the triangles are experimental data points. (The triangles come from tabulated data whilst the circles are from graphs in reference [5].) The polymer concentration where destabilisation first takes place ( $c_F$ ) is given as a function of salt concentration. In the experimental case the concentration of ammonium sulfate in the aqueous solution of HEC and polystyrene particles was varied. (Reproduced from reference [48])

a permanent, rigid bond \* is formed between them. This pair of particles continue to diffuse, coming into contact with other particles and/or clusters and sticking to them. In this way a large fractal structure spanning the whole sample is built up. This is then known as a gel structure. This is illustrated in figure 3.15. As the cluster grows it becomes more tenuous, i.e. the average density decreases.

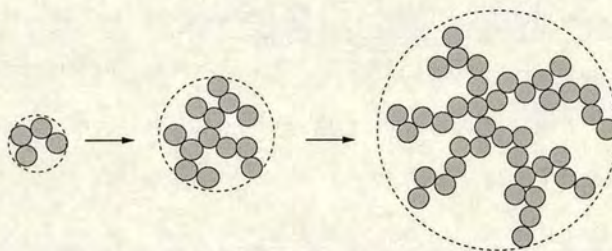


Figure 3.15: Schematic diagram showing the growth of a fractal cluster in DLCA.

This picture of gelation is too simplistic to be truly representative of colloid-polymer mixtures. For reasonable polymer concentrations, the colloidal interaction will be of the order of  $kT$ , so that thermal fluctuations will compete with particle aggregation. This has been modelled by DLCA with finite bond strengths, or “reversible DLCA”

\*this is not a chemical bond

[59, 60]. It was determined that for a bond strength of  $\sim 3kT$  the clusters still grow fast enough to span the system and therefore form a gel. Thermal fluctuations however have been observed in these simulations to cause compaction of the clusters on small length scales. Over time in this simulation it is also observed that the structure breaks into two or three large clusters, which then reform due to thermal motion of the particles. In the real case however the space between the clusters would be filled with solvent and polymer and thermal rearrangements and gravity may lead to the collapse of these structures, known as transient gels.

Haw et al [60] also investigated the case of a bond strength  $\sim kT$ . In this case gelation did not take place as the compactification of the clusters by thermal rearrangement wins over aggregation.

#### 3.1.4.2 Gel Collapse

A substantial amount of experimental work on colloid-polymer gels has been carried out [61, 62, 63]. A characteristic gel collapse has been found to take place in this work. There is a latency time, where little or no settling of the colloid takes place. This is followed by a period of rapid collapse. Finally the colloid compactifies slowly over time. These three stages of collapse are shown in figure 3.16. Oil-in-water emulsions with added polymer also show a similar behaviour, but with the oil rising to the top of the container since it is less dense than water [64].

Small angle light scattering (SALS) studies have also been carried out during the collapse of colloid-polymer gels [62]. The results show the formation of a frozen ring during the latency or delay time. This ring then collapses during the onset of the rapid collapse of the gel structure. Dark-field observations on index-matched colloid-polymer gels have shown the formation of channels and inhomogeneities during the latency time [63].

A discussion of the collapse of gels can be found in reference [63], where the mechanism of the collapse is detailed. The collapse has also been found to depend on the shape and size of the container by Starrs [63].

As the polymer concentration is increased or with a change of container size the sedi-

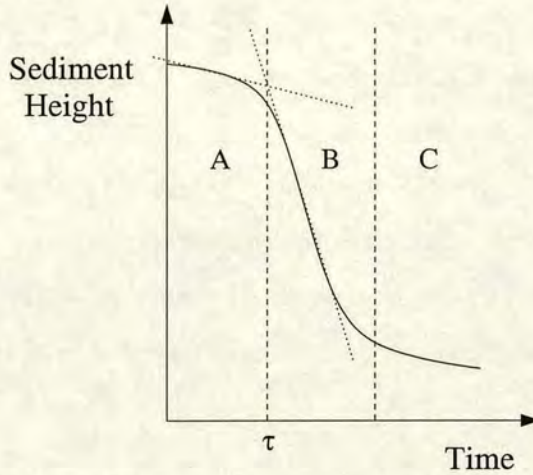


Figure 3.16: Schematic diagram showing the sedimentation profile for a system exhibiting delayed sedimentation. The three stages are shown: A the delay/latency (delay time =  $\tau$ ), B is the region of rapid collapse, and C is the slow compaction. This is the behaviour experimentally observed for colloid-polymer gels [62, 63].

mentation profile can change. Instead of a delayed sedimentation previously described one may also see a so-called creeping behaviour [62, 63]. In this case no latency time is observed. The sediment height decreases with time but there is no rapid collapse.

### 3.1.5 Depletion Restabilisation

As discussed previously, many theoretical and experimental studies have been carried out on the phase separation, or destabilisation of colloidal suspensions due to the depletion effect. The addition of non-adsorbing polymers to a colloidal suspension has also been predicted to induce a stabilisation effect in some regimes. Feigin & Napper [65, 66] predict a kinetic stabilisation of the colloid at high polymer volume fractions. They calculate a segment density profile of the polymer which accounts for internal degrees of freedom of the polymer as well as partially accounting for excluded volume effects. This is combined with a free energy of mixing of the polymer and solvent molecules. While the free energy of mixing was calculated for the interaction between two plates in a solution of polymer coils, it was extended to spherical particles using the Derjaguin approximation. The free energy curves determined show a minimum at low interparticle separation and a maximum at greater separations. At low polymer concentrations both the minimum and maximum are small, and therefore the colloidal suspension is stable.

As the polymer concentration is increased the minimum becomes sufficiently deep to induce flocculation of the particles. The colloidal suspension however is predicted to stabilise at still higher polymer concentrations as the free energy maximum increases in height. The time taken for colloidal particles to aggregate therefore increases. This stabilisation is therefore a kinetic effect, since the equilibrium behaviour is that of phase separation.

The Scheutjens-Fleer-Vincent (SFV) theory [67] also predicts restabilisation of the colloid at high polymer concentrations. However they predict this to be a thermodynamic effect rather than one of kinetics. They calculate the interaction of hard spheres in the presence of nonadsorbing polymer. The pair potential is derived from a lattice theory for interacting polymer near a surface. This is extended to the interaction between hard spheres in the presence of polymer. The polymers are not treated as hard spheres. The depletion thickness was found to be of order  $R_g$  as has been predicted by Asakura and Oosawa [8]. However, SFV theory also predicts a decrease in the depletion thickness when the polymer concentration is greater than the overlap concentration. This therefore leads to a weakening of the depletion attraction, and at high enough polymer concentrations the attraction is so weak that the colloidal suspension restabilises.

The theory of Gast, Hall & Russel for the phase behaviour of aqueous colloidal suspensions with added polymer [48] discussed in section 3.1.2 also predicts thermodynamic restabilisation, like SFV theory.

Experimental evidence for restabilisation at high polymer concentrations has been found for soft spheres by Emmett [68]. The stability diagram determined is shown in figure 3.17. The particles are found to be stable at low polymer concentrations and as this concentration is increased they destabilise. At higher still polymer concentrations the dispersion is observed to restabilise. In view of the subsequent work carried out the restabilisation observed could simply be the appearance of a gel, which have been found in many studies of colloid-polymer mixtures at high polymer concentrations (section 3.1.4). There is no evidence provided by Emmett that the phase found at high polymer concentrations is ergodic and therefore a fluid.



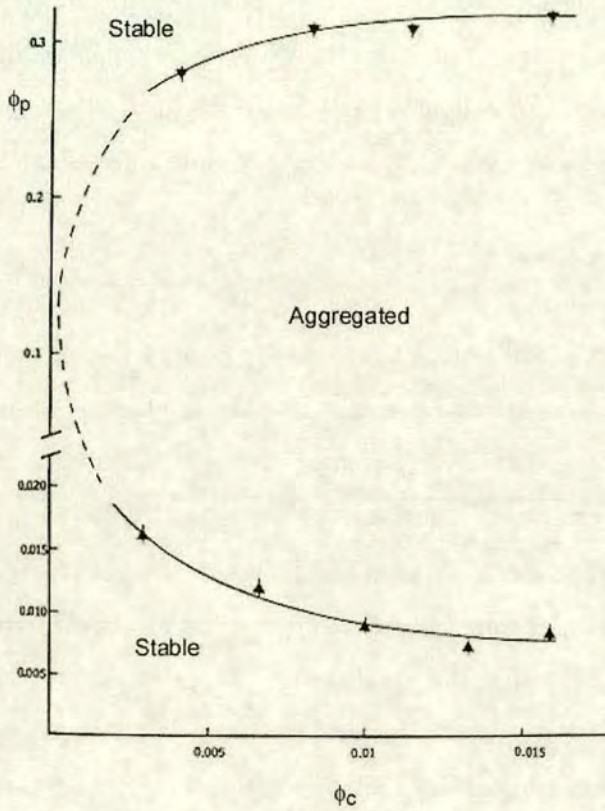


Figure 3.17: Stability diagram for silica spheres ( $a = 153.5nm$ ) in a solution of PDMS in bromocyclohexane as determined by Emmett[68]. The data points and curve represent the stability boundary. As the polymer concentration is increased the solution first destabilises and at still higher polymer concentrations it restabilises. (Reproduced from [68])

### 3.2 Binary Mixtures

The treatment of colloid-polymer mixtures by Lekkerkerker et al. [10] (section 3.1.2) can be extended to mixtures of two sizes of hard-spheres. For a small size ratio (where  $\xi = r_2/r_1$ , where  $r_1 > r_2$ ) the small spheres act as the depletant (i.e. they act like the polymer in colloid-polymer mixtures). The depletion picture is similar to that shown in chapter 2 with the polymer coils replaced by small spheres. By minimising the free energy as discussed in section 3.1.2 the theoretical phase behaviour has been predicted [69]. It is found that the addition of small spheres enlarges the region of fluid-crystal coexistence found in a system of hard-sphere colloids. No thermodynamically stable fluid-fluid phase boundary was found. The results compare favourably to an

experimental investigation carried out by Kaplan et al. [70] at a size ratio,  $\xi = 0.14$ .

Both the experimental and theoretical studies have also shown a region of wall crystal coexisting with fluid at lower small colloid concentration ( $\phi_2$ ) than the fluid-crystal coexistence. At a hard wall there should be a depletion layer inside of which the centre of a small sphere is excluded. The overlap between this wall depletion layer and the depletion layer surrounding a large particle induces a depletion attraction between the wall and the large particle as shown in figure 3.18. This leads to an adsorbed layer of large particles. The large particles within this layer also experience an interparticle depletion attraction, therefore forming wall crystals. This also takes place in colloid-polymer mixtures.

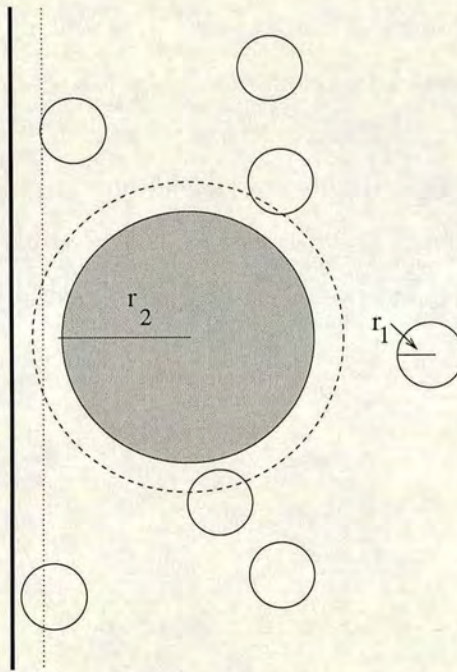


Figure 3.18: Schematic diagram illustrating the depletion interaction at a wall. The dashed line around the large colloid is the depletion zone arising due to the exclusion of the small colloids. These small colloids also result in the dotted line which is the depletion zone of the wall. When these overlap there is an effective attraction between the wall and the large colloidal particles.

It has, however, since been found that the form of the depletion potential is not the same as that of colloid-polymer mixtures. As well as the attraction there is a depletion repulsion at larger interparticle separations. When the depletion force is calculated to third order a secondary minimum is also found [71]. The repulsion corresponds to the

small colloidal particles just fitting in between two larger colloids, thus stabilising the system.

The phase behaviour of binary mixtures with similarly sized particles is also extremely interesting. A variety of crystalline alloy structures are found. Details can be found in Pusey et al. [72]

### 3.3 Rod-sphere Mixtures

Another interesting mixture that has been studied is that of colloidal spheres and colloidal rods. Asakura and Oosawa [73] first mentioned rod-like macromolecules acting as extremely efficient depletants. This can be seen by looking at the simple picture of two colloidal particles in a sea of rods as shown in figure 3.19. A rod-like colloid of length  $L$  and diameter  $D$  occupies a volume  $\pi D^2 L/4$ . The rod is however excluded by the spherical colloid from a volume  $\pi L^3/6$ . This is equivalent to the colloids being depleted by small spheres of diameter  $L$ , as illustrated in 3.19. Rod-like colloids therefore make very efficient depletants. This has been verified experimentally since phase separation has been found to take place at low volume fractions of rods.

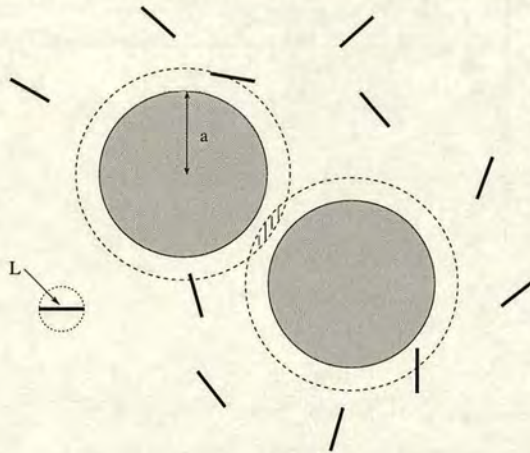


Figure 3.19: Schematic diagram showing the depletion attraction between two spherical colloids in a sea of rods. The dashed lines indicate the depletion zones resulting from the exclusion of the rod-like colloids. The rods have length  $L$  and they effectively deplete in the same way as a small sphere of diameter  $L$ .

The theoretical phase behaviour for rod-sphere mixtures was therefore found [74] by extending the theory for asymmetric binary mixtures [69] discussed in the previous sec-

tion. The behaviour found is qualitatively similar to that for colloid-polymer mixtures. For  $L/2a \lesssim 0.29$  the fluid-crystal coexistence region is simply expanded on the addition of rod-like colloids. Critical and triple points are found for  $L/2a > 0.29$ . The phase behaviour also depends on the aspect ratio,  $L/D$ , of the rods, as detailed in reference [74]. Vliegthart and Lekkerkerker studied the phase behaviour of a mixture of silica coated boehmite rods ( $L = 230nm$  and  $D = 10nm$ ) and silica spheres ( $a = 395nm$ ) in a small window of their predicted phase diagrams. Experimentally phase separation of colloidal spheres ( $\phi = 0.01 - 0.05$ ) was found to take place at a rod volume fraction of  $\phi \approx 0.003$ , while the theory predicts separation around  $\phi \approx 0.005$ . This indicates that the theory is a good predictive guide, however, a more complete phase study is required in order to fully assess the correctness of the theoretical phase diagrams.

### 3.4 Colloid-Micelle Mixtures

Relatively few investigations have been undertaken for mixtures of surfactant and colloid. Many industrial products are essentially just such systems, eg. shampoo is a mixture of an emulsion and wormlike micelles. These mixtures are therefore of both fundamental and industrial importance.

#### 3.4.1 Colloid-Spherical Micelle Mixtures

Piazza and di Pietro [75] have studied a mixture of spherical micelles and colloidal particles. The system studied was PFA colloid (polytetrafluoroethylene copolymer) in an aqueous solution of Triton X100. The nonionic surfactant Triton X100 is known to form spherical micelles, of radius  $r_m$ , up to a concentration of about 40%. The size ratio of the system is  $\xi=0.03$  (where  $\xi = r_m/a$ ). At high enough surfactant concentrations the mixture becomes unstable and separates into colloid-rich and colloid-poor phases. Piazza and di Pietro explained this behaviour in terms of a depletion attraction induced by the spherical micelles.

They compared their experimental results with the theoretical phase diagram predicted using the theory of Lekkerkerker et al. [10] with the spherical micelles taking the place of the polymer coils (since the theory of asymmetric binary mixtures had not been

done at the time). The theory predicts that for a size ratio of  $\xi=0.03$  the surfactant concentration required to induce separation is much higher than that found experimentally. As well as this discrepancy there is also some differences in the type of phase behaviour observed. In order to compare this behaviour with the predictions of the theory of Lekkerkerker et al. the experimental results are scaled in order to agree with the theoretical phase boundary. The scaled experimental results with  $\phi_s^* = 4.3\phi_s$  are shown in figure 3.20 along with theoretical data.

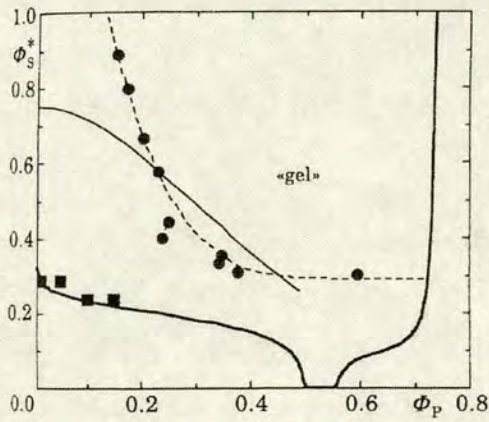


Figure 3.20: Phase diagram for mixtures of colloids and spherical micelles. (Reproduced from [75]). The thick black lines represent the theoretical phase boundaries predicted by the theory of Lekkerkerker et al. [10] for a binary mixture of size ratio 0.03. Squares are the experimental transition points and circles are the gel-gas samples. The dashed line is the approximate boundary of the observed gel region. The full line is the percolation threshold calculated from the Baxter model.

At such a small size ratio the predicted phase behaviour is that of fluid-crystal coexistence at high enough depletant concentration, as indicated by the thick black lines in figure 3.20. Piazza and di Pietro have, however, found the colloid-rich phase to be a gel rather than a colloidal crystal, except for a very narrow strip near the phase boundary as illustrated in the phase diagram. The percolation threshold was calculated using the Baxter model for adhesive (“sticky”) hard spheres [76] and shown on figure 3.20 (black line). The particle concentration ( $\phi_p$ ) for the gel phases shown in the figure agree reasonably with the Baxter model. Gels have been found experimentally at high polymer concentrations in colloid-polymer mixtures 3.1.4. There is therefore a gel line above the fluid-crystal binodal in the phase diagram. In the case of the spherical micelles and col-

loid mixtures the gel region fills most of the region above the binodal. As the mixture is trying to phase separate into colloidal fluid and crystal the concentrated crystal phase reaches the gel line, and therefore the observed behaviour is that of gel-gas separation [77].

The gels found in this study, however, show no structural reorganisation on a time scale of weeks as has been observed in colloid-polymer mixtures. Piazza and di Pietro propose that no structural reorganisation of the gel takes place on the time-scale of weeks because the lifetime of a micelle is much longer than the restructuring time of the polymer coils. Therefore if it is this restructuring that is responsible for the gel collapse then there will be an increased metastability of the gel in surfactant flocculation due to the relatively long lives of the micelles. This is, however, an unconvincing argument since the gel structures found for colloid-polymer mixtures span the whole sample cell, whilst those found by Piazza and di Pietro are found to coexist with a colloidal gas. The gels in the latter case are therefore already well compressed and will only compact more, very slowly, like the compactification stage of the delayed sedimentation of colloid-polymer gels 3.1.4. This is illustrated in figure 3.21. Like colloid-polymer mixtures, the samples investigated by Piazza and di Pietro showed no sign of irreversible aggregation since the dense phase could be completely redispersed when the sample is shaken.

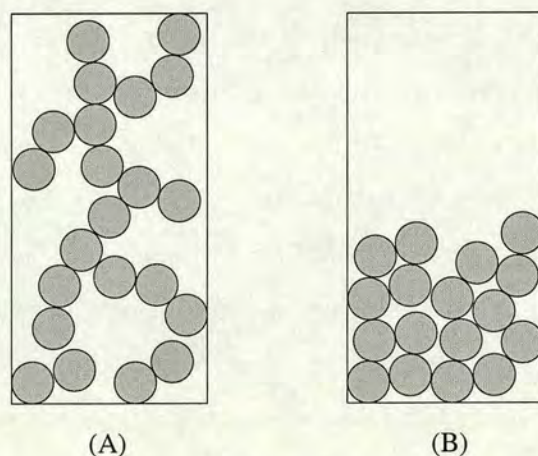


Figure 3.21: Schematic diagram of transient gels (A) before collapse, and (B) after they have collapsed. Figure (B) is similar to the Piazza [75] gel-gas separation, except the upper phase in this diagram has no colloid in it. Figure (B) will compactify slowly over time.

Micelles have also been found to induce creaming of emulsions [78]. Emulsions of oil

droplets in water are formed by the adsorption of surfactant onto the surface of the oil, which stabilises the droplets. If, however, excess surfactant is added, this excess which is not adsorbed by the oil forms micelles which then induce a depletion attraction. This causes flocculation of the emulsion droplets which then rise to the surface, or “cream”. The phase behaviour of a model system of emulsion droplets plus polymer has been investigated in Edinburgh in order to compare the results to that of colloid-polymer mixtures [79].

Direct measurements of the depletion force induced by spherical micelles has also been carried out. Mondain-Monval et al. [80] have measured directly the repulsive force-distance profiles between colloidal droplets stabilised by an ionic surfactant in the presence of the same surfactant micelles. They were particularly interested in the effect of the electrostatic double layer repulsion on the depletion force. It is found that this enhances the depletion attraction as a result of the repulsion between the colloid and the micelles (depletant). This therefore introduces an extra thickness (the screening length,  $\kappa^{-1}$ ) from which the micelles are excluded since they have the same charge as the colloid. This therefore increases the size of the depletion zone.

### 3.4.2 Colloid-Wormlike Micelle Mixtures

Spherical micelle and colloid mixtures are the obvious surfactant analogy of binary mixtures. Wormlike micelles with colloidal particles are therefore a good parallel to colloid-polymer mixtures. There will however be additional effects to consider. The wormlike micelles have an exponential distribution of lengths, and can break and reform as discussed in chapter 2. No experimental phase studies of such a system can be found in the literature. There has however been a theoretical investigation into mixtures of wormlike micelles with small colloidal particles by Sear and Mulder [81]. This regime is different to the well studied colloid-polymer mixtures since the colloidal diameter should be no more than an order of magnitude bigger than the diameter of the wormlike micelles. The theory predicts demixing over a wide range of the ratio for the diameter of the particle to the diameter of the micelle.

Direct measurements of the depletion interaction in semi-dilute solutions of wormlike micelles have been carried out by Richetti et al. [82] The force as a function of separation

is measured between two mica surfaces coated with adsorbed CTAB and immersed in a semi-dilute solution of wormlike micelles of CTAB. Both this investigation and that of Sear and Mulder [81] therefore show that wormlike micelles should act as depletants. How strongly will the micelles deplete though, since they can break up into smaller micelles? Does the distribution of sizes have a large influence on the behaviour? Can their behaviour be modelled as colloid-polymer mixtures? These are just some of the questions which need to be answered and which have been addressed in this thesis.





## Chapter 4

# Experimental Systems & Methods

In this chapter a description of the systems investigated in this thesis is given. These systems are not described in the chronological order in which they were studied, but rather in order of increasing complexity. The experimental methods used in this study are also described in this chapter.

### 4.1 The Systems

The systems studied and the methods of preparation are described in the subsequent sections. A summary of the systems studied is given in table 4.1 for easy reference. Only the main points with regard to sample making are discussed in this chapter. Further details can, however, be found in appendix A.

#### 4.1.1 System A

The nonionic surfactant hexaethylene glycol n-hexadecyl monoether,  $C_{16}H_{33}(CH_2CH_2O)_6OH$ , is more commonly known as  $C_{16}E_6$ . It has been found to form wormlike micelles in aqueous solution [37].  $C_{16}E_6$  is a member of the homologous series of nonionic surfactants discussed in section 2.4. The dilute section of its phase diagram in  $D_2O$  is shown in figure 4.1. The phase diagram of  $C_{16}E_6$  in  $H_2O$  will not vary significantly from this. In system A this solution of wormlike micelles is mixed

Table 4.1: Summary of aqueous systems investigated.

	System A	System B	System C
Colloid	uncharged PEO-stabilised polystyrene latex	charged polystyrene latex <sup>a</sup>	charged polystyrene latex <sup>b</sup>
Surfactant	nonionic surfactant C <sub>16</sub> E <sub>6</sub>	nonionic surfactant C <sub>16</sub> E <sub>6</sub>	anionic surfactant (SLES) and zwitterionic surfactant (CAPB)
Additional Components	none	sometimes salt <sup>c</sup>	sometimes salt and/or octanol

<sup>a</sup>3 different sizes of *surfactant-free* colloid are used in this study

<sup>b</sup>similar size of both surfactant-free and surfactant stabilised colloid are used in this system

<sup>c</sup>these studies will be presented separately in the results chapters

<sup>d</sup>usually salt is used to promote the formation of micelles but a more limited study using octanol has also been carried out

with uncharged polystyrene colloids. These colloids were sterically stabilised with PEO groups. This system is therefore totally uncharged.

#### 4.1.2 Preparation of System A

##### *Chemicals*

The surfactant C<sub>16</sub>E<sub>6</sub> was obtained from Nikkol Ltd., Japan. It was stored under nitrogen in a refrigerator. The uncharged colloidal particles were synthesised in the department by Andrew Schofield, following the method by Ottewill et al. [83, 84]. The colloids were then purified by dialysis for 10 days. The colloid volume fraction was determined by centrifugation as detailed in appendix A. Deionised water from a Millipore purifier was used.

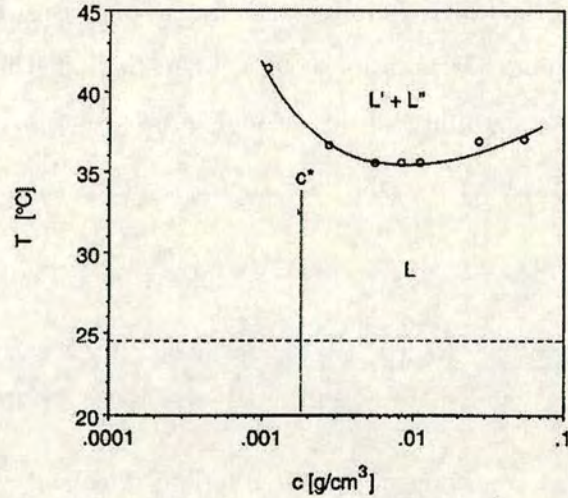


Figure 4.1: Partial phase diagram of the binary system  $C_{16}E_6$  in  $D_2O$  at low surfactant concentrations, reproduced from [37]. The isotropic micellar phase (L) and the miscibility gap ( $L' + L''$ ) and an estimate of the Krafft temperature (dashed line) are shown. The overlap concentration  $c^*$  is also shown.

#### *Preparation of Samples*

The solid surfactant is first weighed into the cylindrical sample vial. The required amount of deionised water is then added. The sample is tumbled a few times by hand until the surfactant is dissolved. The colloid is then added from the stock solution. The sample is subsequently put on a vortex mixer for a minute or two and then placed on a tumbler for a few hours to ensure thorough mixing.

### 4.1.3 System B

System B consists of an aqueous solution of  $C_{16}E_6$  and charged polystyrene latex. Three different sizes of particles, with radii 175nm, 105nm and 70nm, have been investigated. A series of these samples with added salt (NaCl) has also been studied.

#### 4.1.4 Preparation of System B

##### *Chemicals*

The chemicals used are the same as those for system A, with the exception of the

colloid. In this case surfactant free polystyrene latices of three sizes were obtained from The Interfacial Dynamics Corporation (IDC), USA. Sodium Chloride (NaCl) (99.5% pure) is also used in some samples in this system and was obtained from Sigma-Aldrich, UK.

#### *Preparation of Samples*

The samples are prepared gravimetrically in the same way as system A. In some cases though solid salt is also added to the surfactant and water before the colloid.

In the study of system B a range of volume fractions of colloid were investigated. The colloid is, however, supplied at a stock volume fraction between  $\phi_c = 0.06$  and 0.08. A method for concentrating the colloid was therefore required for volume fractions above the stock value. Centrifugation of the colloid was attempted, but it the particles were found to irreversibly aggregate. Dialysis with a weight on top of the dialysis bag was also attempted. Whilst this method worked, it would incur large errors for concentrating small amounts of colloid, since much of the colloid was left sticking to the dialysis bag. The most convenient method was found to be that of evaporation. This was carried out for each sample of high volume fraction required. The necessary amount of latex was put into a sample vial, which was then placed in an incubator at 26°C so that the water could slowly evaporate off. The slow evaporation helped to minimise colloid getting stuck to the walls during the evaporation.

#### **4.1.5 System C**

System C is made up of many components. The mixture of the anionic surfactant sodium lauryl ether sulfate (SLES) and the zwitterionic surfactant cocoamidopropylbetaine (CAPB) in water make the wormlike micelles. The wormlike micelle formation is sometimes promoted by either the addition of salt (NaCl) or octanol. Charged polystyrene latices are added to this system in order to investigate its phase behaviour. The SLES is actually SLES2EO with the structure  $C_{12}H_{25}(OC_2H_4)_2-OSO_3Na$ , but is commonly referred to as SLES as will be the case in this thesis. A phase diagram for this surfactant could not be found in the literature. The zwitterion and the salt are added to promote the formation of the wormlike micelles as discussed in section 2.4.3.

### 4.1.6 Preparation of System C

#### *Chemicals*

Stock solutions of industrial grade SLES (concentration=26.4%w/w) and CAPB (30%w/w) were obtained from Unilever. Sodium Azide ( $\text{NaN}_3$ ) was added to the SLES solution as a preservative, and both this and the CAPB were stored in a refrigerator at about 5°C. A small amount of purified (98.7% pure) SLES was also obtained from Henkel KGaA, Germany, and stored in the fridge. Sodium Chloride (99.5% pure) was obtained from Sigma-Aldrich, UK. Deionised water from a Millipore purifier was also used in these samples. Initially the polystyrene latex particles used were supplied by Rhône-Poulenc, France, however, surfactant-free latices were subsequently obtained from The Interfacial Dynamics Corporation, USA. Using the surfactant-free latices means that there would be no surfactant introduced into the solution by the latices and therefore one avoids potential interference with the micellar properties. This could not be ruled out in the case of the latices supplied by Rhône-Poulenc. Some samples contained n-octanol (supplied by Sigma-Aldrich, UK) rather than salt in order to promote the formation of the wormlike micelles.

#### *Preparation of Samples*

The samples were made gravimetrically. The required weights of SLES, CAPB, deionised water and latex were added to the cylindrical sample vial. The sample was tumbled a few times by hand in order to disperse the latex particles throughout the solution. The NaCl was then added from a stock solution (approximately 20%w/w). N-octanol was added in some cases. The salt (or the octanol) was added last as it increases the viscosity of the sample dramatically as discussed in section 2.4.3 and it would then be difficult to mix the colloid thoroughly in the solution of micelles. The samples were shaken rapidly for a minute or two on a vortex mixer and then placed on a tumbler for a few minutes.

### 4.1.7 Errors in Sample Preparation

The main source of uncertainty in sample preparation is through weighing errors. The concentrations of the stock solutions, were used as supplied, will also have some associ-

ated uncertainty. Lastly there may be some impurities present in the chemicals. Most of the products are highly purified, but this could be a problem for the industrial grade products. A quantitative error analysis is carried out in appendix A.

## 4.2 Characterisation of the Colloid

Most of the experimental studies have been done using the charged polystyrene particles obtained from the Interfacial Dynamics Corporation. These latices come well characterised. The information given by IDC is detailed in chapter 5. The conductivities and the critical coagulation concentrations (ccc) of the charged particles were determined as discussed in the following sections. These measurements are only important in the case of charged particles and were therefore not carried out for the polystyrene particles sterically stabilised by PEO groups (system A).

### 4.2.1 Conductivity Measurements

Conductivity measurements are made in order to study the motion of ions in solution. The conductivity,  $\kappa$ , is defined as

$$\kappa = \frac{1}{\rho} = \frac{l}{RA} \quad (4.1)$$

where  $\rho$  is the resistivity,  $R$  is the resistance, and  $l$  and  $A$  are the length and cross-sectional area of the sample respectively. The units of  $\kappa$  are Siemens per metre ( $\text{Sm}^{-1}$ ). The conductivity depends on the number of ions in solution and on their mobilities.

In order to measure the conductivity of a sample the resistance of the sample is measured using a conductivity cell as one arm of a resistance bridge and finding the balance point. It is unreliable to determine  $\kappa$  simply from this measurement and the measurement of the cell dimensions  $l$  and  $A$ . In practice calibration of a solution of known conductivity (usually potassium chloride) is carried out to determine a cell constant  $C$ , where

$$\kappa = \frac{C}{R} \quad (4.2)$$

Conductivity measurements were carried out using a digital conductivity meter via a platinum electrode (Hanna instruments). A solution of potassium chloride (0.01M)

was used to calibrate this meter. It then allows a quick and simple measurement to be taken simply by placing the electrode and a temperature probe into the sample. This was carried out for each batch of charged polystyrene latices used in this study. The stock solutions ( $\phi = 0.06 - 0.08$ ) were diluted gravimetrically using deionised water to  $\phi \approx 0.01$  in steps. The conductivity of the solutions was measured after each dilution.

There will be a weighing error associated with each dilution of the latex solutions. There will also be a reading error with each conductivity measurement.

#### 4.2.2 Critical Coagulation Concentration

The critical coagulation concentration (ccc) is defined as the concentration of electrolyte which is just sufficient to coagulate a lyophobic sol to an arbitrary defined extent in an arbitrarily chosen time [12]. Therefore it is the relative values of the ccc found using the same coagulation criterion that is important rather than the absolute values. The stability of the charged colloidal solutions used in this study with respect to added sodium chloride was determined experimentally. Many samples, over a wide concentration range, were made up in order to determine an initial estimate of the ccc. This range was then narrowed, until a good estimate of the ccc was found. In this study the ccc was determined to be when the colloidal particles aggregated in a timescale of seconds. The particles do however aggregate more slowly with a lower concentration of salt according to the theory of Overbeek (section 2.2.2) [21]. This has also been investigated for one of the batches of colloid. Experimentally a 1% volume fraction solution of the latex particles was made up. To this the required concentration of salt was added and then the sample was shaken. The sample was subsequently observed.

A source of uncertainty in determining the ccc is the weighing error of the latex solution and the added salt. There will also be an associated error with the concentration of the solution of latices. Determining the ccc is also very subjective. However, as it was only necessary to compare the behaviour of the colloids with each other this was not found to be a problem.



### 4.3 Characterisation of Micelles - Rheology

The micellar solutions with no added colloid were characterised by rheology. Entangled wormlike micelles have a monoexponential stress decay as discussed in section 2.4.4.2. Therefore carrying out oscillatory experiments provides information on the entanglement of the micelles (section 4.3.1.2). The viscosities of the solutions have also been determined. The micellar solutions investigated were made as described in section 4.1, but without adding the colloid. The samples were left overnight to equilibrate at  $26 \pm 0.5^\circ\text{C}$  in the case of the  $\text{C}_{16}\text{E}_6$  system (systems A and B) and at  $20 \pm 1^\circ\text{C}$  for the SLES system (system C).

#### 4.3.1 Background

Rheology is defined as the science of deformation and flow [85, 86]. The flow of matter is everywhere in our daily lives; squeezing toothpaste out of the tube, pouring orange juice from the carton, and pouring shampoo out of the bottle are just a few examples. In this section we give a brief introduction to the basis of rheological measurements.

##### 4.3.1.1 Flow

Consider a cube of side  $d$  and area  $A$  deformed under simple shear by a force  $F$  as shown in figure 4.2. A shear stress

$$\sigma = \frac{F}{A} \quad (4.3)$$

is applied and results in a shear strain,  $\gamma$ , which is the relative deformation under shear. One can also define a shear rate,

$$\dot{\gamma} = \frac{v}{d} \quad (4.4)$$

where  $v$  is the relative speed of deformation of the top layer relative to the bottom layer.

The viscosity of a fluid,  $\eta$ , is a measure of its internal resistance to flow deformation and is given by Newton's postulate as,

$$\eta = \frac{\sigma}{\dot{\gamma}} \quad (4.5)$$

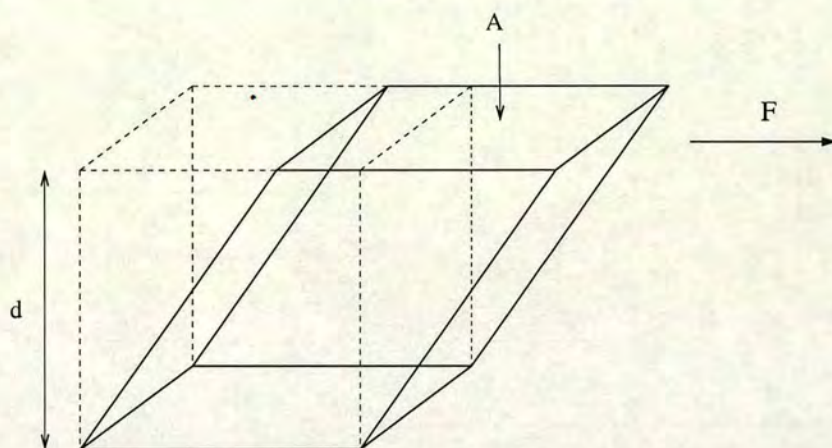


Figure 4.2: The dashed cube, area ( $A$ ) and height ( $d$ ), has been subjected to a simple shear, resulting in the solid rhombohedron. A force,  $F$ , was applied as indicated.

A plot of the shear stress versus the shear rate is known as a “flow curve”. For a Newtonian fluid this is a straight line and therefore the viscosity is constant (figure 4.3). The Newtonian fluid model is an excellent one for most low molecular weight liquids over a very wide range of shear rates. Examples are water and most aqueous solutions, organic liquids, and liquid metals.

Complex fluids, such as concentrated polymer solutions, surfactant solutions and colloidal suspensions are generally non-Newtonian in flow behaviour. Their viscosities are often a function of shear rate (or shear stress) (figure 4.3). If the viscosity decreases with shear rate then the fluid is said to undergo shear-thinning. Conversely, a fluid whose viscosity increases with shear rate exhibits shear-thickening.

#### 4.3.1.2 Oscillation

The behaviour of most substances is dependent on the time-scale on which the stress is applied, e.g. silly putty flows when pulled slowly, but bounces when it is thrown to the ground. When the stress is applied on a short time scale the behaviour is elastic (solid-like) and as the time scale increases one sees increasingly viscous (liquid-like) behaviour. This is an example of a viscoelastic substance. Other examples include glass, shampoo, and toothpaste.

In order to investigate the viscoelastic nature of a substance an oscillatory technique can

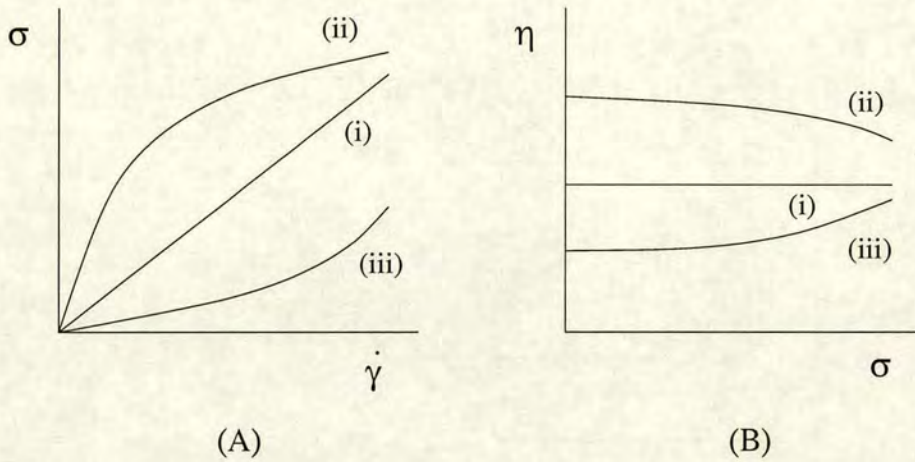


Figure 4.3: (A) Flow diagrams of some common rheological models and (B) shows the corresponding variation of viscosity with shear; (i) Newtonian, (ii) shear thinning and (iii) shear thickening.

be used. The stress is applied in a sinusoidal manner with increasing frequency. This then probes the response of the sample to different time scales. This technique is a non-destructive technique as the sample is simply “wobbled”. It allows the measurement of both the viscous and elastic behaviours of a sample simultaneously.

### Liquids and Solids

Newton’s description of a liquid was introduced in equation 4.5. This model describes the ideal viscous behaviour of fluids. For an applied sinusoidal stress with angular frequency  $\omega$ , and amplitude  $A$ ,

$$\sigma = A \sin \omega t \tag{4.6}$$

a Newtonian liquid produces a sinusoidal strain that is exactly  $90^\circ$  out of phase, with an amplitude denoted by  $B$ ,

$$\gamma = -B \cos \omega t \tag{4.7}$$

A perfectly elastic substance can be modelled by Hooke’s Law. The stress is directly proportional to strain in this case and therefore an applied sinusoidal stress wave (equation 4.6) produces a sinusoidal strain wave that is perfectly in phase,

$$\gamma = B \sin \omega t \tag{4.8}$$

Viscoelastic materials exhibit both elastic and viscous properties to varying degrees.

Therefore when a viscoelastic material is subjected to a sinusoidal stress the resulting strain is out of phase by more than  $0^\circ$  and by less than  $90^\circ$ .

### *Linear Viscoelasticity*

A more general treatment of the viscoelasticity of materials subject to small deformations is given by linear viscoelastic theory [85], where the resulting stress produced by a small step strain at time  $t = 0$  is given by,

$$\sigma(t) = G(t)\gamma \quad (4.9)$$

where  $G(t)$  is the time dependent relaxation modulus. To each incremental strain  $d\gamma(t')$  applied prior to time  $t$  there is a corresponding incremental stress  $d\sigma(t) = G(t - t')d\gamma(t')$ . Assuming the material has time translation invariance (where the material properties are time-independent) then,

$$\sigma(t) = \int_{-\infty}^t G(t - t') \frac{d\gamma}{dt'} dt' \quad (4.10)$$

This is the linearised constitutive equation between shear strain  $\gamma(t)$  and stress  $\sigma(t)$ .

One investigates the linear shear viscoelasticity by applying a small-amplitude oscillatory shear,

$$\gamma(t) = \gamma_0 \exp(i\omega t) \quad (4.11)$$

where  $\omega$  is the frequency and  $\gamma_0$  is the strain amplitude. The corresponding strain rate is thus,

$$\dot{\gamma} = i\omega_0\gamma_0 \exp(i\omega t) \quad (4.12)$$

Substituting equation 4.12 into equation 4.10 gives,

$$\sigma(t) = \int_{-\infty}^t G(t - t') \gamma_0 i\omega \exp(i\omega t') dt' \quad (4.13)$$

which can be simplified by changing the variables ( $t'' = t - t'$ ) to

$$\sigma(t) = \gamma_0 G^*(\omega) \exp(i\omega t) = \gamma(t) G^*(\omega) \quad (4.14)$$

where the complex modulus,  $G^*$  is defined by

$$G^* = i\omega \int_0^\infty G(t'') \exp(-i\omega t'') dt'' \quad (4.15)$$

It can therefore be seen that the stress will be simple harmonic at frequency  $\omega$ , but not necessarily in phase with the strain. It is customary to express  $G^*$  as,

$$G^* = G' + iG'' \quad (4.16)$$

where  $G'$  is the storage modulus and provides information on the in-phase (elastic) part of the modulus and  $G''$  is the loss modulus providing information on the out-of-phase (viscous) component. In general both parts will be frequency-dependent, crossing over from viscous behaviour at low frequencies to elastic behaviour at high frequencies.

As discussed in section 2.4.4.2 wormlike micelles have a monoexponential stress decay, with one relaxation time  $\tau$  and therefore have a relaxation modulus of,

$$G(t) = G_0 \exp(-t/\tau) \quad (4.17)$$

where  $\tau$  is the relaxation time. This corresponds to a Maxwell model, which can be considered as a hookean spring and a newtonian dashpot connected in series. This is the simplest model of a viscoelastic fluid and by integrating equation 4.15 one finds a storage and loss modulus of,

$$G'(\omega) = \frac{G_0 \omega^2 \tau^2}{1 + \omega^2 \tau^2} \quad (4.18)$$

and

$$G''(\omega) = \frac{G_0 \omega \tau}{1 + \omega^2 \tau^2} \quad (4.19)$$

respectively. The relaxation or Maxwell time  $\tau$  is found to be the inverse of the frequency at which curves for  $G'$  and  $G''$  cross (figure 4.4).

A so called ‘‘Cole-Cole’’ plot can be drawn, where  $G''$  is plotted against  $G'$  with frequency parametrically eliminated. This gives a perfect semicircle for a Maxwell fluid and therefore is a convenient way to plot this information.

### 4.3.2 Apparatus and Technique

Rheological measurements were carried out using a TA Carrimed CSL<sup>2</sup>100 rheometer. This instrument can be either stress or strain rate controlled. The latter, however, is done by adjusting the stress to give the required shear rate via a feedback mechanism. This can potentially cause some problems. The rheometer consists of an electronically

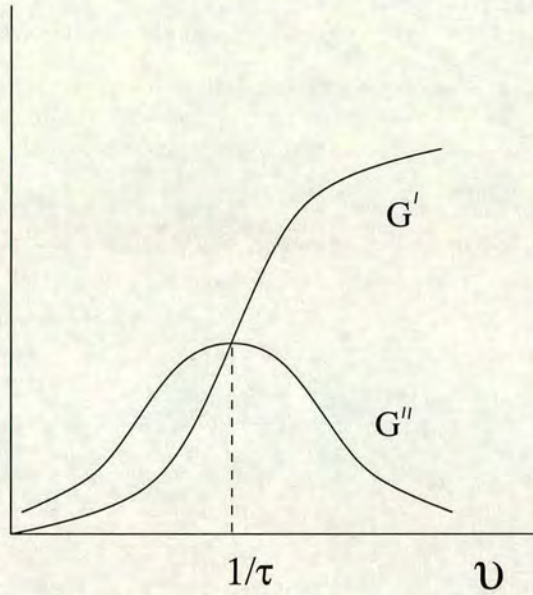


Figure 4.4: Frequency dependence of  $G'$  and  $G''$  for a Maxwell fluid.

controlled induction motor, that drives a spindle to which the chosen geometry is attached. All rotating parts of the instrument are supported by an air bearing in order to minimise the friction effects. A shear stress (or shear strain) is applied and then the subsequent angular displacement is measured by an optical device consisting of a light source and a photo-cell arranged either side of a transparent disc attached to the drive shaft. This is a very sensitive device that can measure movements down to  $2.5\mu rad$ . The software then calculates the strain in the system. The sample is temperature controlled by a Peltier plate system. This allows rapid control of the temperature in a range of  $-10^{\circ}C$  to  $99^{\circ}C$ .

Various geometries can be attached to the rheometer, such as the concentric cylinder, parallel plate, and the cone and plate geometry. The measurements carried out in this work have all been done using a cone and plate with a diameter of 6cm and an angle of  $2^{\circ}$ . The rheometer with this type of geometry attached is illustrated in figure 4.5. The shear rate at a radius  $r$  is given by,

$$\dot{\gamma} = \frac{r\omega}{r \tan \alpha} = \frac{\omega}{\tan \alpha} \quad (4.20)$$

where  $\omega$  is the angular velocity, and  $\alpha$  is the cone angle as shown in figure 4.5. At small angles this expression simplifies to,

$$\dot{\gamma} = \frac{\omega}{\alpha} \quad (4.21)$$

The cone and plate geometry therefore provides a shear rate that is the same everywhere in the liquid provided that the gap angle is small.

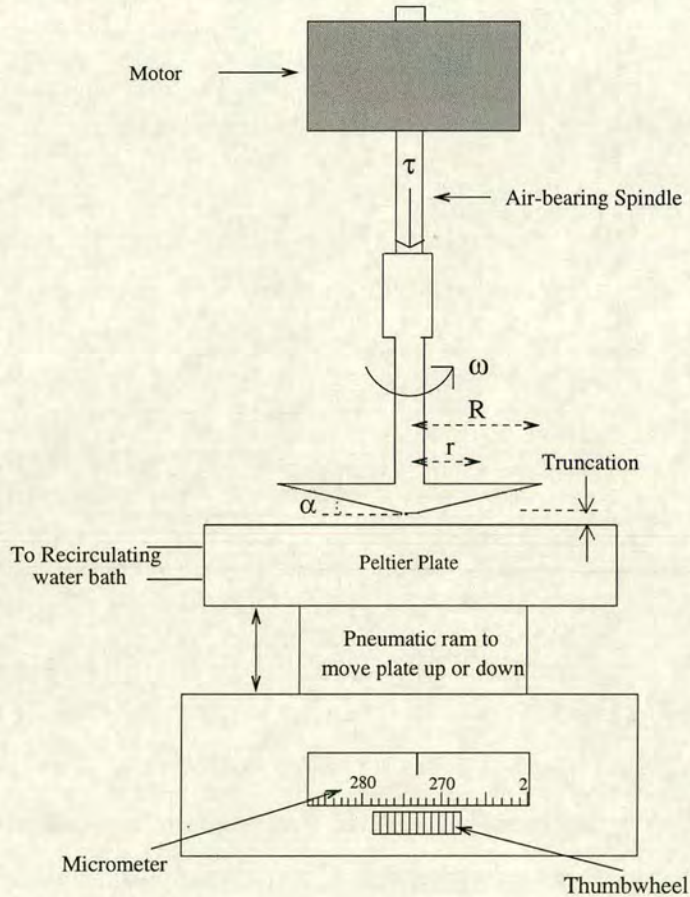


Figure 4.5: Schematic diagram showing the cone and plate geometry attached to the rheometer. The cone is actually truncated with the imaginary tip of the cone just touching the plate. The cone of radius  $R$  and angle  $\alpha$  is subjected to a torque  $\tau$  that results in an angular velocity  $\omega$ .

Once the cone and plate geometry is attached to the rheometer the correct gap between the truncated cone and plate must be set. This corresponds to the (imaginary) apex of the cone just touching the plate. This is done using a deceleration method. A small stress is applied to the cone to set it spinning slowly. The plate is then raised slowly by turning the micrometer thumbwheel (see figure 4.5). This is continued until the geometry no longer spins and then the micrometer reading is taken. The plate is then wound down again by a few hundred microns. With this rough estimate of the zero-point the procedure is repeated, this time more slowly in order to find a more accurate zero-point reading. The plate should then be lowered again by an amount corresponding to the truncation of the cone. For instance, in the case of the 6cm,  $2^\circ$

cone the truncation is  $60\mu\text{m}$ , and therefore with a zero point reading of  $213\mu\text{m}$ , found using the deceleration method described, the micrometer should be set at  $273\mu\text{m}$ . When setting this value, the micrometer should be wound down past this value by about  $50\mu\text{m}$  and approached in the upward direction to eliminate any backlash problems in the screw threads. Setting the gap must be carried out carefully as it is a potential source of error.

Once the gap has been set the ram that the plate sits on is lowered to allow the sample to be loaded. The sample must be loaded correctly otherwise errors will ensue. This is, however, a difficult task and requires a lot of practice. In figure 4.6 a correctly loaded sample is shown alongside one which is overfilled and one which is underfilled. The errors induced by incorrect loading are known as “edge effects”, and their magnitude are highly dependent on the sample properties. Generally if the gap is overfilled (figure 4.6(B)), then some of the excess sample may migrate and sit on top of the geometry. When the sample has a low viscosity this becomes less of a problem and the errors are much reduced. If the gap is underfilled (figure 4.6(C)), the diameter of the geometry is effectively reduced. This will introduce more serious errors than overfilling and should therefore be avoided.

Commonly a syringe or a pipette are used to load a sample onto the rheometer correctly, since the volume required for correct filling can be accurately found and subsequently reproduced time after time. This was carried out for samples of the nonionic surfactant system, but for the ionic surfactant system an alternative method had to be found as the samples are highly viscous and easily go very bubbly. The presence of lots of air bubbles could seriously affect the results. In this case the sample was therefore spooned onto the plate using a spatula. This was more difficult to carry out in a reproducible way than using a syringe, however, with practice a good filling was achieved. There will be some errors arising due to the accuracy of the filling. This cannot, however, be quantified. Experiments were therefore repeated to take account of variations in the fillings.

The viscoelastic nature of the micelles was investigated using an oscillatory shear. A preshear of  $2\text{Pa}$  for 30 seconds was applied in order to remove any history effects due to the loading procedure. A 5% strain oscillatory shear with increasing frequency ( $0.01\text{Hz}$  to  $40\text{Hz}$ ) was applied. This type of experiment allows both the elastic modulus and loss



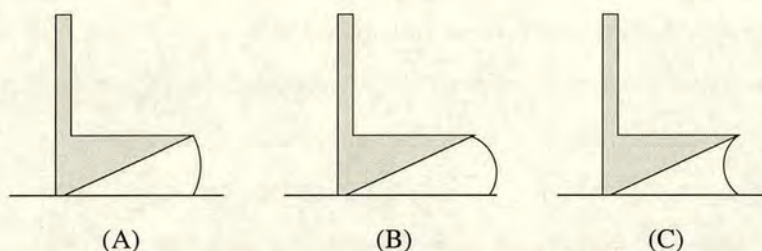


Figure 4.6: Schematic diagram showing the filling of a cone and plate geometry. (A) is correctly filled, (B) is overfilled and (C) is underfilled. Errors are induced if the sample is not loaded correctly.

modulus to be found as a function of frequency. Since the theoretical models of semi-dilute wormlike micelles predicts that the viscoelastic nature of the micelles will fit a Maxwell model (sections 2.4.4.2 and 4.3.1.2), these measurements can allow us to find the crossover to entangled wormlike micelles where Maxwell behaviour is expected. The results can be fitted to a Maxwell model and a viscosity and a relaxation time determined.

The viscosity of the micellar solutions which are not Maxwellian was measured by applying a shear stress to the sample in the linear regime and measuring the shear rate. The linear regime is the low stress part of the flow curve, where the viscosity does not vary with the applied stress (figure 4.3).

#### 4.4 Phase Studies

Samples of systems A and B are prepared as described in section 4.1 and are placed in an incubator at  $26 \pm 0.5^\circ\text{C}$  where they are observed over a period of weeks. The phase study is carried out at  $26^\circ\text{C}$ , above the Krafft temperature (figure 4.1) to ensure the surfactant is soluble, but the temperature is not too high as evidence of branching of the wormlike micelles at higher temperatures has been found [87]. The surfactant  $\text{C}_{16}\text{E}_6$  could only be kept at this temperature for a couple of months before it degraded.

The Krafft temperature of the SLES system is lower than room temperature and therefore the phase samples of system C (prepared as described in section 4.1) were stored in a temperature controlled room at  $20 \pm 1^\circ\text{C}$  and monitored over several months.

In both systems the evaporation of water from the sealed sample vials was determined to be negligible at the temperatures used.

Phase separation in these systems is easily determined by eye as there is a large refractive index mismatch between the polystyrene particles ( $n = 1.591$  at  $20^\circ$ [88]) and the aqueous micellar solution ( $n = 1.33$  at  $20^\circ$ [89]) and thus the solution appears white. If the mixture separates into colloid-rich and colloid-poor phases as has been found for colloids in many mixtures (see chapter 3) a white phase and a slightly cloudy phase would be observed. Note that the micellar solutions without added colloid appear transparent.

## 4.5 Direct Observations

Colloidal particle gels in colloid-polymer mixtures have been extensively studied by Meeker [62] and Starrs [63]. As discussed in section 3.1.4, it has been found that they collapse under gravity in a characteristic manner. There is a delay period, followed by a rapid collapse and then a compaction period. This is known as delayed sedimentation. In order to ascertain whether any of the phase behaviour of colloid-wormlike micelle mixtures mimics this colloid-polymer gel collapse, direct observations of the phase separation were carried out.

Initially the samples that had been used for the phase study of the SLES system were homogenised by a few minutes of vigorous shaking and subsequent tumbling. However when these experiments were repeated, it was found that there was a problem with their reproducibility. Samples which had been well homogenised, even tumbling them overnight, could show differences in their separation behaviour. The delay times etc. could be changed considerably and occasionally there was a changeover from delayed sedimentation to creeping behaviour. The samples, even though they look homogeneous, may contain small aggregates and depending exactly how well the homogenisation process works this may affect the way the colloid behaves. It was therefore decided to make up fresh samples before each observation was carried out in order to minimise the differences found in their sedimentation behaviours. These samples were made up as detailed in section 4.1.6. It should also be noted that the observations are carried

out using the same sized sample vials and constant volume of sample in order to avoid observing size dependent behaviour (section 3.1.4).

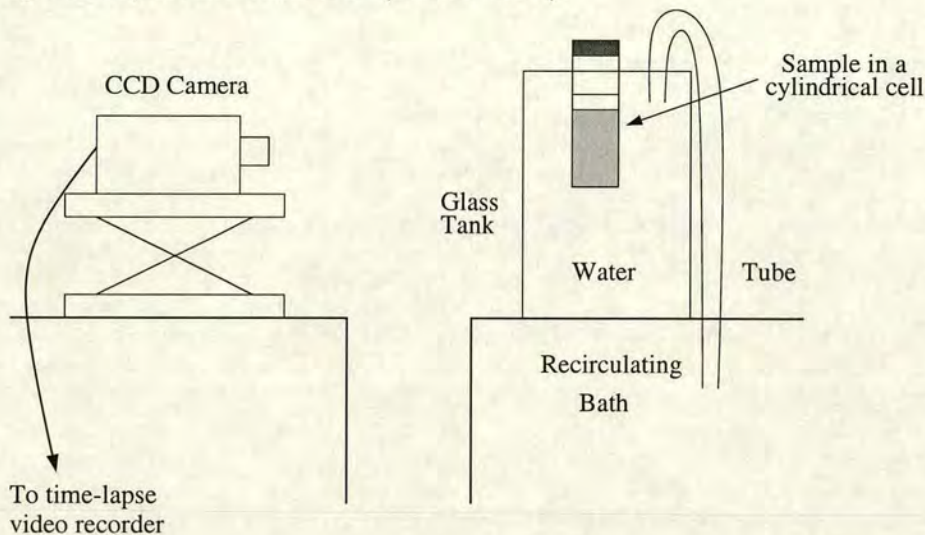


Figure 4.7: Schematic diagram illustrating the direct observation set-up. The sample is placed into a temperature-controlled tank of water that is connected to a recirculating water bath. A CCD camera connected to a time-lapse video recorder is used to record the phase separation of the sample into colloid-rich and colloid-poor phases, as illustrated.

The observations were carried out using the apparatus shown in figure 4.7. The samples were illuminated either from behind in order to see details of the separation or from the front allowing only the sediment height versus time to be found. These observations were carried out in order to ascertain where the crossover of equilibrium phase separation to transient gelation occurs in the SLES/H<sub>2</sub>O/NaCl and SLES/CAPB/NaCl phase diagrams (figures 7.1 and 7.24) A more detailed study was also carried out for one concentration of surfactant and a varying salt concentration.

The sediment height against time taken from the videotapes, is measured directly from the television screen using a ruler. The sediment height from the bottom of the sample to the bottom of the meniscus is measured. The error in this measurement is  $\pm 1$ mm. There is no error in the time at which the measurement is taken, since the video can be paused at the required time. A few points should be noted. Firstly the time delay in putting the sample in the holder and setting up the lighting correctly to begin recording is assumed negligible on the time scale of the separation \*. Secondly in the SLES system the samples are very bubbly after mixing. It therefore takes a few hours

\*the separation takes place on the time-scale of days

for these bubbles to disperse from above and around the meniscus. There is therefore little data for the first few hours of separation and the height of the sample must be measured after the bubbles have disappeared. Thirdly there is a magnification factor introduced by measuring the heights from a large TV screen. This magnification factor is, however, ignored since all the experiments were carried out in the same way and only a comparison between behaviours was required. Similar measurements were carried out on freshly made samples of the  $C_{16}E_6$  system. These samples were not very bubbly after being shaken.

## 4.6 Diffusing Wave Spectroscopy

### 4.6.1 Background

The scattering of light takes place when the electric field of incident light induces a dipole moment in a molecule of a material. This oscillating dipole then reradiates or scatters the light. Most objects in nature scatter visible light strongly. The colours of e.g. flowers, woods and rocks come from strong scattering of light combined with substantial absorption of light of different wavelengths in the visible spectrum. The sky is blue as a result of scattering of white light from molecules in the air. The blue colour is then a result of light of lower wavelengths scattering more than those of high wavelengths. The scattering power of a small particle has a wavelength dependence of  $\lambda^{-4}$  [90].

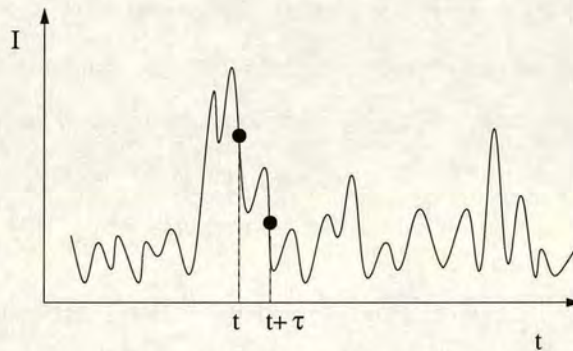


Figure 4.8: Schematic diagram of an intensity trace against time for a light scattering experiment. The dynamics of the system is followed by finding a time correlation function which compares the signal at time  $t$  and a later time  $t + \tau$ , where  $\tau$  is the delay time.

Light scattering has been used extensively in the study of colloidal systems. Static light scattering (SLS) has been used to accurately determine the sizes of colloids and dynamic light scattering (DLS) has been used to investigate dynamics [33, 90]. The scattered photons have undergone phase changes as a result of the scattering events and therefore interfere to produce a highly irregular intensity pattern, known as a “speckle pattern”. As the particles move with respect to one another the intensity of a given speckle fluctuates with time (figure 4.8). The average fluctuation time of a random signal can be determined by calculating a time correlation function (TCF). This is a general technique employed when investigating dynamics using scattering techniques. A TCF compares a delayed version of a signal with the signal itself as shown in figure 4.8. The TCF is defined as follows,

$$\langle I(t)I(t+\tau) \rangle = \lim_{T \rightarrow \infty} \frac{1}{T} \int_0^T I(t)I(t+\tau) dt \quad (4.22)$$

where  $\tau$  is the delay time and  $T$  is long compared with the time scale of the fluctuations. The normalised intensity correlation function,  $g^{(2)}(\tau) = \frac{\langle I(t)I(t+\tau) \rangle}{\langle I(t) \rangle^2}$ , is the experimentally determined quantity and can be related to the correlation function of the electric field,  $g^{(1)}(\tau) = \frac{\langle E(t)E^*(t+\tau) \rangle}{\langle |E(t)|^2 \rangle}$  for a scattered field  $E_s$  following Gaussian statistics, by the Siegert relation [90],

$$g^{(2)}(\tau) = 1 + [g^{(1)}(\tau)]^2 \quad (4.23)$$

The problem with DLS is that the system studied must be almost transparent, eliminating most of the multiple scattering. This is often achieved by matching the refractive index of the colloid to that of the solvent. This is not always possible though and many everyday colloidal suspensions are strongly multiply scattering, such as paint and milk. For slightly turbid systems a technique using two laser beams of different wavelengths, two-colour dynamic light scattering (TC-DLS), can be used. The lasers and optics are aligned in such a way as to eliminate multiply scattered light by cross correlating the scattering intensity from two beams of different wavelength [91].

A technique making use of the multiple scattering called Diffusing-Wave Spectroscopy (DWS) has been recently developed [92, 93]. A source of coherent light (a laser) is incident on a multiply scattering colloidal sample. The photons are then scattered by the colloidal particles several times,  $N$ , before exiting the sample, as illustrated in figure 4.9. For  $N \gg 1$  paths of a photon can be described as random walks

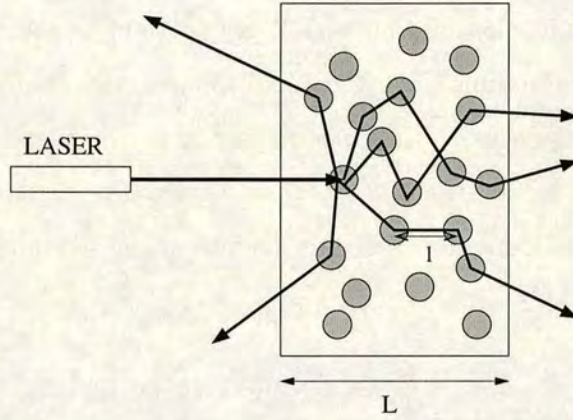


Figure 4.9: Schematic diagram illustrating multiple scattering of light in a colloidal suspension.

with step length  $l^*$ . DWS is therefore independent of the scattering wavevector.  $l^*$  is known as the transport mean free path of the photon and it is the length scale over which the light loses “memory” of its initial direction of propagation. For small particles that scatter isotropically  $l^* \approx l$ , where  $l$  is the mean distance between scattering events (figure 4.9), but for larger particles which preferentially scatter in the forwards direction  $l^* > l$ . The exiting beams again interfere to produce a speckle pattern and the dynamics are followed by TCF’s.

The field correlation function,  $g^{(1)}(\tau)$ , is related to the relaxation processes of the scattering medium. It is found by summing over all scattering paths,  $p$ , as follows [92],

$$g^{(1)}(\tau) = \left\langle \sum_p \frac{\langle I_p \rangle}{\langle I \rangle} \exp(i\Delta\phi_p(\tau)) \right\rangle \quad (4.24)$$

where  $I_p$  is the intensity of path  $p$  and  $\Delta\phi_p(\tau)$  is the phase change of light associated with this path, or more explicitly,

$$\Delta\phi_p(\tau) = \sum_{n=i}^N \mathbf{q}_i \Delta\mathbf{r}_i(t) \quad (4.25)$$

where  $\sum_{n=i}^N$  is a sum over all scattering events in path  $p$ ,  $\mathbf{q}_i$  is the scattering wavevector of the  $i$ th scattering event and  $\Delta\mathbf{r}_i(t)$  is the displacement of scatterer  $i$  ( $\Delta\mathbf{r}_i(t) = \mathbf{r}_i(t) - \mathbf{r}_i(0)$ ).

Each phase change is therefore the sum of all the individual phase changes due to each scattering event in this path. DWS can therefore be used to probe very small motion since small motions of each scatterer add up to a total phase shift of order 1. It is

assumed that the distribution of phases  $\Delta\phi_n$  for paths of length  $n$  is Gaussian. This is a reasonable approximation since the phase is a sum of many random variables. The contribution of all paths to the correlation function is then found and assuming the diffusion equation is valid for the transport of light in the medium, the following expression can be found (the details of this derivation can be found in [92]),

$$\begin{aligned} g^{(1)}(\tau) &= \int_0^\infty P(s) \exp\left(-\frac{1}{3}\langle\Delta r^2(\tau)\rangle s/l^*\right) ds \\ &= \int_0^\infty P(s) \exp(-2Dk^2\tau s/l^*) ds \end{aligned} \tag{4.26}$$

where the second equality is valid for a sample of freely diffusing scatterers with  $P(s)$  the probability of paths of length  $s$ ,  $D$  the diffusion constant, and  $k = 2\pi\eta/\lambda$  the scattering vector.  $P(s)$  depends mainly on the geometry of the scattering sample, the characteristics of the incident beam (focused or extended) and the detection geometry (transmission or backscattering). The expressions for  $P(s)$  and their derivations in these cases can be found in reference [92].

DWS is therefore a complementary technique to DLS and TCDLS since it provides a way of finding quantitative information about particle displacements in the strongly multiply scattering regime. This property allows DWS to be used when investigating concentrated colloidal suspensions. DWS is also much more sensitive to small motions of the scatterers and thus fast time scales, than DLS as mentioned earlier. An added bonus of using DWS is the relatively simple experimental set-up compared to DLS, which is much more sensitive to misalignment than DWS.

## 4.6.2 Experimental Procedure

## 4.6.3 Ergodicity Measurements

### 4.6.3.1 Background

In order to determine whether phases of samples were fluid or gel-like DWS was employed to investigate the ergodicity of the sample. Fluid samples will be ergodic and can therefore explore the entire space of the sample. Gels are non-ergodic, therefore, probing different parts of the sample will result in different intensities and time-averaged

intensity correlation functions (TICF). For non-ergodic systems the time averages and the ensemble averages are therefore not the same, since the time evolution of the system will not lead to all of the statistically possible configurations of particles.

In an ergodic system the limiting values of the TICF's are  $g^{(2)}(q, t = 0) = 2$  and  $g^{(2)}(q, t = \infty) = 1$ . In the case of non-ergodic systems, such as gels or glasses, the long time limit of  $g^{(2)}(\tau)$  is greater than 1 due to the frozen fluctuations which result in a constant part of the scattered intensity. Various methods have therefore been developed in order to find the ensemble average of the systems.

The most simple, but tedious, method for finding the ensemble averaged ICF is simply moving the sample through a series of positions and averaging [94]. An alternative method has been developed by Pusey and van Megen [95], where the ensemble average can be found at a single position. By finding a position where the time-average intensity is the same as the ensemble-average intensity, then the ensemble-averaged correlation function can be easily deduced from the measured TICF. A third method can be employed, where the sample is slowly rotated continuously as the correlation function is measured [96]. Once the decay of the correlation function due to the movement is removed one has the ensemble averaged correlation function.

The method employed in order to determine whether the phase of the sample in this experimental investigation were ergodic or not was the first method. The ensemble averaged correlation function was not required, only whether the phase was ergodic or not. The sample was therefore moved through a number of positions as detailed in the following section. However, to find a true ensemble average would have required longer experiments probing more of the sample.

#### 4.6.3.2 Apparatus & Technique

The apparatus used to investigate the ergodicity of the sample is shown in figure 4.10. Coherent light, of wavelength  $\lambda = 514.5\text{nm}$  from an argon ion laser is directed into the sample. The sample cell sits in a solvent bath of toluene, in a temperature controlled jacket. The sample multiply scatters the incident beam, and the photomultiplier tube (PMT) is used to detect the light a couple of degrees off transmission via a GRIN (GRa-



dient INdex) lens and a single mode fibre. The GRIN lens focuses the scattered light in the entrance of the fibre which carries it to the PMT. Detection just off transmission does not affect the correlation function, since DWS is independent of angle. A polariser is used to measure the horizontally polarised part of the scattered light. By choosing to detect only one direction of polarisation the contrast is increased. The signal detected by the PMT is then correlated by an ALV-5000 correlator (ALV, Germany).

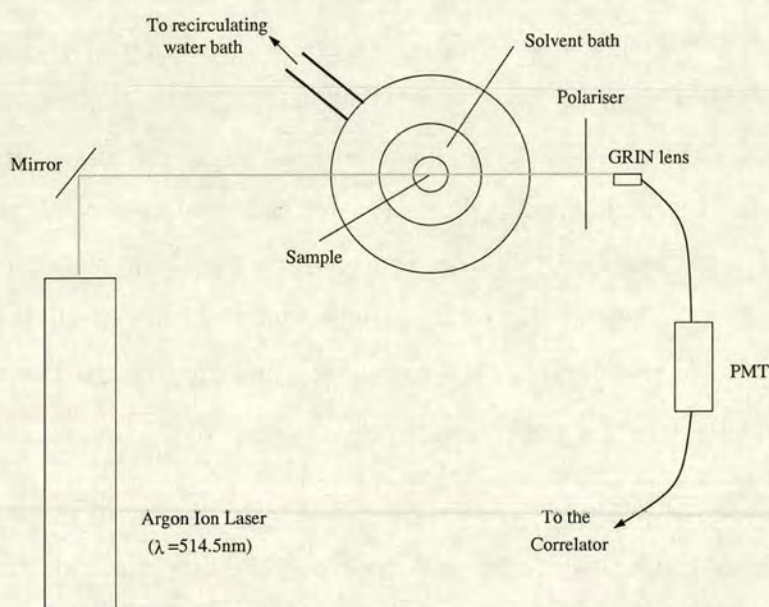


Figure 4.10: DWS set-up for ergodicity measurements. The sample is placed in a bath of toluene which is temperature controlled by recirculating water. The transmitted light is detected by a PMT via a GRIN lens.

Samples of system B were investigated using this method. The samples were placed in the solvent bath at 26°C. The laser intensity used in these measurements was 100mW. Their TICF was measured for 10 different positions of the sample for 1000 seconds each, and an ensemble average of these measurements was calculated. This is not a sufficient number of measurements for a true ensemble average to be found. It is, however, sufficient to determine whether a phase is ergodic or not. This will be discussed in further detail in chapter 6.

#### 4.6.4 DWS During Gel Collapse

The collapse of colloid-polymer gels was discussed in section 3.1.4. Index matched colloid-polymer gels have been found to form inhomogeneities such as channels prior to the rapid collapse. Do the particle dynamics have a characteristic behaviour prior to collapse? Investigations of gels found in system C have been carried out in order to answer this question.

##### 4.6.4.1 Apparatus & Technique

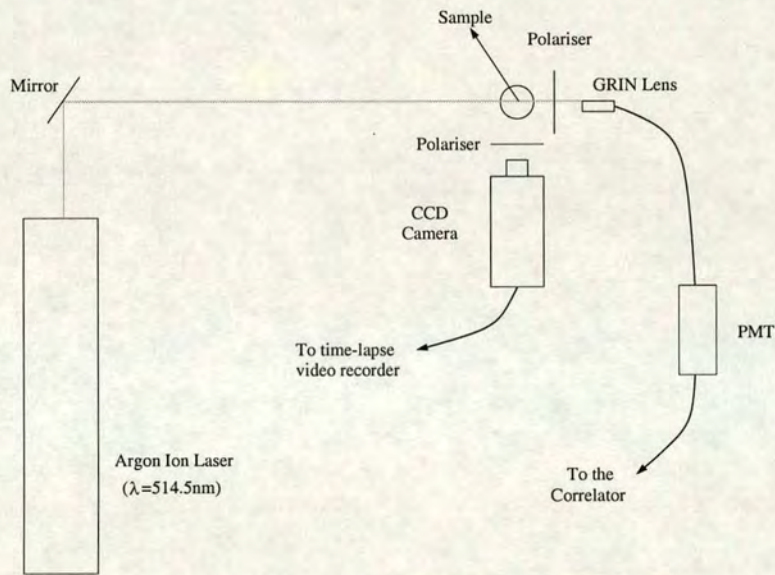


Figure 4.11: DWS set-up to follow gel-collapse. As the gel collapses the scattered light just off transmission is measured by a PMT via a GRIN lens. At the same time the gel collapse is being recorded by a CCD camera connected to a time-lapse video recorder.

The apparatus used in this investigation is similar to that used when probing the ergodicity of the phase samples. It is shown in figure 4.11. The difference with this set up is that the sample is not placed in a temperature controlled solvent bath. Instead the sample is simply placed directly in the beam. The room in which the apparatus is housed is temperature controlled at  $19 \pm 1^\circ\text{C}$ . A CCD camera attached to a time-lapse video recorder is used to visually observe the gel collapse simultaneously with the measurement of the correlation function via the PMT. The TICFs are found by averaging over 15 minutes or 30 minutes depending on the intensity of the signal. The laser intensity used was 50mW. The experiment was allowed to run for a few days, as

the gel was collapsing. It was particularly important in this experiment to measure the scattered light just off transmission since the gel collapse leaves a fairly transparent phase behind which will allow high transmission of light through it and could potentially damage the PMT.

## Chapter 5

# Characterisation of Components

In this chapter the characterisation of the individual components of systems A, B and C are discussed. This information is required in order to help interpret the phase diagrams in chapters 6 and 7.

### 5.1 Characterisation of Colloid

#### 5.1.1 Surfactant-free (IDC) Latices

The main studies in this thesis have been carried out using the well-characterised surfactant-free polystyrene latices from the Interfacial Dynamics Corporation. These latices have, therefore, been studied in more detail than the other colloidal particles used. The main results are discussed in the subsequent sections.

##### 5.1.1.1 *Data from IDC*

The main information on the particles, given by IDC [88], for the four different sizes of particles used is presented in table 5.1.

Table 5.1: Characteristics of surfactant-free charged polystyrene latices.

Particle Radius / nm ( $a$ )	190	175	105	70
Radius Polydispersity / %	3.5	3.4	5.3	2.3
Concentration of Stock Solution / $\text{gcm}^{-3}$	$7.9 \pm 0.1$	$6.0 \pm 0.1$	$8.1 \pm 0.1$	$8.1 \pm 0.1$
Charge Groups per particle ( $z_c$ )	4.1E4	2.8E4	2.0E4	3.1E3

### 5.1.1.2 Calculation of the Screening Length

The data from IDC in table 5.1 can be used to find an estimate of the screening length,  $\kappa^{-1}$ , of the particles in solution. The equation for the screening length, as discussed in section 2.2.2 is,

$$\kappa = \left( \frac{2e^2 n_0 z^2}{\epsilon \epsilon_0 kT} \right)^{1/2} \quad (5.1)$$

Assuming that the deionised water contribution to the screening length is negligible and that the charged groups on the surface of the colloid are fully dissociated then the screening length can be found using the following equation,

$$\kappa = \left( \frac{e^2 z_c \phi}{\epsilon \epsilon_0 kT \frac{4\pi}{3} a^3} \right)^{1/2} \quad (5.2)$$

where  $z_c$  is the number of charge groups per particle of radius  $a$ , and  $\phi$  is the volume fraction of the particles. The values of the Debye screening length calculated in this way are tabulated in 5.2 for the 4 different sizes of IDC latex particles used in our studies.

The values of  $\kappa^{-1}$  found in this way are likely to be poor estimates of the true screening length in the colloidal solutions. The assumption of full dissociation of the charged groups on the particles is doubtful and the solution is likely to contain some salt ions left over from the synthesis of the colloidal particles. A more direct method for finding an estimate of the screening lengths was therefore required. This was done via conductivity measurements as detailed in the following section.

Table 5.2: Debye screening lengths ( $\kappa^{-1}$ ) for IDC latices based on the concentration of counterions, calculated using equation 5.2.

Colloidal Radius /nm	$\kappa^{-1}/nm$				
	<i>Colloidal Volume Fraction</i>				
	<i>0.01</i>	<i>0.02</i>	<i>0.03</i>	<i>0.04</i>	<i>0.05</i>
190	88.5	62.7	51.2	44.4	39.7
175	94.5	67.0	54.7	47.4	42.4
105	52.1	36.9	30.1	26.1	23.3
70	72.0	50.9	41.6	36.0	32.2

### 5.1.1.3 Conductivity Measurements

The conductivity of each IDC latex stock solution was measured as detailed in section 4.2.1. The conductivity of successive dilutions of the stock solutions was found. The graph of conductivity as a function of volume fraction of colloid for each colloid size is shown in figure 5.1. The error in the volume fraction from the dilution of the stock solution is within the size of the data point. The uncertainty in the measurement of the conductivity is plotted as error bars where it is larger than the data point.

It can be seen that there is a substantial difference in the levels of conductivity between the different sizes of latex particles. Solutions of 190nm radius particles, have significantly higher conductivities than the other sizes. For the 175nm and 70nm radius particles the conductivity is small and as the solutions are diluted it levels off to approximately the value of the conductivity of deionised water, which was determined to be about  $18 \pm 0.5 \mu S$ .

As well as the conductivity of various dilutions of the colloidal stock solutions, the conductivities of various concentrations of NaCl solutions were also measured (figure 5.2). The uncertainty in the concentration of the solution is negligible as the weighing errors incurred when making up each solution are very small. The uncertainty in the conductivity reading is shown by the plotted error bars.

CHAPTER 5: CHARACTERISATION OF COMPONENTS

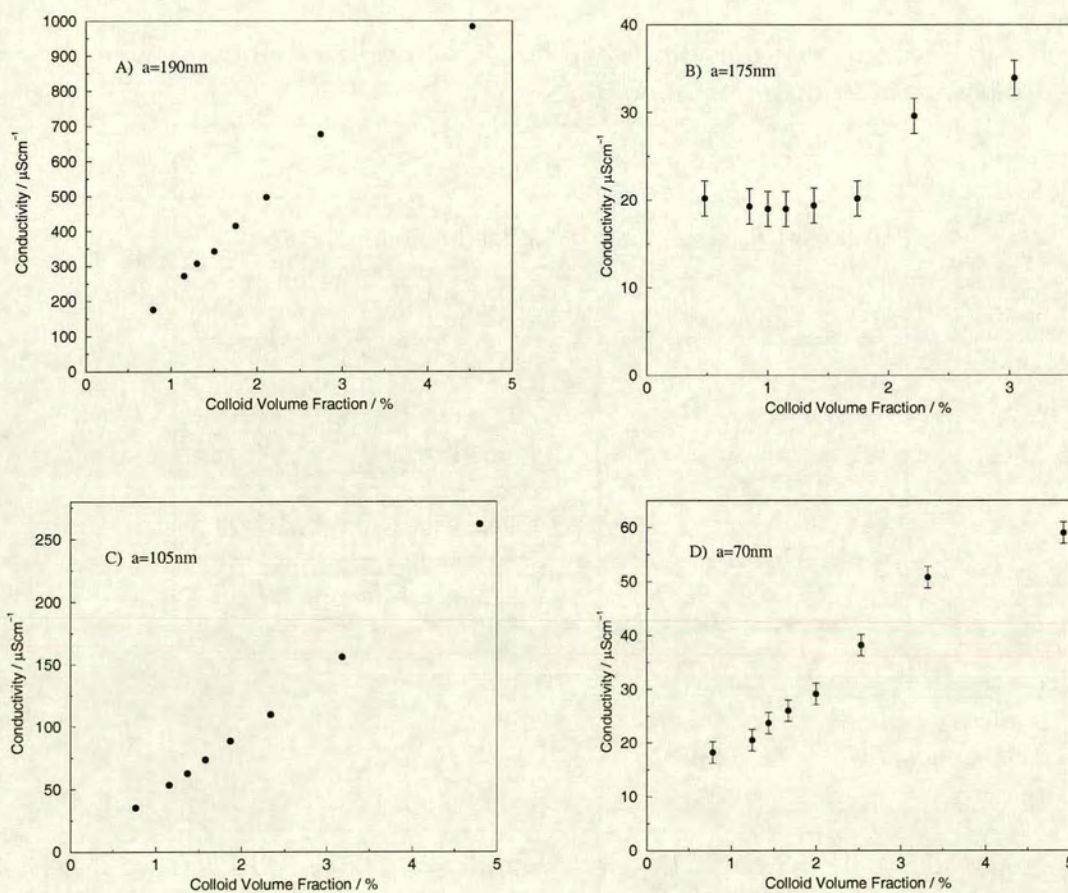


Figure 5.1: Plot of conductivity against volume fraction for the four different sizes of IDC polystyrene latex solutions. The sizes of the particles are indicated on the graphs.

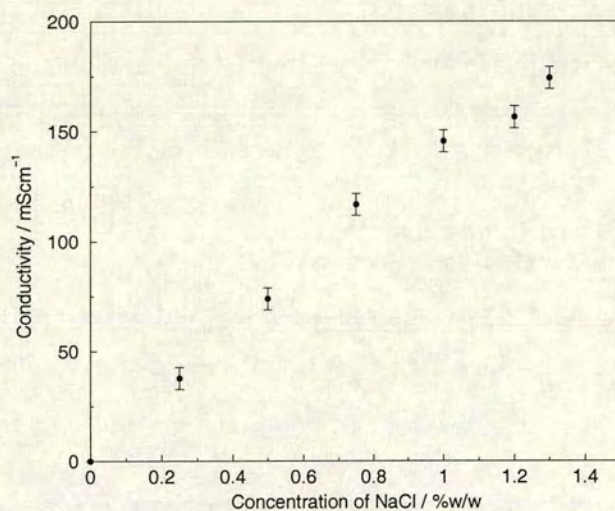


Figure 5.2: Plot of conductivity against concentration of a NaCl solution

## 5.1: CHARACTERISATION OF COLLOID

The conductivity of the NaCl solution was used as a standard so that a value of the screening length for the colloidal suspensions could be determined. This was done by fitting a straight line to the points in figure 5.2. The gradient of the fitted line through the origin is  $140 \pm 5$ . An equivalent NaCl concentration for each volume fraction of the colloidal suspensions was found using their conductivity measurements and this gradient. From this equivalent NaCl concentration a value of the screening length can simply be calculated using equation 5.1. The screening lengths calculated in this way are plotted for each size of latices as a function of volume fraction in figure 5.3.

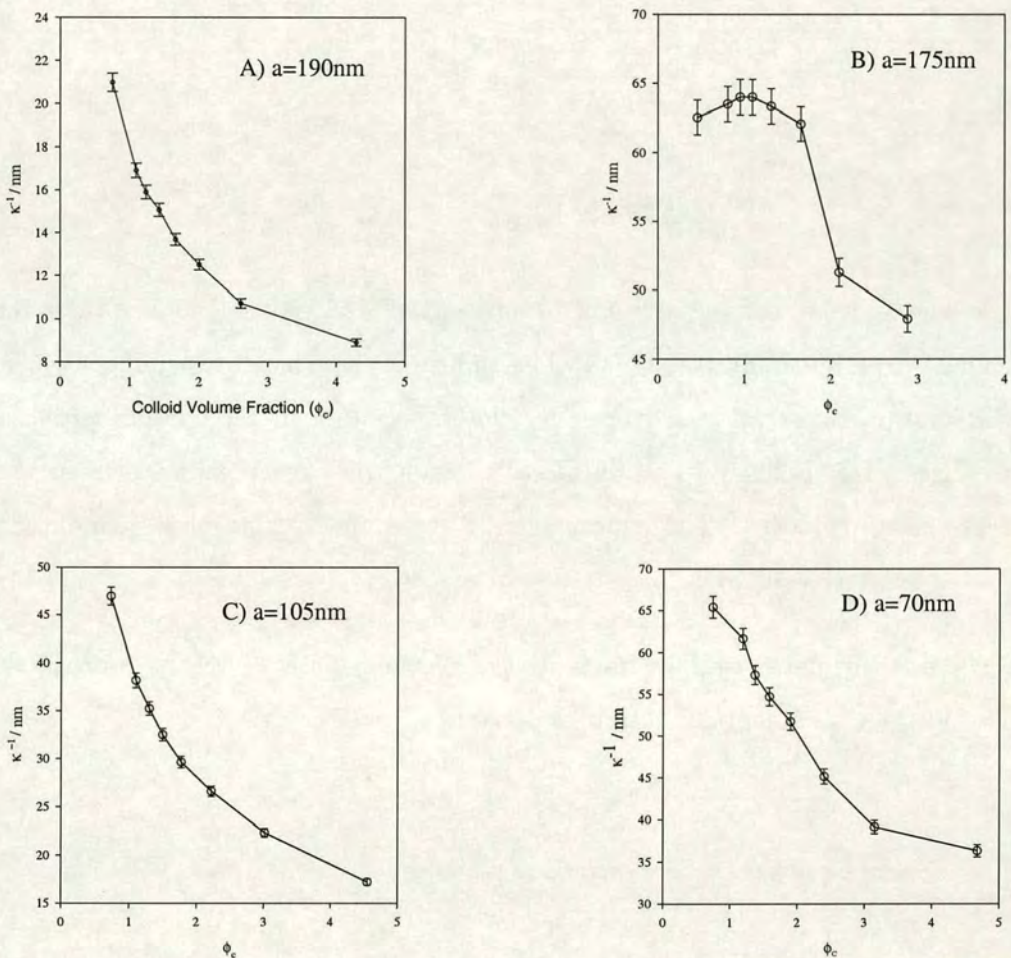


Figure 5.3: Plots of the Debye screening length ( $\kappa^{-1}$ ) against colloid volume fraction,  $\phi_c$ , for IDC latex particles. The size of the particles are indicated on the graphs.

The Debye screening lengths are then tabulated (table 5.3) in order to easily compare them with the calculated values in table 5.2.



Table 5.3: Debye screening lengths ( $\kappa^{-1}$ ) for IDC latices from conductivity measurements.

Colloidal Radius / nm	$\kappa^{-1}/nm$			
	Colloidal Volume Fraction			
	0.01	0.02	0.03	0.04
190	18.5	12.5	10.5	9.5
175	63	53.5	47.5	/
105	41	28.5	23	19.5
70	63.5	50.5	40.5	38

#### 5.1.1.4 Comparison of the values of $\kappa^{-1}$

The calculated values of the screening lengths (table 5.2) are all higher than those determined experimentally (table 5.3). This indicates that there are significantly more ions in solution than expected from only the dissociation of the charged groups on the particles. This is likely to be due to salt ions leftover from the particle synthesis as mentioned previously. The experimentally determined value of  $\kappa^{-1}$  is therefore considered a better estimate.

The 190nm radius particles show the largest discrepancy between the calculated values of  $\kappa^{-1}$  and the experimentally determined values.

#### 5.1.1.5 Critical Coagulation Concentrations

The critical coagulation concentrations (ccc's) of the IDC latices are determined as discussed in section 4.2.2. The values determined along with their associated uncertainties are given in table 5.4. For the 190nm latex particles the critical coagulation concentration was found to lower to about  $1.1 \pm 0.1\%$ w/w, when the time for the particles to aggregate was about 8hours.

The 175nm radius and 70nm radius particles require the least amount of added salt to

Table 5.4: Experimentally determined critical coagulation concentrations (ccc's).

Particle Radius /nm	ccc/%w/w NaCl	ccc/mol l <sup>-1</sup> NaCl
190	1.3±0.1	0.22±0.02
175	1.2±0.1	0.20±0.02
105	1.7±0.1	0.29±0.02
70	1.2±0.1	0.20±0.02

induce aggregation. The value of the ccc for these particles is about the same as the 190nm particles, whilst the 105nm radius particles are found to be significantly more stable to the addition of salt.

At concentrations above the ccc the particle aggregates were sometimes observed to float. This is unexpected as the density of the colloid is higher than the salt solutions. The aggregates could have some trapped air bubbles in them causing them to have a lower density than the dispersion medium, and hence float.

#### 5.1.1.6 DLVO Potentials

As discussed in section 2.2.2 the interaction between charged colloids is usually modelled by the DLVO potential. This potential is an effective potential found by adding the van der Waals attraction to the coulombic repulsion between the particles. As discussed in section 2.2.2 there are many approximations for both the attractive and repulsive potentials. The DLVO potential of the IDC lattices were calculated using the following equations which were introduced in chapter 2.

The van der Waals interaction is found using,

$$V_a = -\frac{A}{12} \left\{ \frac{1}{x(x+2)} + \frac{1}{(x+1)^2} + 2 \ln \left( \frac{x(x+2)}{(x+1)^2} \right) \right\} \quad (5.3)$$

where  $A$  is the Hamaker constant,  $x = H/2a$ , and  $H$  is the distance of closest approach of 2 particles of radii  $a$ . The coulombic repulsion is given by

$$V_R^\sigma = -2\pi\epsilon_0\epsilon_a\psi_d^2 \ln(1 - \exp[-\kappa H]) \quad (5.4)$$

and the surface charge is approximated by,

$$\sigma_d = \epsilon_0 \epsilon \kappa \psi_d \quad (5.5)$$

For highly charged latex particles condensation of the counterions onto the particle's surface has been found to take place [97]. As a result of this an equilibrium is established where the particles have a constant potential. Hence equation 5.4, the constant potential approximation, is used to determine the coulombic repulsion in this system.

The surface potential  $\psi_d$  can be found using the information in table 5.1 and equation 5.5 as follows,

$$\psi_d = \frac{z_c e}{4\pi \epsilon \epsilon_0 \kappa a^2} \quad (5.6)$$

where  $z_c$  is the number of charge groups per particle of radius  $a$ . The surface potential along with  $\kappa$  are then put into equation 5.4 to determine the repulsive part of the potential. The screening has two contributions; the first from the dissociation of the charged groups on the surface of the colloids, and the second from the added electrolyte. Hence the expression used to determine  $\kappa$  is,

$$\kappa^2 = \left( \frac{e^2 z_c \phi}{\epsilon \epsilon_0 k T \frac{4\pi}{3} a^3} + \frac{2e^2 z_s^2 c_s N_a}{\epsilon \epsilon_0 k T M_{w,s}} \right) \quad (5.7)$$

where  $c_s$  is the concentration of added salt,  $z_s$  is the valency of the salt ions and  $M_{w,s}$  is the molecular weight of the salt. It should be noted that the contribution from the counterions of the particles to  $\kappa$  assumes 100% dissociation of the charged groups on the colloid as in section 5.1.1.2. As discussed, the screening lengths were subsequently determined more directly by conductivity measurements and found to be lower. These differences are, however, negligible on addition of salt. In fact the first term of equation 5.7 is found to have very little influence on the the screening length of the system and the values of  $\kappa^{-1}$  are about the same for all of the batches of colloid on addition of salt. Values of the screening lengths for varying salt concentrations are shown in table 5.5. It can be seen that addition of even a small amount of salt greatly reduces the screening length of the colloids.

The DLVO potential was determined for each size of IDC latex by adding the coulombic repulsion (equation 5.4) to the van der Waals attraction (equation 5.3). The value of the Hamaker constant used was  $A = 1.3 \times 10^{-20} \text{J}$  [98]. This is the tabulated value of polystyrene particles in water found in many textbooks [18, 13].

Table 5.5: Calculated screening lengths of IDC lattices on addition of salt.

NaCl Concentration / % w/w	$\kappa^{-1}$ / nm
0.1	2.33
0.25	1.48
0.5	1.04
1.0	0.07

Plots of the DLVO potentials for varying NaCl concentrations for each colloid are presented in figure 5.4.

The calculated DLVO potentials follow the expected trends. At low salt concentrations the repulsive potential is large and long ranged. As salt is added both the size and the range of the repulsion decreases. A secondary minimum begins to emerge and the barrier to the primary minimum becomes smaller. At high enough salt concentration the potential becomes purely attractive.

The quantitative behaviour predicted according to the calculated potentials does not fit the experimental data very well. The values of the ccc found experimentally (table 5.4) are significantly higher (by a factor of 2-3) than the salt concentrations where the attraction dominates in the calculated potentials. The increased stability of the 105nm radius particles compared with the other sizes of particles is nevertheless reflected in the DLVO potentials.

There are a number of reasons for the discrepancy between the calculated potentials and the experimental behaviour. Firstly the determination of the ccc was dependent on an arbitrarily chosen timescale. Therefore a discrepancy in actual values is expected, however, it is unlikely that this could account for about the observed factor of three difference between experiment and theory. Secondly, a range of values of the individual Hamaker constants of polystyrene in vacuum and water in vacuum are found (see table 5.6). Combining these values using equation 2.5 results in a large range of the Hamaker constant of polystyrene in water, from about  $A_{131} = 5 \times 10^{-20} \text{J}$  to  $A_{131} = 4 \times 10^{-23}$  (equation 2.5). This can therefore have a large influence on the van der Waals

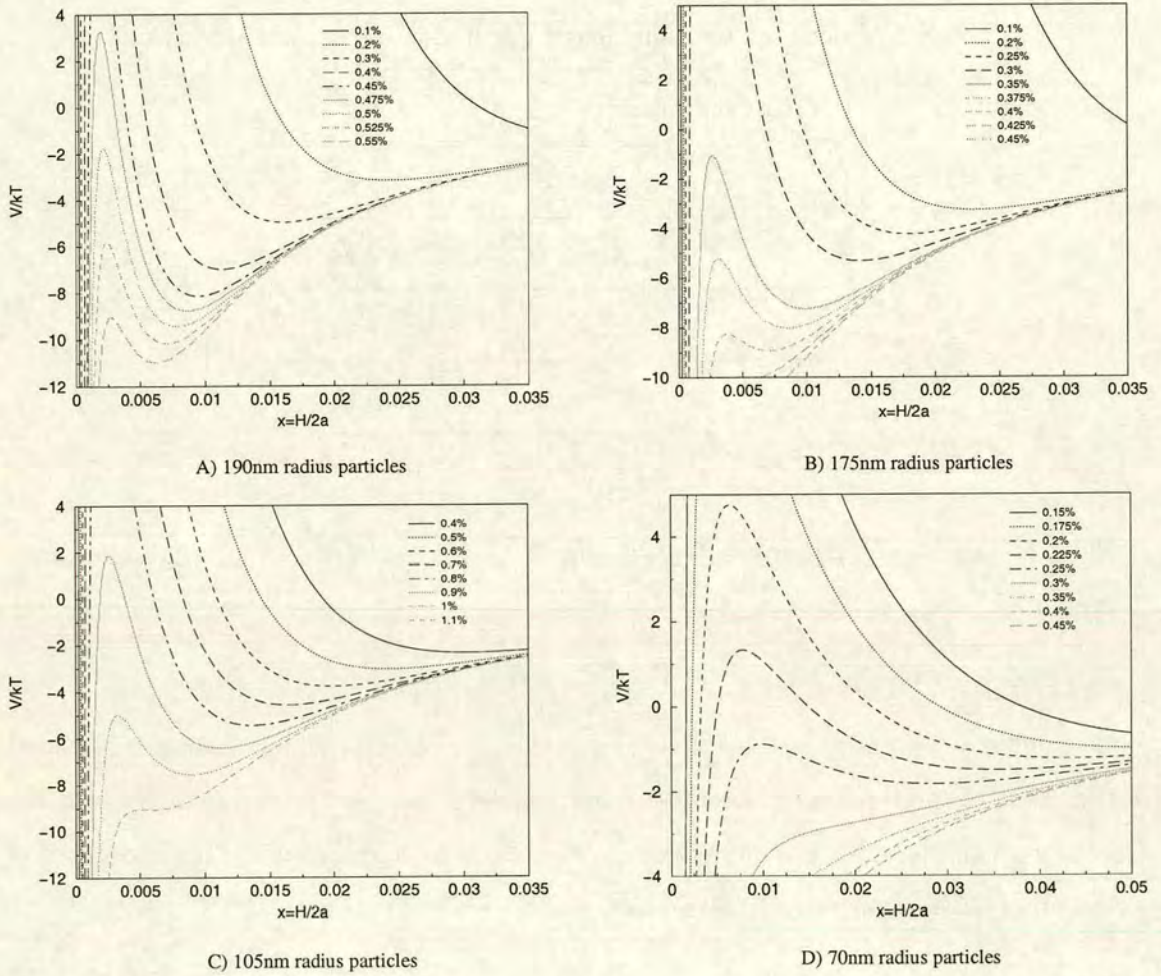


Figure 5.4: DLVO potentials for IDC lattices ( $\phi = 0.01$ ) of size A) 190nm radius, B) 175nm radius, C) 105nm radius and D) 70nm radius as a function of the normalised interparticle distance. The various concentrations of NaCl added is shown as % w/w in the legend.

interactions. Also, the coulombic repulsive potential between the particles used in the calculations is only an approximation (section 2.2.2).

Table 5.6: Values of Hamaker constants [99].

Material	$A_{11}$ (microscopic)	$A_{11}$ (macroscopic)
	$10^{-20}$ J	$10^{-20}$ J
Water	3.3-6.4	3.0-6.1
Polystyrene	6.2-16.8	5.6-6.4

### 5.1.2 Rhône-Poulenc Latices

The charged polystyrene latices purchased from Rhône-Poulenc did not come as well characterised as those from IDC, however the size was known to be approximately 200nm radius. No further characterisations, such as conductivity measurements, were carried out on these latices as they were only used for preliminary studies of the SLES system. The behaviour was subsequently compared to that of the surfactant-free 190nm radius particles from IDC and little difference was found. The majority of points on the SLES phase diagrams (chapter 7) correspond to samples made with IDC latices. The detailed study of the gels formed in this system were also carried out using the IDC latices.

### 5.1.3 PEO-Stabilised Latices

The size of the PEO-coated polystyrene latices synthesised in-house were determined by Abdellatif Moussaïd by static light scattering (see [33] for more details of this technique). They were found to have a radius of 260nm. No further characterisation of these particles was carried out.

## 5.2 Characterisation of $C_{16}E_6$

In the following section the characterisation of the uncharged,  $C_{16}E_6$ , micellar solution is discussed. Firstly, a light scattering study [37] is reported. Secondly, rheological measurements on the system are discussed.

### 5.2.1 Light Scattering Study of $C_{16}E_6$

Schurtenberger et al. have investigated the concentration-induced growth of worm-like micelles for the  $C_{16}E_6/D_2O$  system using light scattering techniques [37]. These measurements and in particular their interpretation are difficult since it is hard to distinguish between the intermicellar interactions and concentration induced growth in the scattering data. The measured static correlation length,  $\xi_s$ , as a function of  $C_{16}E_6$

concentration,  $c$ , is shown in figure 5.5. For  $c < c^*$  the radius of gyration  $R_g$  can be determined using the experimental data as described in [37] using conformation space renormalisation group theory originally developed for polymer solutions [100]. The radius of gyration,  $R_g$ , is determined using the following expressions [37],

$$\langle R_g^2 \rangle = \alpha_s \frac{L^3}{24l_p} \left( 1 - \frac{3}{2N_K} + \frac{3}{2N_K^2} - \frac{3}{4N_K^3} [1 - \exp(-2N_K)] \right) \quad (5.8)$$

where the expansion factor  $\alpha_s$  follows the empirical expression,

$$\alpha_s^2 = \left[ 1 + \left( \frac{N_K}{3.12} \right)^2 + \left( \frac{N_K}{8.67} \right)^3 \right]^{3.17} \quad (5.9)$$

$N_K$  is related to number of persistence lengths,  $l_p$  ( $l_p = 25\text{nm}$  for the  $\text{C}_{16}\text{E}_6$  system), per contour length,  $L$  by,

$$N_K = \frac{L}{2l_p} \quad (5.10)$$

where  $L$  is found using,

$$L = \frac{M_W}{N_A M_L} \quad (5.11)$$

where  $N_A$  is the Avogadro number.  $M_W$ , the micellar molecular weight, is related to the concentration of the surfactant,  $c$ , via the growth law,

$$M_W = 1.29 \times 10^7 c^{1.1} \quad (5.12)$$

$M_L$  is the mass per unit length of the micelle and its value found in the light scattering measurements is  $0.165 \times 10^{-12} \text{gcm}^{-1}$ . Using equations 5.8 to 5.10 from [37]  $R_g$  was found as a function of  $\text{C}_{16}\text{E}_6$  concentration (figure 5.6). In the limit  $c \rightarrow 0$ ,  $\xi_s$  corresponds to  $R_g/\sqrt{3}$  where  $R_g$  is the radius of gyration of the micelle. This is because the lengthscale measured far below  $c^*$  is that of single coils. As the concentration increases the interactions begin to affect the measured correlation length  $\xi_s$ , and therefore a measure of  $R_{g,app}$  is found. The calculations detailed take these interactions into account in order to allow a true value of  $R_g$  to be determined.

At higher concentrations, where  $c > c^*$ ,  $\xi_s$  is no longer dependent on the size of the individual micelles, but is a measure of the mesh-size,  $\xi_M$  of the entangled network. This size decreases strongly with increasing concentration as shown in figure 5.5.

Using the calculated values of  $R_g$  for the dilute regime (figure 5.6) and  $\xi_s$  above overlap from figure 5.5, the concentration dependent size ratio ( $R_g/a$  and  $\xi_s/2a = \xi_M/2a$ ) for

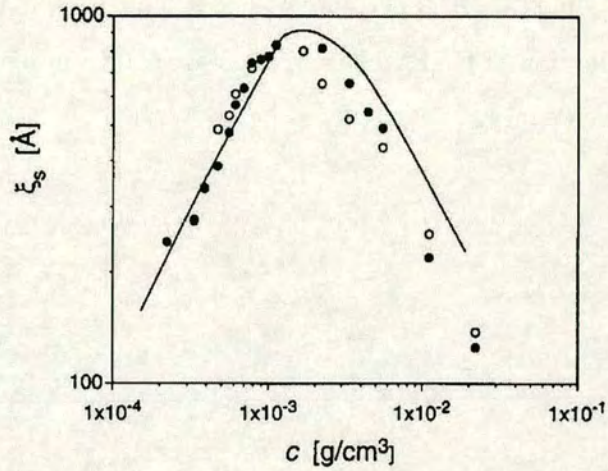


Figure 5.5: Static correlation lengths for the  $C_{16}E_6/D_2O$  system as a function of surfactant concentration. The black and white circles represent the experimental measurements at  $25.5^\circ\text{C}$  and  $32.5^\circ\text{C}$  respectively. The solid line shows the theoretically calculated values. (Figure reproduced from [37])

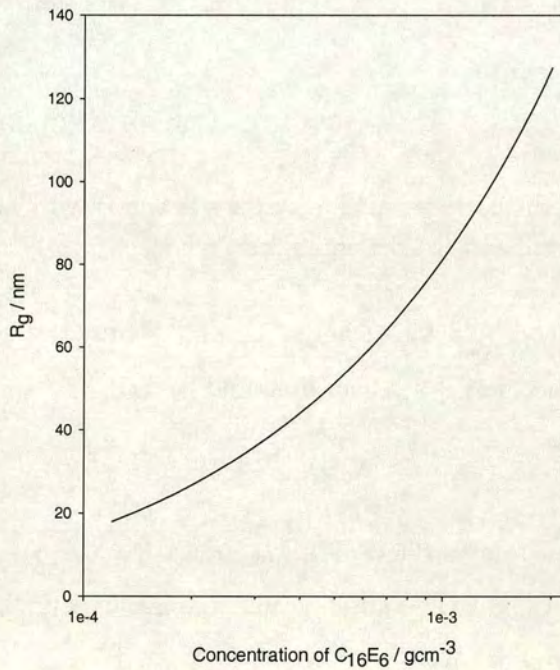


Figure 5.6: Graph showing the variation of the radius of gyration ( $R_g$ ) of the wormlike micelles as a function of  $C_{16}E_6$  concentration in the dilute regime.



the various sizes of colloid used in systems A and B have been determined\*. Plots of the size ratio as a function of  $C_{16E_6}$  concentration are shown in figure 5.7 for both the dilute and entangled regimes.

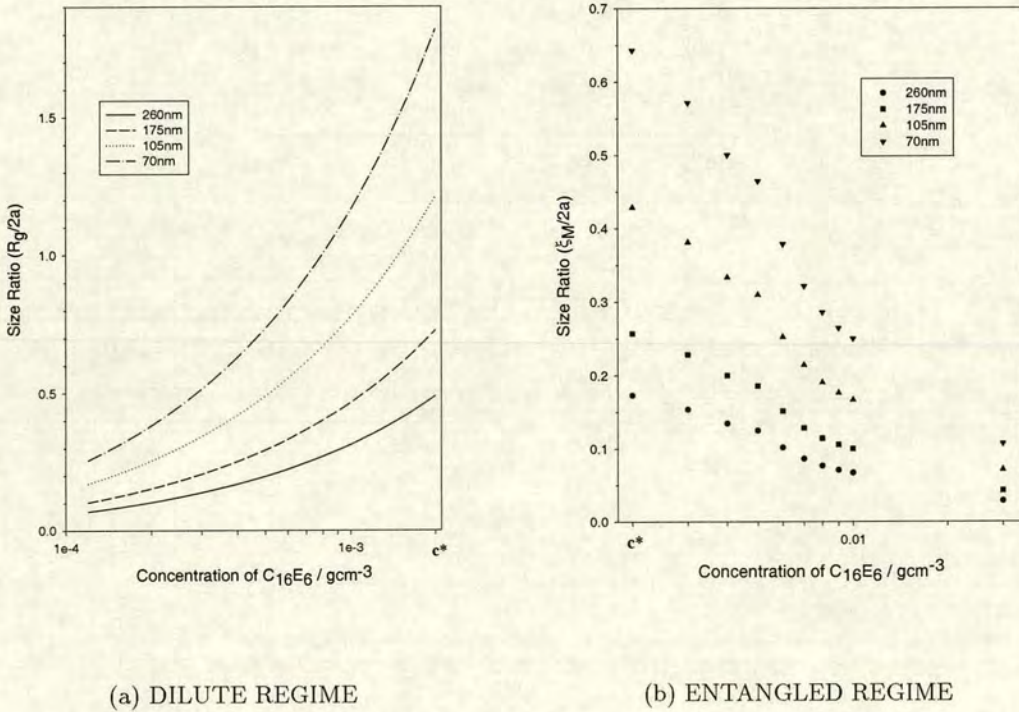


Figure 5.7: Size ratios of the particles used in systems A and B with varying concentration of  $C_{16E_6}$  in (a) the dilute and (b) the entangled regime.

The growth law determined by Schurtenberger et al. [37] can also be used to determine the number density of micelles,  $N$ .  $N$  can be found using

$$N = \frac{cN_A}{M_W} \tag{5.13}$$

where  $c$  is the concentration of surfactant in g/l,  $N_A$  is Avogadro's number and  $M_W$  is the molecular weight of the micelle and is given by equation 5.12. Using equation 5.11 the expression for  $N$  simplifies to,

$$N = \frac{N_A}{1.29 \times 10^7} c^{-0.1} \tag{5.14}$$

A plot of the number of micelles per  $cm^3$  of solution for varying  $C_{16E_6}$  concentration is shown in figure 5.8. It can be seen that the number density of micelles decreases as the

\*The effect of the screening length  $\kappa^{-1}$  is not considered here but will be discussed in chapter 6.

concentration of  $C_{16}E_6$  increases. This is a result of the growth exponent being larger than 1. However, there is only a relatively weak dependence of  $N$  on  $c$  as the number of micelles increases by less than a factor of two over two decades in concentration.

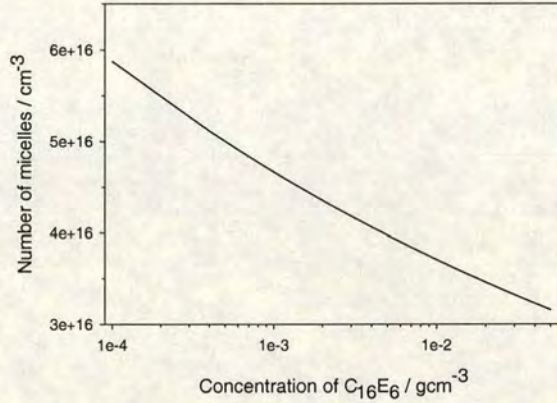
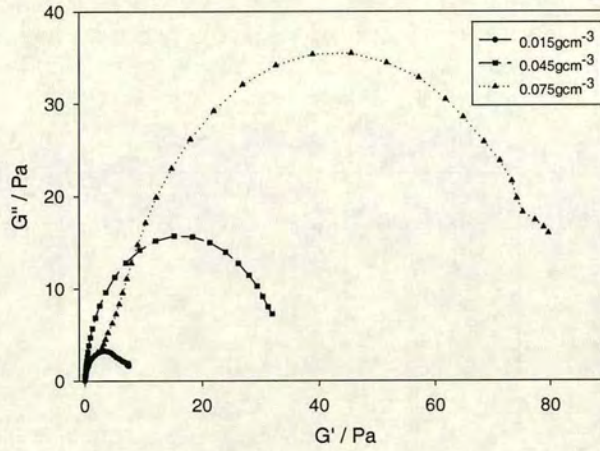


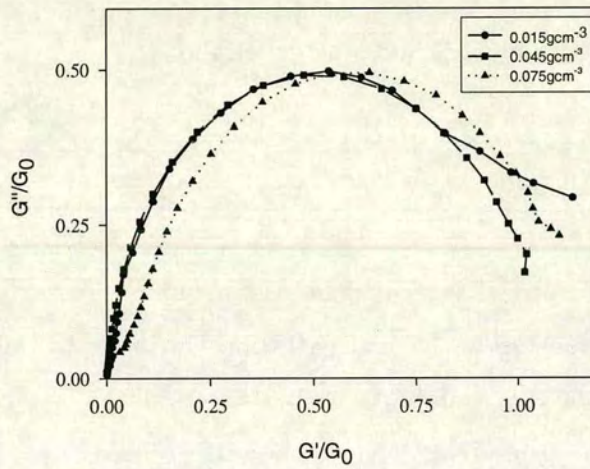
Figure 5.8: Number density of micelles as a function of concentration of  $C_{16}E_6$ , calculated from the light scattering study of Schurtenberger et al. [37].

### 5.2.2 Rheology of $C_{16}E_6$

Rheological measurements (as described in section 4.3) were carried out on a number of samples with varying  $C_{16}E_6$  concentrations in order to determine where the wormlike micelles reach the semi-dilute limit. As discussed in section 4.3, wormlike micelles well within the semi-dilute regime, where the scission time is smaller than the reptation time, have a single relaxation time. Their rheological behaviour is therefore Maxwellian, and is characterised by a semi-circular Cole-Cole plot. Cole-Cole plots for varying concentrations of  $C_{16}E_6$  (without particles) at  $26^\circ\text{C}$  are shown in figure 5.9. It can be seen from this figure that at concentrations above about  $0.015\text{gcm}^{-3}$  the micelles are entangled since the Cole-Cole plot is semicircular (section 4.3). Below this concentration a partial semi-circle is seen in the Cole-Cole plot. This was also found for the SLES system and will be discussed further in section 5.3. According to the rheology, the micelles reach the semi-dilute regime a decade higher in concentration than the overlap concentration determined by light scattering data. Schurtenberger et al [37] found a value of  $c^*$  of about  $0.002\text{gcm}^{-3}$  (section 5.2.1).



(a) Cole-Cole plots



(b) Normalised Cole-Cole plots

Figure 5.9: Viscoelastic behaviour of aqueous solutions of various concentrations of  $C_{16}E_6$ . The erratic behaviour observed at high frequencies has not been included on these plots.

A one-element Maxwell model (see section 4.3) is fitted to this data in order to find the relaxation (Maxwell) time and viscosity of the solution. These values, along with an estimate of  $G_0$ , for a number of surfactant concentrations are shown in table 5.7. The plateau modulus,  $G_0$ , and therefore the viscosity of the micellar solution increases

with concentration. The maxwell (or relaxation) time also increases with an increased C<sub>16</sub>E<sub>6</sub> concentration. These increases are due to the micelles becoming more entangled as the concentration increases.

Table 5.7: Data from fitting a one element maxwell model to the C<sub>16</sub>E<sub>6</sub> rheological measurements.

Surfactant concentration gcm <sup>-3</sup>	Maxwell time seconds	Viscosity Pas	G <sub>0</sub> Pa
0.015	0.080	0.5	6.5
0.025	0.085	0.6	9
0.035	0.090	1.2	13
0.045	0.093	1.4	16
0.075	0.23	16.5	72

Cole-Cole plots are usually normalised by plotting  $G''/G_0$  against  $G'/G_0$  as shown in figure 5.9(b). It can be seen for C<sub>16</sub>E<sub>6</sub> that the viscoelastic behaviour is Maxwellian indicating that the wormlike micelles are entangled.

#### *Temperature Dependence*

The viscoelastic behaviour discussed above was investigated at 26°C. This corresponds to the temperature at which the phase study was carried out. The incubator in which the samples are kept and observed, however, has a temperature of 26±0.5°C and so the effect of this possible temperature fluctuation on the rheological properties was investigated. It was found that there is no significant influence on the viscoelastic behaviour found for temperatures of 25.5°C and 26.5°C. This temperature fluctuation of the incubator should therefore have little effect on the observed phase behaviour, from the point of view of the rheology at least.

### 5.3 Characterisation of SLES system

This system is more complex than that of  $C_{16}E_6$  since additional components such as salt, zwitterionic surfactant (CAPB or cocoamidopropylbetaine) and/or octanol are used to promote the formation of wormlike micelles. In all cases CAPB is added to the SLES to reduce the amount of salt and/or octanol required to tune the micellar behaviour. The effect of all of these added components on the rheological behaviour was determined by varying each one in turn. The effect of added salt, zwitterion and octanol will therefore be discussed in the subsequent sections.

#### 5.3.1 Salt Dependence

Viscoelastic measurements were carried out on the SLES system at  $20^\circ\text{C}$ , as discussed in section 4.3. The behaviour observed for a mixture of 14% SLES and 2% CAPB with different concentrations of NaCl are shown in figures 5.10 and 5.11. Figure 5.10 show an example of the rheological behaviour found when the wormlike micelles have not fully entangled at a salt concentration of 1.5%. The relaxation time is not very small, indicating that the presence of small micelles is not what is causing non-Maxwellian behaviour. It is therefore likely that Maxwellian behaviour has not been seen due to a small scission rate compared with the reptation time. Thus the micelles do not meet the conditions required for Maxwellian behaviour according to the Cates model (section 2.4.4.2).

For 14% SLES and 2% CAPB the micellar solution is observed to give semi-circular Cole-Cole plots at a concentration of about 2.5% NaCl. The Cole-Cole plots, and normalised Cole-Cole plots for 3%, 4% and 5% NaCl are shown in figure 5.11.

A Maxwell model was fitted to the data producing semi-circular Cole-Cole plots. The Maxwell time and viscosities determined, for 14% SLES, 2% CAPB and varying salt concentration, in this way are presented in table 5.8, along with an estimate of the plateau modulus,  $G_0$ . Initially the relaxation (Maxwell) times were found to increase with salt concentration and then decrease again at 5% salt. The increase is due to the micelles becoming more entangled. The subsequent decrease in the Maxwell time is thought to be due to the wormlike micelle becoming branched [101]. In the case

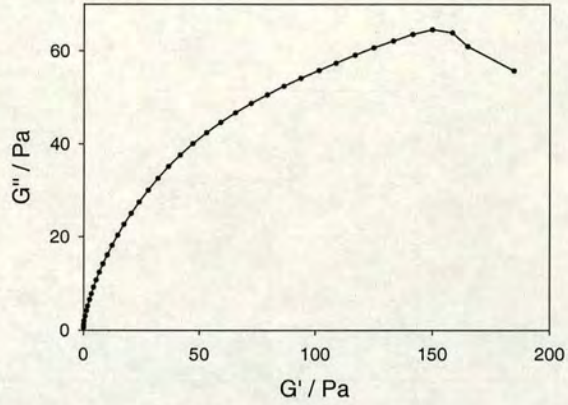


Figure 5.10: Cole-Cole plot for 14% SLES (2% CAPB) and 1.5% salt. The behaviour is not Maxwellian and therefore the wormlike micelles have not reached the semi-dilute regime.

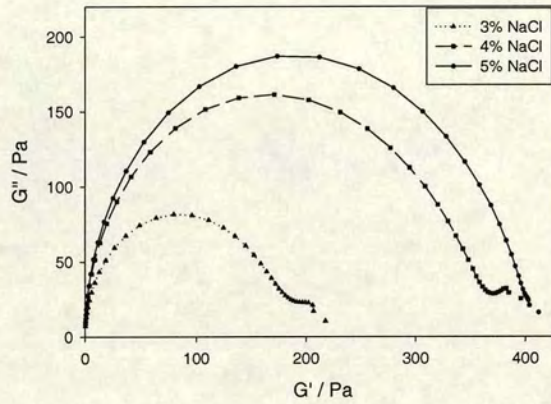
of branched wormlike micelles the branch points are not chemical connections and therefore the worms can slide with respect to spatially fixed connections as shown in figure 5.12 [102]. Reptation can therefore occur along every path of the tree, thus leading to a smaller relaxation time than that found for linear micelles.

Table 5.8: Data from fitting a one element maxwell model to the rheological measurements for solutions with 14% SLES and 2% CAPB and various salt concentrations.

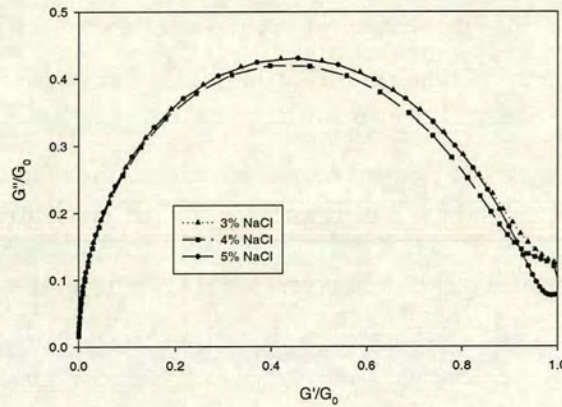
Salt Concentration %	Maxwell time seconds	Viscosity Pas	$G_0$ Pa
2.5	0.15	21	170
3	0.58	111	190
4	0.96	361	370
5	0.40	159	415

As expected the addition of salt promotes the formation and lengthening of the wormlike micelles. This is a result of the reduced effective head group area due to the screening of the coulombic repulsion by the salt ions. (see section 2.4.3 for more details).

The viscoelastic behaviour was probed for a large number of samples with varying SLES



(a) Cole-Cole plots



(b) Normalised Cole-Cole plots

Figure 5.11: Viscoelastic behaviour of 14% SLES (2% CAPB) and varying concentration of salt indicated in the legend. The semi-circular Cole-Cole plots indicate shows Maxwellian behaviour and therefore the wormlike micelles are highly entangled.

and salt concentrations (and a constant SLES to CAPB concentration ratio of 7:1) in order to find a micellar phase diagram. The criterion used to determine the micellar behaviour is discussed using samples of 7% SLES (and 1% CAPB) and varying NaCl concentration (figure 5.13). Three types of behaviour are illustrated in this figure and

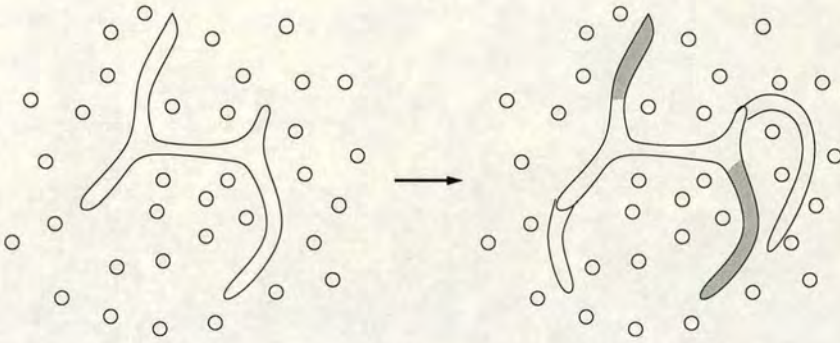


Figure 5.12: Schematic diagram of the reptation of branched micelles. As the branch points of the micelles are not fixed reptation can take place along all branches as shown. The old tube, after reptation is shown as grey tube.

correspond to the three phases found in figure 5.14. Where no viscoelasticity is found the sample is a dilute solution of micelles. As salt is added the micelles grow and begin to entangle. These samples show some viscoelastic behaviour (a partial semi-circular Cole-Cole plot as shown in figure 5.10). At high enough concentrations the behaviour found is Maxwellian, which corresponds to a semi-dilute solution of wormlike micelles (2.4.4.2). The micellar phase diagram (figure 5.14) therefore summarises the behaviour of the micelles in the region where the phase behaviour of added latex was investigated (chapter 7).

### 5.3.2 Effect of Zwitterion

As mentioned, the zwitterion, CAPB, was added to the SLES system in order to promote the lengthening of the wormlike micelles (section 2.4.3). As shown in figure 5.15, the zwitterion is expected to have a head-group area  $a_0$  to length  $l_c$  ratio which is smaller than for the ionic surfactant. The average packing parameter (see figure 2.10) decreases thus favouring the formation of wormlike micelles. This effect was confirmed by viscoelastic measurements (section 4.3) of an SLES/NaCl/H<sub>2</sub>O sample, both with and without added CAPB. The Cole-Cole plots for these measurements are shown in figure 5.16. At 14% SLES and 3% salt Maxwellian behaviour is observed when 2% CAPB is added.

Rheological measurements were carried out on solutions of various concentrations of



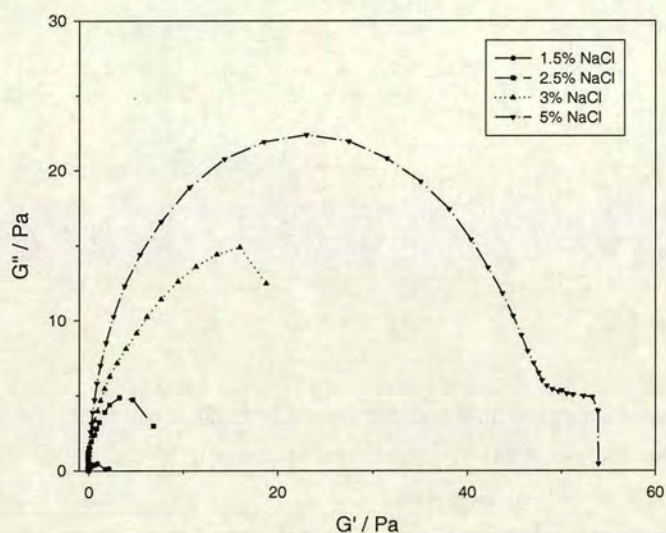


Figure 5.13: Cole-Cole plots for 7% SLES, 1% CAPB and varying NaCl concentration as indicated on the legend. The behaviour changes as the dilute micelles (1.5% NaCl) grow and therefore begin to overlap (2.5% and 3%) until they are in the semi-dilute regime showing the characteristic Maxwellian behaviour (5% NaCl).

SLES and CAPB (with no added salt) in order to determine the micellar phase diagram for this system (figure 5.17). The criterion for determining the phase behaviour is the same as that used for the SLES/NaCl/H<sub>2</sub>O system discussed earlier.

### 5.3.3 Effect of Octanol

Changing the salt and zwitterion concentrations has some effect on electrostatic interactions. (This will be discussed more in chapter 7.) therefore octanol was added in the hope that this could be used to change the micellar properties whilst keeping the electrostatic interactions of the system constant. Maxwellian behaviour was found for a clear solution of 7% SLES, 1% CAPB, 1% NaCl and 0.8% octanol (figure 5.18). In figure 5.18 the rheological behaviour of lower concentrations of octanol are also plotted. The behaviour observed with increasing octanol is similar to that in figure 5.13 where the NaCl concentration is varied.

The octanol therefore acts as a co-surfactant as shown in figure 5.19. It has a much

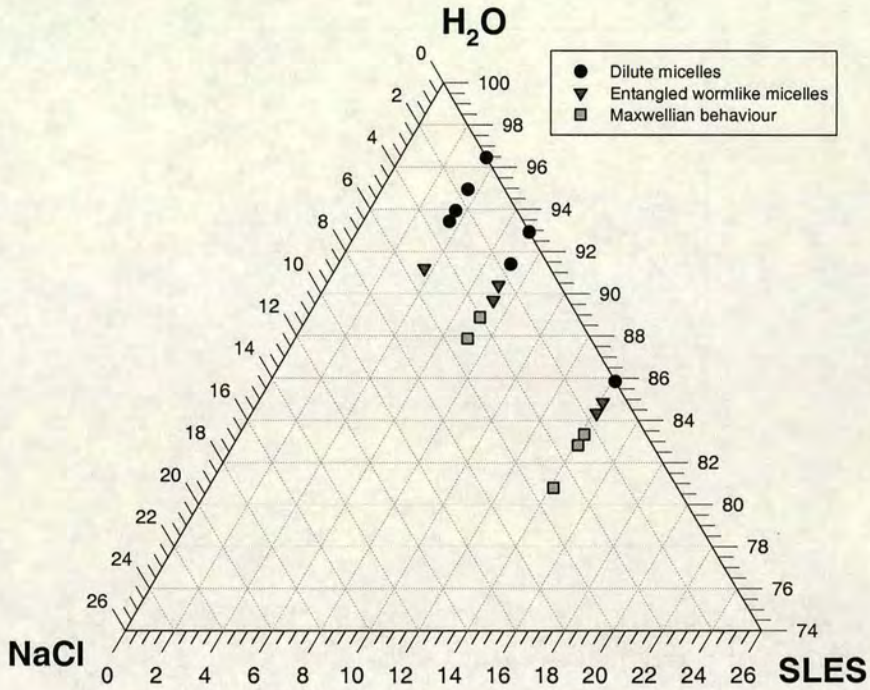


Figure 5.14: Micellar phase diagram for the SLES/NaCl/H<sub>2</sub>O system. CAPB is present in these samples at a constant ratio of SLES:CAPB of 7:1. The phases have been determined by rheological measurements as discussed; dilute micelles show no viscoelastic behaviour, entangled wormlike micelles show viscoelastic behaviour like that of figure 5.10 and the Maxwellian behaviour (section 2.4.4.2) corresponds to the appearance of a semi-circular Cole-Cole plot. The system is therefore well within the semi-dilute regime. The erratic behaviour observed at high frequencies has not been included on these plots.

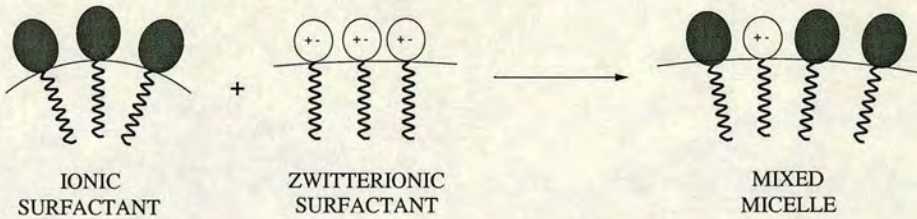


Figure 5.15: Schematic diagram showing the influence of a zwitterionic co-surfactant on the packing of an ionic surfactant. The zwitterionic head group reduces the effective size of the head group of the charged surfactant. This then promotes the formation of wormlike micelles as it reduces the preferred surface curvature.

smaller head group than the SLES molecule and therefore it produces a mixed micelle with a lower interface curvature. Thus wormlike micelles become more favourable than

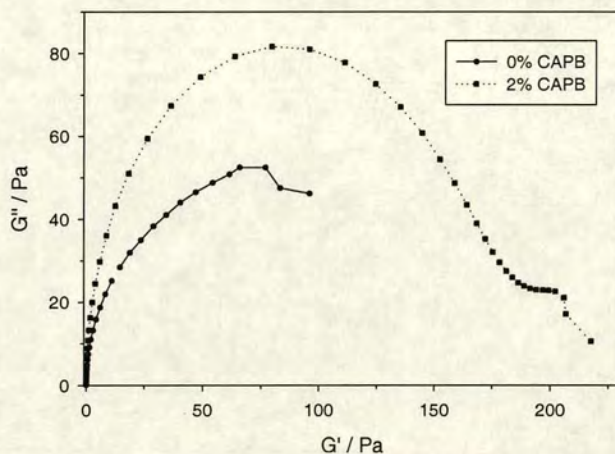


Figure 5.16: Cole-Cole plots for mixtures of 14% SLES, 3% NaCl both with CAPB (at the usual 7:1 SLES to CAPB ratio) and without CAPB.

spherical micelles (section 2.4.3).

Samples of 7% SLES and 1% CAPB with no added salt require so much octanol to get Maxwellian behaviour that the samples become cloudy. The cloudiness causes problems in determining the phase behaviour of the latex particles when added to the surfactant solutions, so it was necessary to add some salt in order to obtain Maxwell behaviour at a lower, non-cloudy, octanol concentration.

### 5.3.4 Temperature Effects

The temperature dependence of the viscoelastic behaviour of the SLES system has been investigated. Essentially no change to the micellar phase diagram determined at 20°C is found over the temperature range 10°C to 30°C. The viscosity and the relaxation time of the micellar solution, however, decreases with increasing temperature.

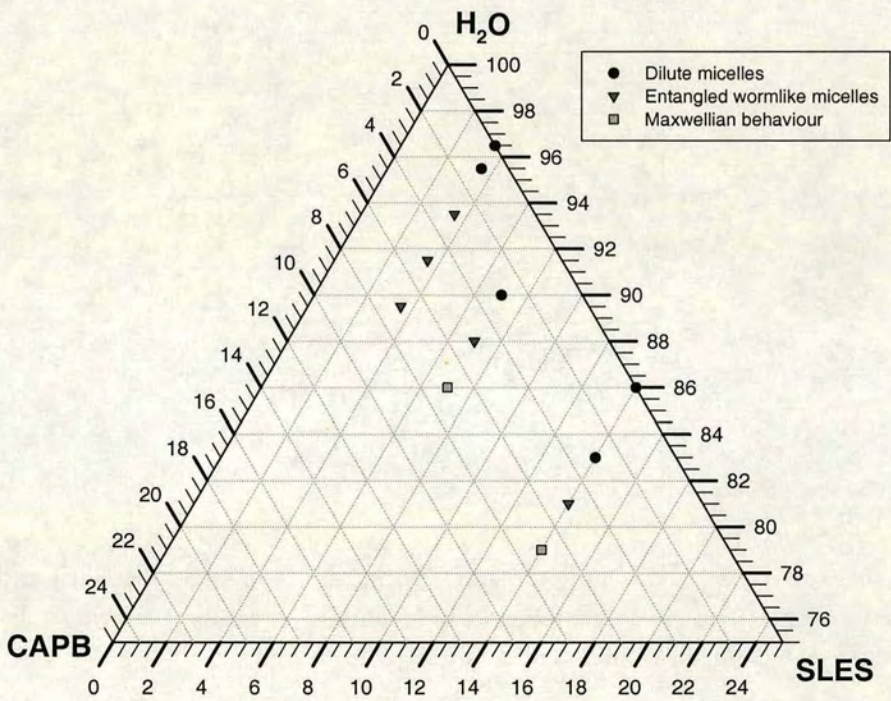


Figure 5.17: Micellar phase diagram for the SLES/CAPB/H<sub>2</sub>O system. There is no salt present in this system. The phases have been determined by rheological measurements as discussed in the SLES/NaCl/H<sub>2</sub>O case.

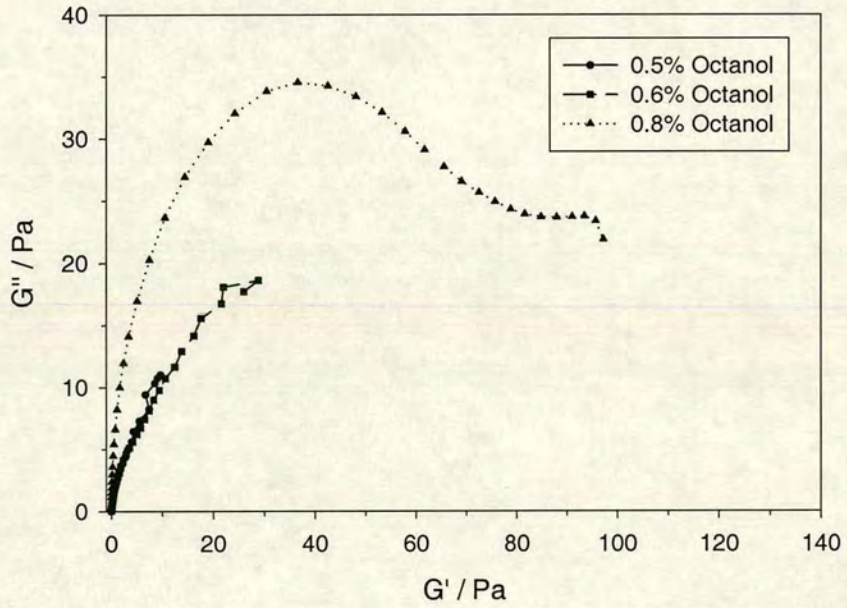


Figure 5.18: Cole-Cole plots for mixtures of 7% SLES, 1% CAPB, 1% NaCl and varying concentrations of octanol as indicated on the legend. The erratic behaviour observed at high frequencies has not been included on these plots.

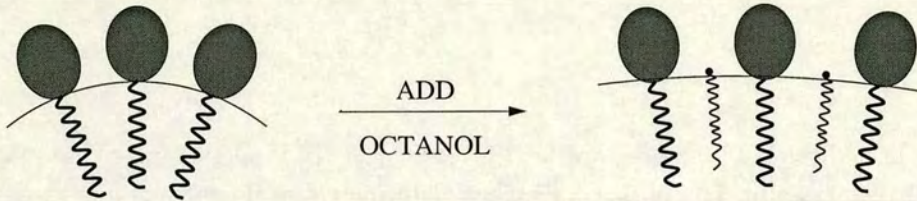


Figure 5.19: Schematic diagram showing the effect on the preferred curvature of an SLES solution on addition of octanol. It can be seen that the addition of the co-surfactant octanol reduces the preferred curvature and thus favours the formation of wormlike micelles.

#### 5.4 Comparison of SLES and $C_{16}E_6$ Systems

This discussion will be between the SLES/NaCl/H<sub>2</sub>O and  $C_{16}E_6$  systems as Maxwell models have been fitted in these cases. It can be seen that the SLES system has a

much higher viscosity (and  $G_0$ ) than the C<sub>16</sub>E<sub>6</sub> system. This is due to the much higher surfactant concentrations in the SLES case. Wormlike micelles in the C<sub>16</sub>E<sub>6</sub> system entangle at a very low surfactant concentration due to the large growth exponent of 1.1 resulting in a few large micelles which can overlap easily.

At the temperatures probed via rheology evidence of branching is found in the SLES system but not for the C<sub>16</sub>E<sub>6</sub> system.



## Chapter 6

# Phase Behaviour of Nonionic Surfactant and Colloid

### 6.1 Introduction

In this chapter the phase behaviour of both uncharged and charged colloids in a solution of wormlike micelles of the nonionic surfactant  $C_{16}E_6$  is discussed. The uncharged colloid case is referred to as system A and the charged colloid case as system B (see chapter 4). In order to discuss the results in terms of the depletion model the differences between polymers and wormlike micelles as depletants must first be explored. The experimental phase diagrams for these systems are then presented and discussed in terms of depletion. A comparison is then made with the well-studied model colloid-polymer mixtures (section 3.1). Theoretical phase diagrams of colloids in a solution of wormlike micelles, based on the depletion model, have also been determined and are compared to the experimental data.

### 6.2 Differences between Wormlike Micelles and Polymer as Depletants

The depletion picture discussed in section 3.1.1 becomes more complex when wormlike micelles rather than polymer coils act as the depletants. These differences will be discussed here and hence it will be shown that a comparison of the colloid-wormlike



micelle phase behaviour with existing colloid-polymer phase diagrams proves difficult.

### 6.2.1 Scission & Recombination of Micelles

Polymer molecules consist of many chemically bonded monomer units. Wormlike micelles are self-assembled aggregates which break and reform. This property could therefore allow micelles to break into smaller micelles or form longer micelles, changing their equilibrium length distribution to allow a minimisation of free energy. In the presence of colloidal particles, the micelles could break into smaller and smaller units, therefore reducing the range of the depletion interaction and thus keep the mixture stable.

### 6.2.2 Concentration Effects

The phase diagrams for colloid-polymer mixtures reproduced in chapter 3 (figure 3.11) are plotted as concentration of polymer against colloid volume fraction. The polymer to colloid size ratio for each plot is constant and the phase behaviour has been found to be highly dependent on this. In the case of the colloid-wormlike micelle mixtures the experimentally controllable variables are the concentration of surfactant and the colloid volume fraction. The two type of plots are therefore apparently similar. However, in the wormlike micelle case the micelle to colloid size ratio changes as the concentration of surfactant is varied. The depletion interaction is therefore affected in two ways. Both the concentration of the depletant changes, altering the depth of the depletion well, and the size ratio changes, altering both the depth and range of the attraction. The colloid-wormlike micelle phase diagram is essentially equivalent to a surface through a 3-d plot of size ratio, concentration of polymer and colloid volume fraction for colloid-polymer mixtures.\*

### 6.2.3 Size Distributions

Polymers have an associated length polydispersity. This polydispersity was chosen to be as small as possible for the model colloid-polymer system studied by Ilett et al. [7],

---

\*This would, however, take no account of the other differences between the micelles and the polymers: the size distribution and the scission and recombination reactions.

and the polymers were assumed to be monodisperse in the theoretical colloid-polymer models discussed in section 3.1. Wormlike micelles are much more polydisperse: they have an exponential size distribution as discussed in section 2.4.4.1. This therefore results in a range of size ratios for the mixture at each surfactant concentration.

#### 6.2.4 Entanglement

Depletion in the entangled regime is fairly difficult to picture. Little study has been carried out in this regime in the model colloid-polymer systems. The important length-scale in the entangled regime is the mesh-size (or blobsize)  $\xi_M$ . The size ratio in this case is therefore assumed to be  $\xi = \xi_M/2a$ . The simplest picture of depletion in the semi-dilute regime is therefore that the colloids are depleted by “blobs” of size  $\xi_M$  [103]. Figure 6.1 is a schematic illustration of the depletion attraction induced between colloidal particles in an entangled network. The mesh is excluded from between the two colloidal particles and therefore there is an unbalanced osmotic pressure inducing an attraction between the colloidal particles. This can alternatively be considered as an entropic effect, where the entropy of the mesh is lower when it is restricted to a confined volume. However, it is unclear whether the size of polymers which are entangled may also affect the depletion interaction.

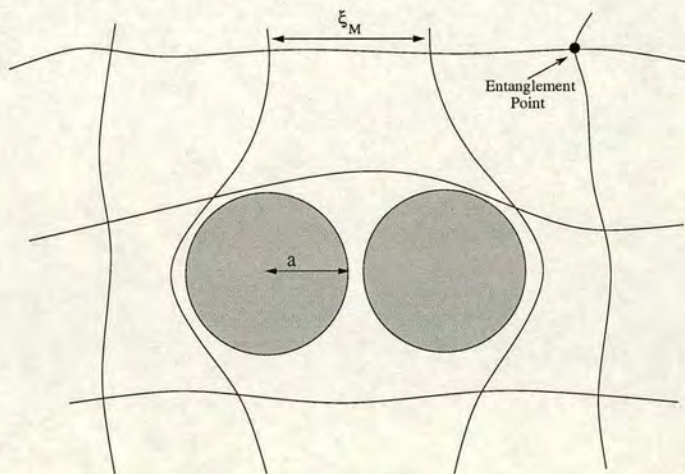


Figure 6.1: Schematic diagram illustrating the depletion attraction for colloids in an entangled polymer solution.

Sear [104] has predicted the phase behaviour of mixtures of small colloidal particles and semi-dilute polymer. Assuming all the interactions are excluded volume interactions

the energy of mixing is zero and therefore only entropy considerations must be assessed in order to determine the phase behaviour of the mixture. There is an entropy increase associated with the mixing of the colloidal particles and the polymer. At the same time, however, there is a decrease in entropy of the individual components, as the polymer reduces the particle's translational entropy and the particles reduce the polymer's configurational entropy. Phase separation will therefore take place when the entropy change of mixing is smaller than the entropy loss of the individual components. This theoretical model predicts that phase separation should begin at  $2a \sim \xi_M$ , where the particles become too large to fit inside the mesh. This entropic argument is essentially the same as the depletion attraction discussed previously, though the simple depletion picture gives no obvious estimate of the size limit for separation.

The situation is more complicated in the case of wormlike micelles than polymers. The entanglement points (see figure 6.1) can move more easily than those in entangled polymer solutions. The micelles' entanglement points can also move by scission and recombination, whereas in the case of polymers they can only move by the slower mechanism of reptation [23]. On addition of colloidal particles to an entangled solution of wormlike micelles the entanglement points could move easily to allow a colloid more freedom to diffuse even if the mesh size is much smaller than the colloid, possibly reducing the effectiveness of the depletion attraction in the entangled regime.

### 6.2.5 Possibility of Branching

There is also evidence in studies of wormlike micelles that branching (section 5.3) may take place [41]. This may affect the depletion interaction. It is minimised in this study by carrying out the observations at a temperature not far above the Krafft temperature, where branching is not found to occur [87]. The possibility of branching is therefore neglected in this thesis.

## 6.3 System A - Uncharged Colloid

### 6.3.1 Experimental Phase Diagram

Figure 6.2 shows the experimentally determined phase behaviour of PEO-coated polystyrene colloid (radius,  $a=260\text{nm}$ ) in an aqueous solution of wormlike micelles of  $C_{16}E_6$  for varying concentration of colloid and surfactant. Included on the right hand y-axis of this diagram are the size ratios, found using the experimentally determined values of  $R_g$  and  $\xi_M$  [37] (section 5.2.1). There are only a few points on this phase diagram since the synthesis of the particles proved difficult, and therefore only a small batch of particles were produced. This, unfortunately, only allowed a limited number of samples to be made. This study is discussed first since, without coulombic interactions, it is the most simple case.

#### *Summary of Observations*

As seen in the phase diagram (figure 6.2) three distinct regions of phase behaviour were observed. At low surfactant concentration the colloid forms a single phase, namely a *colloidal fluid* in the solution of micelles. At a surfactant concentration of about  $0.0025\text{gcm}^{-3}$ , there is a change in behaviour, where the sample separates into *coexisting colloid-rich phase and colloid-poor phases*. At much higher surfactant concentrations, at about  $0.02\text{gcm}^{-3}$ , *colloidal gels* are found.

### 6.3.2 Details of Phase Behaviour

At low surfactant concentrations (the fluid region of figure 6.2) the colloid-wormlike micelle mixture is stable. The sample looks uniformly opaque and no visible changes are observed over a period of about a week. After this time some sedimentation of the particles is observed.

As the concentration of surfactant increases phase separation takes place. In a period of about a day, a much less opaque top phase becomes visible. Over a period of a few days the boundary between the two phases moves downward, after which time no further changes are observed over a period of a few weeks. By tipping the sample bottle it is

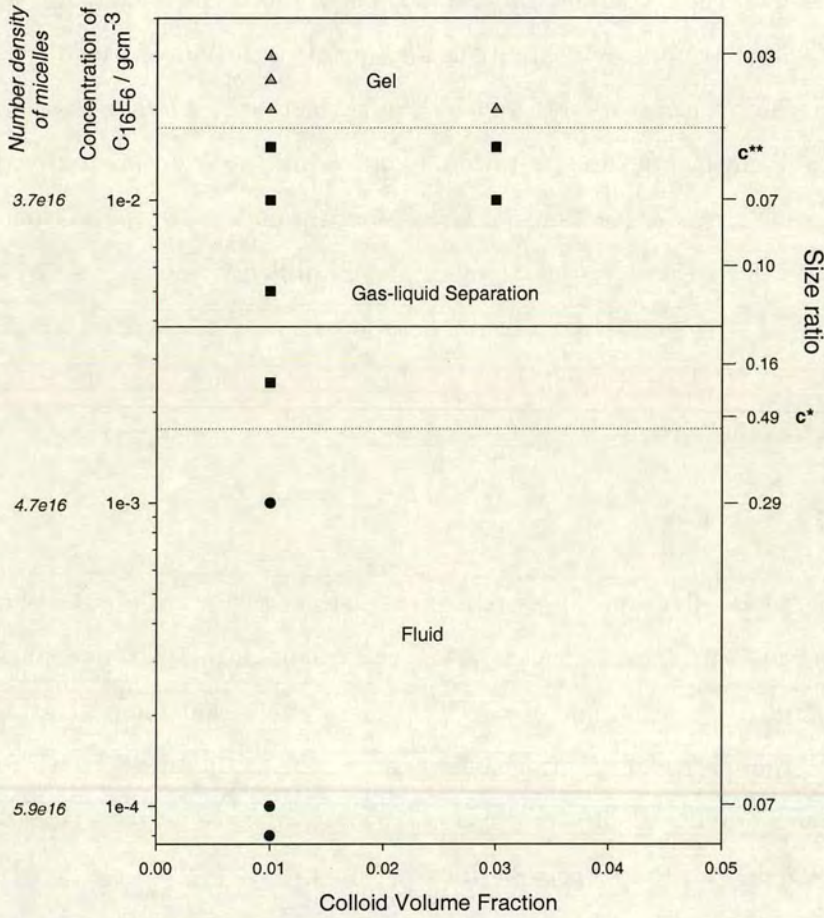


Figure 6.2: EXPERIMENTAL PHASE DIAGRAM OF SYSTEM A. Black circles represent a one phase fluid, black squares represent gas-liquid separation and triangles represent gels. The dotted lines are guides for the eye and are not exact phase boundaries. Additional y-axes indicating the number density of micelles (see figure 5.8) and the approximate size ratio ( $R_g/a$  or  $\xi_M/2a$ ) are shown. Also indicated are  $c^*$ , the overlap concentration (section 5.2.1, and  $c^{**}$ , where Maxwellian behaviour begins to be observed for the micelles (section 5.2.2). The errors associated with the composition of the samples is approximately the size of the symbol. The solid line is the theoretical gas-liquid binodal predicted by the Warren model (section 6.8).

observed that both phases flow like fluids. The colloid in this region therefore seems to have separated into coexisting dilute gas and more dense liquid phases. An interesting point is that the ratio of liquid to gas volume decreases as one moves up in surfactant concentration.

The third region of the phase diagram is the gel region. The samples here look inhomogeneous and have an uneven meniscus indicating solid-like properties. Sometimes channels or fractures in the dense phase can be observed. This behaviour was observed after about a day. The characteristic behaviour of a colloid-polymer gel, “delayed sedimentation” (see section 3.1.4) was, however, not observed. The gel does not settle over a period of a few months.

### 6.3.3 Discussion

The general behaviour observed in this study fits the depletion picture. At low surfactant concentrations a stable colloidal fluid phase is observed since there is too low a concentration to induce a large enough attraction to cause phase separation. It should be noted that as the surfactant concentration increases the number density of micelles in solution decreases, whilst their size increases due to the large associated growth exponent (as shown in section 5.2.1 and indicated on figure 6.2). This is more complicated than the colloid-polymer case, where the number of polymers and therefore volume fraction of depletants increases with concentration. Here the number of depletants decreases as the concentration increases, but the volume fraction of the depletant still increases due to its strong size dependence. The depletion attraction therefore becomes stronger as the concentration of  $C_{16}E_6$  increases, and hence phase separation begins to be observed. As mentioned the partitioning of the colloid between the gas and liquid phases becomes greater as the concentration of  $C_{16}E_6$  increases, since the depletion attraction is becoming stronger. As surfactant concentration is increased further the depletion potential becomes so high that the colloidal particles form a gel, as discussed in section 3.1.4.

## 6.4 System B - Charged Colloid with Added Salt

As mentioned in chapter 4 two studies were made on system B. A study of *charged* colloids (surfactant-free IDC lattices of various sizes) in a solution of *uncharged* wormlike micelles both *with and without added salt* were investigated. The system with salt is discussed first because it is most similar to the uncharged or hard sphere case of system A. This is because the added salt screens the coulombic repulsion between the particles, and therefore results in a small Debye screening length and short-range interactions. The particles, therefore, behave essentially as hard spheres. The added salt was kept to concentrations below the ccc's of the particles (table 5.4) to ensure that the salt itself does not induce aggregation. The addition of salt may have some effect on the packing factors of the surfactant (section 2.4) and therefore the phase behaviour of the surfactant alone at 26°C was checked. It was found that no micellar phase changes took place on addition of up to 1% salt.

### 6.4.1 Experimental Phase Diagrams

For each colloidal size (175nm, 105nm and 70nm radius) a phase diagram with varying surfactant and salt concentration has been determined for a colloidal volume fraction of 1%. Again the size ratios are indicated on these phase diagrams, which are shown in figures 6.3, 6.4 and 6.5.

#### *Summary of Phase Behaviour*

The phase diagrams show similar trends to that of system A discussed previously, except for the low surfactant behaviour. The main observations are:

- *Instability* in the mixture is found at very low surfactant concentrations.
- *Colloidal fluids* are then found.
- *Gas-liquid separation* is observed as the concentration of C<sub>16</sub>E<sub>6</sub> increases.
- *Nonequilibrium gels* appear at higher still C<sub>16</sub>E<sub>6</sub> concentrations.

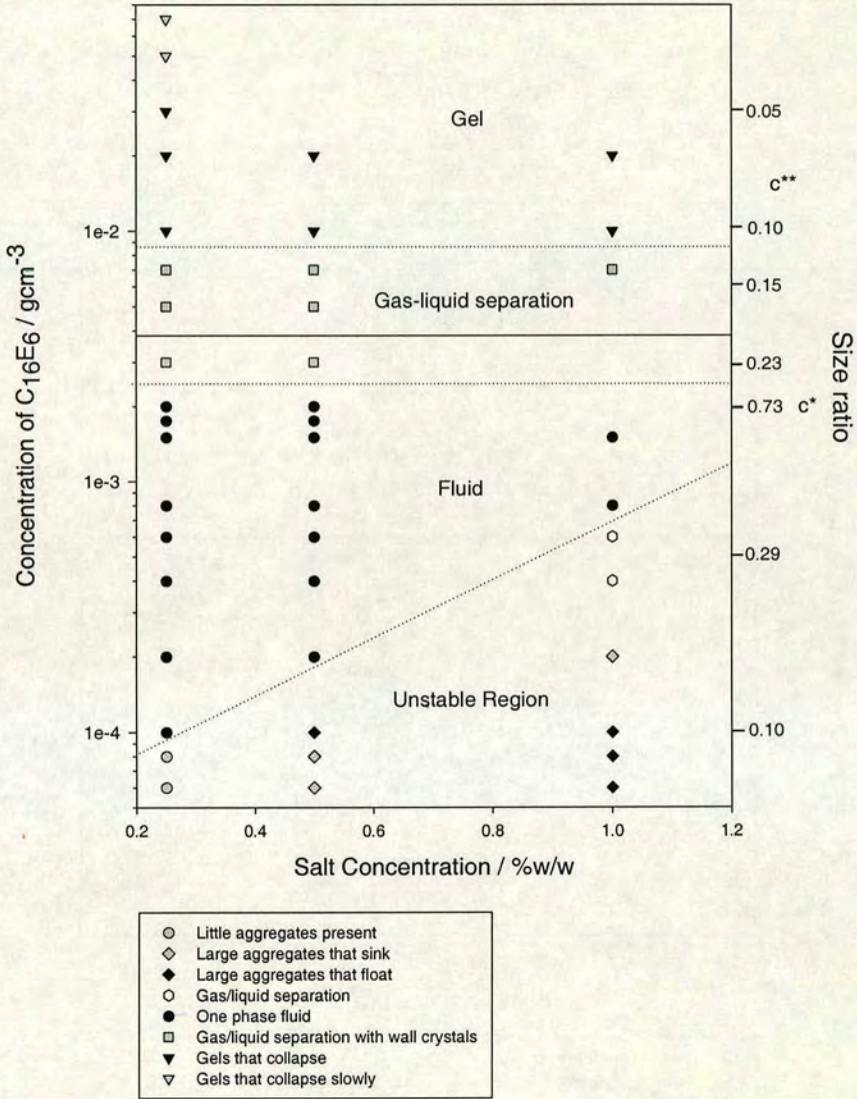


Figure 6.3: PHASE DIAGRAM OF SYSTEM B WITH ADDED SALT - 175NM PARTICLE. Experimental phase behaviour of a 1% volume fraction of latices for varying salt and surfactant concentrations. The legend indicates the behaviour represented by the various symbols. The dotted lines are guides for the eye to separate the various types of behaviour observed, they are not exact phase boundaries. The right-hand y-axis indicates the approximate size ratio ( $R_g/a$  or  $\xi_M/2a$ ). Also indicated are  $c^*$ , the overlap concentration, and  $c^{**}$ , where Maxwellian behaviour begins to be observed for the micelles. The uncertainty in the composition of the samples is smaller than the size of the symbols. The solid line is the theoretical gas-liquid binodal predicted by the Warren model (section 6.8).



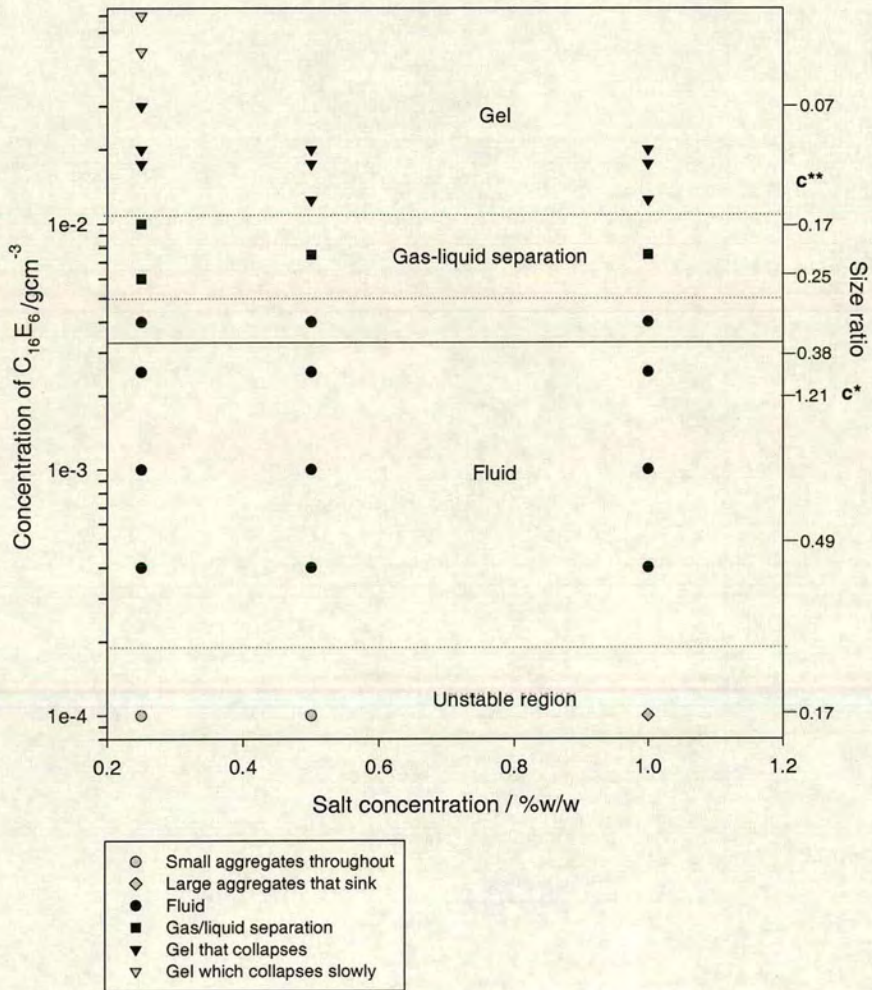


Figure 6.4: PHASE DIAGRAM OF SYSTEM B WITH ADDED SALT - 105NM PARTICLES. Colloid volume fraction and symbols are as for figure 6.3

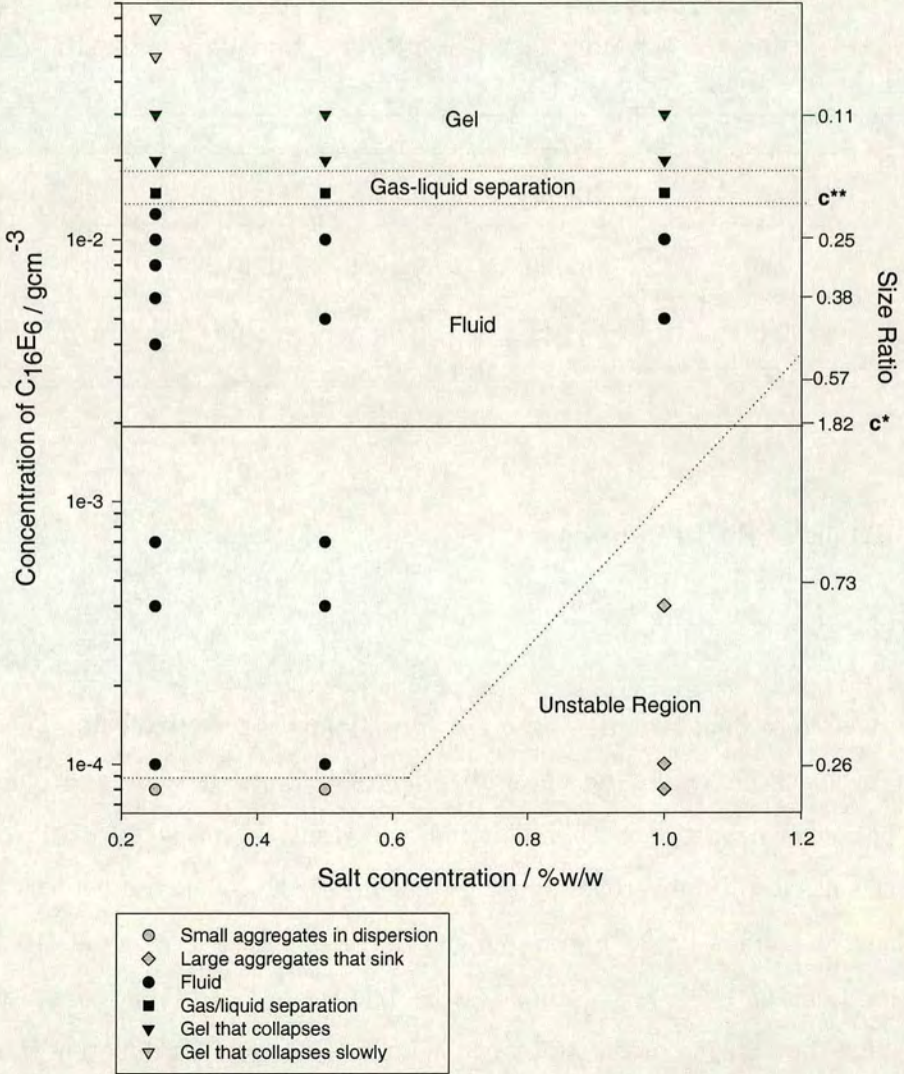


Figure 6.5: PHASE DIAGRAM OF SYSTEM B WITH ADDED SALT - 70NM PARTICLE. Colloid volume fraction and symbols are as for figure 6.3

Approximate surfactant concentrations for the gas/liquid and gel phase boundaries and the corresponding size ratios for each colloidal size are presented in table 6.1.

Table 6.1: Approximate surfactant concentrations of phase boundaries for 1% charged colloid & salt.

Colloidal Radius /nm	Phase Separation		Gel Boundary	
	Boundary /gcm <sup>-3</sup>	Size Ratio	Boundary /gcm <sup>-3</sup>	Size Ratio
175	0.0025	0.25	0.0085	0.12
105	0.005	0.26	0.015	0.16
70	0.015	0.23	0.02	0.20

### 6.4.2 Details of Phase Behaviour

#### *Fluid*

A large one-phase fluid region is observed for all three sizes of colloid. The samples denoted by black circles in the phase diagrams look homogeneous and opaque over a time period of days to weeks.<sup>†</sup> This indicates that the phase is a colloidal fluid, though this has also been verified by measurements of the colloidal dynamics via DWS as outlined in section 4.6.3. Figure 6.6 shows the ensemble average of the intensity correlation function  $g^{(2)}(\tau)$  of a sample in the fluid region ( $a=175\text{nm}$ ). As discussed in section 4.6.3 the baseline in the graph of the intensity correlation function should be 1 for an ergodic sample. In this case the baseline is slightly above 1.0. This is likely to be due the fact that the averaging is done over a relatively short time and that only 10 positions of the sample were probed. In order to check that this is the case and that the sample really is a fluid the ensemble average of  $g^{(2)}(\tau)$  for an aqueous solution of 175nm particles without surfactant was measured in the same way for comparison purposes. The baseline in this case was also found to be higher than 1 by roughly the same amount. The samples in this region were therefore confirmed to be ergodic, i.e.

<sup>†</sup>Sedimentation is observed in the low surfactant concentration (and therefore less viscous) samples.

equilibrium fluids.

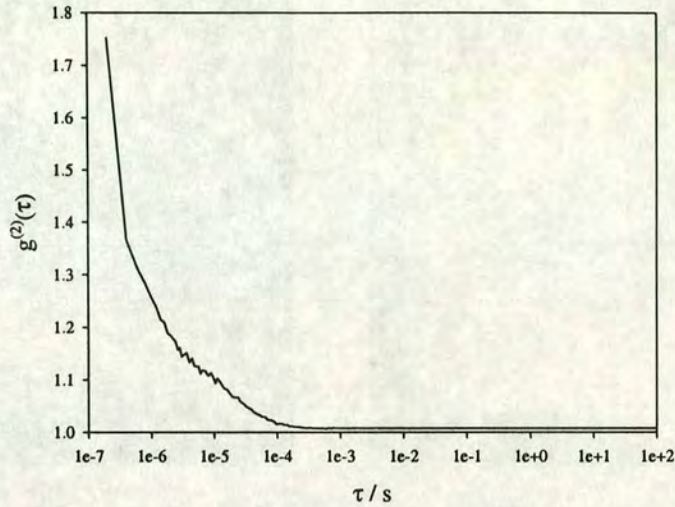


Figure 6.6: Ensemble average of the intensity correlation function  $g^{(2)}(\tau)$  measured by DWS for a fluid phase sample.

### *Phase Separation*

At high enough surfactant concentrations, for all three sizes of colloid, the samples are observed to phase separate over the period of a day into colloid-rich and colloid-poor phases. There are some differences in the phase behaviour for the different sizes of particles. In the case of the 175nm radius particles (figure 6.3) each sample is made up of about 40-45% of the lower more opaque phase and about 55-60% of the upper more transparent phase (see figure 6.7(B)). With such a low volume fraction of colloidal particles present in these samples (1%) it is unlikely that the lower phase is simply a dense colloidal fluid. However, both phases are found to be fluid when the sample cell is tipped up, and the lower phase does not look inhomogeneous. These samples also have wall crystals spanning the two phases, as indicated by iridescence.

The 105nm and 70nm radius particles show slightly different behaviour. The opaque lower phase is a very much smaller proportion of the whole sample, about 2-4% by volume. This phase is also observed to behave as a fluid when the sample bottle is tilted. No wall crystals are observed in these cases.

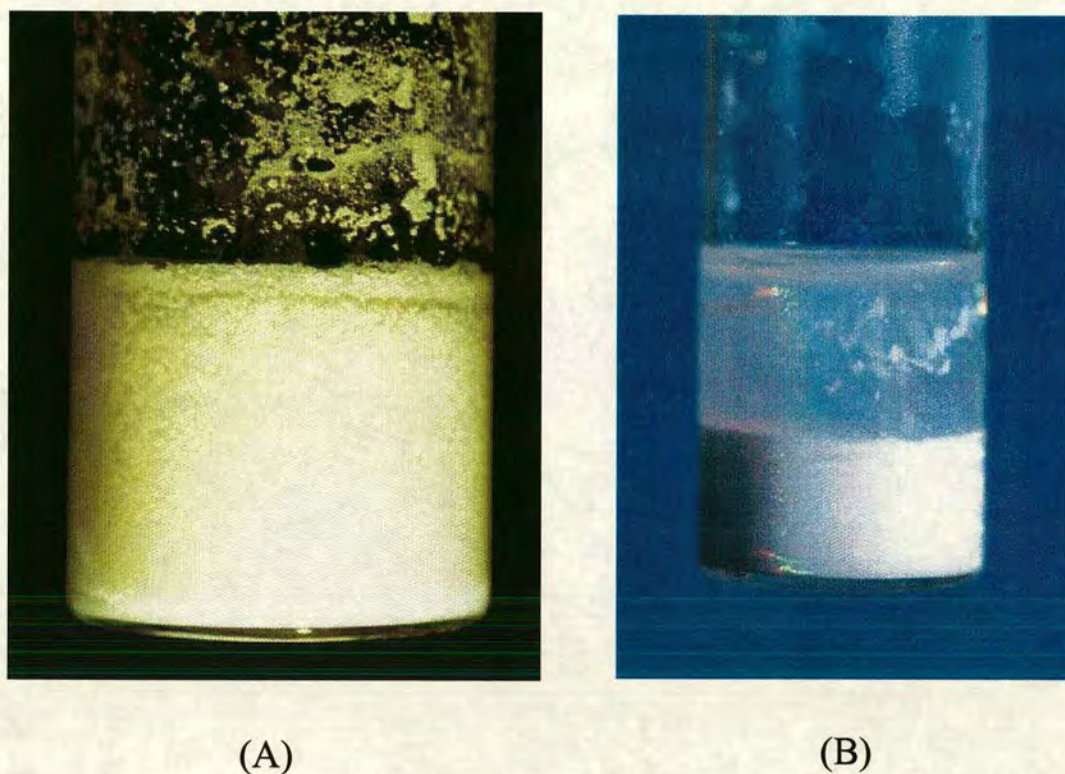


Figure 6.7: Photos of samples of system B with added salt. (A) is a sample at very low surfactant concentrations where the colloid is found to form larger aggregates. (B) is an example of fluid-fluid separation with wall crystals (seen from the iridescence) for the 175nm particle case.

Determining the nature of the phases more precisely is troublesome. Investigating the ergodicity of the lower (opaque) phases of 175nm samples by DWS proved unreliable. By placing the sample into the rig (figure 4.10) the phases are disturbed. This could be overcome by leaving a freshly made sample in the set-up and allowing the phase separation to take place in situ. However, the sample is again disturbed by moving it in order to obtain the ensemble average. The part of the sample probed must also be well below the interface between the two phases otherwise scattering of light from the interface could affect the measurements. The presence of wall crystals also complicates the situation and may have an influence on the scattering measurements. In the case of the 105nm and 70nm radius particle samples the lower phase constituted less than 1mm in height and was therefore impossible to probe by DWS. Therefore in all three cases the behaviour is assumed to be gas-liquid separation and is indicated on the phase diagrams by black squares.

*Gelation*

The phase behaviour changes as the concentration of  $C_{16}E_6$  increases. Around  $0.01\text{gcm}^{-3\dagger}$  in all three cases the samples begin to look inhomogeneous: after about a day the samples look lumpy and long channels appear. Channels have been observed during the collapse of particle gels of colloid-polymer mixtures by Starrs [63]. This and the inhomogeneous, nonergodic nature of the samples indicate that the phase is a colloidal gel. To check that the behaviour was indeed non-ergodic a typical sample was probed by DWS in the same way as the fluid (figure 6.8). The baseline was indeed found to be greater than 1, indicating that the sample was non-ergodic. Over a few days<sup>§</sup> the gels collapse, resulting in an opaque inhomogeneous lower phase and a slightly cloudy upper phase. Photos of a typical gel sample during collapse are shown in figure 6.9. The collapse was investigated by direct observation (section 4.5) for a couple of typical samples. The sedimentation profiles are shown in figure 6.10. They do not show the same collapse behaviour as observed in the case of colloid-polymer mixtures (figure 3.16).

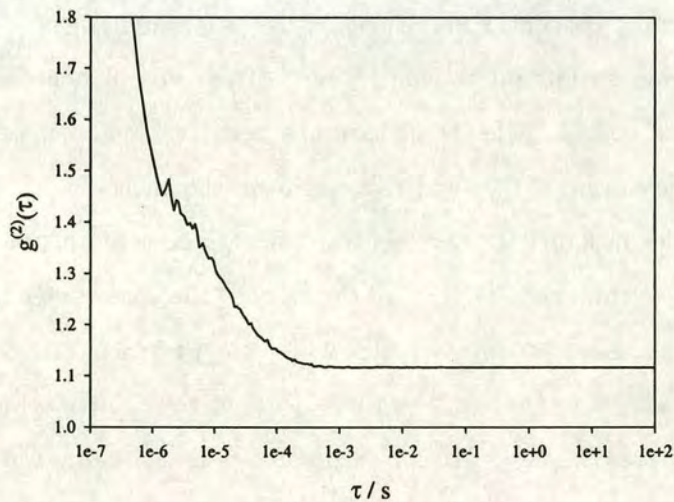


Figure 6.8: Ensemble average of the intensity correlation function  $g^{(2)}(\tau)$  for a gel.

<sup>†</sup>a little higher in the 70nm radius case

<sup>§</sup>The grey inverted triangles in the phase diagrams indicate gels that take longer, on the order of a couple of weeks, to collapse

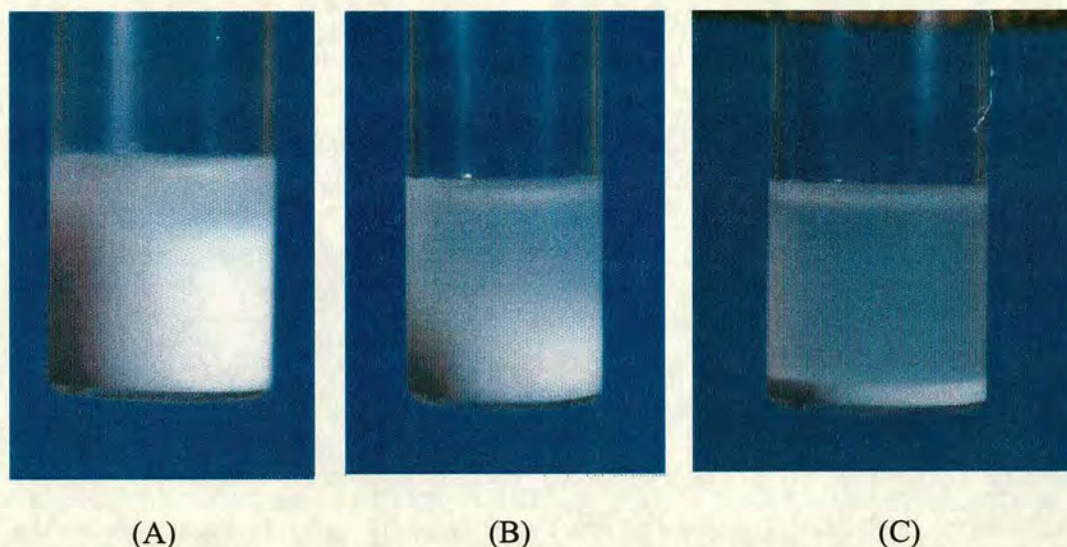


Figure 6.9: Photos showing the various stages of the gels found in system B with added salt. Photo (A) shows the behaviour once collapse has just started, one can see the lump nature of the gel clearly in this photo. Photo (B) shows the gel at a later time, and photo (C) shows the final state of the gel. No further changes were observed over a period of a couple of months. One can see in this gel collapse some colloid is left behind, leaving a colloidal gas phase on top.

#### *Low Surfactant Concentration*

At very low surfactant concentrations the mixture was found to be unstable, before restabilising at higher surfactant concentrations. This type of behaviour is observed for all three sizes of colloid. The behaviour has been studied in most detail for the 175nm radius particles (figure 6.3) and this will form the basis of the following discussion. The grey circles in figure 6.3 represent samples which contain small aggregates of particles (typically  $\sim 1$ mm across) floating throughout the otherwise uniformly opaque sample. The grey diamonds denote samples where the particles form large aggregates (typically a few mm in size) that sink to the bottom of the sample cell, leaving a clear upper phase<sup>¶</sup>(see figure 6.7(A)). The black diamonds indicate the formation of large clusters of colloid that float in the sample, leaving a clear phase at the *bottom* of the sample cell. Again there is no sharp interface between the phases. In both cases where large aggregates are formed the behaviour is irreversible. The white hexagons shown correspond to samples which show apparent gas-liquid coexistence, like that observed

<sup>¶</sup>This, however, is not reminiscent of gas-liquid separation discussed for system A as the colloid is obviously present in large lumps and a sharp interface does not exist between the clear solution and the colloidal lumps.

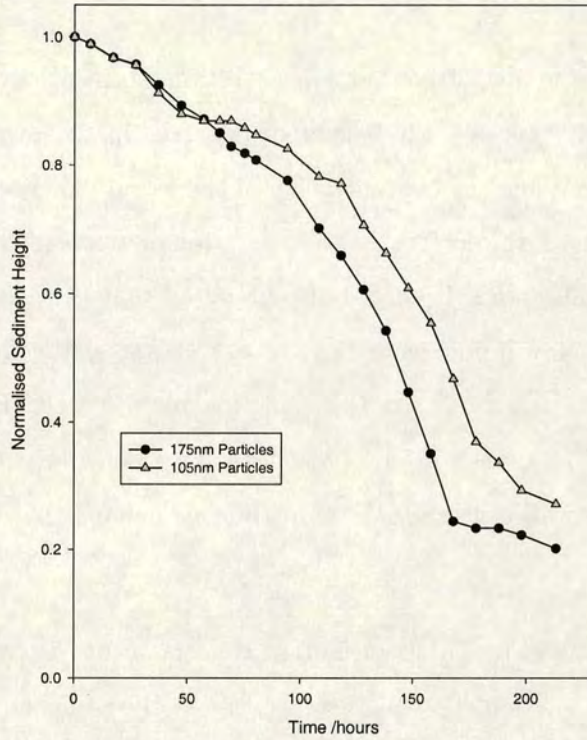


Figure 6.10: Sedimentation profiles of typical gels for system B with added salt. Both samples contain the same concentration of surfactant, salt and colloid and therefore the micellar properties are the same. The different times of collapse are due to the different sizes of colloid as indicated in the legend, with the larger particles collapsing more rapidly as expected. The collapse does not show the expected delayed sedimentation behaviour found for colloidal gels in colloid-polymer mixtures.

in system A. It appears that the mixture is unstable at low surfactant concentration but then becomes more stable as the surfactant concentration is increased, until finally a stable one phase fluid sample reappears. The instability appears to be more pronounced at higher concentrations of added salt. As stated the salt should not induce aggregation of the particles at such salt concentrations. Possible explanations for this unusual behaviour are discussed later in this chapter. Similar trends are found for the 105nm and 70nm particles.



### 6.4.3 Discussion

With the exception of the low surfactant concentration aggregation (at concentrations of approximately  $1 \times 10^{-4} \text{gcm}^{-3}$ ), the behaviour observed in this system is comparable with that of system A. When the concentration of the wormlike micelles is low a stable fluid phase is observed. As the surfactant concentration increases, first phase separation and then gelation are observed. It should also be noted that the gels become stronger, i.e. they take longer to show inhomogeneities and to collapse, as the  $\text{C}_{16}\text{E}_6$  concentration increases. This general behaviour fits the depletion picture well. However, there are still some problems. Why do the 175nm particles have a much larger proportion of the colloid-rich phase and wall crystals? Why do the gels collapse without a pronounced delay period?

The phase boundary moves to higher surfactant concentrations as the particle size gets smaller. This also fits the depletion picture because at the same surfactant concentrations the size ratios are smaller, and therefore the depletion potential well is deeper for the larger particles. Hence a deep enough potential to induce aggregation is found at lower surfactant concentrations for larger particles. It is surprising that there is no influence on the observed behaviour from the stability of the particles. The 105nm particles are found to be significantly more stable on addition of salt than the 175nm and 70nm radius particles 5.4. This is not reflected in the position of the phase boundaries with added salt and surfactant (table 6.1). This therefore indicates that the depletion attraction dominates over electrostatic effects.

The very low surfactant concentration behaviour results were compared with the theory for binary mixtures of colloids [69], and rod-sphere mixtures [74, 105], since surfactant is present as spherical micelles at very low concentrations and then grow into rodlike micelles upon increasing concentration. The volume fraction of surfactant present, however, is much lower than that needed for spherical or rodlike micelles to induce phase separation and thus does not offer a viable explanation. Also, the appearance of the majority of the samples in this regime are similar to colloidal samples with salt above the ccc indicating that it is a charge effect and not a result of the depletion attraction. Somehow the particles overcome their coulombic repulsion and get into the deep primary minimum. The changes in the appearance of the aggregates as the salt

concentration increases is also indicative of this. At low concentrations of salt small aggregates are formed as the nucleation and growth rates will be similar. As the salt concentration increases the growth rate will increase relative to the nucleation and thus larger aggregates will form. For the highest salt concentrations the aggregates might then be more open and probably trap air, causing them to float.

One possible explanation for the low surfactant concentration behaviour is the adsorption of the surfactant onto the surface of the colloid. Evidence exists of the adsorption of telechelic PEO molecules, where a PEO chain is sandwiched between two carbon chains, onto polystyrene particles [106]. The adsorption of  $C_{16}E_6$  onto the particles would cause the counterions to recondense onto the surface of the colloid due to the low dielectric constant of the EO groups. The Debye layer would thus be diminished, as if more salt had been added, allowing the particles to aggregate. This effect is only important when the screening length of the particles is comparable to the length of the surfactant molecule. The latter is about 1-2nm and therefore this behaviour is only found in system B with added salt where the screening lengths are about 1-2nm (table 5.5). This accounts for the aggregation of particles at low surfactant concentration, but what about the restabilisation? This restabilisation at higher surfactant concentrations may be induced once there is a full monolayer coverage of the surfactant on the colloid, where they then become sterically stabilised colloids. This stability has been found by di Basio et al. [107] when full coverage of the polymer PEO onto polystyrene particles is reached. An estimate of the concentration of surfactant at which monolayer coverage takes place for each size of particles has been calculated. The head group area of the surfactant was estimated using the molecular weight per unit length of wormlike micelles of  $C_{16}E_6$  determined by Schurtenberger et al. [37]. The concentration of surfactant required to cover the surface area of a 1% volume fraction of particles of the three sizes was then determined. These values are shown in table 6.2. These estimates roughly agree with the concentration at which restabilisation is observed experimentally for low salt concentration. (The head group area estimate is for  $C_{16}E_6$  with no added salt but this will change with the addition of salt as discussed later.) The curvature effect on the packing of the surfactant molecules onto the colloid is neglected in this estimate.

As the salt concentration increases the concentration of  $C_{16}E_6$  required to restabilise

Table 6.2: Estimates of surfactant concentrations corresponding to monolayer coverage of the particles.

Colloidal Radius nm	Concentration of Surfactant g/cm <sup>3</sup>
175	2E-4
105	3E-4
70	5E-4

the mixture becomes higher as seen in figures 6.3 and 6.5 <sup>||</sup>. The salt reduces the head group area of the surfactant by dehydration of the EO groups as discussed in section 2.4.5.1 and thus allows them to pack more closely together, thus increasing the number of surfactant molecules required to produce monolayer coverage. This would therefore qualitatively account for the increase in surfactant concentration required to restabilise the mixture with a high concentration of salt.

Adsorption of surfactant onto the colloidal surface and subsequent counterion recondensation changes the charge on the colloidal particles which influences its mobility in an electric field. Measurements of the mobility at both low and high surfactant concentrations for system B with added salt would thus allow us to test this hypothesis (see section 8.6).

## 6.5 System B - Charged Colloid, no Added Salt

In the following section the results determined for system B *without* added salt will be presented and discussed. In this case the coulombic repulsion between the colloid is not screened and therefore the colloidal particles have a significantly extensive double layer surrounding them. For various colloidal volume fractions the screening lengths found by conductivity measurements can be found in table 5.3. The colloidal particles in this system have a larger effective radius, seen by neighbouring colloids, of approximately

<sup>||</sup>In the case of the 105nm particles, the smaller number of samples in this region of the phase diagram does not allow us to determine the exact shape of the phase boundary (figure 6.4).

$a + \kappa^{-1}$ , and thus a higher effective volume fraction,  $\phi_{eff}$ , of,

$$\phi_{eff} = \phi \left(1 + \frac{1}{\kappa a}\right)^3 \quad (6.1)$$

where  $\phi$  is the real colloid volume fraction.

The micelles are, however, *uncharged* and so are expected to move into the double layer with no constraints. The micelles should therefore see the real colloid volume fraction. If the micelles can move between two colloids separated by their screening lengths due to the coulombic interaction one might suppose that they should not induce a depletion interaction, as discussed in section 3.1.3 (figure 3.6). The depletant diameter should be larger than  $2\kappa^{-1}$  (as a first approximation) to induce an attraction. How then will this affect the phase diagram?

### 6.5.1 Experimental Phase Diagrams

The experimental phase behaviour of the three different sizes of charged polystyrene latex particles with varying concentration of C<sub>16</sub>E<sub>6</sub> is shown in figures 6.11, 6.12 and 6.13.

#### *Summary of Phase Behaviour*

The phase diagrams show similar trends to that of system A and system B with added salt discussed previously. Differences will be highlighted and discussed in subsequent sections. The main observations are:

- *Colloidal fluids* are found at low surfactant concentrations.
- *Coexisting colloid-rich and colloid-poor phases* are observed as the concentration of C<sub>16</sub>E<sub>6</sub> increases.
- *Nonequilibrium gels* appear at higher still C<sub>16</sub>E<sub>6</sub> concentrations.

Estimates of the phase boundaries and size ratios for each colloidal size are shown in table 6.3.

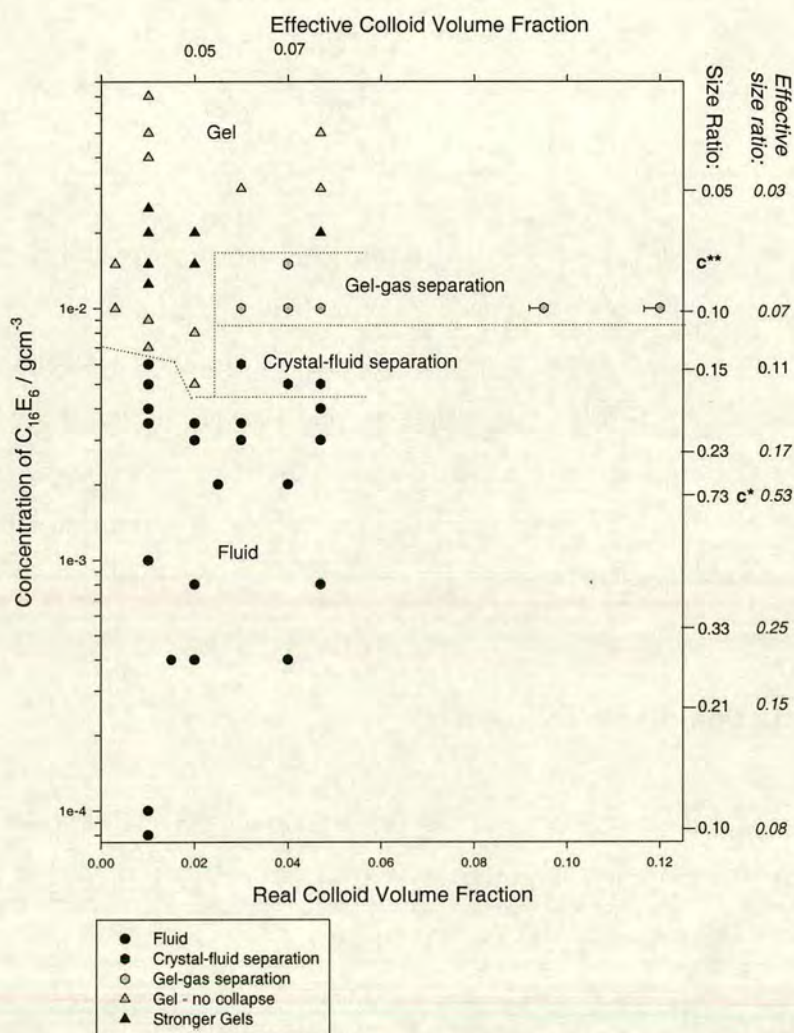


Figure 6.11: PHASE DIAGRAM OF SYSTEM B NO ADDED SALT - 175NM PARTICLES. Experimental phase diagram as a function of surfactant and colloid concentrations for 175nm particles in  $C_{16}E_6$ . The repulsion between the charged lattices is not highly screened in this system and therefore both the real and effective colloid volume fractions are indicated. The effective colloid volume fraction is only given up to 4% real volume fraction as the values of  $\kappa^{-1}$  used to determine them were those found via the conductivity measurements (table 5.2). The variation of the size ratio ( $R_g/a$  or  $\xi_M/2a$ ) and the effective size ratio ( $R_g/(a + \kappa^{-1})$  or  $\xi_M/2(a + \kappa^{-1})$ ) of the system as the  $C_{16}E_6$  concentration increases is also shown on the second y-axis. Also indicated here is the overlap concentration  $c^*$  and the concentration at which Maxwellian behaviour is first observed  $c^{**}$ . The dotted lines are guides for the eye and not phase boundaries. The symbols used are larger than the associated uncertainty, except at high colloid volume fraction where error bars are indicated. The error bars at high colloid volume fractions are not symmetrical as the colloidal solution is concentrated via evaporation. During this procedure some colloid gets stuck to the walls of the vessel and thus the volume fraction of colloid in the sample must be smaller than expected.

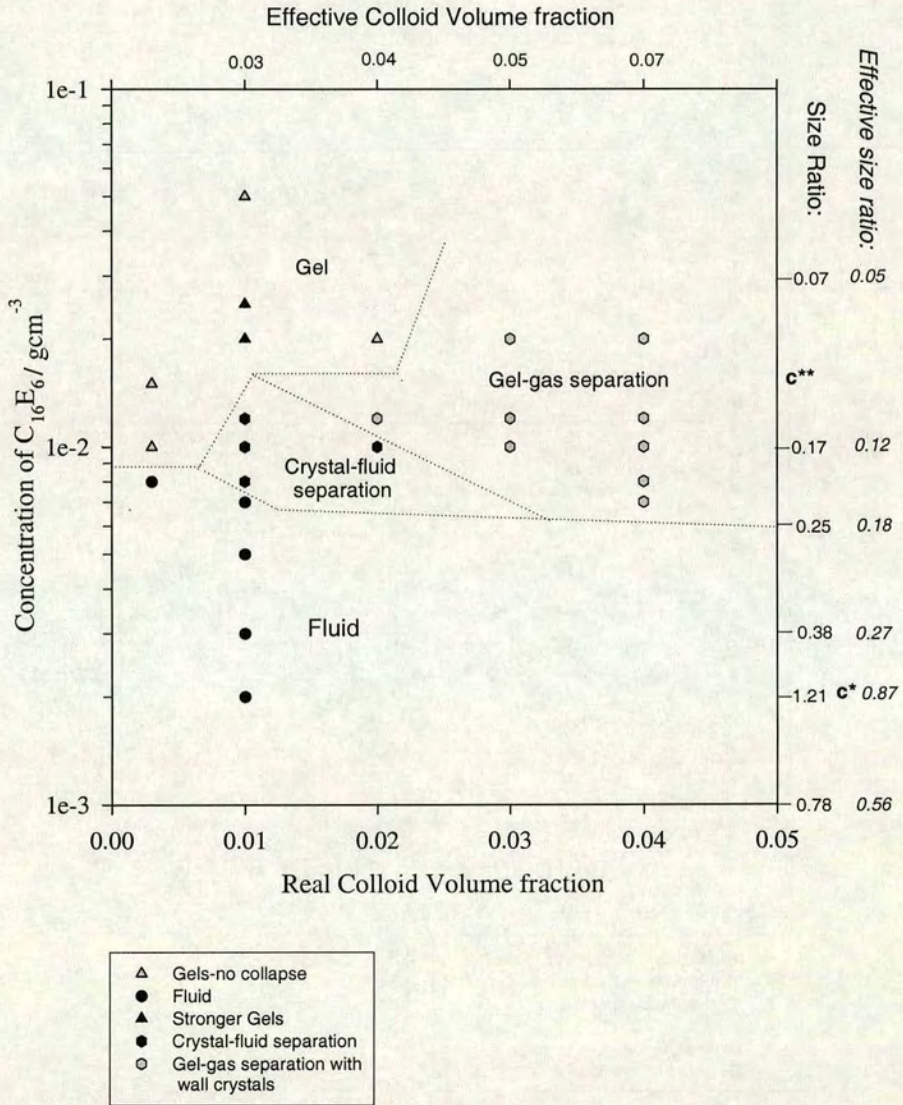


Figure 6.12: PHASE DIAGRAM OF SYSTEM B NO ADDED SALT - 105NM PARTICLES. Symbols etc. as for figure 6.11.

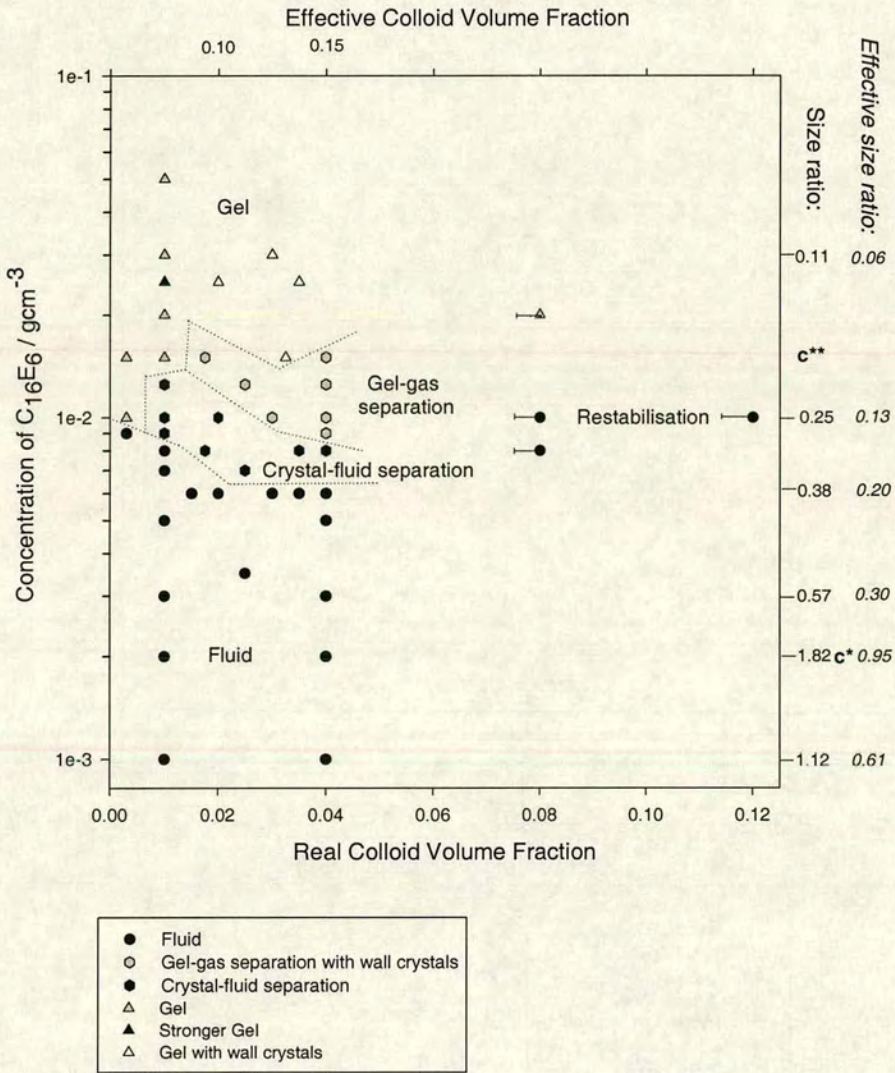


Figure 6.13: PHASE DIAGRAM OF SYSTEM B NO ADDED SALT - 70NM PARTICLES. Symbols etc. as for figure 6.11

Table 6.3: Estimates of surfactant concentration phase boundaries for charged colloid (real volume fraction  $\approx 3\%$ ), no salt.

Colloidal Radius /nm	Phase Separation			Gel Boundary		
	Boundary /gcm <sup>-3</sup>	Size Ratio	Effective Size Ratio	Boundary /gcm <sup>-3</sup>	Size Ratio	Effective Size Ratio
175	0.005	0.19	0.15	0.0125	0.12	0.09
105	0.007	0.25	0.18	0.015	0.16	0.12
70	0.0075	0.33	0.17	0.015	0.23	0.12

### 6.5.2 Details of Phase Behaviour

#### *Fluid*

At low surfactant concentrations and low real colloid concentrations the mixture is a stable one phase fluid. This has been confirmed by carrying out DWS measurements on a typical sample. The baseline of the ensemble average of the intensity correlation function  $g^{(2)}(\tau)$  was found to be very close to 1, similar to that found for a dilute solution of particles in water using the same technique. In the case of the 70nm radius latices (figure 6.13) fluid phases are also found at higher real colloid volume fractions of about 10% at concentrations around  $0.01\text{gcm}^{-3}$ , where separation already takes place for lower colloid volume fractions. It was confirmed by DWS that these samples are indeed fluids. High colloid volume fractions have also been investigated for the 175nm particles. In figure 6.11 the behaviour of samples at 10% and 12% real colloid volume fraction are shown. However, these and additional samples with volume fractions up to 30% at  $\text{C}_{16}\text{E}_6$  concentrations of  $0.01\text{gcm}^{-3}$  were all found to phase separate.

#### *Phase Separation*

Two types of “phase” separation are found in this system, namely crystal-fluid separation and gel-gas separation\*\*. DWS could not be carried out on the separate phases to

\*\*It should be noted that gel-gas separation cannot be an equilibrium state. The term “phase” used



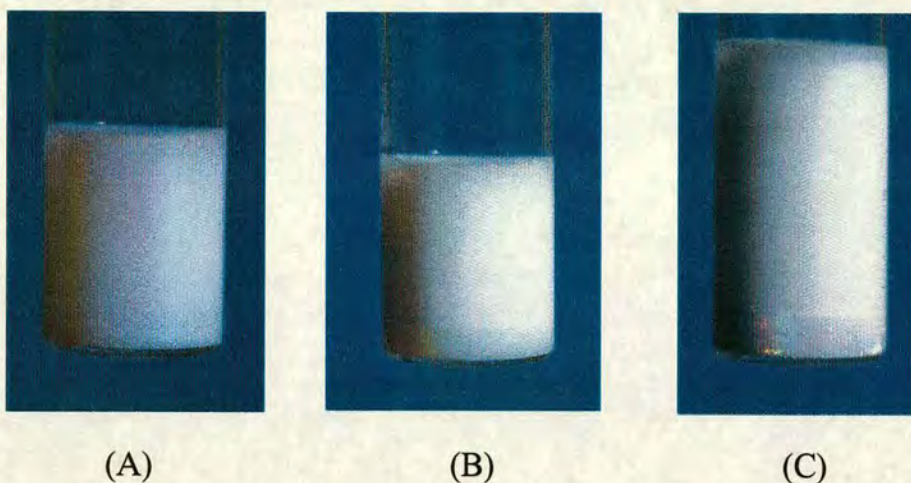


Figure 6.14: Photos of crystal fluid samples for system B with no added salt. Both photos (A) and (B) are 70nm radius particle samples. It can be seen that the behaviours appear quite different. In (A) there are wall crystals throughout the sample while in B there are crystals only in the lower phase. Photo (C) is similar to (B) but is the 175nm particle case. In all three photos it can be seen that the upper fluid phase is still very opaque.

determine whether they were ergodic for the reasons outlined in section 6.4.2. Colloidal crystals are iridescent - the crystal lattice size is comparable to the wavelength of visible light, so that they scatter strongly in the visible spectrum. For the opaque samples studied here it is difficult to tell whether the crystals are simply wall crystals or whether there are crystals in the bulk. The obvious way to investigate this would be by the light-scattering equivalent of x-ray powder crystallography. This was attempted for a typical sample in the crystal-fluid part of the phase diagrams, but the diffuse scattering due to the turbidity of the sample and the small amount of crystal phase observed made the detection of any Bragg peaks impossible. By moving to thin rectangular cells it was hoped these problems could be overcome but the samples did not crystallise. The behaviour observed for a few samples in different cells was not the same as that in the cylindrical cells used to determine the phase diagram.

Two distinct types of “phase coexistence”, crystal-fluid coexistence and gel-gas coexistence were identified on the following basis. In the former case the lower more opaque phase did not move when the samples were tilted. Crystallites appear to be present in the bulk (see figure 6.14), as well as on the walls of these samples. The proportion of the lower phase was also determined by measuring its height. This was then compared

in this context is therefore not strictly correct but it will be continued to be used to describe the observed behaviour.

with the proportion of the sample expected to be taken up if the colloid, of volume fraction  $\phi_{eff}$  (equation 6.1), was close packed at about  $\phi \sim 50\%$ . The crystal phase was therefore found to take up 5-15% of the sample depending on  $\phi$  and the Debye length of the particles. The proportions of crystal phase found experimentally in the crystal-fluid samples agree reasonably well with this estimate. The upper phase in these samples remains relatively opaque indicating a fairly dense fluid. Sometimes wall crystals are also observed in the upper phase.

In the second case, gel-gas coexistence, a significantly larger proportion of the sample was taken up by the more opaque, lower phase. This phase also looked inhomogeneous and lumpy. When these samples were tipped up the bottom phase was seen to move only very slowly. Thus the lower phase is thought to be a gel. The upper phase in these samples is relatively clear, indicating a small amount of colloid being present and this is a colloidal gas. It should be noted that the gel-gas samples also have wall crystals present. Photos of gel-gas coexistence for 105nm radius particles is shown in figure 6.15(A).

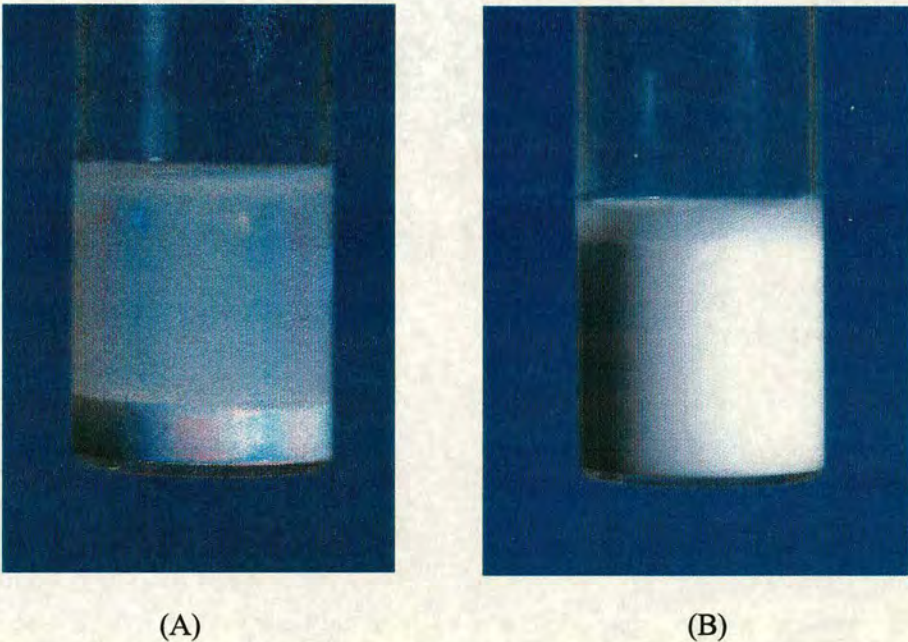


Figure 6.15: Photos of samples for system B with no added salt. (A) is a typical gel-gas sample with wall crystals. (B) is a typical gel. This photo has been taken after a few weeks and this level of separation remains after a period of a few months. The inhomogeneities in photo (B) are not so clear as in system B with salt. An uneven meniscus (at the top of the gel phase) is observed.

*Gels*

Metastable gels are indicated by triangles on the phase diagrams. It was confirmed by DWS measurements that these samples were non-ergodic. The samples in this region are observed to be inhomogeneous, with lumps and channels throughout the sample, though to a lesser degree than observed for gels of system B with added salt. The samples represented by black triangles, however, look completely uniform for a week to two weeks and then begin to look lumpy. These are therefore termed stronger gels in the phase diagrams. After a few months samples in this region still have not collapsed. An uneven meniscus is also observed, above which the top couple of millimetres of the sample looks less cloudy (see figure 6.15(B).) This behaviour is observed to take place over a couple of days for the samples represented by grey triangles but a few weeks to months for those indicated by black triangles.

**6.5.3 Discussion**

In system B without salt one may expect rather different behaviour than in the case of system A and system B with added salt. The large values of the screening length indicate a highly stable colloidal suspension. It would therefore be expected that a higher concentration of surfactant would be required to induce phase separation by depletion. This is the case for both the 175nm and 105nm radius particles but not for the 70nm radius particles (see tables 6.1 and 6.3). This trend seems counter-intuitive and will be discussed in more detail later.

**6.5.3.1 Depletion Picture of Charged Colloid and Uncharged Wormlike Micelles**

Intuitively when considering depletion of charged colloids by uncharged micelles one would expect that a depletion attraction should only be induced when the micelle is larger than the screening length of the colloid, as mentioned earlier. There are, however, a number of reasons why a depletion attraction could indeed be induced in this situation.

Firstly, the size of the micelles considered is their average size both in the dilute and semi-dilute regimes. As discussed though these micelles have an exponential size distri-

bution and therefore even if the average micellar size is too small to induce a depletion attraction there will be larger micelles which will be excluded from between two colloidal particles when they approach one another, as shown in figure 6.16 for the dilute regime.

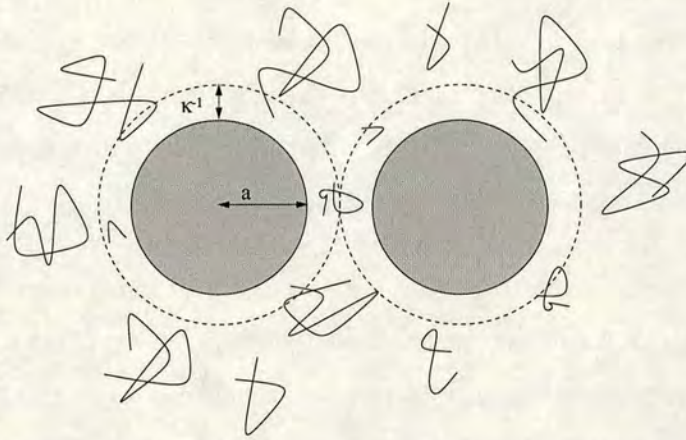


Figure 6.16: Schematic diagram illustrating the effect of a size distribution of wormlike micelles on the depletion interaction between two charged colloidal particles with radii  $a$  and screening lengths  $\kappa^{-1}$ . It can be seen that the uncharged micelles which are smaller than  $2\kappa^{-1}$  can move freely between the colloidal particles, whilst the larger ones cannot and therefore this leads to unbalanced osmotic pressure which induces an attraction between the colloidal particles.

It may also be too simple to assume that the micelle can freely move into the Debye layer. The oily core of the micelle has a low dielectric constant and will therefore be repelled from regions of high electric field [108]. For polyoxyethylene surfactants, such as  $C_{16}E_6$ , the EO headgroups also have a lower dielectric constant than water and therefore for these surfactants it is not only the core of the micelle that is excluded from the Debye Layer. If the micelle was in the Debye layer the electric field lines would either have to go through the oil or around it, in both cases causing a high field energy. The micelles therefore tend to avoid the Debye layer due to this *electrophobic effect*.

The picture of a charged colloidal particle being equivalent to a hard sphere colloid of radius  $a + \kappa^{-1}$  with regard to other colloids is also an oversimplification. The screening length is simply a measure of the fall off of the coulombic repulsion with distance between the particles. The particles are subject to Brownian motion and will be able to approach closer than  $2\kappa^{-1}$ . Even if the closer approach happens only with a small

probability one could still have a depletion attraction between the two particles in the presence of a solution of wormlike micelles with  $R_g < \kappa^{-1}$  in the dilute regime or  $\xi_M < 2\kappa^{-1}$  in the entangled regime.

Another possible effect may also take place in this mixture complicating the picture still further. The average length of the micelles was determined for a solution of wormlike micelles without colloid. However, this may change when the system is perturbed on addition of the colloidal particles. This is a difficult effect to investigate and therefore no information on such a possibility is available.

The effects discussed above show that in a solution of charged colloidal particles and wormlike micelles a depletion attraction, though likely to be less effective, may still arise where in the model colloid-polymer picture one would not expect this. It is difficult to tell which effect should dominate, and in fact a combination of these effects may be taking place. Indeed, as will be seen in the subsequent discussions, no one effect can rationalise all of the experimental data.

6.5.3.2 Discussion of Results in Terms of Depletion

Table 6.4: Values of  $\kappa^{-1}$  found from conductivity measurements for 1% colloid (section 5.1.1.2).

Colloidal Radius nm	$\kappa^{-1}$ nm
175	63
105	41
70	63.5

For all three colloidal sizes there is no phase separation observed in the dilute regime of the micelles. Phase separation begins around the overlap concentration of the micelles ( $c^* = 0.002 \text{gcm}^{-3}$  [37] (section 5.2.1)). The size range of the micelles in the dilute regime is about 18nm to 130nm (figure 5.6). The micelles therefore ought to be large enough to induce a depletion attraction for concentrations from about  $7 \times 10^{-4} \text{gcm}^{-3}$  for the

175 and 70nm particles and from about  $4 \times 10^{-4} \text{gcm}^{-3}$  for the 105nm particles.<sup>††</sup> Phase separation is, however, not observed at all in the dilute regime for system B with no salt, thus there is no evidence of a depletion attraction. The stability of the colloidal particles is likely to result from the long range coulombic repulsion, rather than the absence of a depletion interaction.

Above the overlap concentration for all three sizes of particles phase separation is observed, and at still higher concentrations gels are observed. As shown in figure 5.5 the largest value of the mesh size is 90nm and this decreases as the concentration of  $C_{16}E_6$  increases. Therefore in the simplest picture depletion would not be expected at all for the 175nm and 70nm radius particles since the mesh-size is always smaller than  $2\kappa^{-1}$ . In this picture the 105nm radius particles should only separate up to a concentration of about  $0.003 \text{gcm}^{-3}$ . That phase separation still occurs may be for a number of reasons. It may indicate the importance of the size distribution of the micelles and the oversimplification of considering the colloidal radius to be  $a + \kappa^{-1}$ , when considering if a depletion attraction will take place. Alternatively, the electrophobic effect may be excluding the mesh from the Debye layer, allowing a depletion attraction to be induced.

The other thing to consider here is the validity of the picture of the depletion attraction in the entangled regime, where little study has been carried out. The assumption that depletion is due to blobs of mesh-size  $\xi_M$  (section 6.2) may be too simple a picture. From the predictions of Sear [104], by entropic arguments, discussed earlier one would expect phase separation for all three sizes at all concentrations of  $C_{16}E_6$  above  $c^*$  as the mesh-size is always smaller than the colloidal diameter.

The observation of wall crystals is due to a depletion attraction between colloidal particles and the wall of the sample vial as shown in figure 3.18. It is however unclear why it is observed only in some phase samples.

As found for system B with added salt the phase boundaries move to higher surfactant concentrations for smaller particles (see table 6.3). This is due to the less efficient depletion attraction due to the larger size ratios for smaller particles at the same  $C_{16}E_6$  concentrations.

---

<sup>††</sup>These concentrations are found by comparing the values of  $R_g$  for the micelles found by light scattering [37] and shown in figure 5.6 to the values of  $\kappa^{-1}$ . When  $R_g$  becomes larger than  $\kappa^{-1}$  a depletion attraction is expected.

*Gel Region*

The gels observed do not collapse (within a period of two months) as in model colloid-polymer systems (section 3.1.4). It is therefore impossible to assess how strong the gels are by considering the latency time as is done for colloid-polymer mixtures [63]. By considering the time taken for inhomogeneities to form in gels of system B with no salt it has been noticed that the gels get stronger as the concentration of  $C_{16}E_6$  increases, but then become weaker again as the concentration increases still further. This can be rationalised only if one considers there to be essentially no electrophobic effect \*. There is then a competition between two effects here. Firstly, the increase in concentration of surfactant leads to a larger depletion well depth just as an increase in concentration of polymer does in colloid-polymer mixtures (figure 3.1). Secondly, the mesh size is getting smaller and blobs can fit in between the two colloidal particles easily †, thus reducing the depletion attraction. As the concentration increases, initially the first effect dominates and the gels become stronger. At still higher surfactant concentrations the mesh-size becomes so small that it can easily fit between the colloids resulting in a weaker depletion attraction which then causes the gels to become weaker.

## 6.6 Comparing Phase Boundaries of the Three Systems

System A and system B with added salt are the most similar studies. Therefore qualitatively comparing the phase boundary of system A ( $a = 260\text{nm}$ ) to the  $175\text{nm}$  case for system B with added salt it can be seen that the latter system phase separates at a lower surfactant concentration than is the case for the uncharged colloid. This is reasonable since the colloid has been destabilised by the addition of salt.

Now let us compare the position of the phase boundaries for system B, both with and without added salt (as has been mentioned previously). The  $175\text{nm}$  and  $105\text{nm}$  radius particles mixtures begin to phase separate at higher concentrations of surfactant in the case with no added salt. This is what one intuitively expects since the repulsion between the colloids is smaller in the case of the added salt and therefore one would expect that

---

\*The micelles may still be repelled to some extent from the Debye layer, however, it cannot be the main effect in this part of the phase diagram

†assuming they are not repelled by the double layer

phase separation could be induced more easily. There is, however, a problem. The 70nm radius particles require a smaller concentration of surfactant to induce phase separation in the no salt case.

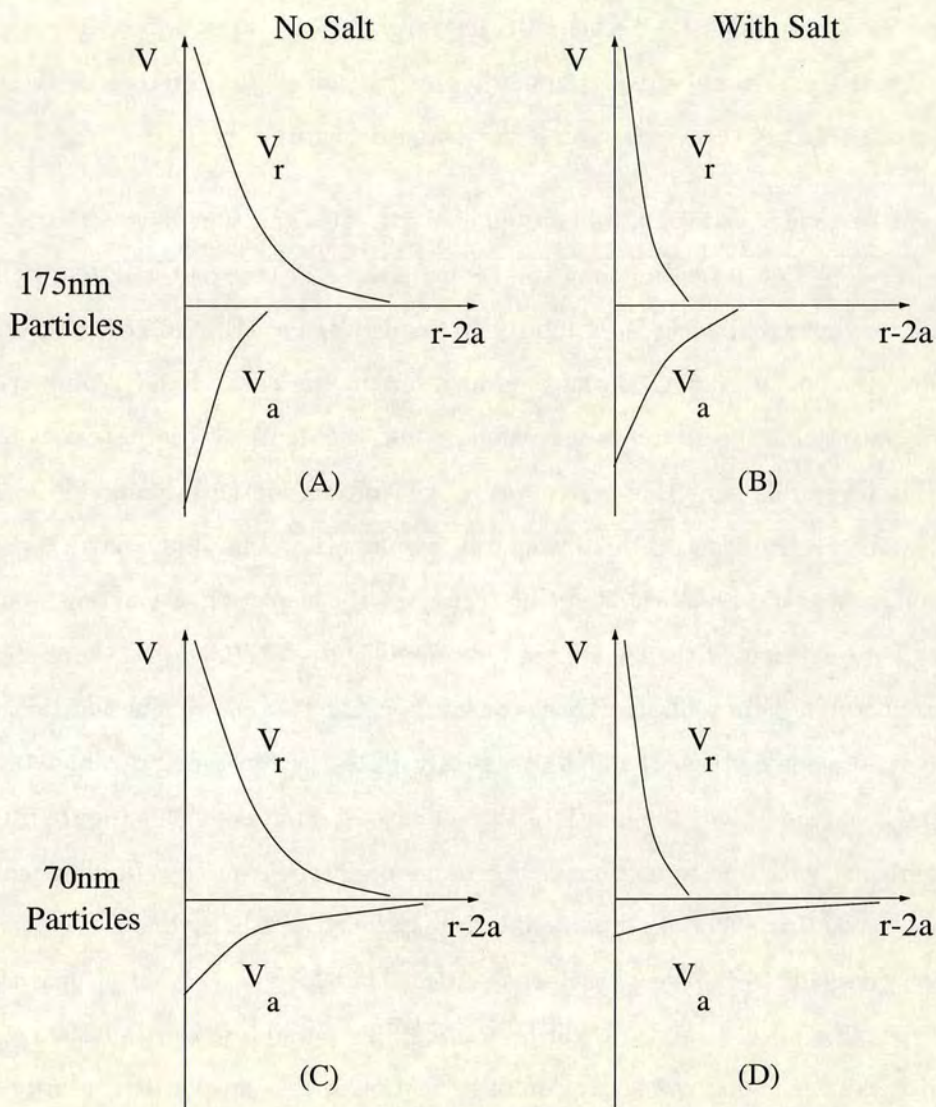


Figure 6.17: Schematic diagram of the depletion attraction ( $V_a$ ) and the coulombic repulsion ( $V_r$ ) as a function of distance ( $r$ ) for 175nm radius particles both without salt (A) and with added salt (B) and for 70nm radius particles without salt (C) and with salt (D). The trends are illustrated for a fixed surfactant concentration.

The situation is therefore more complicated than it first seems. One must consider three effects; the range of the coulombic repulsion, the depth of the depletion potential and the range of the depletion. The size ratio is therefore important as well as the concentration of surfactant and salt. This size ratio at constant  $C_{16E6}$  concentration changes as the particle size changes. In order to rationalise the results the size ratio



must also be assumed to change on the addition of salt. Hence, it is assumed that the size ratio for system B with no added salt is the effective size ratio since. The following rationalisation therefore assumes that the micelles are repelled by the Debye layer as discussed in section 6.5.3.1. A schematic diagram of the changes in both the depletion potential and the coulombic interaction when salt is added for different colloidal sizes at constant surfactant concentration is illustrated in figure 6.17.

The larger particles ( $a=175\text{nm}$ ) have a smaller size ratio and thus have a shorter range and deeper depletion potential than smaller particles \* in the corresponding situation. This is seen when comparing  $V_a$  of figures (A) and (C), and (B) and (D) in figure 6.17. It can be seen in figure 6.17 that by adding salt in the case of the 175nm particles the depletion attraction becomes accessible, while the depth of the potential remains reasonably large. Thus at this surfactant concentration adding salt makes phase separation more likely, hence rationalising the results. For the 70nm particles, at the surfactant concentration illustrated, the range of the depletion attraction is already greater than the range of the coulombic repulsion (figure 6.17(C)). It is therefore imaginable that for these potentials phase separation could take place. On addition of salt the size ratio changes from the effective size ratio to the real size ratio and therefore the range is extended and the depth of the potential becomes smaller (figure 6.17(D)). This combined with the reduction in the range of the coulombic repulsion make the depletion attraction effective, but the depth may be so small (as illustrated) that it is not strong enough to induce phase separation. Therefore in a situation like this the colloid-wormlike micelle mixture will be more stable on addition of salt than without any added salt. A higher concentration of surfactant with a deeper depletion potential (and shorter range) would be required in the case of the added salt to induce phase separation. The “strange” result can therefore be rationalised by considering the coulombic and depletion potentials.

### 6.6.1 Salt Dependence

The phase boundaries in figures 6.3, 6.4 and 6.5 are horizontal in the surfactant-salt plane and are therefore independent of the salt concentration. This is surprising when

---

\*according to the depletion picture discussed in chapter 3

one considers that adding salt reduces the stability of the colloid and one would therefore expect the  $C_{16}E_6$  concentration at which separation begins to become lower as the salt concentration increases. However, the difference in Debye screening lengths going from 0.25% to 1% is small (compared with the change from 0% to 0.25% where a change in behaviour has been observed). This therefore results in the horizontal phase boundaries observed, for system B. There may, however, be some minor differences in the exact positions of the phase boundaries.

## 6.7 Comparison of Experimental Results with Colloid-Polymer Mixtures

### 6.7.1 Phase Separation

The experimental phase behaviour of colloid-wormlike micelle mixtures will now be compared to the experimental study of the model colloid-polymer mixture system of Ilett et al. [7] (section 3.1.3). Overall the phase behaviour of the colloid-micelle mixtures studied in this thesis largely reflects that of colloid-polymer mixtures. At low surfactant concentrations a stable one-phase fluid is found. As the concentration of surfactant increases the depletion attraction becomes stronger and phase separation into colloid-rich and colloid-poor phases results. At still higher concentrations the attraction is so strong that particle gels are formed. While this behaviour has been found in all three systems discussed in this chapter the behaviour is more straightforward for system A and system B with added salt as they are the simpler systems where the colloids behave essentially as hard spheres. The behaviour of these systems compared with the model colloid-polymer system will be discussed first.

#### *System A and System B with added salt*

In both system A and system B with added salt the phase behaviour is similar to that in experimental colloid-polymer mixtures with  $\xi > 0.25$ . Gas-liquid separation is observed in both cases. However, no three phase samples or gas-crystal samples have been found for system A and system B with salt. The triple region observed in the colloid-polymer case (figure 3.12) becomes increasingly narrow at low colloid volume fractions. The triple region is therefore unlikely to be easily found given the varying size ratio with increasing surfactant concentration. Initially one may explain the lack

of gas-crystal coexistence by the colloid polydispersity, but these colloids have been seen to crystallise in system B with no added salt. The reason for the absence of gas-crystal separation is therefore likely to be due to the non-equilibrium gelation behaviour observed at high surfactant concentration reducing the concentration range where one may observe gas-crystal coexistence.

For both systems, at the phase boundary the size ratio is around 0.25, thus the appearance of gas-liquid separation is largely in agreement with what one would expect. However, the size ratios are not always above 0.25 in the gas-liquid coexistence region. At first glance it is therefore expected that a changeover to fluid-crystal separation should be seen. However, the coexistence region extends into the semi-dilute regime, where the definition of  $c^*$  and the size ratio in the entangled regime are somewhat arbitrary. This together with the different behaviour of polymers and wormlike micelles as depletants (section 6.2) make this difference with colloid-polymer mixtures unsurprising.

#### *System B, no salt*

The situation in system B with no added salt is more complex as there is a long range coulombic repulsion between the particles. Thus comparing this with the model colloid-polymer system is more difficult. Crystal-fluid coexistence found in this system indicates that the behaviour is like that of colloid-polymer mixtures with  $\xi < \xi_{CO} \sim 0.25$ . By considering the size ratio to be  $\xi = R_g/a$  in the dilute regime or  $\xi = \xi_M/2a$  in the entangled regime then  $\xi \lesssim 0.25$  where crystal-fluid coexistence is observed for the 175nm and 105nm particles. However, if one instead considers the size ratio in the colloid-micelle mixtures in this system to be  $\xi = R_g/(a+\kappa^{-1})$  or  $\xi = \xi_M/2(a+\kappa^{-1})$  then the size ratio in the crystal-fluid coexistence region is much less than 0.25 for all three sizes of particles. Both size ratios are presented on the phase diagrams (figures 6.11, 6.12 and 6.13), but the latter size ratio where the colloidal radius used is the effective radius gives better agreement between the experimental results for colloid-micelle and colloid-polymer mixtures. With the micelles excluded from the Debye layer the effective size ratio should be used, whereas if the micelles could move freely into the ion cloud then the real size ratio should be used. The experimental results may therefore provide evidence for a strong electrophobic effect (section 6.5.3.1). The complicating factor is,

however, that in the coexistence region the surfactant concentration is above overlap concentration and thus the validity of the comparison with the colloid-dilute polymer experimental results remains unclear.

The gel-gas separation observed for system B with no added salt has not been observed in model colloid-polymer mixtures. It has, however, been found in colloid-spherical micelle mixtures investigated by Piazza and di Pietro [75] (section 3.4.1). In this study the spherical micelles are uncharged while the colloidal particles are charged <sup>†</sup> and is thus similar to system B.

### *General Trend*

For all three systems phase separation begins to take place around  $c^*$ . This is likely to be due to the small surfactant concentrations for the  $C_{16}E_6$  system. The overlap concentration takes place at such a low value as the long micelles (as a result of the large growth exponent) can overlap easily. Thus to induce a strong enough depletion attraction between the particles one must be around the overlap concentration.

### 6.7.2 Gels

The gels found for system A and system B with no added salt do not collapse and therefore are quite different from those found by Ilett et al. [7] in model colloid-polymer mixtures. The gels of system B with added salt do collapse but do not show delayed sedimentation as found in colloid-polymer mixtures. It is unclear why the gels should show such different behaviour. In the case of system B with added salt the strength of the gel increases as the surfactant concentration increases as is the case in colloid-polymer mixtures [63]. However, the concentration dependence of the strength of the gels for system B with no added salt is more complex. It is dependent not only on the concentration of the  $C_{16}E_6$  but also on the mesh size of the entangled network as discussed earlier.

---

<sup>†</sup>Salt is added in this study to screen the electrostatic repulsion, however details of Debye lengths are not given.

### 6.7.3 Depletion Restabilisation

The results of this experimental study do not agree with the Gast et al. [48] or SFV theory [67] (section 3.1.5) where colloid-polymer mixtures are predicted to restabilise above  $c^*$  due to the changeover of the depletion layer from  $R_g$  to the mesh-size. No such restabilisation is observed. This could be due to the differences between depletion by micelles instead of the polymers. It does, however, question the validity of these theories which have not been well tested experimentally.

### 6.7.4 Redispersibility of Samples

A selection of samples made up for the colloid-wormlike micelle phase studies were allowed to phase separate over a few days and then were redispersed by tumbling overnight. The samples were then allowed to phase separate again under the same conditions, but the details of the phase behaviour were not always the same. Each sample on the phase diagram is therefore a freshly made sample rather than a dilution of a previous sample. The latter method was used in the study of the model colloid-polymer system by Ilett et al. as the behaviour was found to be the same when the samples were redispersed. While this is not the case in these samples, it was found that the behaviour of the colloid-wormlike micelle mixtures was reproducible when fresh samples were used.

This behaviour is likely to be due to some particles getting into the deeply attractive primary minimum of the DLVO potential. Tumbling will not break up any resulting small aggregates, thus the behaviour is not strictly reproducible. For the model hard-sphere colloids used by Ilett [7] there is no such primary minimum for the particles to get stuck in.

## 6.8 Comparison with Theory

The theory of Lekkerkerker et al. [10] (section 3.1.2) for colloid-polymer mixtures was extended for the case of colloid-wormlike micelle mixtures by Patrick Warren [109]. The details of the alterations to the existing theory are given below as well as calculated

depletion potentials and theoretical phase diagrams found using this theory.

### 6.8.1 Details of the Theory

#### 6.8.1.1 Assumptions

The phase behaviour of the colloid-wormlike micelle mixture is calculated in the same way as the colloid-polymer mixtures [10] (section 3.1.2). The differences, which have been made to this model, reflect the main differences between wormlike micelles and polymer molecules discussed previously (section 6.2). As the concentration of surfactant is increased the size of the micelles increase according to the accepted growth law (section 2.4.4.1). The growth exponent of this law has been made a variable, since the theory predicts a value of about 0.5, but experiments have found both this value and a value of 1.1 depending on the system (section 2.4.4.1). The monodisperse polymers of the simple colloid-polymer mixtures now have an exponential size distribution. The phase behaviour is then found by minimising the Helmholtz free energy, assuming that the micelles have the same free energy as the equivalently sized polymer. The scission/recombination reactions are also included in the model as it allows the micelle length distributions in each phase to come into equilibrium. More details of this theory can be found in [110].

#### 6.8.1.2 Inputs

The information required to calculate the theoretical phase diagram using the model by Warren [109] is now discussed. In order to calculate the size of the micelles as the concentration is varied one value of  $R_g$  at a known surfactant concentration is required. All other sizes can consequently be calculated from this and the micellar growth law of known growth exponent. The radius and persistence length of the micelles are also required. All of these values can be found from the results of the light scattering study of  $C_{16}E_6$  carried out by Schurtenberger et al. [37] (section 5.2.1). The colloidal radius must also be known (section 5.1).

## 6.8.2 Theoretical Phase Diagrams

The form of the phase boundaries found using the Warren model [109] will be compared to that of colloid-polymer mixtures as well as the experimental results for the colloid-wormlike micelle mixture studies.

Both the spinodals and the binodals are plotted on the theoretical phase diagrams. These lines represent different methods of phase separation. Between the binodal and spinodal lines phase separation is via nucleation and growth of droplets, while within the spinodal line the solution is thermodynamically unstable and concentration fluctuations result in spontaneous phase separation. It is unlikely that any differences between binodal and spinodal samples would have been observed in the experimental study of colloid-micelle mixtures. Both lines are included on the phase diagrams for completeness but the main discussion will therefore be centred around the lower surfactant concentration binodal lines.

### 6.8.2.1 Effect of Growth Exponent

The wormlike micelles of the  $C_{16}E_6$  system have been found by Schurtenberger et al. to have a concentration induced growth with an exponent of 1.1 (size  $\sim c^{1.1}$ ) (see section 5.2.1). This is significantly different to the expected theoretical exponent of 0.5 [38] (section 2.4.4.1). The phase diagram for this system for both of these growth exponents was determined in order to investigate the effect of the growth exponent and to compare the results with the experimental phase diagrams presented earlier in this chapter. The phase diagram corresponding to the experimentally determined growth law (exponent 1.1) is shown in figure 6.18, while that corresponding to the theoretical growth law (exponent 0.5) is shown in figure 6.19.

As mentioned one must input a value of  $R_g$  at a given surfactant concentration, and subsequently values of  $R_g$  at different surfactant concentrations will be calculated via the growth law. In the case of the experimental growth law the starting value chosen is not important as the calculated values will coincide with the experimentally determined values of  $R_g$ . For the theoretical growth law ( $\alpha = 0.5$ ), a starting value of  $R_g$  from the light scattering study [37] is used, but different starting values may have a significant

effect on the phase diagram found. This was therefore investigated by choosing various different starting positions from the light scattering data. It was found that the starting value affects the details of the phase behaviour i.e. the positions of the phase boundaries, but has no effect on the overall trends. The plot shown in figure 6.19 is representative of the behaviour found.

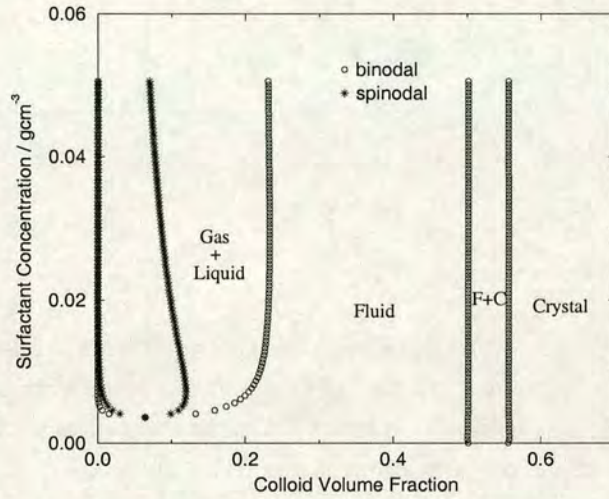


Figure 6.18: Theoretical phase diagram found using the Warren model [109] for 175nm particles in a solution of wormlike micelles of  $C_{16}E_6$ . The worms are assumed to have a growth exponent of 1.1, which corresponds to that found experimentally by Schurtenberger et al. [37]. The results are shown in terms of surfactant concentrations in the free volume. Though not clear on the above scale the gas-liquid binodal line bends back to lower colloid volume fractions as it rises. This behaviour is also seen in the spinodal but is more pronounced in this case.

It can be seen that there are significant differences between the phase diagrams with different growth exponents. The form of the phase diagram for a growth exponent of 1.1 is very different to that observed for colloid-polymer mixtures (figure 3.9). The phase diagram for a growth component 0.5 (figure 6.19) is similar to that observed for colloid-polymer mixtures for a size ratio  $\xi > \xi_{CO}$ , with both a critical point and a triple point being observed.

For a growth exponent of 1.1 a critical point but no triple point is found. The gas-liquid binodal is also observed to bend backwards at high values of the colloid volume fraction. This indicates that a triple point will not be found even at significantly higher surfactant concentrations. (Higher concentrations cannot be calculated in any case as



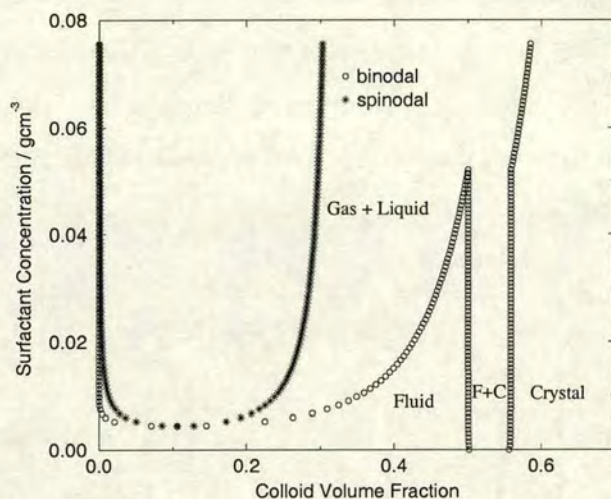


Figure 6.19: Theoretical phase diagram found using the Warren model [109] for 175nm particles in a solution of wormlike micelles of  $C_{16}E_6$ . The worms are assumed to have a growth exponent of 0.5, which corresponds to that found theoretically [38]. The results are shown in terms of surfactant concentrations in the free volume.

the theory is not valid in the semi-dilute regime. This is discussed in more detail in section 6.8.3.3.) The gas-liquid coexistence region may therefore form a closed loop. One would see a restabilisation of the mixture at high colloid volume fractions (see figure 6.18). This has been observed experimentally for the 70nm radius particles (figure 6.5). It provides further evidence for the growth exponent of 1.1 being more suitable than the theoretically predicted value of 0.5 for the  $C_{16}E_6$  system. All subsequent phase diagrams will therefore be calculated for a growth exponent of 1.1. The spinodal line in this phase diagram also bends backwards as the colloid volume fraction increases. The effect on the spinodal is even more pronounced than for the gas-liquid binodal. At high colloid volume fractions the fluid-crystal binodal is the binodal found for hard sphere colloids and discussed in section 2.3.

In order to explain the difference between the phase diagrams with the different growth exponents one may turn to the depletion potentials. The behaviour of colloid-polymer mixtures was originally explained by Asakura and Oosawa [8] and Vrij [9] in terms of depletion potentials. Later Sperry [45] used effective potentials to explain and predict phase behaviour in colloid-polymer mixtures. It therefore appears to be the logical first step in explaining the strange behaviour observed in figure 6.18. The depletion poten-

tials below  $c^*$  (as the theory is only valid in the dilute regime) can also be determined from the theory of Warren [109]. For 175nm radius particles the depletion potentials are shown in figures 6.20 and 6.21, corresponding to growth exponents of 1.1 and 0.5 respectively.

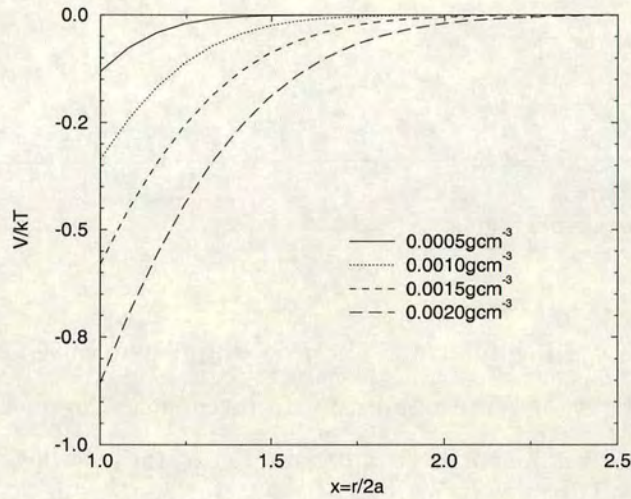


Figure 6.20: Depletion potentials for varying concentration of  $C_{16}E_6$  (growth exponent 1.1) and 175nm radius particles. The x-axis gives interparticle distance in units of the particle diameter.

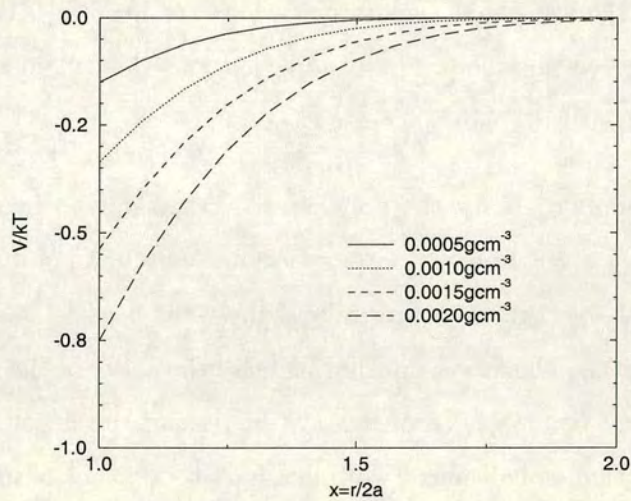


Figure 6.21: Depletion potentials for varying concentration of  $C_{16}E_6$  (growth exponent 0.5) and 175nm radius particles

It can be seen that for the same concentration of  $C_{16}E_6$ , both the range and the depth

of the depletion potential are greater for a growth exponent of 1.1. This does not lead us to a simple explanation of the differences between the phase diagrams for the different growth exponents. Since finding a triple point is a delicate balance between the range and the depth of the attraction, examining the potentials is too simple a picture for rationalising the results.

### 6.8.2.2 *Effect of Polydispersity*

Throughout this chapter the differences between wormlike micelles and polymers have been highlighted. It is therefore interesting to investigate the effect of one of these differences, that of the exponential size distribution of the micelles, on the phase behaviour of the colloid-wormlike micelle mixtures. The phase diagram for a growth exponent of 1.1 for monodisperse worms is shown in figure 6.22 and the corresponding depletion potentials are presented in figure 6.23. The number average mean length is used to define the equivalent monodisperse case.\* It can be seen that the introduction of polydispersity has little influence on the phase behaviour. The exponential size distribution causes the gas-liquid coexistence region to shrink a little. Both the binodal and spinodal curves also show less bending back as the colloid volume fraction is increased compared with the monodisperse case.

The corresponding potentials for the polydisperse case show an increased depth and range of the depletion attraction. This is a result of the presence of micelles both larger and smaller than the average. (This average is the value used to find the potential in the monodisperse case.) The larger micelles increase the range of the attraction, whilst the smaller ones deplete more effectively thus increasing the depth of the attractive well. It has shown that polydisperse wormlike micelles deplete better than monodisperse micelles. This has also been found to be the case for mixtures of colloids and polydisperse polymers [111, 112].

---

\* Other possible definitions of equivalent monodisperse wormlike micelles which give greater/lesser weight to short/long micelles could be made.

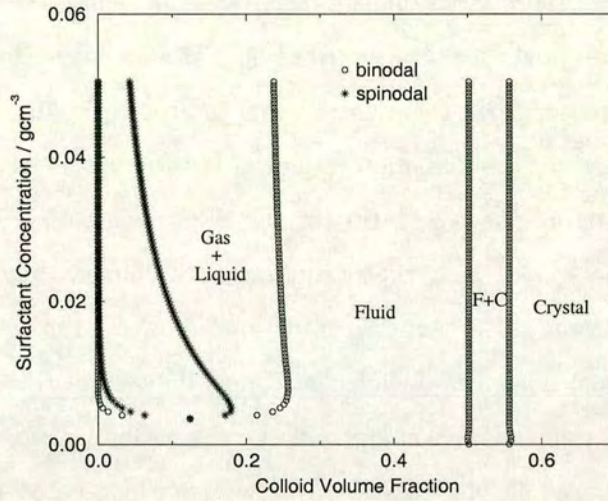


Figure 6.22: Theoretical phase diagram of 175nm particles in a monodisperse solution of wormlike micelles of  $C_{16}E_6$ . The growth exponent is taken to be the experimental value of 1.1. The surfactant concentration is that in the free volume.

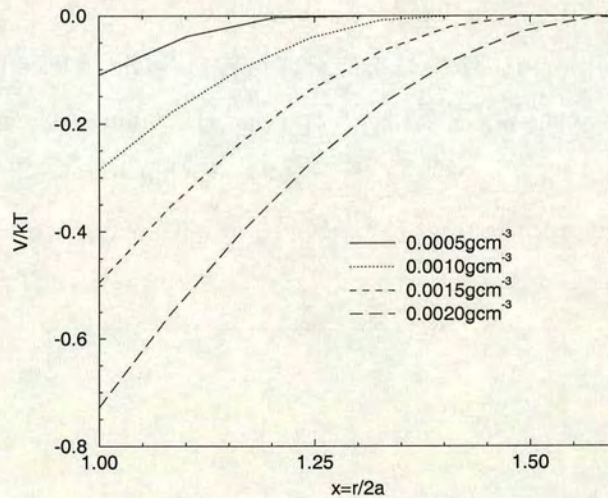


Figure 6.23: Depletion potentials for varying  $C_{16}E_6$  concentration for monodisperse worms with a growth exponent of 1.1 and 175nm radius particles.

### 6.8.2.3 Effect of Size Ratio

The size ratio was found to have a significant influence on the phase behaviour in colloid-polymer mixtures (section 3.1.2). In colloid-polymer mixtures the size ratio can be varied by using either differently sized colloids or polymers. In the case of colloid-

wormlike micelles there is already a range of size ratios present since the micelles self-assemble and have an exponential size distribution. The average size ratio also varies with concentration induced growth. By considering figures 6.20 and 6.21 it can be seen that the range and depth of the depletion potential both increase as the concentration of surfactant and therefore the size ratio (in the dilute regime) is increased. From colloid-polymer mixtures one would expect the range to increase but the depth of the depletion to decrease as the surfactant concentration is increased in the dilute regime as a result of the increase in the size of the micelles. Since the volume fraction of depletants will also be increasing this causes the depth of the attraction to increase. The picture is, also, more complicated in the colloid-wormlike micelle case as it is the average of a distribution of size ratios that is changing. The contribution of the exponential distribution of micelles to the depletion potential therefore makes the situation more complex than that of colloid-polymer mixtures.

One can also change the size ratio more simply by changing the colloidal size. The depletion potentials for 70nm particles and a growth exponent of 1.1 are given in figure 6.24. Comparing these potentials to those of 175nm radius particles in figure 6.20 one can see that the depth of the potential is greater and the range of the attraction shorter for the larger particles. This is what is expected and what has been found in the case of colloid-polymer mixtures (figure 3.1).

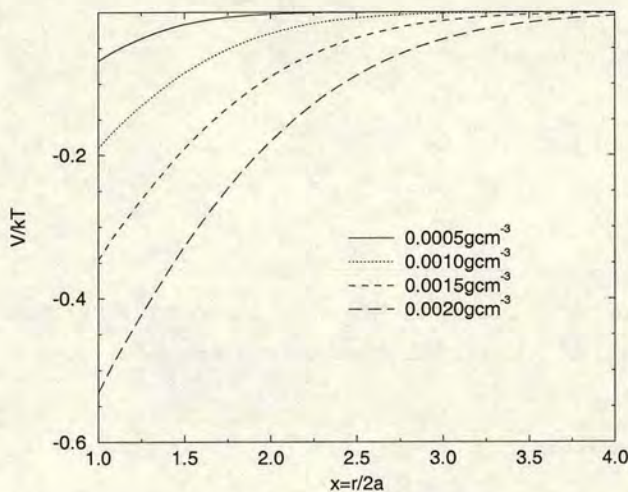


Figure 6.24: Depletion potentials for varying concentration of  $C_{16}E_6$  (growth exponent 1.1) and 70nm radius particles

The theoretical phase diagram for the smallest colloid ( $a=70\text{nm}$ ) used in the experimental investigations was also determined (figure 6.25). It shows the same trends as that of 6.18 discussed in the previous section. The main difference in this case is the smaller gas-liquid coexistence region. The restabilisation at high colloid volume fractions takes place at lower colloid volume fractions in the 70nm radius case than in the 175nm radius case. This is therefore easier to probe experimentally and restabilisation has indeed been found as mentioned previously.

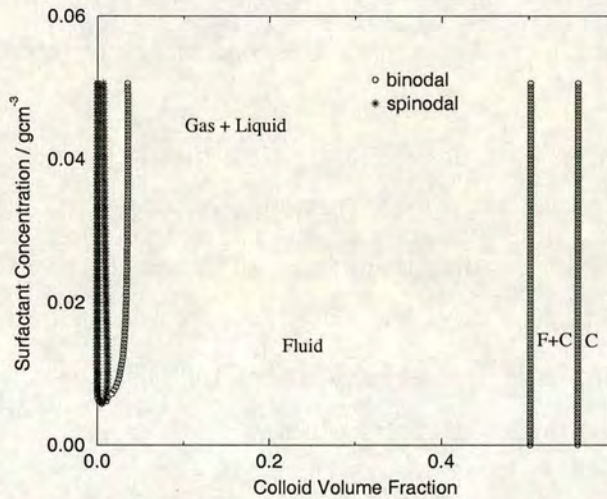


Figure 6.25: Theoretical phase diagram found using the Warren model [109] for 70nm radius particles in a solution of wormlike micelles of  $C_{16}E_6$ . The worms are assumed to have a growth exponent of 1.1, which corresponds to that found experimentally by Schurtenberger et al. [37]. The surfactant concentration shown is that in the free volume.

### 6.8.3 Comparison With Experiment

In the previous discussion the theoretical phase behaviour has been considered mainly in terms of the depletion picture and compared with the existing studies of model colloid-polymer systems. In the following, the experimental phase behaviour of  $C_{16}E_6$  and the various added colloidal particles will be compared to the theoretical phase diagrams. Both the qualitative behaviour and the quantitative positions of the phase boundaries will be considered.

### 6.8.3.1 *Qualitative Behaviour*

The phase behaviour observed in both system A and system B with added salt agrees well with the predicted phase behaviour. The phase separation observed is that of gas-liquid coexistence, in agreement with the theoretical phase behaviour. The gels observed are metastable and are therefore not predicted by this theory.

The observed behaviour of system B with no added salt does not agree with the predicted phase behaviour. Gas-liquid separation is not observed in this case. Restabilisation of the mixture at high colloid volume fractions as a result of the bending back of the gas-liquid binodal has, nonetheless, been observed in the case of the 70nm radius particles. This system is much more complex than that of the essentially hard sphere systems A and B with added salt. In system B with no salt the colloids have a large associated Debye layer surrounding them, increasing their effective size. Charge effects have not been included in the Warren model, where the colloids are assumed to be hard spheres. It is therefore perhaps unsurprising that the phase behaviour observed does not agree well with the theoretical predictions.

In all three systems studied the phase separation only begins to take place around the overlap concentration  $c^*$ . This can be rationalised when one looks at the depletion potentials in the dilute regime, shown in this section. The depths of the potential in this regime are low, getting only as high as  $\sim 1kT$  for concentrations about  $c^*$ .

### 6.8.3.2 *Binodals*

In order to compare the theoretical predictions for phase separation to the experimental phase diagrams presented earlier in this chapter, a plot of the gas-liquid binodals at low colloid volume fraction is shown in figure 6.26, for each size of colloid investigated. In this plot the surfactant concentration is not that in the free volume, but the actual concentration and is thus readily comparable to the experimental results.

The phase behaviour of system A and system B with added salt is in good agreement with the theoretical values. For system A and system B with 175 radius particles the theoretical binodals are at a higher surfactant concentration by less than a factor of

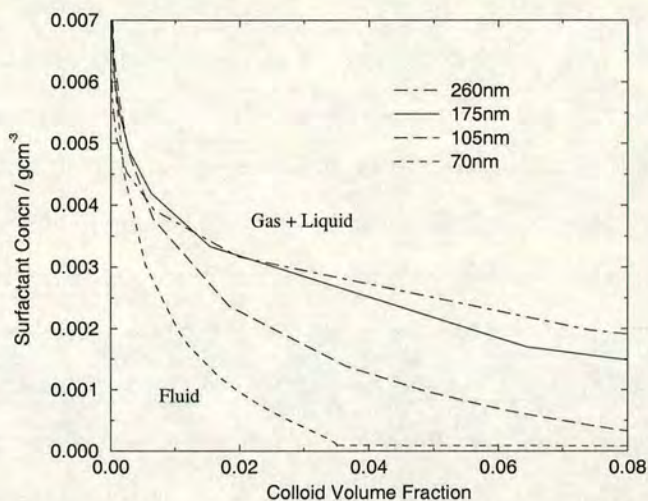


Figure 6.26: Theoretical binodals found using the Warren model [109] for various colloidal sizes. The growth exponent used corresponds to the experimentally determined value of 1.1 [37]. Only the low colloid volume fraction part of the binodal is shown to compare with the experimental phase studies.

2 (see figures 6.2, 6.3, 6.26 and table 6.1). This overestimate of the surfactant concentration required to induce phase separation could be rationalised since the particles are less stable than the theoretically assumed hard sphere particles. However, the 105nm and 70nm radius particles for system B (figures 6.4 and 6.5) have a theoretical phase boundary at a lower surfactant concentration than found experimentally. As the size of the colloid is reduced (and therefore as the size ratio is increased) the Warren model predicts that the phase boundary moves to lower surfactant concentrations. The opposite trend has, however, been found experimentally (table 6.1). Thus while the phase behaviour observed for the individual phase diagrams of system A and system B with added salt agrees well with the Warren model, the size ratio dependence of the surfactant concentration of the phase boundary does not. A recent theoretical study of colloid-polymer mixtures using a macromolecular approach has been carried out by Fuchs and Schweizer [113]. They found that the polymer concentration of the spinodal phase boundary increases as the size ratio increases. This agrees with the trends observed in the colloid-micelle mixtures. Complete phase diagrams have not been found by Fuchs et al. [113] and thus cannot be compared to experiment.

For system B with no added salt the concentration at which phase separation is ob-



served experimentally can be compared with the results of the Warren model despite the differences of the qualitative behaviour. The theoretical prediction gives some indication of the expected concentrations at which the depletion attraction will become strong enough to induce separation. It is, however, more difficult to compare the experimental results to the theoretical phase boundaries. There is no simple way to take account of charge effects. Both the effective size and the volume fraction of the colloid with regard to other colloids become larger due to the extensive Debye layers surrounding the particles. If one considers the simple picture the micelles are uncharged and therefore see the real colloidal radius and volume fraction. However, if there is an electrophobic repulsion of these micelles (section 6.5.3.1), then the effective size ratio and effective volume fraction should be used. It is therefore difficult to see whether binodals should be found for the effective or real values as some of the experimental results discussed support an electrophobic effect, whilst others do not. In any case charge effects are not fully accounted for by the Warren model and good agreement is not expected. For example an important charge effect neglected is the requirement of electroneutrality in each phase.

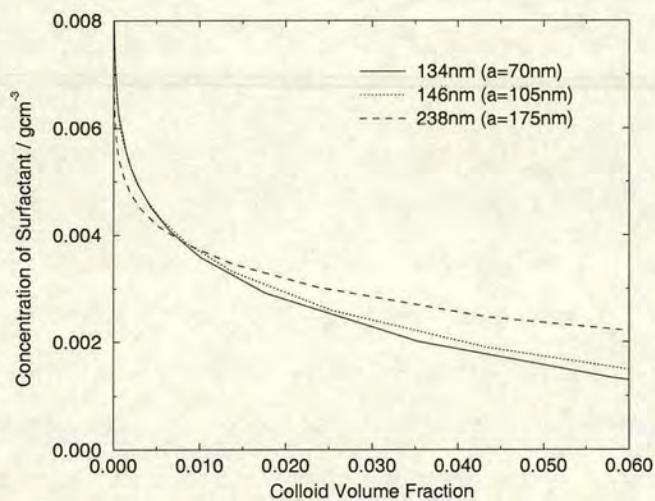


Figure 6.27: Theoretical binodals found using the Warren model [109] for various effective colloidal sizes ( $a_{eff} = a + \kappa^{-1}$ ). The values of the screening length used are those found by conductivity measurements (table 5.3). The values of  $a$ , as well as  $a_{eff}$  are indicated on the legend. The growth exponent used corresponds to the experimentally determined value of 1.1 [37]. Only the low colloid volume fraction part of the binodal is shown to compare with the experimental phase studies

Let us therefore make both types of comparison. Firstly, the system is simply compared to the theoretical phase boundaries found for the case of hard spheres and uncharged wormlike micelles shown in figure 6.26. The theoretical phase boundary is found to be about a factor of 2-4 below the experimental phase boundary (table 6.3). Figure 6.27 shows the binodals for the effective colloidal radii. Using these binodals and the effective colloid volume fractions (figures 6.11 6.12 and 6.13) one can see that the concentrations at which phase separation occurs is lower than that for the real size and volume fraction. The agreement with experiment is therefore worse in this case. In both cases the theoretical model underestimates the surfactant concentration required to induce phase separation. This is consistent with the increased stability of the particles due to the long range coulombic repulsion. Considering charge effects are ignored the agreement between theory and experiment is reasonable. It should also be noted that again the surfactant concentration of the phase boundary increases with colloidal radius theoretically, while the opposite trend is found experimentally.

### 6.8.3.3 *Validity of the Theory*

As discussed in section 6.8.3 the experimental phase diagrams fit quite well the theoretical model of Warren [109]. This is, however, surprising once one considers that phase separation occurs in the experimental system around the overlap concentration, while the theoretical model is only strictly valid for the dilute regime. This model, nonetheless gives good agreement with experiment. This may be simply because the phase boundaries are near the overlap concentration and not very far into the semi-dilute regime.

### 6.8.3.4 *Tielines*

For phase separated solutions tielines show the concentrations of the various components in each of the phases. Tielines have not been included in the theoretical phase diagrams discussed in this section. Since tielines have not been determined experimentally for the colloid-micelle mixtures discussion up until now has only been in terms of phase boundaries. The phase diagram for a growth exponent of 1.1 and 175nm particles with tielines is shown in figure 6.28. The tielines observed for the colloid-wormlike

micelle mixtures are horizontal in the plots of surfactant in the free volume against colloid volume fractions. This is similar to tielines in colloid-polymer mixtures (figure 3.9). In the actual concentration plot the tielines become oblique therefore indicating partitioning of the surfactant as well as colloid between the phases.

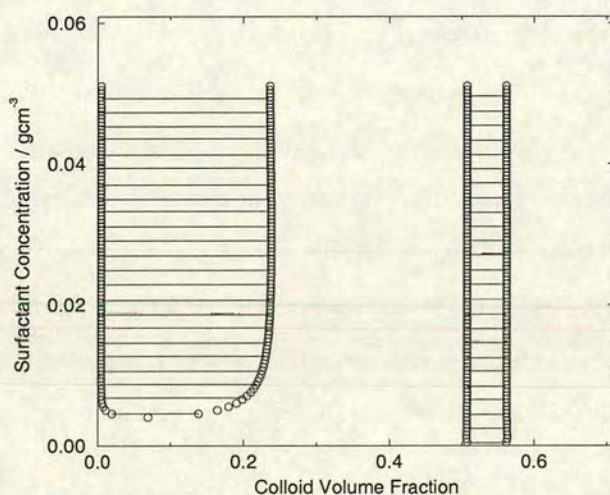


Figure 6.28: Theoretical phase diagram for 175nm particles and a micellar growth law with exponent 1.1. The circles, as before represent the binodal line. Every other tieline is also plotted.

### 6.8.3.5 Conclusion

Both the qualitative phase behaviour and the positions of the phase boundaries are reasonably well predicted by the Warren model for system A and system B with added salt. This model, however, while able to provide a rough estimate of the position of the phase boundaries for system B with no added salt, does not agree so well with the types of phases observed. This is not surprising as electrostatic interactions also play an important role in the behaviour of this system. The largest discrepancy between theory and experiment is the dependence of the phase boundary on the size ratio.

## 6.9 Conclusions

The experimental phase behaviour of colloid-wormlike micelle mixtures presented in this chapter can largely be explained by the depletion attraction. Most of the behaviour fits well into the existing colloid-polymer mixture framework. It is, however, not surprising that some of the details of the behaviour has not been fully rationalised as the system is much more complicated than model colloid-polymer mixtures. The extension of the theory by Lekkerkerker et al. [10] for colloid-polymer mixtures to colloid-wormlike micelle mixtures by Warren [109] has even led to reasonable agreement between experiment and theory.



## Chapter 7

# Phase Behaviour of Ionic Surfactant and Colloid

### 7.1 Introduction

In this chapter the phase behaviour of charged colloids in a solution of charged wormlike micelles is investigated. Under the right conditions, wormlike micelles of the anionic surfactant SLES and the zwitterionic co-surfactant CAPB form in aqueous solution (see section 2.4.3). This has been referred to as system C. It is a more complex system to study since it is a charged many-component system. Also the surfactants used in the study are industrial grade and may therefore contain a large amount of impurities complicating the phase behaviour.

The SLES system has not been well studied and little information is known about the surfactant. The phase behaviour is therefore investigated to find out how far the depletion picture and comparison with the well-studied model colloid-polymer system will take us in understanding a much more complex, industrially-relevant system.

### 7.2 SLES/NaCl/H<sub>2</sub>O Phase Diagram

The phase diagram of a 1% volume fraction of 190nm radius latex particles in an aqueous solution of SLES, CAPB and NaCl is shown in figure 7.1. The concentrations

of SLES and NaCl were varied whilst the SLES to CAPB concentration ratio was kept constant at 7 to 1. This allows the phase behaviour to be represented on a ternary phase diagram (see section 2.4.5.2).

The types of phase behaviour observed are similar to those of system A and system B with added salt. At low surfactant and salt concentrations the mixture is a colloidal fluid. As the surfactant and/or salt concentrations are increased the mixture becomes unstable and separates into coexisting colloid-rich and colloid-poor phases. Increasing the concentrations still further leads to the observation of non-equilibrium colloidal gels.

#### *Comment on Pure SLES*

The phase diagram in figure 7.1 was determined for industrial grade SLES. A small amount of pure SLES was obtained and used to check that impurities present do not have a strong influence on the phase behaviour. Some points on the phase diagram were thus repeated using the pure SLES and the behaviour found was the same.

### **7.2.1 Details of the Phase Behaviour**

The colloidal fluid, as described in chapter 6, is an opaque uniform phase. After a few weeks a clear supernatant begins to appear at the top of the sample. This is a result of sedimentation of the particles.

Gas-liquid coexistence is observed as the surfactant and/or salt concentrations increase. The sample separates into an opaque lower phase and a slightly cloudy upper phase. Both phases are fluids as they move when the sample is tilted. The liquid phase is a small proportion of the total sample as seen in the photo on the far left of figure 7.2.

The phase boundary between the equilibrium phase separation and the formation of gels was determined by carrying out observations of the time-dependence of the separation (as detailed in section 4.5). The gels in this system were found to exhibit the characteristic collapse of delayed sedimentation observed in gels of colloid-polymer mixtures (section 3.1.4). This will be discussed in more depth in section 7.3.

---

<sup>†</sup>this is likely to be an overestimate of  $c^*$

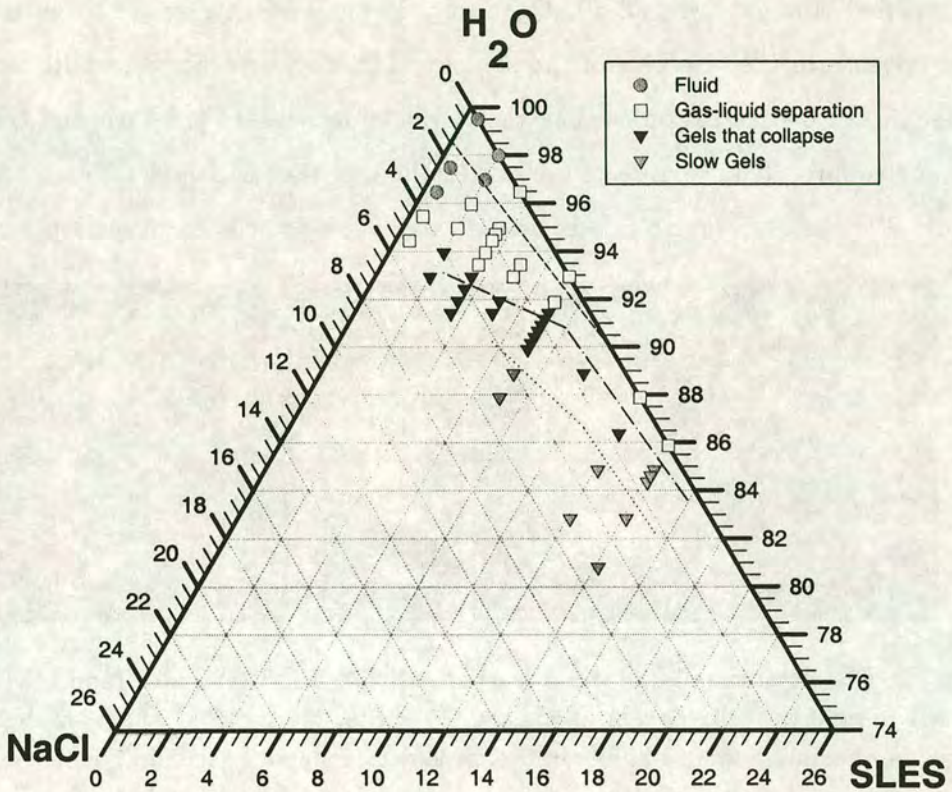


Figure 7.1: Ternary phase diagram of the SLES/NaCl/H<sub>2</sub>O and latex system. The volume fraction of colloid is kept constant at 1%. The co-surfactant CAPB is also present in this system in a constant ratio of 1:7 with the SLES. The various types of behaviour observed are indicated on the legend. The dashed line on the plot corresponds to the ionic strength at the ccc: below this line phase separation is expected, due to the screening of the coulombic repulsion between the colloids. Also indicated on the figure are rough guidelines for the micellar behaviour as shown in figure 5.14. Above the dot-dashed line the micelles are dilute, this line is therefore a rough indication of the value of  $c^*$ . Below the dotted line the measured rheological behaviour is Maxwellian, thus corresponding to semi-dilute wormlike micelles.

The gel region has been split into two sections, one where the gel is observed to collapse over a couple of weeks and the second where the gel collapse happens over the time



scale of many months to years (slow gels). In both cases the gels appear grainy and sometimes have cracks or channels (see figure 7.3). For slow gels this lumpiness can take a number of months to appear. A few of the most viscous samples, with the highest concentrations of surfactant and salt concentration, have not yet collapsed, after a period of about two and a half years<sup>†</sup>. The gels become slower to collapse due to the increase in the viscosity of the sample. The viscosity change results from the increase in salt concentration causing the wormlike micelles to lengthen and therefore to entangle more. The collapse of the gels in the less viscous samples (black triangles in figure 7.1) has been investigated in detail and will be discussed in section 7.3.

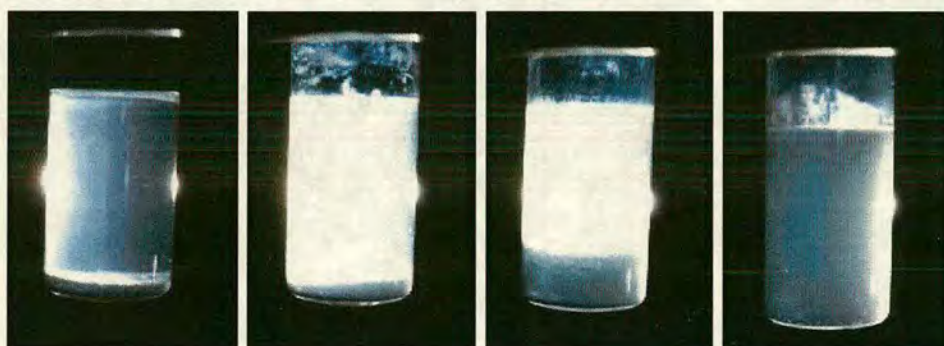


Figure 7.2: Photos of samples of the salt series with 7% SLES, 1% latex (and 1% CAPB). From left to right the salt concentrations are; 0%, 1.5%, 3% and 5%. The phase behaviour changes from equilibrium gas-liquid on the far left, to collapsed gels and finally, on the far right, to a slow gel where inhomogeneities have appeared over a period of a few months.

In figure 7.2 the appearance of the phases in samples with 7% SLES (and 1% CAPB) with an increasing amount of added salt is shown. The behaviour is observed to change from gas-liquid coexistence on the far left, to gels that have collapsed over a few days to a few weeks and finally to a slow gel where inhomogeneities have only appeared after a few months. It can be seen that the relative volume of colloid-rich phase present increases as the concentration of salt increases. At the same time the upper phase becomes less cloudy, although this is difficult to see in the photographs. This indicates that there is greater partitioning of the colloid between the phases as the salt concentration increases.

It should be noted that in this system wall crystals have not been observed in any of

<sup>†</sup>The phase behaviour is observed over a much longer period of time in this system as the high viscosities make the dynamics slow and the surfactant does not decompose as rapidly as the  $C_{16}E_6$  system.

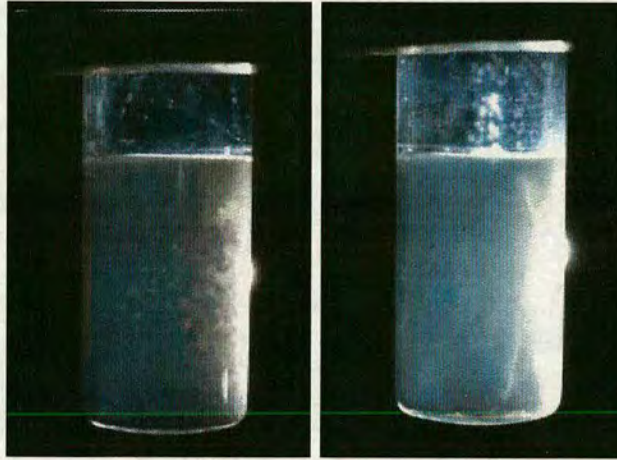


Figure 7.3: Photographs of “slow gels”, where a lumpy texture and cracks form over a few months. The sample on the left contains 14% SLES (2% CAPB) and 1.5% NaCl and clearly shows a grainy structure. The sample on the right contains 14% SLES (2% CAPB) and 5% NaCl and illustrates the appearance of cracks, as well as lumps, in the gel samples. Both samples contain colloid at a volume fraction of 1%.

the samples.

#### 7.2.1.1 Creaming Behaviour

Unexpected behaviour has been observed for samples containing relatively high concentrations of surfactant and salt, 14% SLES, 2% CAPB and 5% NaCl, and is shown for colloidal volume fractions of 1% and 2% in figure 7.4. These samples are highly viscous but over time, as well as becoming inhomogeneous as expected for slow gels, the latex particles have been observed to cream, that is to rise to the top of the sample. In the case of the 1% colloid volume fraction a clear phase appears at the bottom of the sample cell. The 2% volume fraction sample shows a definite opacity gradient with the top of the sample being more white than the bottom. The density of the 5% salt solution is about  $1.032\text{gcm}^{-3}$  [89], which is below that of the latex particles ( $\rho = 1.055\text{gcm}^{-3}$ ). If one, however, considers the  $\text{Na}^+$  counterions of the SLES molecules, assuming 100% dissociation, then the density of this solution is about  $1.057\text{gcm}^{-3}$ , which is just greater than the particles. This therefore explains the creaming behaviour.

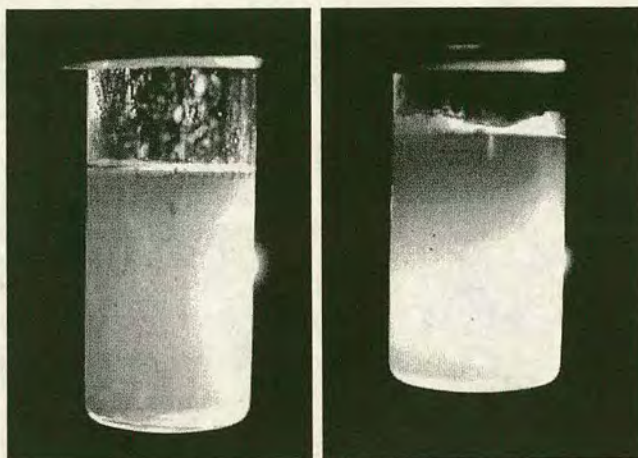


Figure 7.4: Both samples shown contain 14% SLES 2% CAPB and 5% NaCl. The one on the left has a colloid volume fraction of 1% whilst that on the right has a volume fraction of 2% particles. Creaming is observed: the particles are more concentrated at the top of the sample.

### 7.2.2 Discussion in terms of colloidal interactions

The majority of points on the phase diagram in figure 7.1 have concentrations of salt above that of the critical coagulation concentration (ccc) of the colloid determined (table 5.4). As well as the added salt, the anionic surfactant also has counterions which dissociate and thus contribute to the screening of the coulombic repulsion between the charged colloidal particles. The dashed line of figure 7.1 corresponds to the ionic strength at the ccc, and therefore simply considering the DLVO potentials everything below this line would be expected to phase separate and above it the samples would be stable. It can be seen, however, that phase separation is observed above this line, at 0% salt. The micelles must therefore be inducing the phase separation. At this point in the phase diagram the micelles may either be spherical micelles or small, dilute wormlike micelles, as the changeover between these two phases is continuous and difficult to detect. In either case though the dilute micelles must be inducing an attractive force between the particles via the depletion mechanism (section 2.2.4 and chapter 3).

At a surfactant concentration of 0.5% the mixture unexpectedly remains stable up to concentrations much higher than the equivalent ccc. A possibility for the increase in the stability of the colloid is the adsorption of the SLES onto the particle surface. This has been confirmed by a study of the salt-induced aggregation of the IDC latex

both with and without added SLES, where adding SLES was indeed found to make the particles more stable [114]. This adsorption of the surfactant is likely to happen in all the samples, due to the hydrophobic nature of the latices, but in the 0.5% surfactant case there will be little leftover surfactant available to make micelles as a result. A combination of the reduction in concentration of micelles available to deplete and the increased stability of the colloidal particles, due to the adsorption of the surfactant onto the particles, leads to the stable behaviour observed up to about 4% NaCl for the 0.5% SLES samples.

### 7.2.3 Conclusion

The behaviour observed in the SLES/NaCl/H<sub>2</sub>O system is similar to that found in system A and system B with added salt and can therefore be explained by a depletion attraction induced by the micelles. It is, however, difficult to reach concrete conclusions about the micellar effects on the colloidal phase behaviour from the study of the SLES/NaCl/H<sub>2</sub>O system (figure 7.1) as the addition of salt to the SLES/CAPB mixture has two effects. A method of separating the electrostatic and depletion interactions is therefore required in order to better understand what is happening in the phase diagram. This will be discussed fully in section 7.4.

## 7.3 Detailed Studies of Gels

The process of the gel collapse for the SLES/NaCl/H<sub>2</sub>O system has been studied in detail in two ways. Firstly direct observations were carried out to follow the collapse of the gels and therefore determine the delay times and how they change as the properties of the micelles are changed. The sedimentation process was also followed by diffusive-wave spectroscopy (DWS) (section 4.6) in order to probe the dynamics of the colloidal particles throughout the gel collapse. An interesting question to address here is whether DWS measurements could be used to predict when the gel will collapse. As well as being of fundamental interest this could also prove useful in shelf-life predictions of shampoos and other industrial products.

### 7.3.1 Observations

Direct observations were carried out in order to determine the phase boundary between equilibrium phase separation and gel collapse as mentioned earlier. A more detailed study of the collapse process for a constant SLES concentration of 7% (and CAPB concentration of 1%) for varying salt concentrations was carried out. Photographs of samples at early and late stages of gel collapse are shown in figure 7.5 and the sedimentation profiles determined as discussed in section 4.5 are shown in figure 7.6.

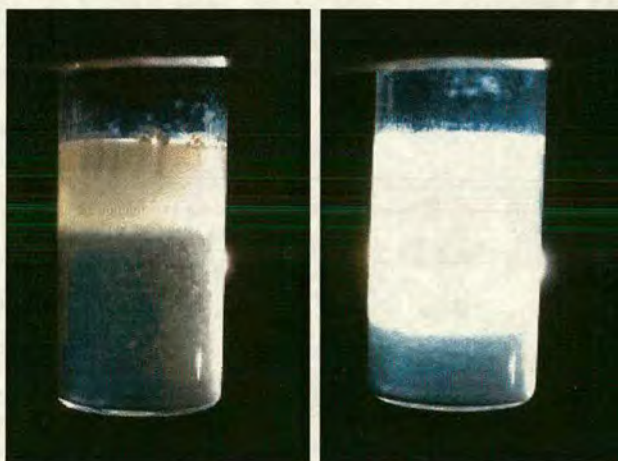


Figure 7.5: Photographs of a sample at both early and late stages of gel collapse.

Figure 7.6 shows the sedimentation profile for 7% SLES (and 1% CAPB) and an increasing concentration of salt from 1.75% to 3%. It can be seen that delayed sedimentation takes place for concentrations up to 2.5% NaCl. This behaviour roughly mimics that observed in colloid-polymer mixtures (section 3.1.4). However, there is a noticeable drop in the sediment height before the onset of the delay. This was also observed by Meeker in colloid-polymer gels [62] and initially thought to be a meniscus effect. The meniscus in the case of the colloid-wormlike micelles studied in cylindrical cells is, however, much less pronounced than that of the square cells used to study colloid-polymer mixtures by Meeker. In colloid-polymer mixtures the stronger gels, with longer latency times, were observed to show this settling effect even when the meniscus was minimised by filling the sample cells to the top. The latency times of the gels studied in colloid-polymer mixtures are short (usually a few hours) compared with those of gels in colloid-wormlike micelle mixtures where they are typically a couple of days. In light of the studies of Meeker [62] it is therefore not surprising that there is a significant change

in sedimentation height prior to the expected delayed sedimentation picture (figure 3.16) for colloid-wormlike micelles, where the latency time is much longer than that of colloid-polymer mixtures. The reasons for the settling behaviour, however, remain unclear.

For salt concentrations of 2.75% and 3% 'creeping behaviour' is observed. This was also observed in gels of colloid-polymer mixtures at high polymer concentrations [63](section 3.1.4).

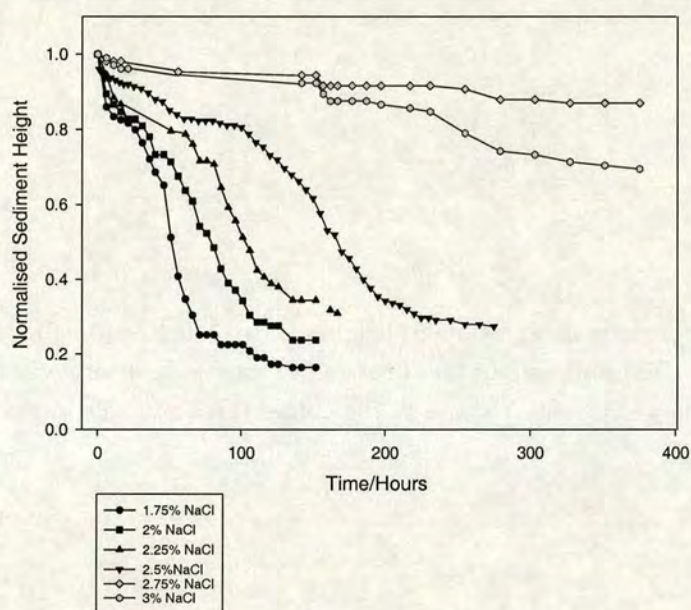


Figure 7.6: Plots of normalised sediment heights versus time for samples with 7% SLES (and 1% CAPB) and various NaCl concentrations.

The increase in viscosity as the salt concentration is increased will have a great impact on the sedimentation profiles observed. Therefore to probe the real gel behaviour due to the colloidal interactions the normalised sediment heights were plotted as a function of an "effective time", where the viscosity is divided out. In this plot (figure 7.7) the salt dependence of the latency times is essentially reversed.

In order to explain this one must think about the effect of the salt on both the colloidal interactions and on the wormlike micelles. As the salt concentration increases the coulombic repulsion between the charged particles becomes screened and therefore the

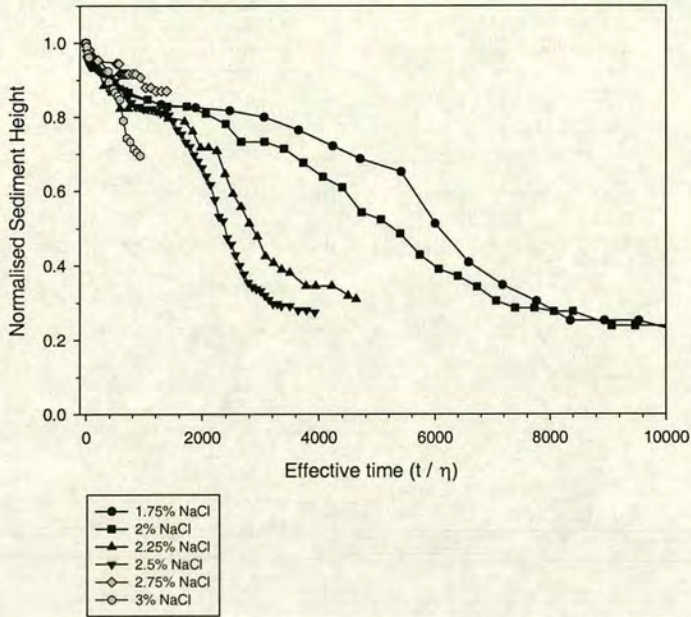


Figure 7.7: Plots of normalised sediment heights versus effective time for samples with 7% SLES (and 1% CAPB) and various NaCl concentrations. The effective time ( $t/\eta$ ) removes the effect of the large viscosity change as the concentration of salt increases.

DLVO potential becomes more attractive and shorter ranged (see figure 5.4(A)). At the same time the salt causes the micelles to grow and thus become more entangled. For all the salt concentrations investigated we are above  $c^*$  (see figure 5.14), where the important lengthscale is the mesh-size which decreases as the salt concentration increases. If one assumes that depletion in the entangled regime is due to blobs of size  $\xi_M$  then the width of the depletion zone will decrease as the salt concentration increases. This therefore leads to a stronger, shorter range depletion attraction (section 3.1.1). One possible explanation for the salt dependence of latency time is that the resulting shorter range attraction allows the particles to form more dense clusters since the particles can approach more closely at higher salt concentrations. These dense clusters will settle more quickly under gravity therefore resulting in the reduction of the effective latency time at high salt concentrations.

### 7.3.2 DWS

DWS experiments were carried out during the gel collapse, of a sample containing 7% SLES, 1% CAPB and 2.1% NaCl, as detailed in section 4.6.4. Two sets of results, corresponding to the top and the bottom of the sample (see figure 7.8), will be discussed in this section. The experiments were repeated and the trends were found to be reproducible.

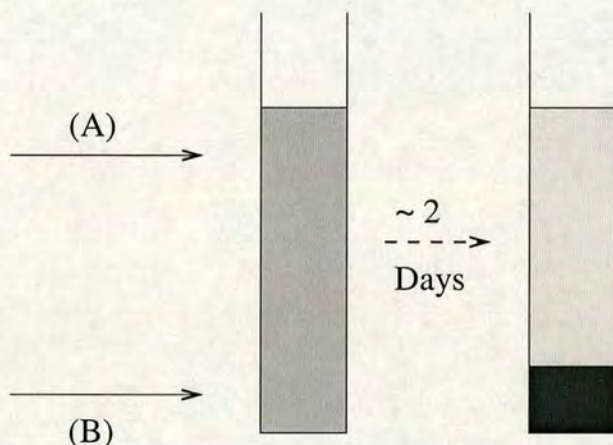


Figure 7.8: Schematic diagram of positions of the gel sample probed by DWS during its collapse over time. (A) corresponds to the position of the laser beam for investigation of the *top* of the sample, while (B) is the position of the laser beam for investigating the *bottom* of the sample. It should be noted that the laser beam is kept away from the interfaces in order to avoid scattering of the light from the interface.

#### 7.3.2.1 Results

The DWS measurements were carried out in a taller, narrower sample cell than those used so far, in both the phase studies and for the direct observations shown in section 7.3.1. Since the delay time of colloid-polymer gels has been determined to be dependent on the shape and size of sample vial [63], a direct observation on a 7% SLES (1% CAPB) and 2.1% NaCl sample in this sample vial was carried out. The results of this along with times determined from the observations of the sample during the DWS experiment are shown in figure 7.9.

It can be seen that the gel collapse is slower during the DWS experiment than during direct observation of the collapse in the same vial. There may be a slight variation



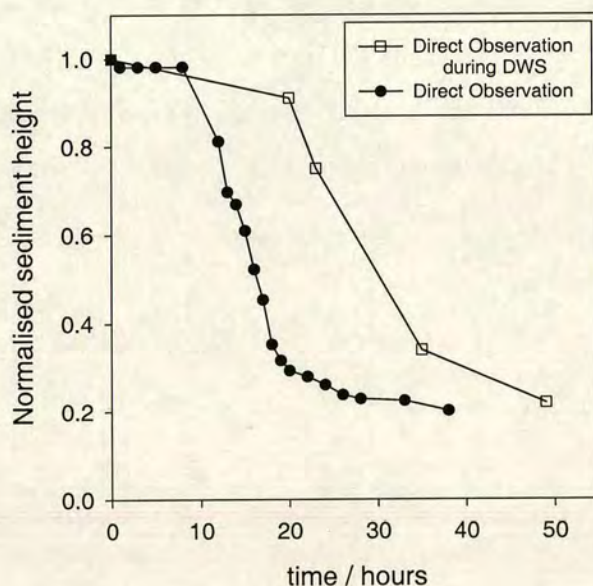


Figure 7.9: Sedimentation profiles of a 7% SLES, 1% CAPB and 2.1% NaCl sample in a tall, thin cylindrical cell. The black circles represent the sedimentation profile observed when the sample was illuminated by an incoherent light source (section 4.5). The white squares correspond to the observed collapse during the videoing of both the top and the bottom parts of the sample while DWS measurements were carried out (section 4.6.4).

in temperature in these two experiments. The DWS experiment was carried out in a temperature controlled room at  $19 \pm 1^\circ\text{C}$ , while the observation was carried out at  $20 \pm 1^\circ\text{C}$ <sup>§</sup>. At lower temperatures the sample becomes more viscous and thus will cause the gel collapse to become slower. However, such a small temperature variation is unlikely to cause the collapse to slow down as significantly as shown in figure 7.9. DWS experiments have been carried out for this sample with a water bath in place keeping the temperature at a value of  $20 \pm 0.5^\circ\text{C}$ . The gel collapse is again found to be slower than determined by direct observation with an incoherent light source. The laser therefore appears to be having some effect on the kinetics of the sample. It is, however, unclear how exactly this could be causing the gel to collapse more slowly.

<sup>§</sup>The direct observation of this sample was carried out in a temperature controlled room and not in a water bath as the sample was too tall to view it all in the set-up of figure 4.7

*Top*

A plot of average intensity<sup>¶</sup> against time for the top of the sample is shown in figure 7.10. Photos of the direct observations during the gel collapse are shown in figure 7.11. A few intensity correlation functions,  $g^{(2)}(\tau)$ , are presented in figure 7.12 to illustrate the main changes with time, as the gel collapses.

In figure 7.10 the intensity increases dramatically at about 21 hours, at the same time the gel interface is observed to begin to pass through the laser beam (figure 7.11). This change also coincides with a slowing down of the dynamics as seen in the plot of the correlation functions (figure 7.12). The direct observations showed that after about 24 hours the interface had passed through the beam (figure 7.11 - 24.5 hours), at this time the average intensity is found to have dropped again and begins to fluctuate around an approximately constant level. The fluctuations observed are likely to be a result of aggregates of the particles left in the less cloudy upper phase falling through the beam. This has been seen by direct observation, though it cannot be seen in figure 7.11.

One can rationalise the changes in average intensity (figure 7.10) and in the correlation functions (figure 7.12) over time by considering the changes in the sample. The initially uniformly opaque sample results in a large amount of multiple scattering and therefore the intensity found just off transmission is rather low. This stays approximately constant during the delay time. As the gel interface passes through the beam the intensity increases sharply, this is likely to be due to scattering of the light by the interface. Once the interface has passed through the laser beam the intensity levels off (although is subject to significant fluctuations as discussed previously) to a higher value than was found previously. This is because the laser is now probing an only slightly turbid phase. There is therefore much less multiple scattering of the light, which therefore results in a larger intensity just off transmission. As the gel collapses the dynamics slow down (figure 7.12). Initially (up to about 20 hours) this is likely to be due to the formation of the gel phase. After the gel interface has passed through the laser beam the dynamics slow down even more dramatically. This is likely to be a result of much less multiple scattering taking place. The photons therefore must travel further or for longer times to produce a complete phase change as there are less particles present to contribute to

---

<sup>¶</sup>averaged over each 15 minute run

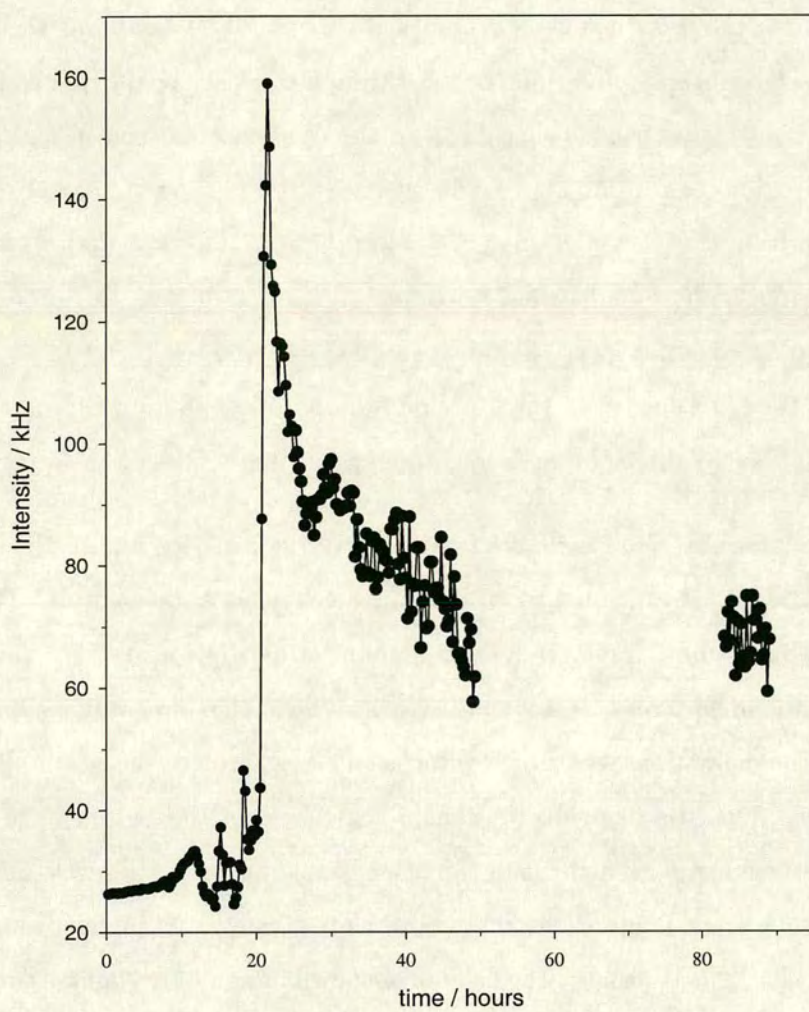


Figure 7.10: Intensity (averaged over 15 minutes) versus time for the top of the gel sample during its collapse

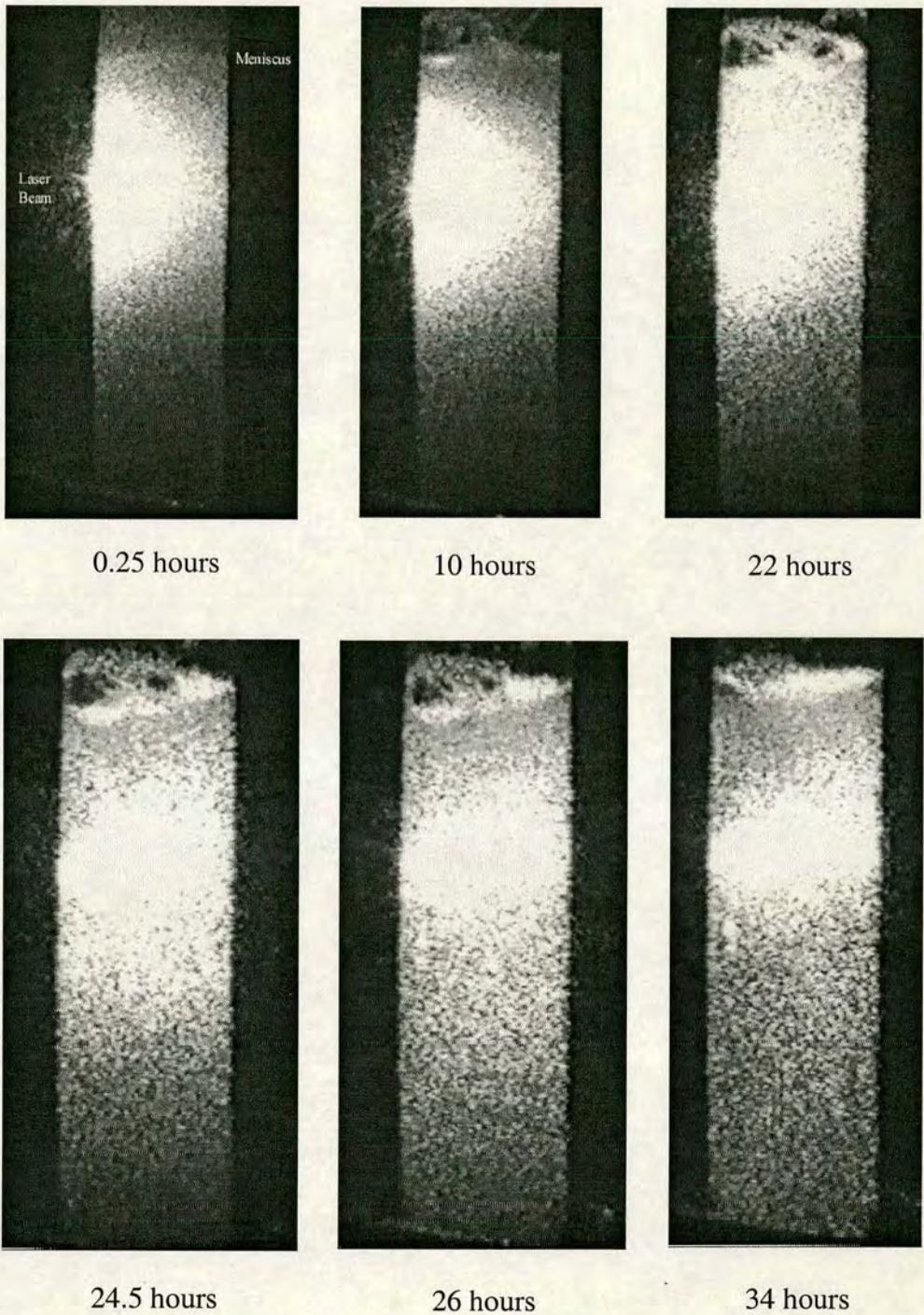


Figure 7.11: Images of the top of the sample over time during the DWS experiment. As the interface of the collapsing gel passes through the laser beam the area of the laser beam observed gets larger (22 hours). Near the end of the separation (34 hours) the laser beam passes straight through the sample cell. In all cases the speckle pattern, due to the scattered light can be observed.

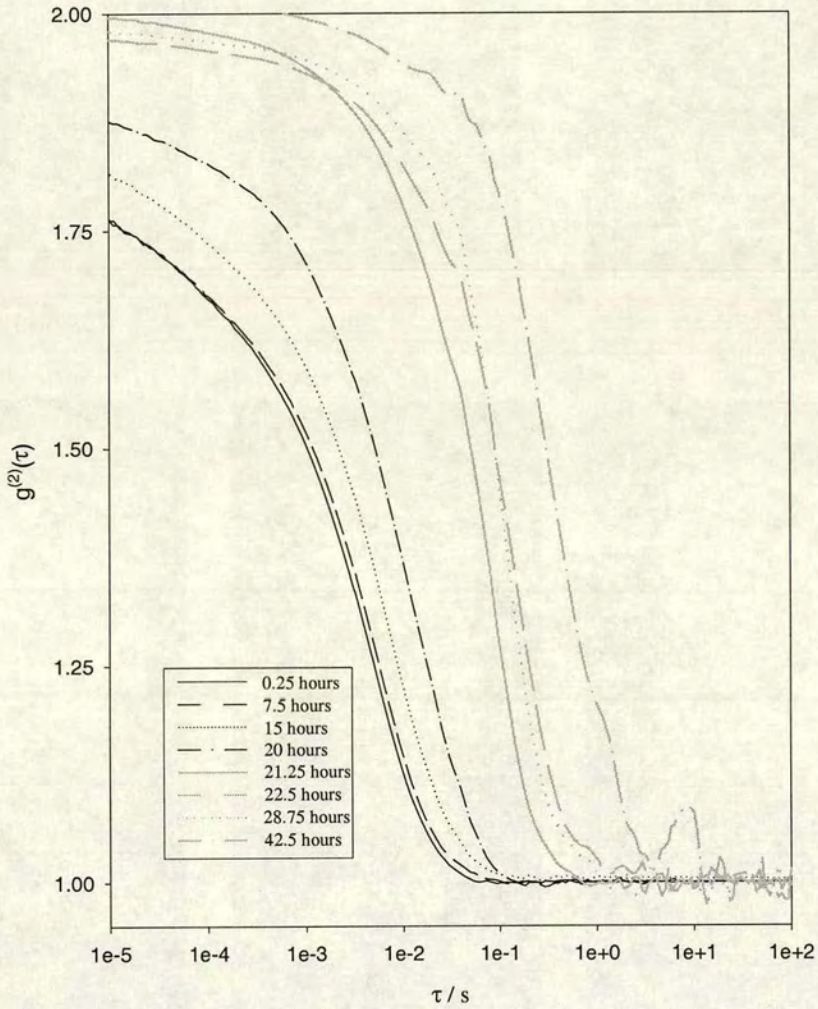


Figure 7.12: Intensity correlation functions ( $g^{(2)}(\tau)$ ) (averaged over 15 minutes) for the top of the gel sample as it undergoes delayed sedimentation.

the phase change. The dynamics therefore slows down.

### *Bottom*

The results are presented in the same way as those corresponding to the top of the sample. The plot of average intensity against time as the gel collapses is shown in figure 7.13. Images of the bottom of the sample during the DWS experiment are shown in figure 7.14 and the form of the correlation functions over time is shown in figure 7.15.

As observed in the case of the top of the sample, there is a large peak in the observed average intensity as a function of time (figure 7.13). The intensity begins to rise after approximately 15 hours. The corresponding direct observation and correlation function at this time are shown in figures 7.14 and 7.15 respectively. Little change is observed in both cases between the beginning of the experiment to about 22-23 hours into the experiment. At this point the correlation functions are observed to change shape as shown in figure 7.15. No noticeable changes in the sample are seen in the observations until 23 hours have passed, where the sample is observed to look lumpy. This lumpiness then coarsens over time, as the gel collapses. The gel interface can clearly be seen in the observations at about 35 hours as indicated in figure 7.15 <sup>||</sup> From about 35 hours the gel is compactifying and the intensity is observed to level off.

Let us try and rationalise the main changes of the average intensity and correlation functions over time by considering the changes in the part of the sample being probed. Before the gel begins to separate the intensity rises sharply. This may be due to the formation of aggregates of particles which then span the sample cell. As the gel collapses the bottom phase becomes more concentrated in colloidal particles and therefore the amount of multiple scattering observed increases. This results in a decrease in the average intensity of the signal observed just off transmission. The dynamics of the particles are observed to slow down as the gel forms, this slowing down is not as dramatic as that seen in the top part of the sample. This could be a result of two competing effects. Firstly, as the sample gels, large aggregates, which diffuse more slowly, are formed. Secondly, the density of the sample increases, thus resulting in

---

<sup>||</sup>Some detail is lost in the printing and therefore the interface is not too easy to see in the stills shown here.

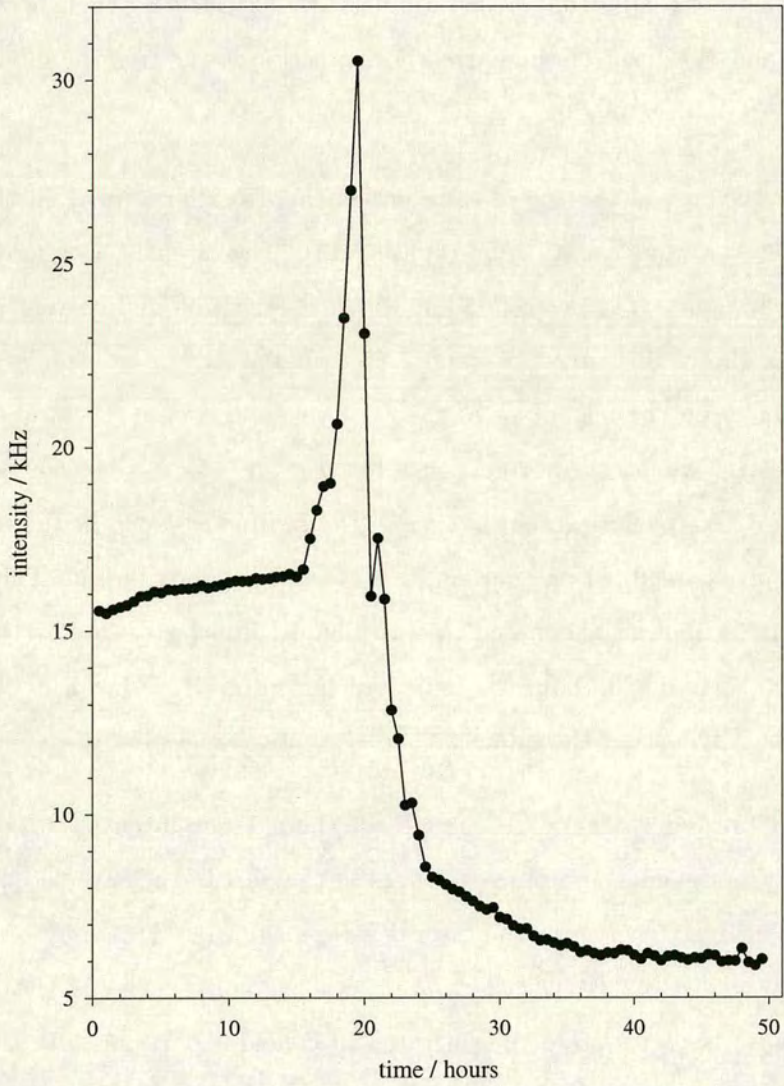


Figure 7.13: Intensity (averaged over 30 minutes) versus time for the bottom of the gel sample during its collapse.

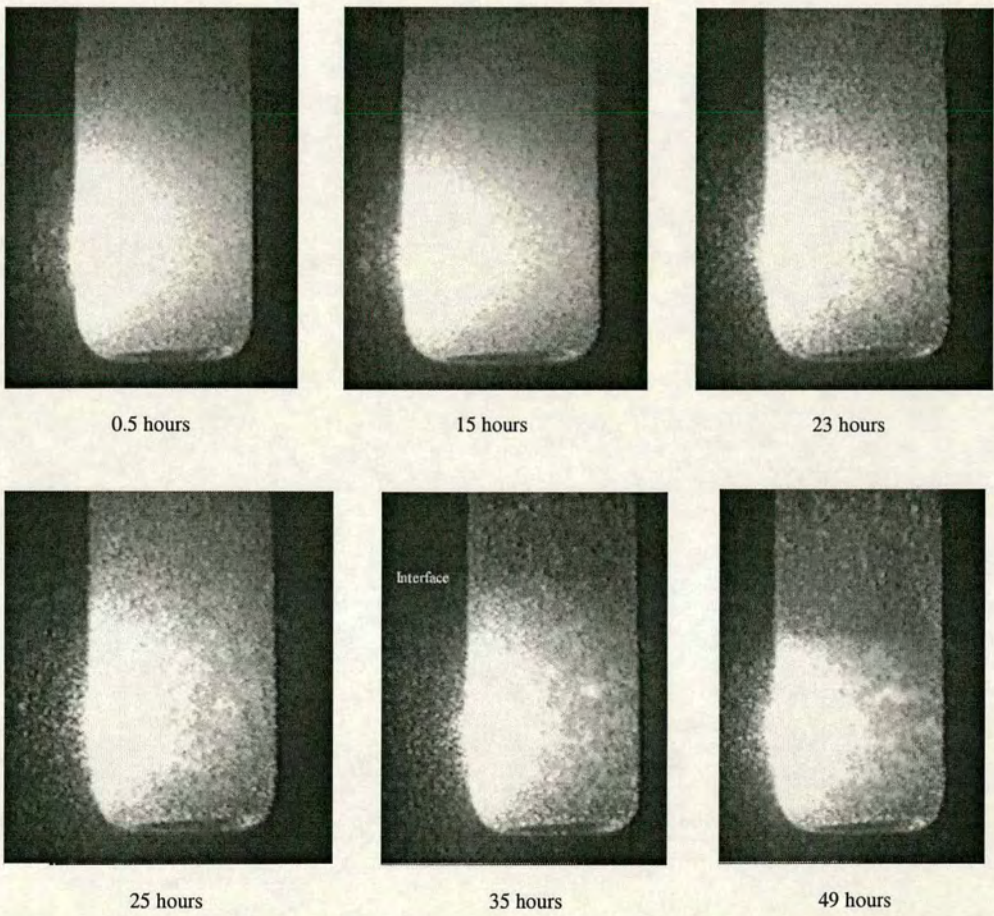


Figure 7.14: Images of the bottom of the sample over time during the DWS experiment. As the gel collapses the sample becomes lumpy. This can be seen from 23 hours onwards in the images. After 35 hours the gel interface can be seen a little above the laser beam. This interface moves down slowly as the gel compactifies until at 49 hours the interface is just at the top of the incident laser beam.



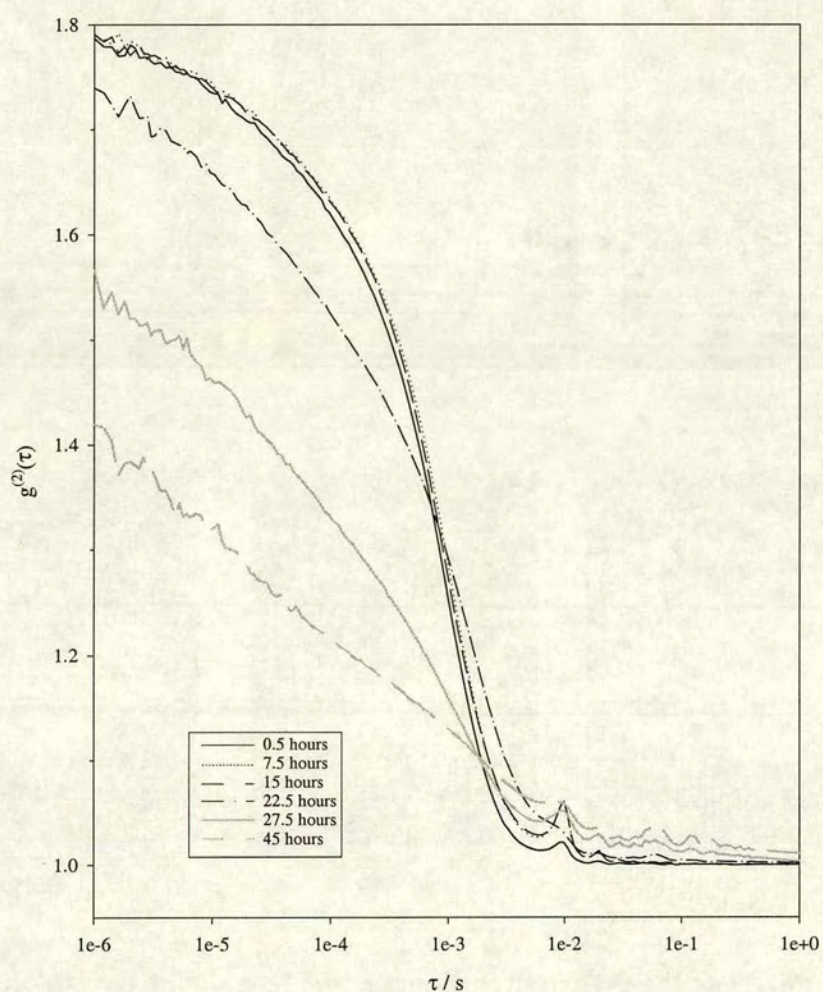


Figure 7.15: Intensity correlation functions ( $g^{(2)}(\tau)$ ) (averaged over 30 minutes) for the bottom of the gel sample as it undergoes delayed sedimentation

more multiple scattering and hence faster dynamics. From about 22 hours, as the gel is collapsing, the shape of the correlation function changes. This effect will be discussed in the subsequent section.

### 7.3.2.2 *Fitting*

According to equation 4.25 (section 4.6) a mixture of scatterers with different dynamics is expected to give a single broad relaxation of  $g^{(2)}(\tau)$  with an average relaxation time, rather than two separate relaxation modes. This is because in each scattering path a mixture of the different species will be probed. Menon and Durian [115] have investigated the dynamics of a three-dimensional granular medium, where two distinct relaxation modes are observed in the correlation function. They determined the mean-squared displacement of the scatterers,  $\langle \Delta r^2(\tau) \rangle$ , using the following approximation for the field correlation function in the transmission geometry [92],

$$g^{(1)}(\tau) \sim \exp(-(L/l^*)^2 k^2 \langle \Delta r^2(\tau) \rangle) \quad (7.1)$$

where  $L$  is the sample thickness,  $k$  is the scattering wavevector, and  $l^*$  is the transport mean free path, which was calculated from the total amount of light transmitted through the sample,  $T$ , according to [92],

$$T = \frac{5l^*/L}{1 + 4l^*/3L} \quad (7.2)$$

The mean squared displacements for a few correlation functions from the bottom part of the sample have been calculated and are shown in figure 7.16. At 5 hours and 20 hours two different modes are observed in these plots. There is a fast mode, and a slower mode which has a gradient of about 1, as indicated on the plot. The slow mode is therefore diffusive motion. At 37.5 hours the plot of  $\langle \Delta r^2(\tau) \rangle$  is rather different. It is broad with a gradient, indicated on figure 7.16 of about 0.14.

The correlation functions found during the collapse of the colloid-wormlike micelle gel (figures 7.12 and 7.15) are not monoexponential and seem to correspond to two relaxation modes. The field correlation functions,  $g^{(1)}(\tau)$ , were therefore analysed by the inverse Laplace transform (ILT), using the fitting program CONTIN [116] which

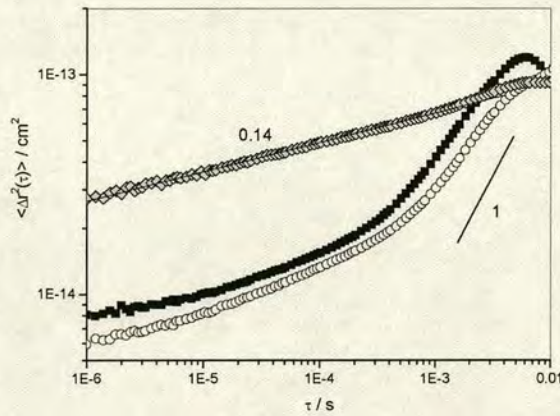


Figure 7.16: Plots of mean squared displacements,  $\langle \Delta r^2(\tau) \rangle$ , for a few correlation functions from the bottom of the sample during gel collapse. Black squares correspond to the correlation function measured after 5 hours. The plots with white circles, and grey diamonds are found for the correlation functions after 20 hours and 37.5 hours respectively.

calculates the distribution of relaxation times  $G(\ln \tau)$  according to,

$$g^{(1)}(\tau) = \int_0^\infty G(\ln \tau) \exp(-t/\tau) d \ln \tau \quad (7.3)$$

An example of the fit and the corresponding relaxation modes are shown in figure 7.17, 7.18 and 7.19. In figure 7.17 three peaks are found. The peak at high characteristic time  $\tau$  is ignored since the statistics are not good in this part of the correlation function. At 20 hours (figure 7.18) the correlation function looks smoother than that at 5 hours and the ILT gives two peaks. At even later times (figure 7.19) the ILT of the correlation function results in 4 peaks as  $g^{(1)}(\tau)$  is rather broad. However, to follow the changes in the observed dynamics during the gel collapse we will only consider the two peaks illustrated since they correspond to similar characteristic times as the peaks highlighted in figures 7.17 and 7.18. The correlation functions for the top of the sample are treated in a similar way. The time and amplitudes of the two peaks as the gel collapses over time for the top and the bottom of the sample are hence shown in figures 7.20 and 7.21 and figures 7.22 and 7.23 respectively.

The graphs of amplitude and  $\tau$  versus time for the two peaks through both the top and the bottom of the sample cell show a large scatter of values. This is because lumps of particles pass through the beam, resulting in a vastly altered signal. As these events are random this results in the large scatter in the characteristic time and amplitudes

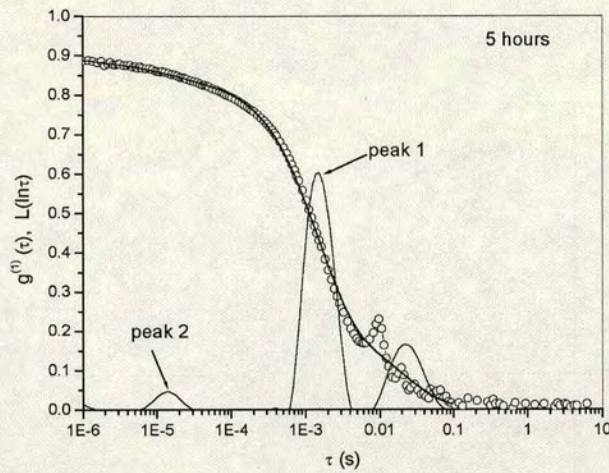


Figure 7.17: The correlation function through the bottom of the sample after 5 hours is shown by the open circles. The superimposed black line is the fit and the peaks correspond to the ILT of this fit.

of the peaks. Some trends can, however, be observed.

#### *Top*

For the top of the sample the amplitude of both the slow, main, mode (peak 1) and the fast mode (peak 2) is found to decrease. The characteristic relaxation time ( $\tau$ ) of peak 1 begins to increase at about 22 hours, as the gel interface passes through the beam. For peak 2, the fast mode, no trends are observed, the characteristic relaxation time is simply subject to a large scatter of values.

#### *Bottom*

For the bottom of the sample both the amplitude and the relaxation time of peak 1 (the slow mode) decreases with time, as the gel collapses. At the same time the amplitude and relaxation times of peak 2 (the fast mode) increase with time. This therefore accounts for the change in shape of the correlation function with time seen in figure 7.15.

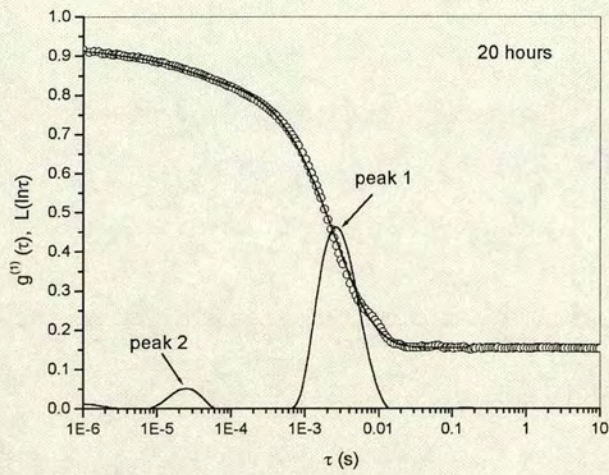


Figure 7.18: The correlation function through the bottom of the sample after 20 hours is shown by the open circles. The superimposed black line is the fit and the peaks correspond to the ILT of this fit.

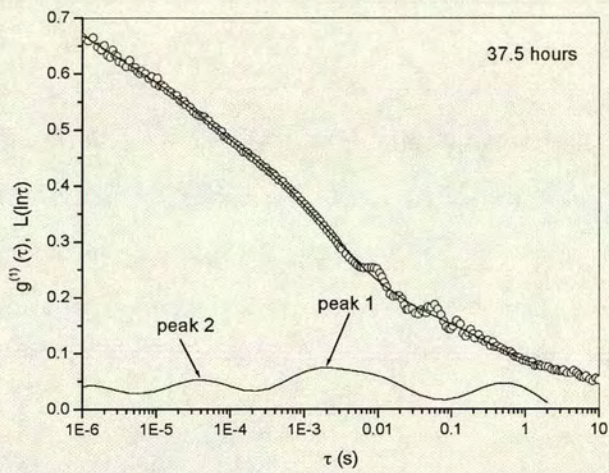
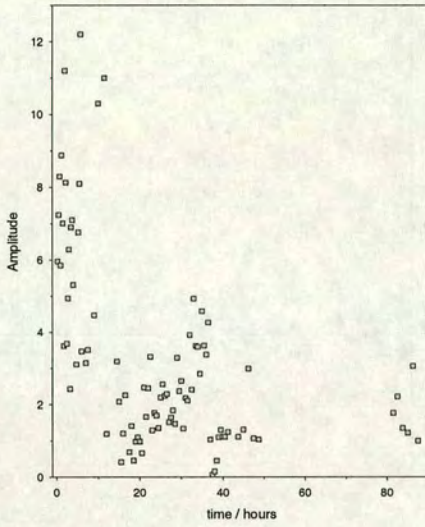
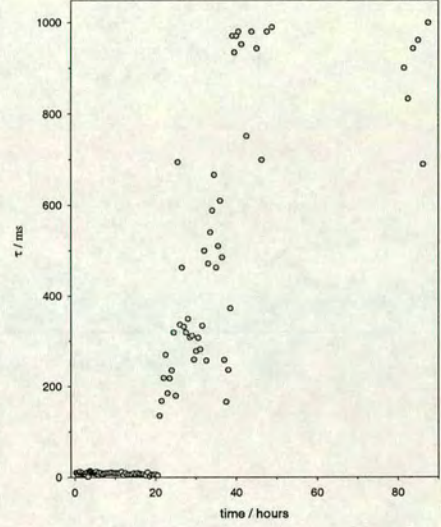


Figure 7.19: The correlation function through the bottom of the sample after 37.5 hours is shown by the open circles. The superimposed black line is the fit and the peaks correspond to the ILT of this fit.

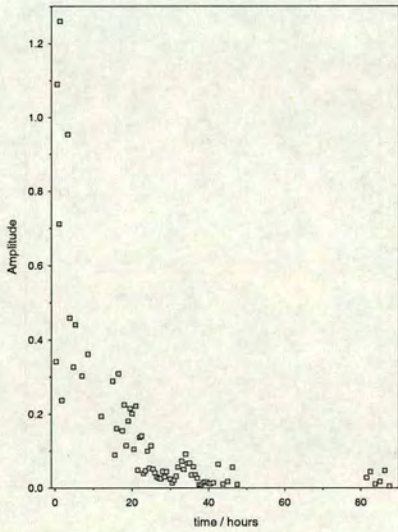


(a) Amplitude

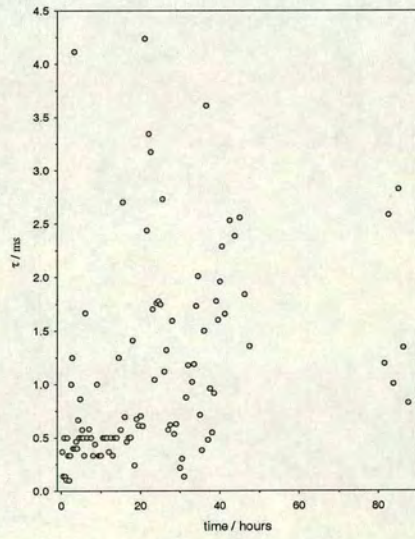


(b) Relaxation time

Figure 7.20: Time and amplitude of peak 1 of a Laplace transform of the DWS data through the top of the gel as it collapses

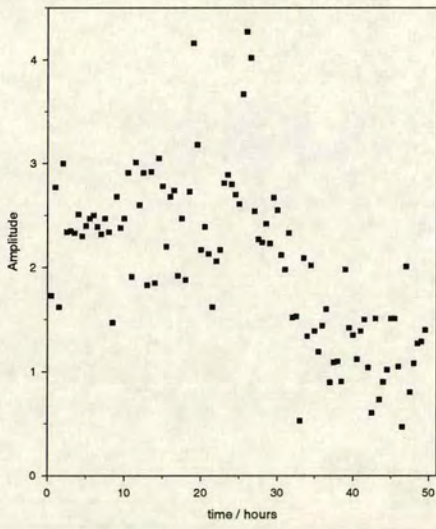


(a) Amplitude

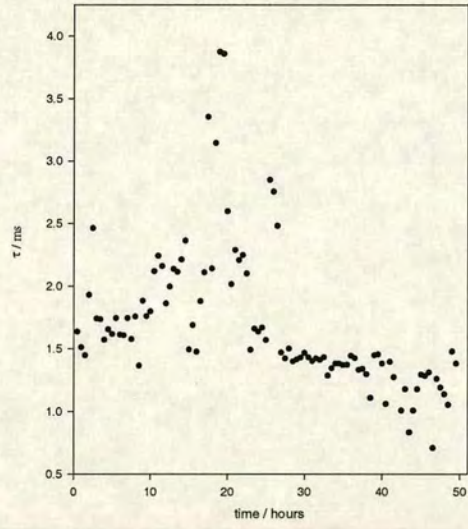


(b) Relaxation Time

Figure 7.21: Time and amplitude of peak 2 of a Laplace transform of the DWS data through the top of the gel as it collapses.

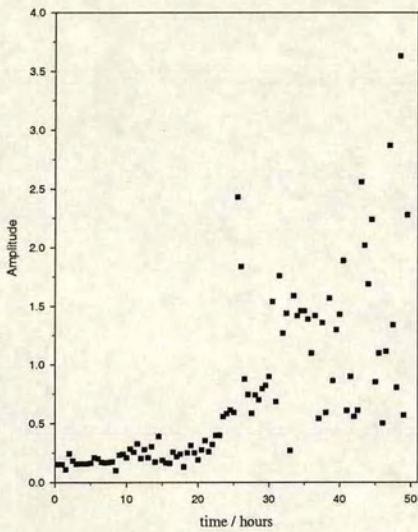


(a) Amplitude

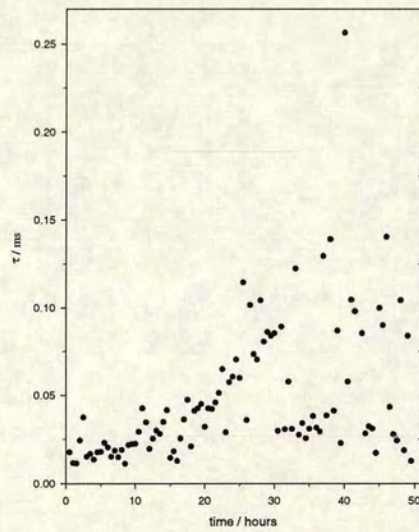


(b) Relaxation Time

Figure 7.22: Time and amplitude of peak 1 of a Laplace transform of the DWS data through the bottom of the gel as it collapses.



(a) Amplitude



(b) Relaxation Time

Figure 7.23: Time and amplitude of peak 2 of a Laplace transform of the DWS data through the bottom of the gel as it collapses.

### 7.3.2.3 Conclusion

The DWS experiments on the gel during its collapse show reproducible trends which can be rationalised by considering the behaviour of the sample at the position the laser is probing. This is aided by the use of simultaneous direct observation of the sample while the DWS measurements are being made. The complicated nature of the behaviour, however, makes it difficult to analyse the DWS results in more detail.

These experiments were carried out to investigate whether the onset of collapse could be easily predicted by measurement of the dynamics of the system. This would then provide a quick and simple test for shelf life of many industrial products. Unfortunately, however, these results show that little change is observed to take place before collapse begins in this system at least.

## 7.4 Distinguishing between Charge Effects and Depletion Effects

Electrostatic and depletion interactions are distinguished by adding a nonionic species which promotes the lengthening of the wormlike micelle without altering the coulombic interaction. This has been done in two ways. Firstly instead of having the SLES and CAPB in a constant ratio and adding salt, the concentration of the zwitterion CAPB\*\* was varied and no salt was added. Secondly octanol was added to the SLES/CAPB system. Both of these methods change the structure of the micelles (see section 5.3) while essentially keeping the electrostatic interactions constant. The results of these studies will be discussed in the following sections.

---

\*\*The zwitterion is classified as a charged surfactant, but it carries both a positive and negative charge and therefore is effectively neutral. It will result in a much smaller change in the electrostatic interaction when it is varied compared with adding salt to the system. Counterions of the CAPB will nonetheless contribute to some screening of the coulombic repulsion.



7.4.1 Varying Zwitterion

7.4.1.1 Results

A ternary phase diagram of the experimentally determined behaviour for varying SLES and CAPB concentrations (with no added salt) for a 1% volume fraction of 190nm radius particles is shown in figure 7.24.

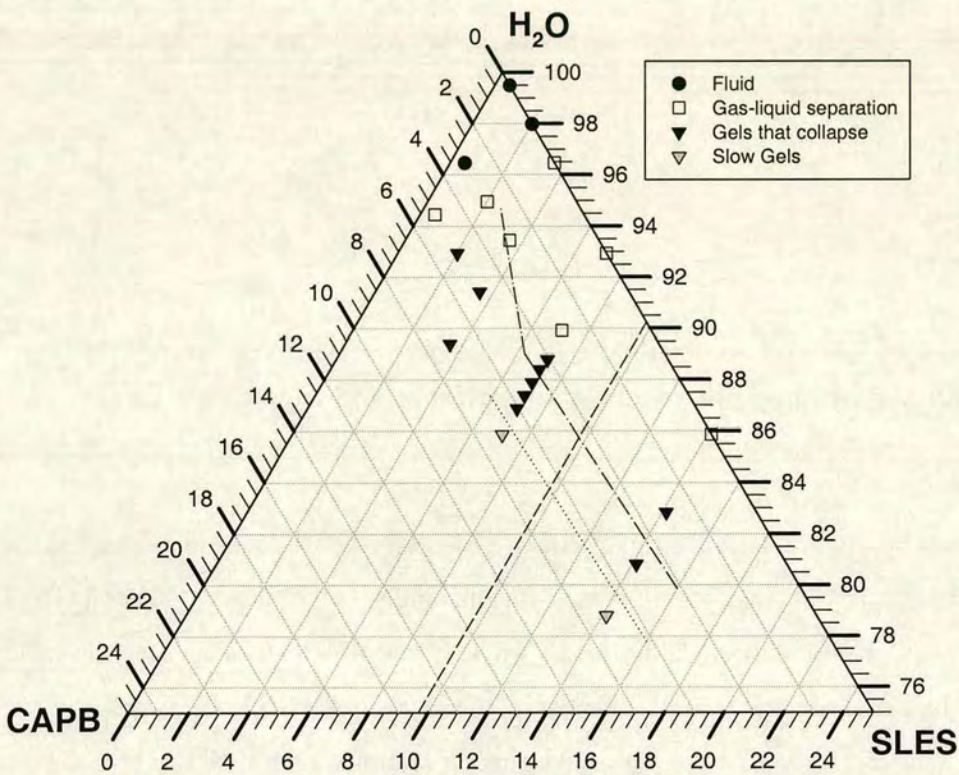


Figure 7.24: Ternary phase diagram of the SLES/CAPB/H<sub>2</sub>O system. No salt is added to this system and therefore the electrostatic interactions will remain approximately constant. This is indicated by the dashed line which corresponds to the ionic strength at the ccc. Below this line phase separation is expected when DLVO potentials alone are considered. Also indicated on this figure is the behaviour of the micellar solution (from figure 5.17). The dot-dash line is a rough estimate of  $c^*$ : below this line the micelles are entangled. The concentration of SLES and/or CAPB must however be increased further, as indicated by the dotted line, in order to find Maxwellian behaviour.

The behaviour found is similar to that of the SLES/NaCl/H<sub>2</sub>O system (figure 7.1); fluids, gas-liquid coexistence and gels which collapse via delayed sedimentation are all observed. The gels are again split into two types of behaviour according to how quickly they coarsen and subsequently collapse.

### 7.4.1.2 Discussion

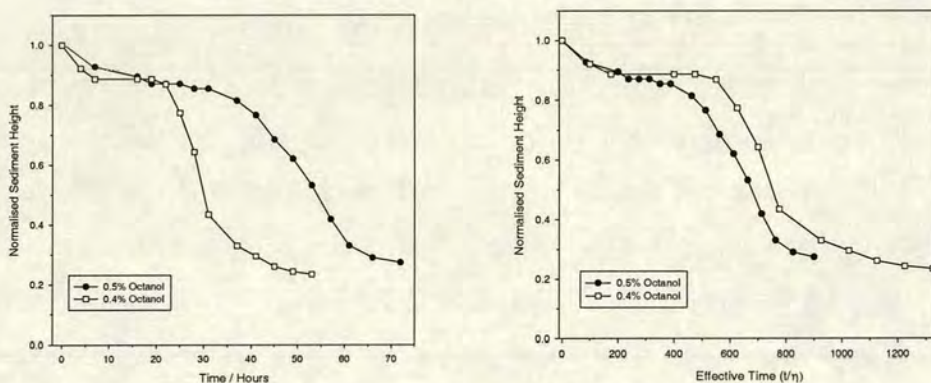
In section 5.3 it was shown that adding more CAPB to the SLES has a similar effect on the micelles as adding salt to the system. It therefore causes the micelles to grow longer and to become more entangled. The addition of CAPB will have little effect on the electrostatic interactions between the colloidal particles. The zwitterion will have some associated counterions which will contribute to screening of the coulombic repulsion, however this effect will be far less pronounced than in the case of added salt. Given that the phase behaviour is similar to that of the SLES/NaCl/H<sub>2</sub>O system, we conclude that the dominant interaction in both cases is likely to be the depletion attraction induced by the micelles. The phase behaviour observed certainly fits this picture as it is similar to the more simple, uncharged C<sub>16</sub>E<sub>6</sub> system (chapter 6). This will be discussed in full in section 7.5

### 7.4.2 SLES/CAPB/Octanol System

Octanol is uncharged and therefore by adding this to a solution of SLES and CAPB it induces the growth and entanglement of the wormlike micelles (section 5.3) without affecting the coulombic interaction between the colloidal particles. This method is more effective than adding CAPB in separating the depletion and electrostatic interactions. A phase diagram with varying SLES and octanol concentrations has not been determined as the phase behaviour and appearance of the micellar system when octanol is added is found to be quite complex. The main problem is that the amount of octanol required to induce Maxwellian behaviour of the micelles is so high that the micellar samples become cloudy making them unsuitable for carrying out the phase study. In order to get back to a clear micellar phase some salt had to be added to the mixture of SLES/CAPB too.

7.4.2.1 Results

Due to these problems, the effect of adding octanol to the SLES/NaCl/H<sub>2</sub>O system was investigated and compared to the behaviour without octanol. In figure 7.1 it can be seen that a sample with 7% SLES (and 1% CAPB), 1% NaCl and 1% volume fraction of latex phase separates into coexisting liquid and gas phases. When a small amount of octanol is added to this composition a gel is observed. The sedimentation profiles of two concentrations of added octanol, 0.4% and 0.5% which correspond to 1 molecule of octanol to 4.5 and 5.5 molecules of SLES respectively, are presented in figure 7.25.



(a) Normalised sediment height against time

(b) Normalised sediment height against effective time ( $t/\eta$ )

Figure 7.25: Sedimentation profiles of samples with 7% SLES, 1% CAPB and 1% NaCl with two different amounts of added n-octanol.

7.4.2.2 Discussion

The rheological behaviour of the 0.5% octanol sample with no added colloid is shown in figure 5.18. The 0.4% octanol sample shows similar behaviour. In both cases the micelles have begun to entangle but are not in the semi-dilute regime where Maxwellian behaviour is observed. The addition of octanol has the same rheological effect on the micelles as adding more salt to the system (see figures 5.13 and 5.18). Therefore finding similar behaviour for the colloid-micelle mixtures with either more salt (about 1.75% - see figure 7.6) or added octanol shows that the dominant effect is the depletion

attraction.

It should also be noted that by increasing the amount of octanol added to the system the observed delay time in the gel collapse is longer. However, as with the SLES/NaCl/H<sub>2</sub>O system this dependence is reversed once the viscosity of the micellar solutions is taken into account. This effect must therefore be primarily due to the mesh-size of the micellar network becoming smaller and hence the depletion attraction becoming more short range. The resulting gels become more dense with decreasing mesh-size and therefore collapse more rapidly.

## 7.5 Discussion & Comparison with Other Systems

### *The Depletion Picture*

In system C both the colloid and the wormlike micelles are charged. The depletion attraction should therefore be enhanced as the depletion layer becomes larger due to the mutual repulsion between the particles and the micelles. This effect was observed by Mondain-Monval et al. [80] and is discussed in section 3.4.1. At 0% salt the strong depletion attraction induced by the charged micelles at high surfactant concentrations is enough to overcome the strong repulsion between the colloidal particles.

It is not surprising that the behaviour observed in system C is similar to that of system A and system B with added salt since all the studies of system C point to the dominance of the depletion attraction over the coulombic interactions. System C therefore behaves essentially something like a hard sphere system. At high salt concentration this is expected, but at low salt concentration it is not as the Debye length is large. This behaviour therefore provides evidence that to a first approximation the charged colloids interact, with each other and with the charged micelles, as colloids with an effective hard sphere radius,  $a + \kappa^{-1}$  and an effective volume fraction  $\phi_{eff}$ . These values will vary with salt concentration.

### *Size Ratio Effect*

In the C<sub>16</sub>E<sub>6</sub> systems the variation of the size ratio, as the concentration of the surfactant was varied, was highlighted in the phase diagrams in chapter 6. In chapter 6

the question of which size ratio to use for system B with added salt was raised. Whilst the intuitive first answer to this was the usual size ratio ( $\xi = R_g/a$  or  $\xi = \xi_M/2a$ ) because the uncharged micelles should not be influenced by the Debye layer, the results give better agreement with size ratios involving the effective colloidal radius ( $\xi = R_g/(a + \kappa^{-1})$  or  $\xi = \xi_M/2(a + \kappa^{-1})$ )<sup>††</sup>. For the SLES system both the colloid and the depletant are charged and hence the size ratio considered should take account of their mutual repulsion. The size of the micelles in this system is unknown as light scattering studies have not been carried out on them. It is nonetheless known that in the dilute regime,  $R_g$  of the micelles will increase as the micelles grow (and thus as salt/surfactant/zwitterion/octanol concentrations are increased) and above the overlap concentration the mesh-size will decrease as the concentration of micelles increases. Where the micelles have been induced to grow by the addition of octanol and zwitterion, rather than salt, the effective colloidal radius will remain approximately constant and thus in the dilute regime the size ratio will increase, while above entanglement it will decrease again.

In the case of the SLES/NaCl/H<sub>2</sub>O system the salt induces growth of the micelles and reduces the screening length. Hence in the dilute regime the effective size of the colloid is reduced, while the radius of gyration of the micelles increases, therefore giving a large increase in the size ratio. Above the overlap concentration the decrease in the effective size of the colloids is accompanied by a reduction in the mesh size. The change in the size ratio above  $c^*$  is therefore minimised and will depend on which effect is more pronounced.

The difference in the variation of the size ratios for the SLES/NaCl/H<sub>2</sub>O (figure 7.1) and the SLES/CAPB/H<sub>2</sub>O (figure 7.24) systems have not shown any effect on the observed phase behaviour. Since the actual values of the size ratios are unknown it is hard to say whether this is surprising or not. In both cases the behaviour is similar to that observed for colloid-polymer mixtures above the cross-over size ratio.

---

<sup>††</sup>The micelles may, however, be repelled from the Debye layer due to their low dielectric constants. This has been discussed in chapter 6.

*Gels*

The gels observed in system C, unlike those of systems A and B, collapse by delayed sedimentation like gels in colloid-polymer mixtures. The similarity of the gels found for system C with those of colloid-polymer mixtures is another indication that the dominant effect in system C is indeed depletion. The effective order in which gels collapse in system C is, however, different to that in colloid-polymer mixtures. In the latter case the delay times are found to increase as the polymer concentration is increased [62]. The increase in concentration of polymer will increase the depth of the attractive well, but no change in the size ratio occurs and hence no change in the range of the depletion attraction will take place. In system C the effective delay time decreases with both increasing salt (figure 7.7) and/or SLES (figure 7.1). This effect has been explained in terms of the range of the attraction rather than its depth (see section 7.3.1). The shorter range attraction promotes densification of the colloidal structure, which in turn promotes faster collapse and sedimentation.

It should also be noted that in both the phase diagrams with varying salt (figure 5.14) and varying zwitterion (figure 5.17), gel behaviour appears when the micelles begin to entangle. The depletion potential has become strong enough as a result of the depletants becoming smaller (as the changeover from  $R_g$  to  $\xi_M$  takes place) and/or the concentration of the surfactant increasing. Slow gels also appear in both cases approximately where Maxwellian behaviour begins to be observed since the viscosity of the system is much larger in the semi-dilute regime.

**7.5.1 Comparison with Theory**

In chapter 6 the experimental phase diagrams were compared to theoretical phase diagrams produced from the Warren model [109]. Unfortunately a similar comparison cannot be made for system C, since the theoretical model cannot take account of charge effects. For the  $C_{16}E_6$  system the growth of the micelles is simply a result of the increase in concentration of the surfactant, but in the SLES/NaCl/H<sub>2</sub>O system both increases in the surfactant and salt concentrations promotes micellar growth. Hence even if a growth law was known for the SLES/NaCl/H<sub>2</sub>O system it would be impossible to input this into the Warren model to find the corresponding theoretical phase diagram.

## 7.6 Conclusions

It can be seen that the phase behaviour of a complex system of colloid-wormlike micelle mixtures discussed in this chapter can be qualitatively explained via the depletion mechanism. This is surprising considering the large number of components present and the charged nature of both the colloid and the micelles. This study therefore shows that the behaviour of realistic, complicated systems consisting essentially of colloid-wormlike micelle mixtures, such as shampoos, can largely be rationalised by considering the dominant colloidal interaction, namely the depletion attraction.

## Chapter 8

# Conclusions

In this chapter the main results of the phase studies detailed in chapters 6 and 7 are discussed. The main conclusions of these studies will be highlighted and then suggestions for possible further work are made.

### 8.1 Depletion Interaction due to Wormlike Micelles

In both of the main results chapters the details of the phase behaviour are discussed in terms of the depletion interaction. It should, however, be emphasised that this is the first study of the phase behaviour of colloid-wormlike micelle mixtures and therefore finding that the depletion force is indeed an important interaction in these mixtures is a significant result. The studies of wormlike micelles with colloids to be found in literature are limited. Theoretical investigations of mixtures of small colloidal particles and wormlike micelles [81], and direct force measurements of the depletion attraction due to worms at a surface [82] have been carried out (section 3.4.2). These studies, and depletion by other species such as polymers and spherical micelles indicate that wormlike micelle should deplete when mixed with a colloidal solution but hard evidence of this did not exist until now. As the micelles self-assemble they can break and reform. Therefore there was a possibility that the micelles could have broken up into small micelles in the presence of colloidal particles in order to reduce the effectiveness of the depletion attraction and thus keep the mixture stable.



## 8.2 Comparison with Experimental Studies of Colloid-Polymer Mixtures

Throughout this thesis the behaviour has been compared to that of the well studied model colloid-polymer mixtures. Wormlike micelles and polymers though similar in some respects have many important differences which could affect the depletion interactions. The size of the wormlike micelles has an exponential distribution and its average depends on concentration. The micelles can also break and reform unlike polymers. One aim of this study was to investigate how these differences would affect the phase behaviour observed. It has been found that despite these differences the phase behaviour of colloid-wormlike micelle mixtures qualitatively mimics that of model colloid-polymer mixtures.

The experimental studies carried out involve a few systems; a totally uncharged system (system A), a mixture of charged colloids and uncharged micelles (system B), and a mixture of charged colloids and charged micelles (system C). The main results found in these systems will be discussed in the subsequent sections.

### 8.2.1 System A and System B with Added Salt: Approximate Hard-Sphere Systems

System A, system B with added salt can be approximated to hard sphere systems. The phase behaviour observed in these cases is similar to that of colloid-polymer mixtures above the cross-over size ratio ( $\xi_{CO}$ ). One-phase fluids have been observed at low surfactant concentration, then as the concentration of  $C_{16}E_6$  increases the system begins to phase separate into coexisting liquid and gas phases due to the depletion attraction. As the strength of this depletion attraction increases further non-equilibrium gels are observed. This region of the phase diagram will be discussed in section 8.4. The size ratio in the wormlike-micelle mixtures changes as the concentration of surfactant changes so it is more difficult to compare the results with colloid-polymer mixtures. Nevertheless, for system A and system B with added salt the gas-liquid phase boundary is at a size-ratio of around  $\xi = 0.25$ , therefore one would expect to see gas-liquid coexistence.

In these systems most of the phase separation takes place above the overlap concentra-

tion,  $c^*$ . The behaviour found in the entangled regime is similar to that of the dilute regime, indicating the same type of depletion interaction is taking place. Depletion restabilisation (section 3.1.5) predicted by SFV theory [67] and by Gast et al. [48] as the depletion layer size changes to the mesh-size is not observed in these systems.

### 8.2.2 System B with no Added Salt: Strong Electrostatic Interactions

System B without added salt is a much more complex system to consider since the colloids have an extensive Debye layer associated with them which restricts how closely the colloids can approach one another. It was therefore no surprise to observe a more complex phase diagram. At low surfactant concentration a one phase colloidal fluid was found. As the concentration of surfactant increases first crystal-fluid coexistence then gel-gas separation are seen. As before at higher surfactant concentrations non-equilibrium gels are found.

In this system it is unclear from the experimental evidence whether the micelles can freely enter the Debye layer surrounding the particles, as one would expect for uncharged species, or if the micelle's low dielectric constant results in a repulsion between the micelles and the double layer. Phase separation in this system only takes place above  $c^*$ , where the mesh-size is mostly smaller than the screening length of the colloid. If one assumes that depletion takes place by blobs of size  $\xi_M$  then no depletion attraction should take place here. Since it does this may provide evidence for a repulsion between the micelles and the double layer, due to the low dielectric constant of the micelles. However, the micelles exist as an entangled network in this regime and it may be too simple a picture to expect depletion of blobs to be the only effect.

Comparing the experimental results for system B with no added salt and colloid-polymer mixtures a size-ratio of less than 0.25 is expected since crystal-fluid separation is observed. For all colloidal sizes studied,  $\xi < 0.25$  only when the effective size ratio, where the colloid is assumed to be a hard-sphere of radius  $a_{eff} = a + \kappa^{-1}$  is used. Again this may be a result of the repulsion between the micelles and Debye layer. However, given the differences between polymers and wormlike micelles, and the fact that here we are in the entangled regime, some disagreement between colloid-polymer mixtures and colloid-wormlike micelles is to be expected.

Despite some of the, as yet, unanswered questions posed by this system, the results on the whole agree well with a depletion attraction and the existing colloid-polymer mixture framework.

### 8.2.3 System C: An Industrial System

System C is a complicated fully charged system, with many components. Initially the phase behaviour of latex in a solution of wormlike micelles, with varying surfactant (SLES) and salt concentrations, and a constant surfactant to co-surfactant (CAPB) ratio was used. The phase behaviour found is similar to that of system A and system B with salt. At low surfactant/salt concentrations a stable fluid is found, then as the number and size of the micelles found grows gas-liquid coexistence is found. At higher still surfactant/salt concentrations a metastable gel phase is found. Since added salt both induces the growth of the micelles and screens the coulombic repulsion it is difficult to conclude that the phase behaviour observed is a result of the depletion attraction induced by the micelles, even though the behaviour is similar to that found in the more simple systems. In order to separate the depletion and electrostatic interactions the concentration of the zwitterionic co-surfactant CAPB was varied as well as the SLES, and no salt was added to the system. The electrostatic interactions were therefore kept approximately constant, whilst the size and concentration of the micelles were varied. The phase behaviour observed is similar to that of varying salt/SLES. This therefore indicates that the depletion attraction is the dominant force in this system. This was also confirmed by adding octanol to an aqueous sample of SLES/NaCl/CAPB/Latex. The octanol induced lengthening of the micelles, and this caused the sample to change from coexisting gas-liquid to a gel. Again this indicates the importance of the depletion attraction.

## 8.3 Theoretical Predictions of Phase Behaviour

The method of determining phase behaviour of colloid-polymer mixtures of Lekkerkerker et al. was extended to colloid-wormlike micelle mixtures by Warren [109]. This model takes account of the main differences between polymers and wormlike micelles as

depletants. Like the model of Lekkerkerker et al. it takes no account of charge effects. Light scattering studies have been carried out on the  $C_{16}E_6$  system [37], providing the necessary data to determine theoretical phase diagrams. The phase behaviour predicted agrees well with system A and system B with added salt. Reasonable agreement of the phase boundary, though not of the actual details of the phase behaviour also exists for system B with no added salt. The experimental study of system C cannot be compared to theory as it is a fully charged system, where the growth of the micelles is induced both by the concentrations of surfactant and salt/co-surfactant.

The predictions of the phase diagram have also been found to be highly dependent on the growth exponent of the concentration-induced growth of the micelles. With the experimentally determined value of 1.1, a critical point but no triple point is found. The gas-liquid binodal in this case is also observed to bend back giving rise to a stable region at high colloid volume fractions (below the melting volume fraction 0.494). This restabilisation has been observed in the case of  $C_{16}E_6$  with charged 70nm particles (but with no salt) indicating this effect is indeed real. For a growth exponent of 0.5 a phase diagram with both critical and triple points like that of colloid-polymer mixtures is found. The depletion potentials alone do not explain this phenomenon.

The theoretical model is valid only in the dilute regime and therefore it is surprising that the agreement with experiment is so good as most of the phase separation observed takes place above  $c^*$ .

## 8.4 Non-equilibrium Behaviour

In all three systems non-equilibrium behaviour has been observed at high surfactant concentrations. This occurs where the depletion attraction becomes strong enough that the colloids aggregate in a space-filling structure that spans the sample. In system A and system B with no added salt the gel structures do not collapse, while those of system B with added salt and system C do. The gel collapse in system B is not via delayed sedimentation as expected and observed in gels of colloid-polymer mixtures. The reasons for this are as yet unclear. Delayed sedimentation is observed for gels in system C though the gel collapse unexpectedly becomes effectively faster as the

surfactant concentration increases. This can be explained by considering the reduction in the range of the depletion potential as the surfactant concentration increases. This results in more dense clusters forming, which collapse more quickly under gravity.

Diffusive-wave spectroscopy has been used to probe the dynamics of the colloidal particles during gel collapse. The qualitative behaviour has been found to be reproducible and can be rationalised by considering the collapse process and the region of the sample probed. Quantitative analysis, however, proved difficult due to the complicated nature of the study. It was hoped that some clue to the imminent collapse would be found during the delay period by DWS. Unfortunately this has not been the case, and therefore it looks unlikely that this method could be used to test the potential shelf-life of industrial products.

### **8.5 Application to Complex Systems**

The most important conclusion to be drawn from this work is the the universality of solutions which can be approximated as a colloid-depletant mixture. This includes many industrial products such as shampoos. The phase behaviour can largely be explained by the existing model of simple colloid-polymer model.

### **8.6 Suggestions for Further Work**

Aqueous sterically stabilised colloids are difficult to synthesise and therefore most of the experiments in this thesis involve the use of charged colloids. By adding salt we have estimated the system to a hard-sphere case when explaining the results. However, a better comparison with theory could be made for a more realistic hard-sphere case by moving to micelles in organic solvents where many model hard-sphere colloids exist. One such micellar system would be that of lecithin in either cyclohexane or iso-octane with small amounts of added water used to induce the micellisation. This system, however, provides practical difficulties for a phase study as the amount of water in solution varies the properties drastically and it is difficult to keep constant due to changes of the humidity of air. This system would also be useful in providing a test for the differences of the phase behaviour for growth exponents of 1.1 and 0.5 as the

lecithin has been found to show both growth behaviours, depending on the conditions [36](section 2.4.4.1). The difference in behaviour, if confirmed, could provide an indirect method of determining the growth exponent of the micelles.

Many of the problems encountered in explaining the phase behaviour observed here were due to the relatively uncharted territory of the entangled polymer regime. Phase studies of colloid-polymer mixtures in this regime would be difficult due to the high viscosity of the samples. The phase separation may take a relatively long time to happen, and only metastable states may be observed. Nonetheless if the study could be carried out it may yield important information.

In section 6.4 the low surfactant concentration behaviour has been rationalised by the adsorption of surfactant molecules onto the surface of the colloid. Partial coverage destabilises the particles, allowing aggregation to take place. At monolayer coverage the colloid becomes sterically stabilised. This effect is only observed for system B with added salt, as the screening length in system B without added salt is too large to allow this adsorption to take place. There is no concrete evidence for the adsorption of the surfactant. If the adsorption causes recondensation of counterions onto the surface of the colloid, then the charge on the colloid should go down. The charge on the colloid should then be measured as a function of surfactant concentration both with and without added salt. This can be done in a number of ways e.g. electrophoresis or electro-osmosis, where the motion of colloid in an electric field is determined [12].

The possibility of a repulsion between uncharged micelles and the double layer around charged colloids has been suggested in section 6.5.3.1. This electrophobic effect gives good agreement with some experimental data and not others. A theoretical investigation into this effect, and a more simple experimental investigation perhaps of nonionic spherical micelles and charged colloid could be undertaken.

The phase behaviour of the systems studied could also be investigated more quantitatively. Tielines could be found by measurement of the components in each phase. These measurements would be difficult, but may be done by neutron scattering.



# List of Figures

2.1	Schematic diagram of the structure of the double layer and the corresponding potential versus distance curve. . . . .	9
2.2	DLVO potentials for a typical colloidal suspension. . . . .	13
2.3	Schematic diagram of a sterically stabilised colloid. . . . .	15
2.4	Schematic diagram of the depletion attraction. . . . .	16
2.5	Schematic diagram of hard-sphere phase behaviour. . . . .	17
2.6	A 2-d representation of entropically driven freezing. . . . .	18
2.7	Experimental phase diagram of charge-stabilised colloids. . . . .	20
2.8	Schematic diagram of a surfactant molecule. . . . .	21
2.9	Schematic diagram of the adsorption of surfactant molecules at both air/water and oil/water interfaces. . . . .	23
2.10	Schematic diagram of the geometric packing factors for surfactant molecules. . . . .	23
2.11	Table showing the dependence of micellar geometry on the packing parameters. . . . .	25
2.12	Schematic diagram of a wormlike micelle. . . . .	26
2.13	Schematic diagram illustrating the state of a solution of wormlike micelles with increasing surfactant volume fraction. . . . .	27



## LIST OF FIGURES

2.14	Schematic diagram of the reptation reactions of a polymer. . . . .	29
2.15	Schematic diagram of the scission-recombination reactions of wormlike micelles. . . . .	30
2.16	Schematic representation of the temperature effect on non-ionic surfactants. . . . .	32
2.17	Schematic phase diagram for nonionic surfactants. . . . .	33
2.18	Experimental phase diagram of $C_{12}E_5$ . . . . .	34
2.19	Schematic ternary phase diagram. . . . .	35
2.20	Partial ternary phase diagram of the AOT-NaCl- $H_2O$ system. . . . .	36
3.1	Schematic diagram illustrating the effect of size ratio on the depletion potential. . . . .	40
3.2	Theoretical phase diagram for colloid-polymer mixtures according to theory of Gast Hall & Russel. . . . .	42
3.3	Theoretical phase diagram for colloid-polymer mixtures according to theory of Gast Hall & Russel. . . . .	43
3.4	Theoretical phase diagram for an aqueous colloid-polymer mixture with varying size ratio. . . . .	45
3.5	Schematic diagram of the effectiveness of the depletion attraction in the presence of an electrostatic repulsion. . . . .	45
3.6	Schematic diagram of depletion of charged colloidal particles by polymers.	46
3.7	Theoretical phase diagram for an aqueous colloid-polymer mixture with varying ionic strength. . . . .	46
3.8	Schematic diagram illustrating the common tangent approach for determining phase behaviour. . . . .	48

3.9	Phase behaviour of colloid-polymer mixtures predicted by Lekkerkerker et al. . . . .	49
3.10	Phase behaviour of colloid-polymer mixtures predicted by Lekkerkerker et al. . . . .	50
3.11	Experimental phase diagrams of colloid-polymer mixtures. . . . .	52
3.12	Theoretical phase diagrams of colloid-polymer mixtures for varying size ratio. . . . .	52
3.13	Comparison of theoretical and experimental results for charged colloids and polymer - size ratio dependence. . . . .	53
3.14	Comparison of theoretical and experimental results for charged colloids and polymer - dependence on salt concentration. . . . .	54
3.15	Schematic Diagram of Diffusion Limited Cluster Aggregation (DLCA). . . . .	54
3.16	Schematic diagram of the sedimentation profile for a system exhibiting delayed sedimentation. . . . .	56
3.17	Experimental evidence for depletion restabilisation. . . . .	58
3.18	Schematic diagram of the depletion interaction at a wall. . . . .	59
3.19	Schematic diagram of the depletion interaction in a rod-sphere mixture. . . . .	60
3.20	Phase diagram for colloid-spherical micelle mixtures. . . . .	62
3.21	Schematic diagram comparing transient gels before collapse, after collapse and coexisting gel-gas samples. . . . .	63
4.1	Partial phase diagram of the binary system $C_{16}E_6$ in $D_2O$ . . . . .	69
4.2	A cube under simple shear. . . . .	75
4.3	Flow diagrams of common rheological models. . . . .	76
4.4	Frequency dependence of $G'$ and $G''$ for a Maxwell fluid. . . . .	79

## LIST OF FIGURES

4.5	Schematic diagram of the rheometer with cone and plate geometry attached. . . . .	80
4.6	Filling of cone and plate geometry. . . . .	82
4.7	Schematic diagram of the direct observation apparatus. . . . .	84
4.8	The intensity trace in a light scattering experiment. . . . .	85
4.9	Schematic diagram of multiple scattering in a colloidal suspension. . . . .	87
4.10	DWS set-up for ergodicity measurements. . . . .	90
4.11	DWS set-up to follow gel collapse. . . . .	91
5.1	Plots of conductivity against volume fraction for IDC lattices. . . . .	96
5.2	Plot of conductivity against concentration of a NaCl solution. . . . .	96
5.3	Plots of $\kappa^{-1}$ against volume fraction for IDC lattices. . . . .	97
5.4	DLVO potentials for IDC lattices. . . . .	102
5.5	Static correlation lengths for the $C_{16}E_6/D_2O$ system. . . . .	105
5.6	$R_g$ as a function of $C_{16}E_6$ concentration in the dilute regime. . . . .	105
5.7	Size ratios of particles & wormlike micelles of $C_{16}E_6$ . . . . .	106
5.8	Number density of micelles as a function of concentration of $C_{16}E_6$ . . . . .	107
5.9	Cole-Cole plots for varying concentration of $C_{16}E_6$ . . . . .	108
5.10	Cole-Cole plot for SLES/NaCl/ $H_2O$ system before wormlike micelles become highly entangled. . . . .	111
5.11	Cole-Cole plots of SLES/NaCl/ $H_2O$ system in the semi-dilute regime. . . . .	112
5.12	Schematic diagram of the reptation of branched micelles. . . . .	113

5.13	Cole-Cole plots as the NaCl concentration is varied for the SLES/NaCl/H <sub>2</sub> O system. . . . .	114
5.14	Micellar phase diagram for the SLES/NaCl/H <sub>2</sub> O system. . . . .	115
5.15	Schematic diagram showing the influence of a zwitterionic co-surfactant on the packing of an ionic surfactant. . . . .	115
5.16	Cole-Cole plots for the SLES/CAPB/H <sub>2</sub> O system. . . . .	116
5.17	Micellar phase diagram for the SLES/CAPB/H <sub>2</sub> O system. . . . .	117
5.18	Cole-Cole plots for SLES/NaCl/H <sub>2</sub> O system with added octanol. . . . .	118
5.19	Schematic diagram showing the effect on the preferred curvature of an SLES solution on addition of octanol. . . . .	118
6.1	Schematic diagram illustrating the depletion attraction for colloids in an entangled polymer solution. . . . .	123
6.2	Experimental phase diagram of system A. . . . .	126
6.3	Experimental phase diagram of system B with added salt - 175nm particles. . . . .	129
6.4	Experimental phase diagram of system B with added salt - 105nm particles. . . . .	130
6.5	Experimental phase diagram of system B with added salt - 70nm particles. . . . .	131
6.6	Ensemble average of $g^{(2)}(\tau)$ for a fluid phase sample. . . . .	133
6.7	Pictures of samples for system B with added salt. . . . .	134
6.8	Ensemble average of $g^{(2)}(\tau)$ for a gel. . . . .	135
6.9	Photos showing the various stages of the gels found in system B with added salt. . . . .	136
6.10	Sedimentation profiles of typical gels for system B with added salt. . . . .	137

## LIST OF FIGURES

6.11	Experimental phase diagram for system B with no added salt - 175nm particles. . . . .	142
6.12	Experimental phase diagram for system B with no added salt - 105nm particles. . . . .	143
6.13	Experimental phase diagram for system B with no added salt - 70nm particles. . . . .	144
6.14	Photos of crystal-fluid samples for system B with no added salt. . . . .	146
6.15	Photos of more samples for system B with no added salt. . . . .	147
6.16	Schematic diagram illustrating the depletion interaction from a size distribution of micelles for charged colloids. . . . .	149
6.17	Depletion and repulsive potentials for 175nm and 70nm particles, with and without added salt. . . . .	153
6.18	Theoretical phase diagram of 175nm particles in a solution of worms with growth exponent 1.1. . . . .	161
6.19	Theoretical phase diagram of 175nm particles in a solution of worms with growth exponent 0.5. . . . .	162
6.20	Depletion potentials for varying concentration of $C_{16}E_6$ (growth exponent 1.1) and 175nm radius particles. . . . .	163
6.21	Depletion potentials for varying concentration of $C_{16}E_6$ (growth exponent 0.5) and 175nm radius particles. . . . .	163
6.22	Theoretical phase diagram of 175nm radius particles in a monodisperse solution of worms (growth exponent=1.1). . . . .	165
6.23	Depletion potentials for varying $C_{16}E_6$ concentration for monodisperse worms with a growth exponent of 1.1 and 175nm radius particles. . . . .	165
6.24	Depletion potentials for varying concentration of $C_{16}E_6$ (growth exponent 1.1) and 70nm radius particles. . . . .	166

6.25 Theoretical phase diagram of 70nm radius particles in a solution of worms with growth exponent 1.1. . . . . 167

6.26 Theoretical binodals for various colloidal sizes in a solution of wormlike micelles with a growth exponent of 1.1. . . . . 169

6.27 Theoretical binodals for various effective colloidal sizes in a solution of wormlike micelles with a growth exponent of 1.1. . . . . 170

6.28 Theoretical phase diagram with tielines for 175nm particles (growth exponent=1.1. . . . . 172

7.1 Experimental phase diagram of SLES/NaCl/H<sub>2</sub>O and latex system. . . 177

7.2 Photos of phase separation for 7% SLES and increasing salt concentration.178

7.3 Photos of slow gels. . . . . 179

7.4 Photos of samples where the latices cream. . . . . 180

7.5 Photos of early and late stages of gel collapse in the SLES system. . . . 182

7.6 Plots of sediment heights versus time for 7% SLES and various NaCl concentrations. . . . . 183

7.7 Plots of sediment heights versus effective time for 7% SLES and various NaCl concentration. . . . . 184

7.8 Schematic diagram of positions of the gel sample probed by DWS during its collapse. . . . . 185

7.9 Sedimentation profile of a 7% SLES, 1% CAPB and 2.1% salt sample in a light scattering cell. . . . . 186

7.10 Average intensity versus time for the top of the sample during gel collapse.188

7.11 Video images of the top of the collapsing gel sample during the DWS experiments. . . . . 189

## LIST OF FIGURES

7.12	Intensity correlation functions over time during gel collapse - Top. . . .	190
7.13	Average intensity versus time for the bottom of the sample during gel collapse. . . . .	192
7.14	Video images of the bottom of the collapsing gel sample during the DWS experiment. . . . .	193
7.15	Intensity correlation functions over time during gel collapse - Bottom. .	194
7.16	$\langle \Delta r^2(\tau) \rangle$ for a few correlation functions from the bottom of the sample during gel collapse. . . . .	196
7.17	Correlation function for the bottom of the sample after 5 hours, together with its fit and the corresponding ILT. . . . .	197
7.18	Correlation function for the bottom of the sample after 20 hours, together with its fit and the corresponding inverse Laplace transform. . . . .	198
7.19	Correlation function for the bottom of the sample after 37.5 hours, together with its fit and the corresponding inverse Laplace transform. . . .	198
7.20	Amplitude and relaxation time of peak 1 of a Laplace transform of the DWS data through the top of the gel as it collapses. . . . .	199
7.21	Amplitude and time of peak 2 of a Laplace transform of the DWS data through the top of the gel as it collapses. . . . .	199
7.22	Amplitude and relaxation time of peak 1 of a Laplace transform of the DWS data through the bottom of the gel as it collapses. . . . .	200
7.23	Amplitude and relaxation time of peak 2 of a Laplace transform of the DWS data through the bottom of the gel as it collapses. . . . .	200
7.24	Phase diagram of SLES/CAPB/H <sub>2</sub> O system. . . . .	202
7.25	Sedimentation profiles of SLES/CAPB/NaCl/Octanol samples. . . . .	204
A.1	Schematic diagram showing the colloidal suspension after centrifugation.	238

# List of Tables

4.1	Summary of aqueous systems investigated. . . . .	68
5.1	Characteristics of surfactant-free charged polystyrene latices. . . . .	94
5.2	Debye screening lengths ( $\kappa^{-1}$ ) for IDC latices based on the concentration of counterions, calculated using equation 5.2. . . . .	95
5.3	Debye screening lengths ( $\kappa^{-1}$ ) for IDC latices from conductivity measurements. . . . .	98
5.4	Experimentally determined critical coagulation concentrations (ccc's). . . . .	99
5.5	Calculated screening lengths of IDC latices on addition of salt. . . . .	101
5.6	Values of Hamaker constants [99]. . . . .	102
5.7	Data from fitting a one element maxwell model to the C <sub>16</sub> E <sub>6</sub> rheological measurements. . . . .	109
5.8	Data from fitting a one element maxwell model to the rheological measurements for solutions with 14% SLES and 2% CAPB and various salt concentrations. . . . .	111
6.1	Approximate surfactant concentrations of phase boundaries for 1% charged colloid & salt. . . . .	132
6.2	Estimates of surfactant concentrations corresponding to monolayer coverage of the particles. . . . .	140



LIST OF TABLES

6.3 Estimates of surfactant concentration phase boundaries for charged col-  
loid (real volume fraction  $\approx 3\%$ ), no salt. . . . . 145

6.4 Values of  $\kappa^{-1}$  found from conductivity measurements for 1% colloid (sec-  
tion 5.1.1.2). . . . . 150

# Bibliography

- [1] P.N. Pusey and W. van Megen. Phase-behaviour of concentrated suspensions of nearly hard colloidal spheres. *Nature*, 320:340, 1986.
- [2] R.G. Laughlin. *The Aqueous Phase Behaviour of Surfactants*. Academic Press, 1994.
- [3] R. Strey, R. Schomacker, D. Roux, F. Nallet, and U. Olsson. Dilute lamellar and  $L_3$  phases in the binary water- $C_{12}E_5$  system. *J. Chem Soc. Faraday Trans.*, 86(12):2253–2261, 1990.
- [4] O. Ghosh and C.A. Miller. Liquid-crystalline and microemulsion phase behaviour in alcohol-free aerosol-AOT/oil/brine systems. *J. Phys. Chem.*, 91(17):4528–4535, 1987.
- [5] P.R. Sperry, H.B. Hopfenberg, and N.L. Thomas. Flocculation of latex by water-soluble polymers: Experimental confirmation of a nonbridging, nonadsorptive, volume-restriction mechanism. *Journal of Colloid and Interface Science*, 82(1):62–76, 1981.
- [6] P.B. Sperry. Morphology and mechanism in latex flocculated by volume restriction. *Journal of Colloid and Interface Science*, 99(1):97–108, 1984.
- [7] S. M Ilett, A. Orrock, W.C.K. Poon, and P.N. Pusey. Phase behaviour of a model colloid-polymer mixture. *Phys. Rev. E*, 51(2):1344–1352, 1995.
- [8] S. Asakura and F. Oosawa. *J. Chem. Phys.*, 22:1255, 1954.
- [9] A. Vrij. Polymer at interfaces and the interactions in colloidal dispersions. *Pure and Applied Chemistry*, 48:471–483, 1976.

## BIBLIOGRAPHY

- [10] H.N.W. Lekkerkerker, W.C.K. Poon, P.N. Pusey, A. Stroobants, and P.B. Warren. Phase behaviour of colloid and polymer mixtures. *Europhys. Lett.*, 20(6):559–564, 1992.
- [11] P.B. Warren. A theory of void formation in charge-stabilized colloidal suspensions at low ionic strength. *Journal of Chemical Physics*, 112(10):4683–4698, 2000.
- [12] D.J. Shaw. *Colloid & Surface Chemistry*. Butterworth Heinemann, fourth edition, 1994.
- [13] J.N. Israelachvili. *Intermolecular and Surface Forces*. Academic Press, 2nd edition edition, 1991.
- [14] R. Hogg, T.W. Healy, and D.W. Fuerstenau. *Trans. Faraday Soc.*, 62:1638, 1966.
- [15] G.R. Wiese and T.W. Healy. *Trans. Faraday Soc.*, 66:490, 1970.
- [16] J.Th.G. Overbeek. Recent developments in the understanding of colloid stability. *J. Colloid Interface Sci.*, 58:408–422, 1977.
- [17] R.J. Hunter. *Foundations of Colloid Science Volume I*. Oxford, 1989.
- [18] W.B. Russel, D.A. Saville, and W.R. Schowalter. *Colloidal Dispersions*. Cambridge University Press, 1989.
- [19] B.V. Deryagin and L. Landau. *Acta Phys Chim. URSS*, 14:633, 1941.
- [20] E.J.W. Verwey and J.Th.G. Overbeek. *Theory of the stability of lyophobic Colloids*. Elsevier, 1948.
- [21] H. Reerink and J.Th.G. Overbeek. *Discuss. Faraday Soc.*, 18:74, 1954.
- [22] N. Fuchs. Über die stabilität und aufladung der aerosole. *Z. für Physik*, 89:736–743, 1934.
- [23] P.G. de Gennes. *Scaling Concepts in Polymer Physics*. Cornell University Press, 1991.
- [24] A.P. Gast, W.B. Russel, and C.K. Hall. An experimental and theoretical study of phase transitions in the polystyrene latex and hydroxyethylcellulose system. *Journal of Colloid and Interface Science*, 109(1):161–171, 1986.

- [25] P.D. Patel and W.B. Russel. An experimental study of aqueous suspensions containing dissolved polymer. A. phase separation. *Journal of Colloid and Interface Science*, 131(1):192–200, 1989.
- [26] W.W. Wood and J.D. Jacobson. Preliminary results from a recalculation of the monte carlo equation of state of hard spheres. *Journal of Chemical Physics*, 27:1207, 1957.
- [27] W.G. Hoover and F.H. Ree. Melting transition and communal entropy for hard spheres. *Journal of Chemical Physics*, 49(8):3609–3617, 1968.
- [28] W. van Meegen and I. Snook. *Chem. Phys. Lett.*, 35:399, 1975.
- [29] S.J. Brenner. *J. Phys. Chem.*, 80:1473, 1976.
- [30] C.J. Barnes, D.Y.C. Chan, D.H. Everett, and D.E. Yates. *J. Chem. Soc. Farad. Trans. II*, 74:136, 1978.
- [31] A. Kose, M. Ozaka, K. Takano, Y. Kobayashi, and S. Hachisu. Direct observation of ordered latex suspension by metallurgical microscope. *J. Colloid Interface Sci.*, 44:330–8, 1973.
- [32] W.B. Russel. *Dynamics of Colloidal Systems*. University of Wisconsin Press, 1987.
- [33] P.N. Pusey. *Liquids, Freezing and the Glass Transition*, chapter 10. Elsevier, 1991.
- [34] G. Platz, C. Thunig, J. Polike, W. Kirchhoff, and D. Nickel. *Colloids Surf. A*, 88:113, 1994.
- [35] M.E. Cates. Flow behaviour of entangled surfactant micelles. *J. Phys.:Condens. Matter*, 8:9167–9176, 1996.
- [36] G. Jerke, J.S. Pedersen, S.U. Egelhaaf, and P. Schurtenberger. Static structure factor of polymerlike micelles: Overall dimension, flexibility, and local properties of lecithin reverse micelles in deuterated isooctane. *Phys. Rev. E*, 56(5):5772–5788, 1997.
- [37] P. Schurtenberger, C. Cavaco, F. Tiberg, and O. Regev. Enormous concentration-induced growth of polymer-like micelles. *Langmuir*, 12(12):2894–2899, 1996.

## BIBLIOGRAPHY

- [38] M.E. Cates and S.J. Candau. Statics and dynamics of worm-like surfactant micelles. *J.Phys: Condens. Matter*, 2:6869–6892, 1990.
- [39] S.J. Candau and M.E. Cates. to be published.
- [40] P. Schleger, G. Ehlers, B. Farago, D. Richter, and A. Wischnewski. Clear signatures of reptation in entangled linear polymers. <http://www.ill.fr/AR-98/page98/30soft.htm>, 1998.
- [41] S.J. Candau, A. Khatory, F. Lequeux, and F. Kern. Rheological behaviour of wormlike micelles - effect of salt content. *Journal de Physique IV*, 3:197–209, 1993.
- [42] E.K. Wheeler, P. Izu, and G.G. Fuller. Structure and rheology of wormlike micelles. *Rheologica Acta*, 35(2):139–149, 1996.
- [43] C. Grand, J. Arrault, and M.E. Cates. Slow transients and metastability in wormlike micelle rheology. *J. Phys. II France*, 7:1071–1086, 1997.
- [44] J.H. Clint. *Surfactant Aggregation*. Blackie, 1992.
- [45] P.R. Sperry. A simple quantitative model for the volume restriction flocculation of latex by water-soluble polymers. *J. Colloid Interface Sci.*, 87(2):375–383, 1982.
- [46] J.F. Joanny, L. Leibler, and P.G. de Gennes. *J. Polym. Sci., Polym. Phys.*, 17:1073, 1979.
- [47] A.P. Gast, C.K. Hall, and W.B. Russel. Polymer-induced phase separations in nonaqueous colloidal suspensions. *J. Colloid Interface Sci.*, 96(1):251–267, 1983.
- [48] A.P. Gast, C.K. Hall, and W.B. Russel. Phase separations induced in aqueous colloidal suspensions by dissolved polymer. *Faraday Discuss. Chem. Soc.*, 76:189–201, 1983.
- [49] N.F. Carnahan and K.E. Starling. *J. Chem. Phys.*, 53:600, 1970.
- [50] K.R. Hall. *J. Chem. Phys.*, 57:2252, 1972.
- [51] W.R. Smith and D. Henderson. *Molec. Phys.*, 19:411, 1970.
- [52] L. Verlet and J. Weis. *J. Phys. Rev. A*, 5:939, 1972.

- [53] J.M. Kincaid and J. Weis. *J. Molec. Phys.*, 34:931, 1977.
- [54] W.C.K. Poon, J.S. Selfe, M.B. Robertson, S.M. Ilett, A.D. Pirie, and P.N. Pusey. An experimental study of a model colloid-polymer mixture. *J. Phys. II France*, 3(7):1075–1086, 1993.
- [55] H. de Hek and A. Vrij. Interactions in mixtures of colloidal silica spheres and polystyrene molecules in cyclohexane i. phase separations. *Journal of Colloid & Interface Science*, 84(2):409–422, 1981.
- [56] J. Edwards, D.H. Everett, T. O’Sullivan, I. Pangalou, and B. Vincent. Phase separation in model colloidal dispersions. *J. Chem. Soc., Faraday Trans. 1*, 80:2599–2607, 1984.
- [57] A.P. Gast, W.B. Russel, and C.K. Hall. An experimental and theoretical study of phase transitions in the polystyrene latex and hydroxyethylcellulose system. *J. Colloid Interface Sci.*, 1985.
- [58] T. Vicsek. *Fractal Growth Phenomena*. World Scientific, 2nd edition edition, 1994.
- [59] M.D. Haw. *Computer Simulation of Aggregation and Gelation in Colloidal Suspensions*. PhD thesis, University of Edinburgh, 1996.
- [60] M.D. Haw, M. Sievwright, W.C.K. Poon, and P.N. Pusey. Cluster-cluster gelation with finite bond strength. *Advances in Colloid and Interface Science*, 73:71, 1997.
- [61] W.C.K. Poon, A.D. Pirie, and P.N. Pusey. Gelation in colloid-polymer mixtures. *Faraday Discussion*, 101:65–76, 1995.
- [62] S.P. Meeker. *Low Shear Rheology and Delayed Sedimentation of Colloidal Systems*. PhD thesis, University of Edinburgh, 1997.
- [63] L. Starrs. *Collapse of Transient Gels in Colloid-Polymer Mixtures*. PhD thesis, University of Edinburgh, 1999.
- [64] A. Parker, P.A. Gunning, K. Ng, and M.M. Robins. How does xanthan stabilise salad dressing? *Food hydrocolloids*, 9(4):333–342, 1995.
- [65] R.I. Feigin and D.H. Napper. Stabilization of colloids by free polymer. *J. Colloid Interface Sci.*, 74:567–571, 1980.

## BIBLIOGRAPHY

- [66] R.I. Feigin and D.H. Napper. Depletion stabilization and depletion flocculation. *J. Colloid Interface Sci.*, 75:525–541, 1980.
- [67] G.J. Fleer, J.M.H.M. Scheutjens, and B. Vincent. The stability of dispersions of hard spherical particles in the presence of nonadsorbing polymer. *ACS Symposium Series*, 240:245–263, 1983.
- [68] S.N. Emmett. *Phase Transitions in Dispersions of Weakly Interacting Colloidal Particles*. PhD thesis, University of Bristol, 1990.
- [69] W.C.K. Poon and P.B. Warren. Phase behaviour of hard-sphere mixtures. *Europhysics Letters*, 28(7):513–518, 1994.
- [70] P.D. Kaplan, J.L. Rouke, A.G. Yodh, and D.J. Pine. Entropically driven surface phase separation in binary colloidal mixtures. *Phys. Rev. Lett.*, 72:582–585, 1994.
- [71] Y. Mao, M.E. Cates, and H.N.W. Lekkerkerker. Depletion forces in colloidal systems. *Physica A*, 222:10–24, 1995.
- [72] P. Bartlett, R.H. Ottewill, and P.N. Pusey. *Journal of Chemical Physics*, 93:1299, 1990.
- [73] S. Asakura and F. Oosawa. *J. Polym. Sci.*, 32:183, 1958.
- [74] G.A. Vliegenthart and H.N.W. Lekkerkerker. Phase behaviour of colloidal rod-sphere mixtures. *J. Chem. Phys.*, 111(9):4153–4157, 1999.
- [75] R. Piazza and G. di Pietro. Phase separation and gel-like structures in mixtures of colloids and surfactant. *Europhys. Lett.*, 28(6):445–450, 1994.
- [76] R.J. Baxter. *J. Chem. Phys.*, 49:2770, 1968.
- [77] W.C.K. Poon. Private Communication.
- [78] J. Bibette, D. Roux, and B. Pouligny. Creaming of emulsions: the role of depletion forces induced by surfactant. *J. Phys. II France*, 2(3):401–424, 1992.
- [79] P. Baggot, S.U. Egelhaaf, and W.C.K. Poon. In preparation.
- [80] O. Mondain-Monval, F. Leal-Calderon, J. Phillip, and J. Bibette. Depletion forces in the presence of electrostatic double layer repulsion. *Phys. Rev. Lett.*, 75(18):3364–3367, 1995.

- [81] R.P. Sear and B.M. Mulder. Phase behaviour of mixtures of wormlike micelles and mixtures of wormlike micelles with small colloidal particles. *J. Phys. Chem.*, 101:4839–4844, 1997.
- [82] P. Kekicheff, F. Nallet, and P. Richetti. Measurement of depletion interaction in semi-dilute solutions of worm-like surfactant aggregates. *J. Phys. II France*, 4(5):735–741, 1994.
- [83] R.H. Ottewill, R. Satgurunathan, F.A. Waite, and M.J. Westby. Non-ionic polystyrene latices in aqueous media. *British Polymer Journal*, 19:435–440, 1987.
- [84] R.H. Ottewill and R. Satgurunathan. Nonionic latices in aqueous media. Part 1. preparation and characterization of polystyrene latices. *Colloid & Polymer Sci.*, 265:845–853, 1987.
- [85] H.A. Barnes, J.F. Hutton, and K. Walters. *An Introduction to Rheology*. Elsevier, 1993.
- [86] R.W. Whorlow. *Rheological Techniques*. Ellis Horwood, 1992.
- [87] P. Schurtenberger. Private Communication to S.U. Egelhaaf.
- [88] Interfacial Dynamics Corporation. Data Sheets, 1999.
- [89] D.R. Lide. *CRC Handbook of Chemistry and Physics*. CRC, 76th edition, 1995–1996.
- [90] B.J. Berne and R. Pecora. *Dynamic Light Scattering*. Wiley, 1976.
- [91] P.N. Segre, W. van Meegen, P.N. Pusey, K. Schatzel, and W. Peters. 2-color dynamic light-scattering. *J. Mod. Optic.*, 42(9):1929–1952, 1995.
- [92] D.A. Weitz and D.J. Pine. *Diffusing-wave spectroscopy*, chapter 16, page 653. Oxford Science Publications, 1993.
- [93] G. Maret. Diffusing-wave spectroscopy. *Current Opinion in Colloid & Interface Science*, 2:25–257, 1997.
- [94] J.G.H. Joosten, E.T.F. Geladé, and P.N. Pusey. Dynamic light scattering by nonergodic media: Brownian particles trapped in polyacrylamide gels. *Phys. Rev. A*, 42(4):2161–2175, 1990.



## BIBLIOGRAPHY

- [95] P.N. Pusey and W. van Megen. *Physica A*, 157:705, 1989.
- [96] J.Z. Xue, D.J. Pine, S.T. Milner, X.I. Wu, and P.M. Chaikin. Nonergodicity and light scattering from polymer gels. *Phys. Rev. A*, 46(10):6550–6563, 1992.
- [97] T. Gisler, F. Schulz, M. Borkovec, H. Sticher, P. Schurtenberger, B. D’Aguanno, and R. Klein. Understanding colloidal charge renormalization from surface chemistry: Experiment and theory. *J. Chem. Phys.*, 101(11):9924–9936, 1994.
- [98] V.A. Parsegian and G.H. Weiss. Spectroscopic parameters for computation of van der Waals forces. *J. Colloid Interface Sci.*, 81:285–289, 1981.
- [99] J. Visser. Adhesion of colloidal particles. In E. Matijevic, editor, *Surface and Colloid Science*, volume 8, pages 3–84. Wiley-Interscience, 1976.
- [100] Y. Oono. *Adv. Chem. Phys.*, 61:301–437, 1985.
- [101] F. Lequeux and S.J. Candau. *Structure and Flow in Surfactant Solutions*, chapter 3. ACS Symposium Series 578, 1994.
- [102] F. Lequeux. Reptation of connected wormlike micelles. *Europhys. Lett.*, 19(8):675–681, 1992.
- [103] J.F. Joanny, L. Leibler, and P.G. de Gennes. *J. Polym. Sci., Polym. Phys.*, 17:1073, 1979.
- [104] R.P. Sear. Entropy-driven separation in mixtures of small colloidal particles and semidilute polymers. *Phys. Rev. E*, 56(4):4463–4466, 1997.
- [105] Y. Mao, M.E. Cates, and H.N.W. Lekkerkerker. Depletion stabilization by semidilute rods. *Phys. Rev. Lett.*, 75(24):4548–4551, 1995.
- [106] L. Ouali, J. François, and E. Pefferkorn. Adsorption of telechelic poly(ethylene oxide) on colloids: Influence on colloid stability. *Journal of Colloid and Interface Science*, 215, 1999.
- [107] A. Di Biasio, F. Bordini, C. Cametti, and P. Codastefano. Evidence for a crossover region in the aggregation of PEO-coated polystyrene particle suspensions. *J. Chem. Soc., Faraday Trans.*, 94:3477–3480, 1998.
- [108] M.E. Cates. Private Communication.

- [109] P. Warren. Private Communication.
- [110] L.A. Galloway, P.B. Warren, W.C.K. Poon, S.U. Egelhaaf, and M.E. Cates. In preparation.
- [111] R.P. Sear and D. Frenkel. Phase behaviour of colloid plus polydisperse polymer mixtures. *Phys. Rev. E*, 55(2):1677–1681, 1997.
- [112] P.B. Warren. Phase behaviour of a colloid and binary polymer mixture: Theory. *Langmuir*, 13:4588–4594, 1997.
- [113] M. Fuchs and K.S. Schweizer. Structure and thermodynamics of colloid-polymer mixtures: A macromolecular approach. *Europhys. Lett.*, 51(6):621–627, 2000.
- [114] S. Haddon. Phase diagrams of colloid-surfactant systems. Undergraduate Research Project, *University of Edinburgh*, 1999.
- [115] N. Menon and D.J. Durian. Diffusing-wave spectroscopy of dynamics in a three-dimensional granular flow. *Science*, 275:1920–1922, 1997.
- [116] S.W. Provencher. A constrained regularization method for inverting data represented by linear algebraic or integral equations. *Comput. Phys. Commun.*, 27:213, 1982.

BIBLIOGRAPHY

# Appendix A

## Sample Making - More Details

### A.1 System A

#### A.1.1 Finding the Volume Fraction of the Colloid

An approximate estimate of the volume fraction of the PEO-coated polystyrene latices was found using centrifugation. A known weight of colloid is centrifuged at 3000rpm until the colloid and the water have separated. In reality, however, when the supernatant of mass,  $M_w$ , is discarded it contains some colloid. The mass of the colloidal solution remaining,  $M$ , is determined. Assuming that the colloid is randomly close packed, with a volume fraction of  $\approx 0.64$ , and assuming the density of polystyrene is about  $1\text{gcm}^{-3}$ , then the volume fraction of the remaining sediment is,

$$\phi = 0.64 = \frac{M_c}{M_c + M'_w} \quad (\text{A.1})$$

where  $M = M_c + M'_w$  is the mass of the sediment,  $M_c$  is the colloid mass and  $M'_w$  is the mass of the remaining water in the sediment (figure A.1).

Adding water of mass  $M_{add}$  to the sediment to disperse the mixture allows the volume fraction of this solution,  $\phi_{new}$  to be found via,

$$\phi_{new} = \frac{M_c}{M_c + M'_w + M_{add}} = \frac{\phi}{1 + \frac{M_{add}}{M}} \quad (\text{A.2})$$

It can be seen from the above assumptions that only an approximate value of the volume

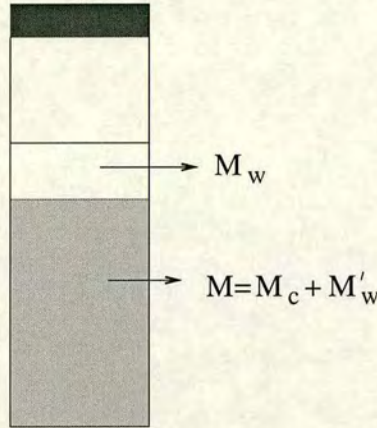


Figure A.1: Schematic diagram showing the colloidal suspension after centrifugation.

fraction of the stock solution used to make samples of system A is found. However, the same stock solution is used throughout, thus the relative concentrations are correct.

## A.2 System B

### A.2.1 Finding the Required Colloid Volume Fraction

The IDC latex particles used for most of the phase studies come as a stock solution of  $x$ g of solid per  $100\text{cm}^3$  of solution. The literature value for the density of the particles is  $\rho_l = 1.055\text{gcm}^{-3}$  [88]. The volume fraction of the stock solution,  $\phi_0$ , is therefore,

$$\phi_0 = \frac{x}{100\rho_l} \tag{A.3}$$

To make up a sample of volume  $V_t$  with a volume fraction of  $\phi$  requires a volume  $V_l = V_t\phi$  of latices and thus requires a volume

$$V = \frac{V_l}{\phi_0} = \frac{100V_l\rho_l}{x} \tag{A.4}$$

of the stock solution. The samples are, however, made gravimetrically and therefore an estimate of the density of the solution  $\rho_{sol}$  is required in order to determine the mass of stock solution to be measured. An approximate expression for the density of the solution is,

$$\rho_{sol} = \frac{x + \rho_w(100 - \frac{x}{\rho_l})}{100} \tag{A.5}$$

where  $\rho_w$  is the density of water. Hence the mass of the stock solution required,  $M$ , is,

$$M = \frac{100V_l\rho_{sol}\rho_l}{x} \quad (\text{A.6})$$

## A.2.2 Sample-making

The samples of system B are made up as discussed in chapter 4. Usually the samples are 3g, but larger volume samples are made up as the concentration of the  $C_{16}E_6$  becomes low in order to minimise the associated weighing uncertainties.

### A.2.2.1 Sample Error Calculation

Neglecting the uncertainty in the concentration of the stock solution of latex particles the errors involved with sample making are weighing errors. The associated uncertainty of the balance used is estimated as  $\pm 0.0005\text{g}$ . For a typical sample of system B with no added salt the errors are as follows,

$$\text{Weighing error of } C_{16}E_6 = \frac{0.0005}{0.03} = \pm 1.7\%$$

$$\text{Weighing error of particles} = \frac{0.0005}{0.4} = \pm 0.13\%$$

$$\text{Weighing error of water} = \frac{0.0005}{2.57} = \pm 0.02\%$$

There is also an error in the concentration of the solution. This is largest for the 175nm particles and is,

$$\text{Error in stock solution} = \frac{0.1}{6.0} = \pm 1.7\%$$

It can therefore be seen that the weighing errors of the particles and the water are negligible and the uncertainty in the sample can be estimated by combining the weighing error of  $C_{16}E_6$  and the error in the stock solution. Thus the total error in the solution is about 2.4%. This is quite a small uncertainty and is smaller than the size of the symbols used on the phase diagrams.

Similar results are determined for system B with added salt.

## A.3 System C

### A.3.1 Sample-making

The technique described in section A.2.1 is also used for preparing samples with a volume fraction  $\phi$  of IDC colloid in system C. A similar method is also used to make up the samples from a stock Rhône-Poulenc latices of known initial volume fraction. The surfactant stock solutions are of a given % w/w and therefore the % w/w required in a phase sample is easily determined. The order in which components are added is discussed in chapter 4.

The samples used for the phase study for system C are 20g samples. In order to carry out direct observations on system C, smaller cells were required and thus 7g samples were subsequently made in smaller cylindrical vials. The volume of all samples was kept constant throughout the observations in order to minimise any size dependence of the gel collapse as has been found for colloid-polymer mixtures [63].

#### A.3.1.1 Uncertainties

Errors are assessed for system C in a similar way to system B described previously. The samples are, however, larger in this system and therefore the relative weighing errors are very small. The symbols used to represent the samples in the phase diagrams are therefore larger than the associated uncertainty.